

Theory of Discreteness of Charge Effects in the Electrolyte Compact Double Layer

C. A. BARLOW, JR. AND J. ROSS MACDONALD
*Central Research Laboratories, Texas Instruments Incorporated,
Dallas, Texas*

Contents

I. Introduction	2
II. Qualitative Discussion	3
1. Gross System Considered	3
A. Double-Layer Structure	3
B. Definition of Terms	7
C. Experimental Methods	10
2. Discreteness Effects	11
3. Types of Imaging	16
4. The Question of Order	19
5. Role of the Diffuse Layer	33
6. The Concept of an Inner-Region Dielectric Constant	43
7. Complications in the Compact Layer	53
A. Nonlinearities	53
B. Solvation	56
III. Quantitative Discussion	57
1. Introduction	57
2. Examining the Question of Order	58
3. Diffuse-Layer Screening	72
IV. Methodology	81
1. Some Exact Array Methods	81
2. Approximate Methods	91
V. Discussion of Results: Nonpolarizable Adions	102
1. Local Potentials	102
A. Single Imaging	102
B. Other Imaging Conditions	114
2. Micropotentials	119
A. Early Work	119
B. Conductive-Conductive Imaging	128
C. Single Imaging	136
D. Other Imaging Conditions	144
VI. Discussion of Results: Average Quantities	161

1. Permanent/Polarizable Dipoles	161
2. Nonpolarizable Adions	169
3. Polarizable Adions	173
VII. Discussion of Results: Local Potentials—Polarizable Adions	177
Appendix I. C-C Imaging for a Single Charge	183
Appendix II. Distribution Function for Nearest Neighbors without Interaction	186
List of Symbols	188
References	194

I. Introduction

“The more complicated the system considered, the more simplified must its theoretical description be. One cannot demand that a theoretical description of a complicated atom, and all the more of a molecule or a crystal, have the same degree of accuracy as of the theory of the simplest hydrogen atom. Incidentally, such a requirement is not only impossible to fulfill, but also essentially useless. . . . An exact calculation of the constants characterizing the simplest physical system has essential significance as a test of the correctness of the basic principles of the theory. Once, however, it passes this test brilliantly, there is no sense in subjecting it to further tests as applied to more complicated systems. The most ideal theory cannot pass such tests, owing to the practically unsurmountable mathematical difficulties unavoidably encountered in applications to complicated systems. In this case all that is demanded of the theory is a correct interpretation of the general character of the quantities and laws pertaining to such a system. The theoretical physicist is in this respect like a cartoonist, who must depict the original not in all details, like a photographic camera, but simplify and schematize it in a way as to disclose and emphasize the most characteristic features. Photographic accuracy can and should be required only of the description of the *simplest* systems. A good theory of complicated systems should represent only a good “caricature” of these systems, exaggerating the properties that are most difficult, and purposely ignoring all the remaining inessential properties.”

J. Frenkel

This article begins with a qualitative discussion of those frequently neglected aspects of the electrolyte double layer concerned with discreteness effects. In this discussion, details of the mathematical aspects of the problems associated with the system are subordinated in favor of a thorough appraisal of the physical aspects. We have attempted here to give a clear enough account of the situation that, were the reader to read only this part of the article, he would nonetheless obtain an appreciation of most of the phenomena active in the compact layer. The following two parts are intended to supplement this first part by giving much of the

mathematical detail and apparatus omitted in the qualitative discussion. Particularly the latter of these two parts, titled “Methodology,” should prove useful to the reader interested in performing accurate potential calculations. The final part of the paper is a critical review of important work in this field with emphasis upon comparing the various models and approximations used as well as the results following from these treatments.

There have been numerous reviews published concerning electrolyte double-layer behavior, structure, and theoretical understanding. We have tried to discover and list all major reviews of this area which have appeared since 1935 and have dealt with the interface between an electrolyte solution and a metal. We have appended some critical assessment of the reviews after the listing of many of them (19,22,24,28,39–41,46,48,58,79,87,98,100,102,104,105,117). The list of reviews, while longer than any previously given, is probably not comprehensive. Further, since the present work is not intended to be a review of reviews, the assessments are by no means complete and emphasize, when pertinent, discussions of discreteness effects. To increase their usefulness to the reader, the titles have been included for all reviews.

Because of the existence of the many earlier reviews on the general double layer, we believe it is unnecessary to give a thorough discussion of this general area and its background. We shall limit such background material to the minimum required for support and intelligibility of the succeeding discreteness-of-charge material we shall cover. We shall not be concerned herein with interaction of double layers, a subject with considerable literature (29,30,59,72), some of which is related to discreteness effects (57,73,74). A useful table of charge and diffuse-layer potential for NaF based on Grahame’s (50) data has been published by Russell (112).

II. Qualitative Discussion

1. Gross System Considered

A. Double-Layer Structure. A stylized picture of the two main parts of the equilibrium electrical double layer at the interphase region between a metal electrode and an electrolyte

solution is shown in Fig. 1. The parts are separated by the outer Helmholtz plane (OHP), which conventionally defines the plane of closest approach of the charge centroids of diffuse layer ions. Such ions are generally solvated and are held in average positions by the balance between diffusive forces and the electric field in the region. It may sometimes be more appropriate to define the OHP as the plane at the perpendicular distance from the electrode where the dielectric constant of the inner region rises very rapidly

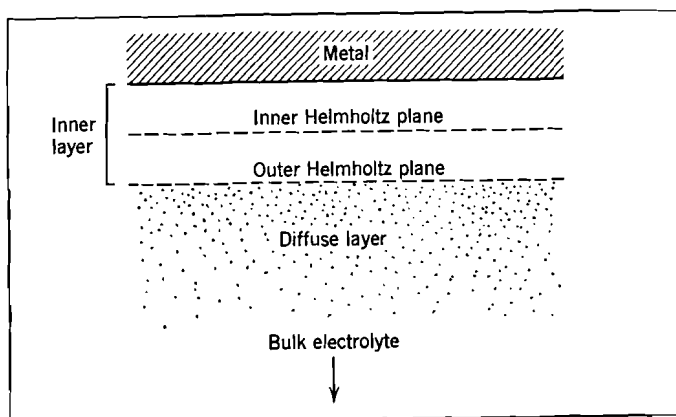


Fig. 1. Schematic diagram of the usual electrolyte double layer (104).

toward the bulk value (56,95). The inner or compact layer, which is thought to be a reasonably close-packed monolayer (43,56,84,106), contains solvent molecules and, in the case of specific adsorption, contains adions as well. The adions are not considered to be solvated, at least in the direction toward the electrode. Thermal equilibrium only applies when the electrode is ideally polarizable. Note that the term "polarizable" will be used in two entirely different ways throughout this article. The first usage will always involve the pair of words "ideally polarizable" and corresponds to the standard usage in electrochemistry that the electrode is blocking and thus no discharge occurs there. The more frequent appearance throughout this review of the term "polarizable" (and different grammatical forms of this word) refers to the induction of electric dipole moments within the material of the double layer by electric fields present therein.

Figure 2 shows the specific adsorption situation based on Stern's (118) model of the inner layer. When the specifically adsorbed ions are of a single type, an inner Helmholtz plane (IHP) may be defined which marks the distance of closest approach of the charge centroids of the adions. The adions are held at the IHP by both specific, or chemical, forces and nonchemical electrostatic forces.

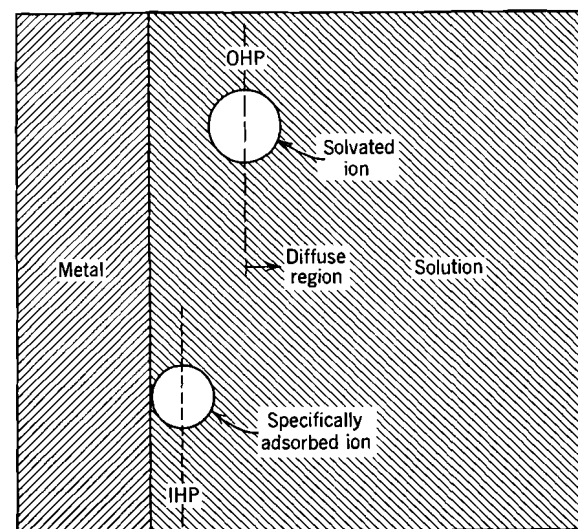


Fig. 2. Schematic diagram showing positions relative to the electrode surface of solvated and specifically adsorbed ions (87).

A very detailed picture of the interphase region is presented in Fig. 3. Although it is almost certainly wrong in some of its details, it well illustrates the possible complexity of this region. Note that it is unlikely that the average boundary between adsorbed solvent molecules in the inner region and the ions in the diffuse region should remain the same distance from the electrode in the neighborhood of adions (87). The OHP is therefore actually not likely to be a plane at all. All major calculations of double-layer structure have, nevertheless, ignored this complication. Such neglect is illustrative of the usual practice of treating what is actually a three-dimensional problem as a two- or one-dimensional one instead.

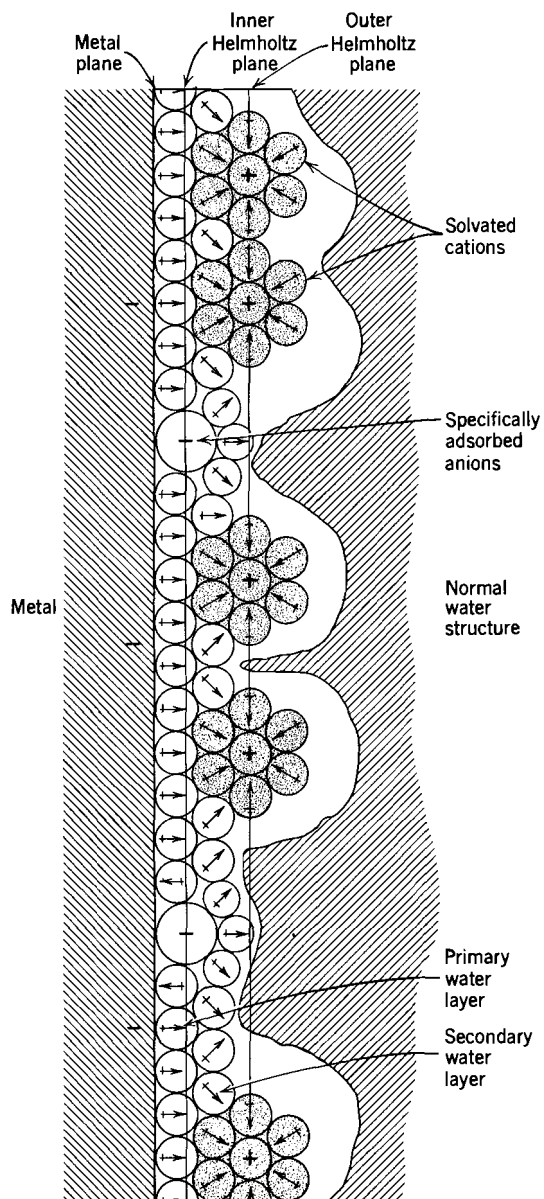


Fig. 3. Hypothetical detailed structure of the electrolyte double layer (10).

B. Definition of Terms. Figure 4 is a diagrammatic representation of local potential variation in the double layer in the direction perpendicular to the plane electrode into the solution. A number of quantities needed in discussing discreteness or other calculations are defined in this figure. The electrode surface plane is here denoted by ESP.

The thickness of the inner region is $d \equiv \beta + \gamma$. It is not likely that β and γ vary very much with the average charge density on the metal, q , or the adion charge density, q_1 (80,84). It will frequently be convenient to normalize distances with β ; the following quantities may then be defined: $Z \equiv z/\beta$; $Z_0 \equiv d/\beta$; $\Gamma \equiv \gamma/\beta$; and $\lambda \equiv \gamma/d \equiv \Gamma/(1 + \Gamma)$. We define Γ^{-1} as $B \equiv \beta/\gamma$.

We shall denote actual local potentials or potential differences by the symbol ψ and average potentials (appropriate for smeared rather than discrete charges) by V . Although Fig. 4 is drawn in

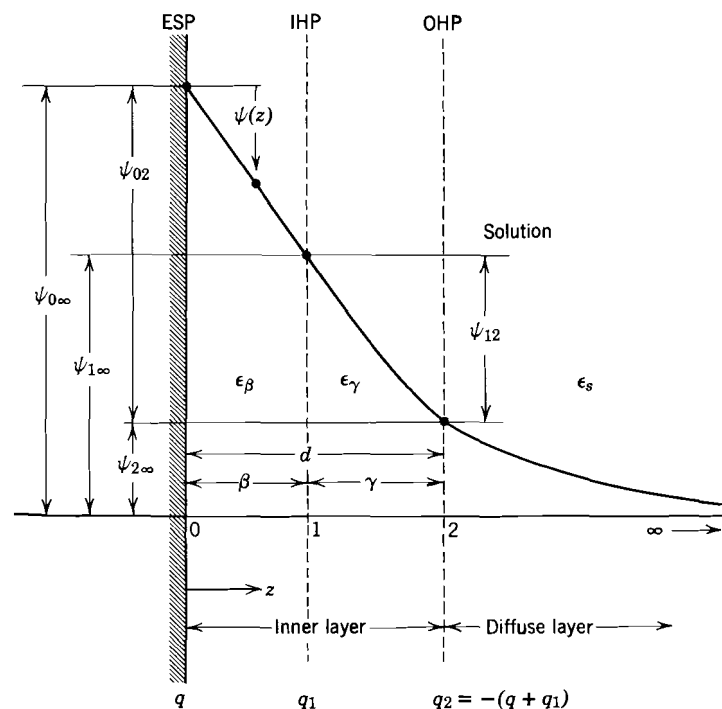


Fig. 4. Schematic diagram of potential variation in the double layer showing definitions of pertinent quantities.

the conventional way with the zero of potential far out in the solution, it is convenient to define the actual potential $\psi(z)$ so that $\psi(0) = 0$, as shown. We shall not usually include adion self-image contributions to the potential in the quantity $\psi(z)$. As drawn in Fig. 4, $\psi(z)$ illustrates the local potential variation along a positive perpendicular line to the ESP which does not pass through or too near any actual charges. The perpendicular

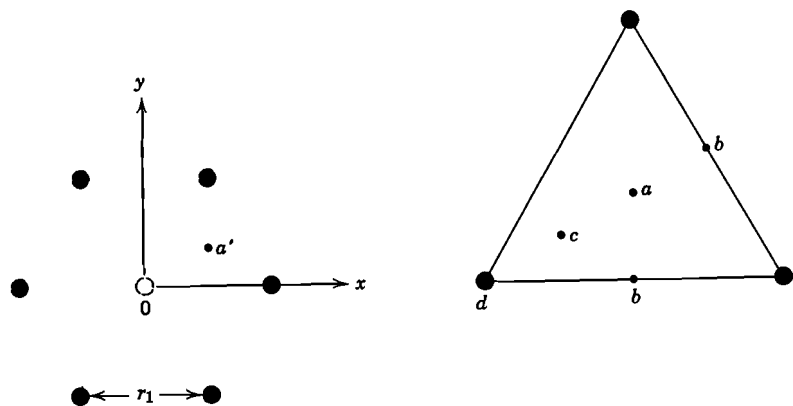


Fig. 5. Hexagonal arrangement of adions on the IHP. An adion has been removed from point 0. The letters designate various array points of interest.

line through the point 0 of Fig. 5, where an adion has been removed from a rigid hexagonal array, is of particular interest, as we shall see later, in micropotential calculations. Note that the nearest neighbor separation of the array, r_1 , is shown on Fig. 5 as well as the x, y coordinate system. The distances x and y may also be normalized with β to give $X \equiv x/\beta$ and $Y \equiv y/\beta$. Unless explicitly noted, we shall generally be concerned with local potentials on the line defined by $X = Y = 0$.

Different authors have employed many different designations for the various average or local potential differences (p.d.'s) shown in Fig. 4. We have therefore elected to use here the neutral definitions illustrated. Thus, $\psi_{02} \equiv \psi_0 - \psi_2 \equiv \psi(0) - \psi(\beta + \gamma)$. The corresponding average p.d. is $V_{02} \equiv V_0 - V_2 \equiv V(0) - V(\beta + \gamma)$.

Figure 4 also illustrates the domains of applicability of three dielectric constants. The use of a dielectric constant ϵ_s in the

diffuse layer of magnitude not much less than that of the solvent bulk value is usually a good approximation, especially when a one-dimensional treatment of the diffuse layer is itself a good approximation. The rapid transition (here approximated as a discontinuity) from an inner-region dielectric constant to the bulk value may not actually occur exactly at the conventional OHP (95) as shown. The division of the inner-layer dielectric constant into two separate values by the IHP (87) is intended to allow for the dielectric effect of a partial solvation shell of an adion lying between the adion and the OHP. It is customary to neglect this possible complication and employ a single position-independent dielectric constant, $\epsilon_1 \equiv \epsilon_\beta \equiv \epsilon_s$, for the entire inner layer. In some calculations (80, 84), the possibility of field-dependent dielectric saturation in the inner region has been included, but ϵ_1 is frequently taken independent of q and q_1 . The use of a dielectric constant at all in this region is certainly a considerable approximation (5,6,85,87) (see Section II-6) and can lead to inaccurate results even for ratios of local to average potentials. In such ratios, even a variable ϵ_1 introduced in the usual way will cancel completely; nevertheless, such results are still inaccurate because of errors in the potentials occasioned by the use of a conventional dielectric constant at all.

Let N denote the number of adions per unit area. If N_s is the value of N corresponding to a complete monolayer of adions, then $N = \theta N_s$, where the fractional coverage θ satisfies $0 \leq \theta \leq 1$. Now if z_v is the effective valence of adsorbed ions and e the proton charge, the adion charge density, q_1 , is given by $q_1 \equiv z_v e N \cong 1.602 \times 10^{-13} z_v N$, when q_1 is expressed in $\mu\text{coul}/\text{cm}^2$ and N in cm^{-2} .

If the adions are arranged in a fixed square array, then the nearest neighbor distance for two adions will be $N^{-1/2}$. Actually, the structure that minimizes the interaction energy of adions is not a square array but a hexagonal one. Consequently, in all regular array calculations performed for the present system, the structure is assumed hexagonal. Note, however, that for all but the highest attainable surface charge densities, the difference in energy between these two structures is so slight that at room temperature equilibrium between these two phases occurs when the two are present in roughly equal concentrations over the electrode surface. For simplicity, we shall ignore the presence of

the higher-energy structure, as its properties are almost identical to the hexagonal-structure properties in any case (45,85). If r_1 is the nearest neighbor distance for a hexagonal array, then $N = (\frac{2}{3})^{1/2} r_1^{-2} \cong 1.1547 r_1^{-2}$. Alternatively, $r_1 \cong 43.011 \times 10^{-8} [z_0/q_1]^{1/2}$ cm, when q_1 is expressed in $\mu\text{coul}/\text{cm}^2$. It will be convenient to define $R_1 \equiv r_1/\beta$ and $\xi \equiv z/r_1 \equiv Z/R_1$.

At the point of zero charge (PZC), also termed the electrocapillary maximum (ECM), $q = 0$. Another condition of interest, even though it is infrequently attained in electrolytes, is that for which $q = -q_1$. Then $q_2 = 0$, and the electrode is sometimes termed grounded. When $q_2 = 0$, the value of $\psi(z)$ a large (or "infinite") distance from the electrode will be designated $\psi_\infty \equiv V_\infty$. Here "infinite" means that $z \gg r_1$ but denotes a distance still small compared with the minimum linear extent of the adsorbed charge region.

Using an inner-region dielectric constant intended to account for the electronic polarizability of adions and solvent molecules as well as the orientational polarizability of solvent molecules having permanent dipole moments, one may write

$$\begin{aligned} V_\infty &= 4\pi\beta z_0 e N / \epsilon_1 = 4\pi\beta q_1 / \epsilon_1 \\ &\cong 1.12941 \times 10^7 \beta q_1 / \epsilon_1 \end{aligned} \quad (1)$$

where in the last equation β is in cm and q_1 in $\mu\text{coul}/\text{cm}^2$. Although V_∞ is an average potential, it has frequently been denoted as ψ_∞ rather than V_∞ . We shall use the two designations interchangeably herein. Note that for $q_2 = 0$, $V_\infty = -V_{0\infty}$. In general, a uniform D field contribution, ψ_e , is a part of any inner-layer local or average potential. The full local potential is thus given by $\psi(z) = \psi_a(z) + \psi_e(z)$, where $\psi_a(z)$ is the part arising directly from the discrete adions and their images. Note that V_{02} may be written $V_{02} = V_\infty[\Gamma + Z_0(q/q_1)]$, where $Z_0 \equiv 1 + \Gamma$.

C. Experimental Methods. There are two principal ways of gaining information about the double layer at an ideal polarized electrode (22,46). The two methods are the electrocapillary method and the differential capacitance method. To obtain desired quantities such as charge components from measurements of interfacial tension or differential capacitance, differentiation and integration of measured curves are required.

These processes generally introduce some uncertainty into the results, but differential capacitance measurements are more sensitive to double-layer structure than interfacial tension ones.

Several methods of employing the above measurements to yield ionic surface charge excesses have been developed (12,27,87). Since a statement to the contrary has been made (28), it is important to point out that although the above kinds of measurements and calculations deal with macroscopic (average) quantities such as q and q_1 , they may be appreciably affected by charge discreteness effects as discussed later. No theory or method of analyzing experimental data which is derived only from a consideration of average charges and potentials can be expected to come close to representing adequately the effects, even average ones, of the discrete, three-dimensional structure of the double layer.

2. Discreteness Effects

Discreteness in the double layer is important because the dimensions over which the potentials and fields appreciably vary therein are of the same magnitude as the sizes and separations of the charged and polarizable entities themselves. Although we shall concentrate on discreteness effects in the inner layer, they are also important in the diffuse layer and could be of some importance at the electrode, since even a "smooth" liquid metal electrode is made up of discrete atoms and electrons on the microscopic scale with which we are concerned. That discreteness effects in the electrode are not likely to be of much importance for liquid metal electrodes is indicated, however, by the lack of much change in differential capacitance when going from liquid to solid gallium, mercury, and Wood's metal electrodes by means of a small temperature change (114). On the other hand, considerable difference between differential capacitance curves obtained with liquid mercury and liquid gallium has been observed (44).

Consider the very simple case of an inner layer consisting first only of nonpolarizable solvent molecules each having a permanent dipole. Even here the discreteness of the molecules is important. The molecules, even though adsorbed at the electrode, will be continually moving in the plane and vibrating and rotating

because of their thermal energy. The electric field of the permanent dipoles will interact with the conducting electrode, inducing image dipoles therein. By images, we mean that the charge distribution which is induced in the conducting layer by a given discrete or continuous monopole or multipole charge distribution outside the layer produces the same potential outside the layer as that which would be produced if a perfect mirror image of the inducing distribution existed at an equivalent position behind the imaging plane. Since images do not actually exist, there is no p.d. between the imaging plane and the images as there would be if the image were made up of real charges.

The time-average local field acting at any given dipole arises from several sources, including that of its own image and all surrounding dipoles and their images. Clearly then, the time-average dipole moment of the array (regular or disordered) will depend upon a self-consistent field which itself is different depending upon whether all surrounding dipoles are discrete or are uniformly smeared into a real dipole sheet and the corresponding image sheet. Thus, the V_∞ potential arising from such a discrete two-dimensional array of dipoles with at least some freedom to rotate will depend on the discreteness of the dipoles, even though V_∞ is itself a space-average or smeared quantity.

Next consider the important case of an array of polarizable ions adsorbed on a conducting electrode. Assume that the ions are hexagonally arrayed and that there is nothing between them, as would be the case for adsorption from a gas phase. It has been shown (89) that, even in this simple case, the discreteness of the charges is crucial in determining V_∞ . No ϵ_1 is explicitly introduced *ad hoc* into the calculation of V_∞ , but the existence of a nonzero adion polarizability, α , leads to an effective ϵ_1 which depends on adion spacing, r_1 . Further, the presence of adion polarizability leads to other influences on V_∞ which cannot be logically represented by a dielectric constant. The V_∞ obtained with $\alpha \neq 0$ can be much less in magnitude than that with $\alpha = 0$ and V_∞ may even change sign at certain adion spacings.

In the electrolyte double layer with specific ionic adsorption, one has a situation even more complex than a combination of the above two situations. Polarizable ions are surrounded by polarizable solvent molecules having rotatable permanent dipole

moments instead of by vacuum as in the adsorption from a gas phase. Thus far, there have been no treatments of electrolyte double-layer capacitance or potentials which adequately take discreteness into account. This may appear surprising since Frumkin (38,39), in the early 1930's, seems to have been the first to suggest that the discreteness of the electrolyte double layer might be important. Although much of the succeeding discussion will deal with various theoretical approaches to the discreteness problem, it is by no means yet solved satisfactorily in the electrolyte case.

Although Frumkin first drew attention to the possible importance of discreteness in the electrolyte double layer, its importance for adsorption from a gas phase was recognized considerably earlier. Particularly important was the accurate calculation by Topping (125) in 1927 of the mutual potential energy of a plane, hexagonal array of ideal, nonpolarizable dipoles. The useful results of this calculation have been obtained in approximate form a number of times by authors (34,66) unaware of Topping's work, and even today his calculations are seemingly not well-known by electrochemists (9,10).

In 1939, Esin and Markov (33) reported that the potential at the ECM ($q = 0$), measured versus potassium iodide concentration with respect to a constant reference electrode, varied anomalously rapidly. In accordance with Stern's (118) theory of the double layer, they observed a linear dependence of the above p.d. upon the logarithm of concentration (or activity) but found a slope greater than the value kT/e expected from Stern's theory. According to this theory, a tenfold increase in concentration at $T \approx 23^\circ\text{C}$ should lead to an increase of the ECM potential by $(kT/e) \ln 10 \approx 58$ mV. The appearance of a considerably greater increase has been termed by Grahame (52) the Esin-Markov effect.

To help put in focus the attempts which have been made to explain the Esin-Markov effect, we will briefly review the simplest theory (32) of it. First let us assume at least for $\theta \ll 1$ that the adsorption isotherm has the form $q_1 = Ac_0 \exp\{-e\psi_{1\infty}/kT\}$, where A is a constant, and c_0 is the concentration of ions in the bulk of the electrolyte. The p.d. $\psi_{1\infty}$ has been termed the micro-potential by Ershler (32). Next, observe that the ECM double-layer p.d., $V_{0\infty}$, is almost surely going to be nearly proportional

to q_1 —unless there are strong nonlinearities in the dielectric response of the compact layer—because the p.d. across the (nonlinear) diffuse layer is small compared with the p.d. across the inner layer. Setting $V_{0\infty} \cong V_{02}$, and $\psi_{1\infty} \cong \psi_{12}$, and taking logarithms, one may therefore write

$$\ln V_{02}|_{\text{ECM}} \cong \ln c_0 - (e/kT)\psi_{12}|_{\text{ECM}} + \text{constant} \quad (2)$$

Accordingly,

$$\frac{dV_{02}|_{\text{ECM}}}{d \ln c_0} = V_{02}|_{\text{ECM}} \left\{ 1 - \left(\frac{e}{kT} \right) \frac{d\psi_{1\infty}}{dV_{02}} \Big|_{\text{ECM}} \frac{dV_{02}}{d \ln c_0} \Big|_{\text{ECM}} \right\} \quad (3)$$

from which one obtains

$$\frac{dV_{02}|_{\text{ECM}}}{d \ln c_0} = \left\{ \frac{kT}{eV_{02}|_{\text{ECM}}} + \frac{d\psi_{12}}{dV_{02}} \Big|_{\text{ECM}} \right\}^{-1} \left(\frac{kT}{e} \right) \quad (4)$$

The point of the above result is that as $|V_{02}|$ increases the quantity $|kT/eV_{02}|$ will tend to become small compared with $|d\psi_{12}/dV_{02}|_{\text{ECM}}$, and we may write for appreciable $|q_1|$

$$\frac{dV_{02}|_{\text{ECM}}}{d \ln c_0} \cong \left(\frac{dV_{02}}{d\psi_{12}} \Big|_{\text{ECM}} \right) \left(\frac{kT}{e} \right) \quad (5)$$

Under the simplest assumptions, $dV_{02}/d\psi_{12}|_{\text{ECM}}$ is just a constant geometrical factor, such as $\lambda^{-1} \equiv 1 + B$, and we are thus led to expect a limiting slope for $V_{02}|_{\text{ECM}}$ vs. $\ln c_0$ of $\lambda^{-1}kT/e \approx 2kT/e$. It is now clear that whatever the actual form of the adsorption isotherm, the Esin-Markov effect can be discussed in terms of the interdependence of $V_{0\infty}$ and $\psi_{1\infty}$, or approximately of V_{02} and ψ_{12} . The ratio $\Lambda \equiv \psi_{12}/V_{02}$ is thus of much importance in discussing discreteness effects and will appear frequently in the rest of this article.

In 1943, Esin and Shikov (34) tried to explain the above effect by recourse to the discrete nature of the double layer. Unfortunately, as we shall see later, their model of the double layer was very crude and overexplained the effect, yielding about 200 mV instead of about the 100 mV observed by Esin and Markov. Parsons (103) has analyzed the Esin-Markov effect in considerable detail and shows that it may occur at any point on the electrocapillary curve, not just at $q = 0$. Parsons also suggested that the failure of the Stern theory to explain the Esin-Markov effect arose not from the neglect of discreteness effects but from

the use of an incorrect form of the adsorption isotherm. We believe the Esin-Markov effect can only be described adequately with a correct isotherm, which itself takes proper account of discreteness effects.

Figure 6 shows qualitatively the difference in the dependence of potential on distance in the neighborhood of two planes of smeared-out charge and two containing discrete charge. It will be seen that the full p.d. produced by the layers occurs just across

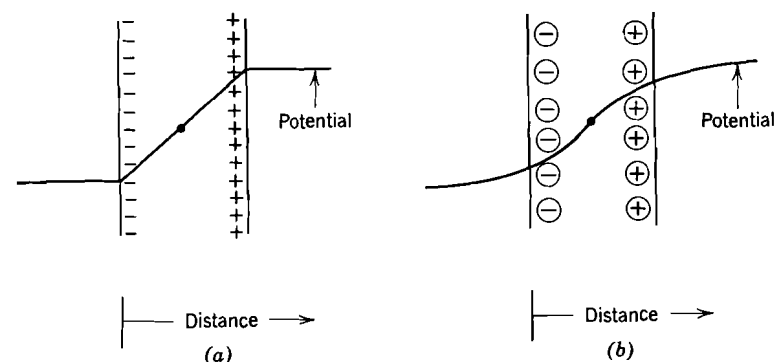


Fig. 6. Schematic diagram of the potential distribution produced by (a) two parallel planes of continuous charge, and (b) two parallel planes containing discrete charges.

the two smeared planes of charge, but only a part of this total p.d. occurs between the two planes when the charges are discrete. Esin and Shikov's use of this reduced potential still led to an overestimate of the Esin-Markov effect. Ershler (32), using an improved model which we shall discuss later, obtained in 1946 somewhat better agreement between theory and the Esin-Markov effect.

To recapitulate, discreteness effects are almost certainly important in comparing theoretical calculations of the average potential difference across the inner layer, V_{02} , with experimentally derived values of this quantity. It follows that discreteness is also certain to be of importance in any theory of the inner-layer differential capacitance of the double layer which can represent the experimental situation and data adequately. Finally, discreteness is of great importance in determining the potential $\psi_{1\infty}$ at the position of an adsorbed ion. As we have seen,

it is this potential, the micropotential, which appears at least approximately in an adsorption isotherm and determines the relation between q and q_1 .

Suppose a given adion is removed from its place at the IHP into the bulk of the solution. The average energy necessary to accomplish this is $-z_0 e \psi_{1\infty}$, provided $\psi_{1\infty}$ in Fig. 4 is measured along the line of removal of the ion.* Most writers in the present area have ignored in practice the contribution $\psi_{2\infty}$ (or $V_{2\infty}$) to $\psi_{1\infty}$ and actually have calculated ψ_{12} rather than $\psi_{1\infty}$. When the contribution to $\psi_{1\infty}$ arising from the potential drop in the diffuse layer, which is frequently small and may often be well approximated by an average rather than local potential, is omitted the p.d. significant in determining the energy of adsorption necessary to move an adion from the OHP to the IHP is ψ_{12} . This quantity must be a local potential difference; it depends strongly on discreteness effects and has also been termed the micropotential.

Although the importance of double-layer discreteness effects was suggested more than 35 years ago and a good many calculations have been made over the years attempting to include the influence of discreteness realistically, there are as yet no theories available which incorporate all discreteness effects (discreteness-of-charge, discrete permanent and induced dipoles, and finite-size effects of molecules and ions), especially when thermal motion is also included. One purpose of the present review is to evaluate the limitations of earlier discreteness calculations and, hopefully, thereby exhibit the need for and point the way toward improved future analyses.

3. Types of Imaging

The two boundary regions of the inner or compact part of the double layer may be quite different under various circumstances.

* As we have pointed out elsewhere (6,92), the energy of adsorption should generally include a contribution from so-called rearrangement effects (not included above). On the other hand, the micropotential as defined here, which properly excludes such effects, may still be used in a statistical-thermodynamic treatment of adsorption. Such a usage may be shown to be exact for ordered structures, and is often quite accurate even for rather disordered ones. We shall not take the opportunity to elaborate herein on the statistical thermodynamics of adsorption isotherms.

Such differences can have profound effects on the structure and behavior of the compact layer itself. In order to describe possible situations, we shall for the present employ dielectric constants, remembering, however, that their introduction is an approximation which blurs some discreteness effects, especially for the inner layer.

Let the effective dielectric constant of the material to the left of the ESP be ϵ_0 . This material may be a conducting electrode, air, oil, or a dielectric solid. As usual, take ϵ_1 as the effective dielectric constant of the inner region and ϵ_s as that of the region to the right of the OHP. Let ϵ_2 denote either ϵ_0 or ϵ_s , depending on the situation considered. Next, recognize that the situations at the two boundaries of the inner region can themselves affect the effective ϵ_1 . We therefore regard ϵ_1 as fixed but consistent with the boundary conditions of the inner layer.

The region to the right of the compact layer will be considered to be the usual diffuse layer. Three conditions in it are, however, of special interest. At very high solute concentration, the effective Debye length in the diffuse layer will be very small compared to other characteristic lengths in the double layer. The diffuse layer is then conventionally approximated by a metallic conductor at the OHP. Second, when $q = -q_1$ and $q_2 = 0$, the diffuse region ceases to exist on the average. Note, however, that in the neighborhood of adions, a field will still penetrate beyond the OHP, tending to create a local diffuse region of opposite charge. Finally, in the limit of very low solute concentration, the concentration of mobile ions in the diffuse layer will be so low under some conditions that their contribution to electrical conductivity effects at the OHP and into the diffuse layer may be neglected (26). Then, only dielectric constant changes in the neighborhood of the OHP remain important.

Table I summarizes some of the imaging situations possible. When $\epsilon_0 = \epsilon_1 = \epsilon_s$ as in the first row, there is no imaging at either boundary, and we designate this situation $O-O$. This is a limiting condition, not likely to be of physical significance. The first four rows in the table apply when neither the ESP nor the OHP is actually conducting or may be well approximated as conducting. The second row defines the situation where there is no dielectric discontinuity to induce dielectric imaging at the

TABLE I
Imaging Possibilities

Imaging designation	Left boundary region		Right boundary region	
	Dielectric	Conducting	Dielectric	Conducting
<i>O-O</i>	ϵ_1	No	ϵ_1	No
<i>O-D</i>	ϵ_1	No	ϵ_s	No
<i>D-O</i>	ϵ_0	No	ϵ_1	No
<i>D-D</i>	ϵ_0	No	ϵ_s	No
<i>C-O</i>	—	Yes	ϵ_1	No
<i>C-D</i>	—	Yes	ϵ_s	No
<i>C-C</i>	—	Yes	—	Yes
<i>O-C</i>	ϵ_1	No	—	Yes
<i>D-C</i>	ϵ_0	No	—	Yes

ESP but where there is such a discontinuity at the OHP (i.e., $\epsilon_s \neq \epsilon_1$).

When the ESP is conducting, the transition from a dielectric region to the conducting plane also induces imaging. Here, the image of a charge or dipole is of the same magnitude as the charge or dipole moment of the real entity. When only dielectric imaging is present, however, the image magnitude is always less than that of the real element except in the limit where one of the dielectric constants involved becomes infinite.

The *C-C* case was earlier termed "infinite imaging." It is the situation first defined and partially treated for adions by Ershler (32). As in a hall of mirrors, a real adion charge is imaged an infinite number of times, with each image charge having the same magnitude as the original charge. There are also an infinite number of images of each adion in the *C-D*, *D-C*, or *D-D* cases but the image magnitudes progressively decrease as their apparent distance from the IHP increases. Finally, in the *D-O*, *O-D*, *O-C*, and *C-O* cases, each adion is imaged only once, again with full magnitude only in *O-C* and *C-O* cases. The *C-O* case has been termed single imaging (6) and is very important for adsorption of ions from a gas phase ($\epsilon_s \simeq 1$) onto a conducting substrate.

In conclusion, it should be mentioned that the diffuse layer will in general be neither an ideal dielectric nor a good conductor.

Then, both its dielectric aspects and its mobile ions are important in inducing a complicated type of imaging at and near the OHP. This possibility has not been included in the table and no completely adequate treatment of the boundary value problem involved has yet been given. Luckily, there seem to be situations of interest where the diffuse layer can either be ignored or treated as a good conductor. Theoretical analysis has been carried out for both of these limiting conditions and some approximate calculations treating the intermediate situation have been made.

4. The Question of Order

One of the most important and difficult questions to answer as a prerequisite to any adequate treatment of the compact layer is that of how the various particles arrange themselves over the surface. If the electrode surface itself provides preferred sites, then the possibilities are greatly reduced, and the question is simplified once the existence of preferential sites becomes established. While certain electrode surfaces seem to exhibit this behavior and lead to "immobile" or "localized" adsorption, the case which has provided the greatest challenge and interest to workers in the field is the opposite situation, "mobile" adsorption. In particular, the liquid-mercury electrode is widely believed to be effectively smooth on an atomic scale; even if there should instantaneously exist preferential sites for ionic or molecular adsorption, the motion of the mercury ions on the surface of the electrode would eliminate such inhomogeneities on the time scale of macroscopic experiments. Accordingly, it is likely that the mercury electrode has little or no order of its own to impose upon the overlying adsorbate layer. The same statement should certainly apply to the diffuse layer as well.

In the absence of an orderly preferred arrangement of the adsorbed particles relative to any given point on the electrode surface, there remains the distinct possibility that as a result of the various interactions within the compact layer, a relative ordering is established among the particles in the compact layer. The particles could still form an array, for example, which would be free to move relative to the electrode. It is this question of the relative arrangements of particles in the compact layer which we are going to discuss.

Even describing the arrangement of particles becomes more difficult as the number of different types of particles increases; one has more questions to answer. What do things look like in the neighborhood of a type-*A* particle, a type-*B* particle, etc.? Even a single question becomes manifold; in the neighborhood of a type-*A* particle, where are the closest type-*A* neighbors, type-*B* neighbors, etc.? If the complexity of the description increases rapidly with number of components, the difficulty of theoretical prediction may increase even faster. Although an adequate picture of the arrangements applying in the actual compact layer is our ultimate goal, we will do well to understand a simpler system, where a single species of ion is present on the surface and the effects of further adsorbed species, such as solvent molecules, are either ignored or perhaps crudely accounted for. After we have obtained a better insight into this idealization, we will be in a better position to discuss the actual system with its additional complexities. This plan is not overly cautious; even the idealized problem has thorny aspects, and no one has obtained a clear picture of the arrangement even in a one-component system under the most general circumstances. There are general statistical mechanical principles which apply, of course, but such principles alone do not always give a clear picture of the situation. One must usually augment these general laws with the knowledge of which approximations to apply, this knowledge usually proceeding from a fairly adequate intuitive grasp of the situation. It is this intuition which is most difficult to achieve in the present system. The usual practice, in view of these difficulties, is to make analogies with things we understand and have developed arithmetical procedures to cope with. Thus, we may begin by assuming that the compact-layer ions arrange themselves on a regular array as in a solid, an arrangement of great simplicity and familiarity, and then test this hypothesis by estimating whether or not the disruptive influence of thermal motion is sufficient to sensibly destroy this arrangement. Other authors have sometimes chosen a different starting guess, such as an almost random arrangement, the interactions being considered as small perturbations which inflict slight regularity upon the otherwise uncorrelated particles. This procedure too is an analogy with a familiar system, i.e., with weakly nonideal gases. Yet another guess is that the system

is highly ordered by short-range steric forces within short distances, but that at further distances the departures from randomness of arrangement induced by the other interactions are small enough to be considered once again as a perturbation. Again, this starting point is tantamount to drawing an analogy with ordinary liquids. Later in this article we will indicate why the present system is not well described by any of these analogies, either as a two-dimensional quasi-solid, quasi-gas, or quasi-liquid.

At this point it should be clear to the reader from the diversity of description which we note above that there is much to be desired in our overall understanding of the compact layer. Much of the published work on this subject employs one of the foregoing models—this is one of the major sources of difference among the various treatments. Too few workers have been sufficiently concerned with determining the appropriateness of the models employed, and too often a physical picture of what is happening is not provided. In our own work, which is not always free of the foregoing shortcomings, we have generally taken the regular array model as our starting point, a procedure which we repeat here. In the next few sections, however, we will attempt to examine the adequacy of this model as completely and carefully as is practical. Not only do we wish to be exempt from our own criticism above, but also there is much one may learn from such an exercise. After we have established the limits of validity of this model, we will consider alternatives when appropriate. Before embarking on this program, however, we shall illustrate what differences are to be expected following from different postulated arrangements in the compact layer.

Consider a system in which nonpolarizable ions are adsorbed on an ideal polarizable electrode, and assume that they form a mobile adsorbed layer and that there are no additional species in this layer. We shall determine the potential for such a system assuming first that the only correlation between the positions of different ions is that induced by a steric hard-core repulsion between ions; the distance of closest approach between ion centers is denoted by r_{1m} . Next, we obtain the potential for an alternative situation where the ions are arrayed on a regular hexagonal lattice. It is the comparison between the results

obtained for these two different types of ionic arrangement which will provide a measure of the importance of ordering in the compact layer.

In Section II-5 of this article we discuss how the diffuse layer alters the potential in the inner region. However, for our present purposes of demonstrating how ordering may affect the system, it is simplest to avoid the further complexities brought about by the diffuse layer, and so we shall here make the incorrect assumption that the diffuse layer plays no role in producing and influencing potentials in the compact layer. Accordingly, the results we obtain here are only illustrative of the general dependence of various system quantities upon ordering.

Under the above conditions, the potential in the compact layer arises only from the adsorbed ions and the charges on the electrode surfaces. In fact, if the electrode is a conductor, its surface is an equipotential; the potential anywhere in the compact layer may be determined from a knowledge of the ion positions and the average electrode surface charge density by means of the familiar method of images. According to this method, the potential in general consists of two contributions: The first is the potential arising from the adions and their electrical images in the ESP (the images therefore lie on the plane $z = -\beta$); the second contribution is a linearly varying potential, or uniform field part, $\psi_e(z)$, arising from the excess charge density on the electrode. This excess charge density is the amount by which the average electrode surface charge density differs from that required to establish the field of the fictitious images. In the present C - O single-imaging case, where the only imaging plane is the ESP, this excess charge density is given by $(q + q_1)$; thus, the uniform field potential is given by $\psi_e(z) = -4\pi(q + q_1)z$. Remark that for the present situation there is no electric polarization in the compact layer, and therefore, there is no necessity to consider a dielectric constant here. In the remainder of this discussion we simply set $q = -q_1$, corresponding in this case to grounding the ESP, and therefore we may eliminate further consideration of ψ_e in what immediately follows.

If we neglect electric multipole moments, permanent and induced, of the adsorbed ions, then the surface-averaged potential in the compact layer is independent of arrangement. It is in fact

identical to the potential one would have if the actual ions were evenly smeared over the IHP—this conclusion incidentally is independent of the role played by the diffuse layer. The average potential one obtains is given by $V(z) = 4\pi z_e N z$ for $0 < z < \beta$; for $z > \beta$ the potential is the constant $V_\infty \equiv 4\pi q_1 \beta$. How does this compare with the time-average local potential seen by any particular ion arising from all other ions and their images? (We shall ignore the potential arising from the self image of the selected ion, as this is independent of arrangement and thus can be considered as a “chemical” addition to the adsorption energy, for example. It thus does not add anything to the present discussion.) When potential is measured with reference to the bulk of the solution, this quantity, the micropotential, does depend on ionic arrangement even in the present case of zero α .

For the first arrangement of ions, the local potential $\psi_a(\beta)$ is that arising from a uniform surface charge q_1 on the IHP except for a circular vacancy (about the given ion) of radius r_{1m} ; the image of this IHP charge likewise possesses a circular vacancy of the same radius. It is straightforward to show that the potential for this case is given by

$$\begin{aligned}\psi_a(\beta) &= 2\pi q_1 \{ [4\beta^2 + r_{1m}^2]^{1/2} - r_{1m} \} \\ &= \psi_\infty \{ [4 + R_{1m}^2]^{1/2} - R_{1m} \} / 2\end{aligned}\quad (6)$$

where $R_{1m} \equiv r_{1m}/\beta$. We see that the potential $\psi_a(\beta)$ differs from the average potential at the IHP, the macropotential, by the constant factor $\{ [4 + R_{1m}^2]^{1/2} - R_{1m} \} / 2$. It often happens that interactions other than steric effects cause R_{1m} to be larger than one might think. In fact, we sometimes may set $R_{1m}^2 \gg 4$, obtaining $\psi_a(\beta) \cong R_{1m}^{-1} \psi_\infty$; the micropotential is then smaller than the macropotential by the factor R_{1m}^{-1} , which by hypothesis is much smaller than unity. Let us now compare this result with that obtaining for the hexagonal array. For this case the potential is roughly that of a hexagonal array of ideal dipoles, each of dipole moment $2z_e e \beta$, at a position removed from the plane of the dipoles by the amount β . Carrying out the necessary sum over different dipoles in the array, we find

$$\psi_a(\beta) \cong 18q_1 \beta^2 N^{1/2} \cong \frac{3}{2} R_1^{-1} \psi_\infty \quad (7)$$

Thus, for this case the ratio of $\psi_a(\beta)$ to ψ_∞ is not even constant with surface density N . It is similar to the first result except that r_{1m} has been replaced with the variable r_1 . Incidentally, this is our first example of the fact that an array produces the same sort of micropotential as a uniform sheet with a circular vacancy of radius more or less equal to r_1 . This is a fact which we will use a great deal later on.

In the preceding, we have had an example of how a local potential may be drastically affected by arrangement, a detail of the system structure. This particular local quantity, $\psi_a(\beta)$, essentially the micropotential, has a great influence on system properties, insofar as it determines the equilibrium density of ions adsorbed under given conditions. The reader may still be left with the impression that we have cheated a bit, that we have deliberately chosen to examine that local quantity most likely to influence the system as a whole. He might say, "You show the micropotential is sensitive to structure, but once you tell me q_1 , I have no further need for the micropotential. How then can one assert that, given q_1 , the system properties are sensitive to arrangement?" As an exhibit that not only local potentials but also average potentials might be dependent on inner-layer structure, we consider a variation on the previous example. This time we let the ions possess a polarizability α . Under this condition the average potential for all $z > \beta$ is given by $V = \psi_\infty + 4\pi N\alpha\mathcal{E}$, where \mathcal{E} is defined as the electric field acting to polarize a given ion. It is through the dependence of \mathcal{E} upon arrangement that the average potential becomes structure sensitive. We shall examine the case of no correlation for $r > r_{1m}$ and hard-core repulsion for $r < r_{1m}$.

The field \mathcal{E} at a given ion in this case consists of three parts: the contribution from the other ions and their images, the contribution from the other induced dipoles and their images, and the contribution from the image of the given ion and its polarization P . The first contribution is given by

$$\mathcal{E}_1 = E_\infty [1 + (R_{1m}/2)^2]^{-1/2} \quad (8)$$

where $E_\infty \equiv -\psi_\infty/\beta$. The second contribution may be shown to be

$$\mathcal{E}_2 = -2\pi NP\beta^{-1} [R_{1m}^2 (R_{1m}^2 + 4)^{-3/2} + R_{1m}^{-1}] \quad (9)$$

Finally, the self-image contribution is

$$\mathcal{E}_3 = (4\beta^2)^{-1} [\beta^{-1}P - z_v e] \quad (10)$$

Upon introducing the substantive equation

$$P \equiv \alpha\mathcal{E} = \alpha[\mathcal{E}_1 + \mathcal{E}_2 + \mathcal{E}_3] \quad (11)$$

one arrives at the ugly-looking result

$$P = -\alpha \frac{\beta^{-1}\psi_\infty [1 + (R_{1m}/2)^2]^{-1/2} + z_v e (4\beta^2)^{-1}}{1 + 2\pi\alpha N\beta^{-1} [R_{1m}^2 (R_{1m}^2 + 4)^{-3/2} + R_{1m}^{-1}] - (J/4)} \quad (12)$$

where $J \equiv \alpha/\beta^3$. Once again invoking $R_{1m} \geq 2$ leads us to

$$V \cong \psi_\infty - 4\pi N\alpha [2\psi_\infty/\beta R_{1m} + z_v e/4\beta^2] \times [1 - (J/4) + 4\pi\alpha N\beta^{-1} R_{1m}^{-1}] \quad (13)$$

Perhaps this expression for V is not very illuminating until one puts numbers into it. It turns out that the factor

$$[1 - (J/4) + 4\pi\alpha N\beta^{-1} R_{1m}^{-1}]$$

may become rather small; when this occurs the contribution to V from the polarization may be appreciable. It is only in the limit of low surface density that this contribution assumes a simple form. In this limit we find

$$V \doteq [1 - (J/2)][1 - (J/4)]^{-1}\psi_\infty \quad (14)$$

Now we find the average potential in the array situation. Once again $V = \psi_\infty + 4\pi N\alpha\mathcal{E}$ for all $z > \beta$. This time one finds, however, that while \mathcal{E}_3 is the same as before, $\mathcal{E}_1 + \mathcal{E}_2$ is a different expression: $\mathcal{E}_1 + \mathcal{E}_2 \cong -11r_1^{-3}(P + 2z_v e\beta)$. Employing the same substantive relation leads to

$$P \cong -z_v e(J/4) [1 + 88R_1^{-3}] [1 + 11R_1^{-3}J - (J/4)]^{-1} \quad (15)$$

We immediately obtain

$$V \cong \psi_\infty [1 - (J/4)] \{1 + 88R_1^{-3}\} \{1 + 11R_1^{-3}J - (J/4)\}^{-1} \quad (16)$$

Again, the expression we have obtained for V is not very transparent; however, we note that again there is a factor in the denominator which may be quite small. When we take the low density limit $R_1 \gg 2$, we find as we should that the expression for V is the same as the one found for the random arrangement.

How is it then that we assert a structure dependence? The point is that in going to the low-density limit we only consider the case where the polarizing field is determined almost solely by the self-image. The structure sensitivity can only exist in the domain where \mathcal{E} is determined by the surroundings of an ion (other than its self-image). Thus, we find most unpleasantly that the comparisons should be carried out in the regime where the equations are fairly complicated. We therefore resort to a numerical comparison for the particular case $R_1 = R_{1m} = 4$, $J = 1$. Upon substituting these values into the exact expressions, one obtains for the uncorrelated and array cases, respectively, $V \approx 0.62\psi_\infty$, and $V \approx 0.36\psi_\infty$. There is thus a 72% change in the inner-layer potential drop in going from the ordered to the disordered arrangement in our example. The difference between the two types of arrangement as far as overall potentials are concerned may be even more than this, but generally it is much less. However, this example should illustrate how even an average potential may be structure sensitive. Remark that physically the primary source of structure sensitivity for such average quantities is the "feedback term" in Eqs. 11 and 14 for P . The feedback referred to is contained in such factors as

$$[1 + 4\pi N\alpha\beta^{-1}R_{1m}^{-1} - (J/4)]^{-1}$$

or

$$[1 + 11R_1^3J - (J/4)]^{-1}$$

which result from the fact that the system of induced dipoles produces a field which acts back on the dipoles themselves. Under certain conditions, this field may be as large or larger than the field initiating the polarization. When this occurs, the polarization may grow to a large value, the value very sensitive to the size of the feedback. In this case, a change in structure would alter the feedback a bit and perhaps drastically change the resulting polarization, effective dielectric constant, and average potentials. (Had we chosen for our numerical example a situation where J was closer to four, the situation would have been much more dramatic.)

Having seen that the arrangement of particles in the inner layer may greatly affect various local and average properties of that layer, we now return to the main business of estimating the

degree of order which is actually present in spite of the disorganizing effect of thermal motion. As stated earlier, our present method consists in initially assuming perfect order, that is, a rigid hexagonal array, and then calculating roughly how far away from its proper site any given ion will typically move at thermal energies. We remark that the motion we are concerned with is that of the given ion relative to its immediate neighbors. There is no meaning to the question of how far it will be able to move relative to remote ions. In a three-dimensional system such a question admits of a finite answer; in a two-dimensional system the correlation between positions of two particles falls off indefinitely as the separation between such particles increases. We shall discuss this matter at greater length later in this article. We note for the present that it is really the motion relative to immediate neighbors which is the important thing to find anyway. *Only the immediate neighbors have such an influence upon our given ion that their precise positions relative to it significantly affect system properties.* We have already noted this important fact indirectly when we remarked upon the approximate equivalence of a hexagonal array and a uniform distribution with a vacancy of appropriately chosen radius. It turns out that the approximation becomes quite close when applied to the fields produced by those ions other than the immediate neighbors. Furthermore, when the alteration of potential by the diffuse layer is considered, this insensitivity to relative positions of other than immediate neighbors is greatly enhanced over what obtains when the diffuse layer has no effect. This too will become more apparent later in the article.

Our present rough criterion for the validity of the hexagonal structure under completely general adsorption conditions is, in accordance with the foregoing remarks, the following. Considering all ions except a given one to be fixed at sites on a hexagonal array, determine the energy necessary for the given ion to move "appreciably" away from its proper position. In all cases, "appreciable" motion is taken to mean some given fraction of the array spacing r_1 . The reason for considering appreciable motion as a fixed percentage of r_1 is that, ultimately, we are interested in finding the conditions insuring that thermal motion induces a moderate fractional change in the local potentials and fields

acting at any ion. This requires that motion relative to the spacing r_1 be considered. There is of course some arbitrariness about the actual choice of the "given fraction." It all depends on how much precision is to be demanded from the hexagonal arrangement. Clearly, if all predictions are to be good to one part in 10^5 , a much smaller fractional motion ($\sim 10^{-5}$) should be used in the criterion than if one demands only "good qualitative agreement" for the model. We have chosen the latter demand, implying that our criterion does not establish where the hexagonal model is good to one part in 10^5 , but rather where the model is just a bit better than a model which ignores the coulomb-induced arraying tendencies of the system. (A much clearer picture of the situation is obtained when one repeats the calculations for more than one choice of "the given fraction." This is done later in this article, thereby removing much of the unpleasantness associated with having to make arbitrary assignments.) Having established the energy U required to move the given ion by the significant amount, we next compare this energy with kT for various values of the system parameters. When the ratio is less than 0.1, the typical random-model expansion parameter, $1 - \exp(-U/kT) \cong U/kT$, is quite small and may be neglected. Under such circumstances this random model is quite appropriate. When the ratio U/kT is greater than 0.1 but less than 1.0, we assert that no clear-cut array is formed, but that the interactions are progressing from a domain where they may be considered as perturbations to a domain where they are too large to be so considered. When the ratio is about 1.0 or so, we assert that array structure is present, but that thermal motion exercises a nonnegligible influence of order $\exp(-U/kT)$. This is a difficult regime to be handled accurately by any model. For a ratio somewhat greater than 1.0, the Boltzmann factor $\exp\{-U/kT\}$ drops rapidly enough that thermal motion becomes a perturbation on the basically ordered arrangement. When the ratio is 2.0 or greater, the Boltzmann factor suggests that thermal perturbation is of the order of a 15% or less effect and may be ignored. We thus say that for ratios less than 0.1 the system is random, for ratios greater than 2.0 the system is regularly arrayed, and the crossover takes place about where

$$\exp(-U/kT) \approx 1 - \exp(-U/kT) \quad (17)$$

or where $\exp\{-U/kT\} \approx \frac{1}{2}$. This crossover occurs when $U/kT \approx 0.7$; however, to avoid the false implication that a sharp phase transition is pictured, we round the number 0.7 to unity thereby underestimating somewhat the pertinence of the hexagonal model. It will sometimes happen, as we shall see, that the range $0.1 \leq U/kT \leq 2.0$ is associated with a very narrow domain of certain system parameters. When this occurs, there is a more abrupt transition between the regimes of disorder and array structure, a diminishing of the significance of the difficult intermediate (transition) region, and a reduction in the sensitivity of the conclusions concerning validity of one or the other model to specific arbitrary assignments.

We consider first the artificial situation where only the ESP images the nonpolarizable adions (the only species present)—actually this is the circumstance for adsorption from a gas phase of ions onto a conducting or dielectric electrode. We are interested in the energy required to move an adion from point 0 to point a' in Fig. 5. This (and the five symmetrically equivalent directions) is the direction which presents the softest potential barrier to the ion, and therefore this is the direction contributing most to the fluctuation of the given ion's position. For large enough R_1 , one may safely approximate the ions and their images as ideal dipoles for purposes of calculating the potentials. With this approximation, the electric field produced by the six nearest neighbors at point 0 is given by $-6(2z_v e \beta)/r_1^3$. The potential produced by these neighbors at point 0 in the IHP is approximately $12z_v e \beta^{-1} R_1^{-3}$. Arguing that the change in potential from 0 to a' should be roughly the same size as the potential at 0 and that the total potential should be roughly that produced by the six nearest neighbors alone, we find* for the energy U to move an adion from 0 to a'

$$U \cong 12(z_v e)^2 \beta^{-1} R_1^{-3} \equiv (3\sqrt{3}/2\pi)(z_v e) R_1^{-1} \psi_\infty \quad (18)$$

Numerically, $U \cong (4/5)z_v e R_1^{-1} \psi_\infty$; the agreement with what we will determine exactly in later sections of the article is very good considering the casual way the calculation was done. The approximate values of $0.08z_v e \psi_\infty$ and $0.16z_v e \psi_\infty$ for $R_1 = 10$ and 5,

* Both of these assumptions represent an error of about a factor of 2, but the errors compensate and our final answer is pretty good.

respectively, compare well with the correct answers, $0.086z_0e\psi_\infty$ and $0.13z_0e\psi_\infty$. Finally, we find U/kT for $T = 300^\circ$ and $z_0 = 1$

$$U/kT \cong 6600R_1^{-3}/\beta \text{ (\AA)} \quad (19)$$

Picking $\beta \approx 2 \text{ \AA}$, our equation tells us that $U/kT \approx 1$ for $R_1 \approx 15$, or $r_1 \approx 30 \text{ \AA}$. The ratio becomes equal to 2 for an R_1 value only 20% smaller: $R_1 \approx 12$ or $r_1 \approx 24 \text{ \AA}$. These values correspond to very low surface charge densities. To obtain q_1 in practical units ($\mu\text{coul}/\text{cm}^2$), one may use the numerical relation $q_1 \cong 1.850 \times 10^3 z_0 r_1^{-2} \text{ (\AA)}$. For the values $r_1 = 30 \text{ \AA}$ and 24 \AA , we therefore find when $z_0 = 1$, $q_1 \approx 2 \mu\text{coul}/\text{cm}^2$ and $q_1 \approx 3.2 \mu\text{coul}/\text{cm}^2$. In terms of the conventional fractional surface coverage θ , equal to $(N/N_s) \equiv (R_{1m}/R_1)^2$, the above surface charge densities correspond to $\theta = 2\text{--}3\%$. Thus, for the present single-imaging case, the situation is very clear-cut. For all surface densities large enough to be of probable interest, the dominant feature of the system is its array-forming behavior; the hexagonal model for this case is excellent except perhaps at elevated temperatures. Incidentally, we see from the very strong arraying tendencies of this system, even at low surface densities, that if a neutral species is added to the surface, provided its addition does not significantly moderate the interaction between ions, then the relative positions of the ions among themselves will be fixed by the above energetic considerations, and the neutral species will simply occupy the remaining space on the surface. Thus, in this case the solution of the two-component problem follows immediately from the emphatic behavior of the one-component system. As for the question of the possible moderation of the interaction by the neutral species, this is an interesting question which is discussed later on.

If it were not for the diffuse-layer effect upon the potential, our account of order in a compact layer containing only nonpolarizable adions could end here with the decision heavily in favor of the hexagonal array.* It does not happen that way, however, for reasons which will only become completely clear in the next section. We therefore turn now to considering a closer representation

* We have not actually ruled out the possibility of a different lattice structure and, as a matter of fact, the square array has only a slightly higher energy. For single imaging, the difference is 1.5%, so that the hexagonal arrangement is only strongly preferred for $R_1 \leq 4.5$ or $r_1 \leq 9 \text{ \AA}$, an ion density which for reasons which will become apparent later is probably unattainable for the single-imaging situation.

of the actual situation, that where the OHP maintains itself as an equipotential surface to good approximation, with consequent effects upon the inner-layer potentials. We shall, of course, have to borrow certain results obtained later in this article; however, that is all right since we are not concerned yet with deriving potentials so much as we are with examining certain consequences of them.

In the C-C infinite-imaging regime, the potential arising from a given ion and its image in the ESP is very effectively attenuated, or "screened," at moderate lateral distances (parallel to the IHP) from that ion. The potential variation in the IHP is drastically smoothed, and ions can move over the IHP much less inhibited by interactions than for the case where screening is absent. Roughly, the ratio of U , the energy to move the ion from point 0 to point a' , to thermal energy is given for $\beta = \gamma$ by*

$$U/kT \approx 200 \times 10^{-2R_1/7} \quad (20)$$

Again desiring the value of R_1 for which the ratio equals unity, we obtain that the crossover condition is met for $R_1 \approx 8$, or for $r_1 \approx 16 \text{ \AA}$. (A closer estimate actually gives $R_1 \approx 7$, or $r_1 \approx 14 \text{ \AA}$.) Note that the interaction is rising very rapidly, doubling for a change in R_1 of about unity. (Again, a closer inspection of the accurate variation shows that in this range of R_1 , the interaction doubles whenever R_1 decreases by about $\frac{2}{3}$.) Since the variation is so rapid with R_1 , we seem to have an example of the circumstance referred to earlier where the transition region is quite abrupt and the decision as to the pertinence of a given model is insensitive to arbitrary assignments. In this case, the hexagonal model seems appropriate for charge densities in excess of about $9 \mu\text{coul}/\text{cm}^2$. This value of surface charge density which approximately marks the beginning of the lattice domain is just large enough to be uncomfortable: It falls within the range of typical experiments, thereby supporting a lattice model over part of the range and denying its validity over the remaining part. This is particularly unfortunate because matters yet to be accounted for—such as presence of neutral species in the compact layer—in conjunction with the sensitivity of our conclusions to changes in system parameters, might alter this critical surface charge density a significant amount in either direction and, correspondingly,

* As one might expect, the effect of screening depends upon the value of Γ ; we will defer a detailed consideration of the dependence upon this parameter until Section III of this article.

could affect our final assessment of the lattice model. Nonetheless, our later considerations do not change this value very much; the resulting changes are probably to decrease this critical surface density somewhat. In essence then, we find that the array model does not span the whole range of experimental interest, but it does seem to span the major part of it ($9\mu\text{coul}/\text{cm}^2$ to about $40\mu\text{coul}/\text{cm}^2$). The fact that the entire experimental range is not pre-empted by the array model seems to indicate that for this system no one model is adequate. One must use the array model where appropriate, a less ordered model at lower surface coverages, and perhaps develop a joining procedure in the rather narrow transition region.*

We may again argue as we did for the single-imaging case that for $R_1 \leq 7$, the ionic interactions emphatically dominate, and that therefore the addition of neutral particles to the layer, assuming they do not reduce the interaction appreciably, will simply involve those neutral particles filling up the spaces between the ions. Whereas this is probably essentially correct, we are beginning to encounter problems with this picture for smaller R_1 values. The basic problem is that with $R_1 = 7$, the separation between ionic centroids is about 14 \AA , of which perhaps 4 \AA is accounted for by the hard ionic cores. This leaves about 10 \AA , just enough room for three water molecules. For a little lower value of R_1 , one of the waters would have to find another spot. Clearly, when the ionic separations are only a few solvent molecular diameters in size, steric effects become important and our picture of "filling up the empty space with neutral particles" becomes less defined. We will have further occasion to discuss the interesting behavior of the compact layer with its neutral species in later sections.

Finally, we consider what the state of the system is likely to be for much smaller surface coverages than for $R_1 \approx 7$. It has already been stated that the motion of different ions is essentially

* One interesting feature which emerges as an outcome of the rapid transition from disorder to order is the speculation that at the transition, just below a charge density of $9 \mu\text{coul}/\text{cm}^2$ or so, depending on actual values of β and γ , there will be a large entropy-change contribution to the free energy of adsorption. This would tend to inhibit further adsorption, hastening the onset of saturation in the q_1 versus q isotherm.

uncorrelated in this regime. We now wish to consider a matter which will modify this conclusion slightly, but in a very interesting way. In the next section, we point out that as a result of the short screening distance established by the diffuse layer, two ions may approach each other much closer than they otherwise could; the unscreened interaction energy is many times kT at those close distances where the screening first begins to lose its effectiveness. Accordingly, at such distances, the energy necessary to move the ions slightly closer together may be much larger than the energy to reach the given starting configuration. As such increments are typically many times thermal energy, the ions are almost always unable to penetrate closer, and the effect is that of a "hard core" interaction between ions. Because this hard core differs from the "true" hard core of the ions, and because it only acts between ion pairs, not between an ion and neutral particle, we refer to it as the coulombic hard core, which is generally effective in preventing close approaches between ions at ordinary temperatures rather than the "true" hard core. We find that the radius of this coulombic core is nearly twice the ordinary steric hard-core radius for C-C imaging. We therefore find that, even at low coverages, the coulombic interaction plays a role, doubling the effective hard-core radius of the ions and thus quadrupling the excluded area per ion. This effect will be discussed later. Next, we consider the manner in which the diffuse layer so drastically alters the potentials in the system.

5. Role of the Diffuse Layer

We have already discussed the fact that the diffuse layer modifies the potential in the compact layer. There are three ways in which this comes about. First, the presence of mobile ions in the vicinity of the OHP leads to what has been termed a "screening" effect on the potential resulting from a given ion on the IHP. The mechanism for this screening is simply the strong repulsion between the adion and the charges (of like sign) in the diffuse layer. The mobile diffuse-layer ions tend to avoid coming close to adions of the same sign, preferring to take up those positions near the OHP of lower potential energy. This tendency is somewhat disrupted by thermal motion, of course, but provided this energy is small compared with the variations of potential over

the OHP produced by the adions and their images in the ESP one may approximate the situation—at least for purposes of visualizing the system—by saying that diffuse-layer ions near the OHP arrange themselves so as to assume the lowest possible energy. In this respect, the ions behave like the charges on the surface of an ideal conductor; hence the approximate effect of these ions is the same as for an ideal conductor placed in the vicinity of the OHP. The outcome of this approximate model is that IHP charges are imaged conductively in the OHP, and their potentials fall off more rapidly with distance than in the absence of such imaging. This behavior of the potential, resulting from induced variations of charge in the diffuse layer, is, except for the geometry of the situation, analogous to what occurs when a charged object is immersed in a space-charge region, thus the name “screening.”

The second modification which is brought about by the diffuse layer comes from the fact that the diffuse layer is a dielectric material. Although the notion of a dielectric constant is questionable as applied to the compact layer, it is a much more justifiable concept when applied to the diffuse layer. Indeed, we may with little error regard the dielectric polarization of the diffuse layer as though the diffuse layer were a dielectric continuum. The dielectric constant of this continuum may vary as the OHP is approached from the solution side; however, it is generally assumed that the dielectric constant is constant all the way up to the OHP. Whatever the detailed model of the diffuse-layer dielectric constant, the effect of this polarization is again to image charges more or less in the OHP. This type of imaging is not perfect as is conductive imaging, however, the image charge being reduced in magnitude by a factor dependent on the size of the dielectric-constant variation at the OHP.

The third effect of the diffuse layer is, via the first two effects, to change the degree of order of the adions. Thus, if the first two effects of the diffuse layer are sufficient for given coverage to smooth the potential variations in the IHP to magnitudes less than thermal energy, then the arraying tendencies of the adions will be too weak, and the arrangement of the adions will be somewhat random. The effect of such loss of order has already been discussed in Section II-4.

Let us now estimate the potential in the compact layer assuming the adions are arrayed on a hexagonal lattice and that both the ESP and OHP are conductive imaging planes. We will shortly consider the case of dielectric imaging at the OHP. We begin by noting that the potential variation parallel to the IHP has the same periodicity as the lattice. Accordingly, we may write

$$\psi(\mathbf{r}) = \text{constant} + A\hat{z} + \sum_{\mathbf{k}} f_{\mathbf{k}}(\hat{z}) \exp(i\mathbf{k} \cdot \mathbf{r}) \quad (21)$$

where A is a constant to be determined from boundary conditions at the ESP, \hat{z} is here the normal distance from the field point, \mathbf{r} , to the source plane, and $\{\mathbf{k}\}$ designates those vectors parallel to the IHP, producing functions $\{\exp(i\mathbf{k} \cdot \mathbf{r})\}$ having the proper periodicity. Now the smallest \mathbf{k} vector producing a function periodic on the array has the magnitude $|\mathbf{k}| = (4\pi\sqrt{3})/3r_1$. If we require $\psi(\mathbf{r})$ to satisfy Laplace's equation almost everywhere in the compact layer, we find that for this smallest \mathbf{k} vector, the function $f_{\mathbf{k}}$ is given by $f_{\mathbf{k}} = B \exp[-(4\pi\sqrt{3}\hat{z})/3r_1]$, where B is another constant. For all larger \mathbf{k} vectors, the exponential decay in \hat{z} is faster and we ignore these contributions in the following discussion.

If one refers to the infinite imaging situation of Fig. 26(d), it is clear that successive nonideal dipole sheets are separated by $\Delta z = 2d = 2\beta(1 + \Gamma)$. The contributions from successive sheets to the part of the potential which varies in planes parallel to the IHP are in the ratio $\exp[-(8\pi\sqrt{3})(1 + \Gamma)/3R_1]$. For $\Gamma = 1$, this ratio may be written $\exp(-29R_1^{-1})$. Thus, for all values of $R_1 \leq 6.3$, the contributions of successive planes are in ratios $\leq 10^{-2}$, whereas for $R_1 \leq 12.6$ the ratios are $\leq 10^{-1}$. Accordingly, we do not make too great an error if we replace the infinite regress of images by three nonideal dipole sheets, the first lying about the ESP, the second and third lying about the planes $z = \pm 2d$. This approximation may not be accurate enough for large R_1 or for a meticulous treatment of the potential near the ESP or the OHP (for then we would have thrown away contributions as large as the smallest of the three which were retained); however, for most purposes it should suffice. Now if we employ a superscript zero to denote single imaging and define $\psi_a^0(x, y, z)$ as the potential arising from the nonideal sheet centered at the ESP, then the actual C-C imaging potential $\psi_a^{(2)}(x, y, z)$ (which

does not include a possible uniform field contribution arising from excess charge on the ESP) is given for $z \leq d$ approximately by*

$$\psi_a^{(2)}(x, y, z) \cong \psi_a^0(x, y, z) + \psi_a^0(x, y, z + 2d) - \psi_a^0(x, y, 2d - z) - 4\pi q_1 z(1 + \Gamma)^{-1} \quad (22)$$

For the present case of conductive imaging at the OHP, we may readily find the charge on the ESP for which there is no uniform field contribution. Noting that when the true potential is identical with $\psi_a^{(2)}$, the average p.d. across the compact layer vanishes [because $\psi^{(2)}(0) = \psi_a^{(2)}(\beta + \gamma) = 0$], we may use Gauss's law to establish that $q\beta + (q + q_1)\gamma = 0$; thus, there is no excess charge on the ESP provided that $q = -\lambda q_1$. Accordingly, the uniform field contribution, which in general must be added to the $\psi_a^{(2)}$ of the C-C imaging case, is $\psi_e(x, y, z) = -4\pi\epsilon_1^{-1}z(q + \lambda q_1)$, where the bogus dielectric constant ϵ_1 should not be taken seriously but is merely a reminder that polarization effects within the compact layer must somehow be taken into account. In the absence of the diffuse-layer effects, the local potential would have been $\psi^0(x, y, z) = -4\pi(q + q_1)z + \psi_a^0(x, y, z)$, where we have set $\epsilon_1 \equiv 1$ here and in the following. The whole question of dielectric effects in the inner layer will be discussed in Section II-6. A comparison with our conductive-imaging result shows that the effect of the (conducting) diffuse layer is, for given q and q_1 , to add a potential, $\psi_a^0[x, y, z + 2\beta(1 + \Gamma)] - \psi_a^0[x, y, 2\beta(1 + \Gamma) - z]$, to that obtained when one neglects the diffuse layer. In Table II, we give the values of potential $\psi(x, y, \beta)$, normalized in accordance with $\Psi(x, y, \beta) \equiv \psi(x, y, \beta)/\psi_\infty$, for C-O single imaging where the diffuse layer is neglected, and for the C-C imaging situation with $\Gamma = 1$. The potentials applying to an incomplete lattice situation are shown for two points in the IHP; point 0 corresponds to the site of a removed adion, and point a' is a point of three-fold symmetry before one of the three neighboring adions is removed.

* The reader will naturally wonder where the term $-4\pi q_1 z(1 + \Gamma)^{-1}$ came from. It turns out that this is the potential arising from the infinite image sets which have been neglected up to now. Only portions of the potential which vary in directions parallel to the IHP fall off exponentially by our previous argument. We are still left with this uniform-field part, which is not the same as that arising from excess charge on the ESP, ψ_e . This whole matter is further discussed in Section IV-1.

The charge density on the electrode in all cases is taken to be $-q_1$; however, the difference $\Psi(a') - \Psi(0)$ is independent of this choice. There are two sets of numbers listed for the conductive-imaging situation. The first numbers represent accurate data acquired by methods discussed later in this article, and the numbers in parentheses were obtained by the approximate method just described. One notes the decreasing utility of this approximation for increasing R_1 . The reason that the absolute accuracy is so poor for $R_1 = 10$ is that the terms neglected in the

TABLE II
Normalized Potentials on the IHP^a

R_1	Single imaging			Infinite imaging		
	$\Psi^0(0)$	$\Psi^0(a')$	$\Delta\Psi^0$	$\Psi(0)$	$\Psi(a')$	$\Delta\Psi$
2	0.556	0.668	0.112	0.556(0.556)	0.708(0.708)	0.152(0.152)
5	0.284	0.413	0.129	0.504(0.46)	0.543(0.54)	0.039(0.08)
10	0.149	0.235	0.086	0.500(0.35)	0.505(0.49)	0.005(0.14)

^a Here, $\Delta\Psi \equiv \Psi(a') - \Psi(0)$.

model are less than 10% for a *complete* lattice (no vacancy). Since the absolute magnitude of the potential at point 0 diverges for the complete lattice, our 10% figure arrived at earlier (for $R_1 = 12.6$) is of no use in establishing an upper bound on the error for this case. Happily, we have the accurate data for direct comparison here.

One of the most significant features shown in the table is the smoothing effect of conductive imaging at the OHP. While for single imaging the potential variation from point 0 to point a' is roughly 10% of ψ_∞ over a wide range of coverages, the presence of conductive imaging at the OHP causes this variation to drop to 4% at $R_1 = 5$ and to 0.5% at $R_1 = 10$. Thus, we see that even though the potential at point 0 is actually increased by the diffuse-layer imaging, the variations of potential over the IHP are greatly decreased; it is therefore the variation in potential which is "screened" by the diffuse layer. The effect of screening at given d naturally decreases for C-C imaging as Γ departs in either

direction from unity; from symmetry we note that for given r_1 , the unnormalized potential $\psi_a^{(2)}$ evaluated on the IHP is invariant under the replacement $\beta \leftrightarrow \gamma$ and thus $\Gamma \rightarrow \Gamma^{-1}$. Later we will illustrate more specifically the dependence upon Γ . We have used the data for $\Psi^{(2)}(a') - \Psi^{(2)}(0)$ to calculate the ratio $U^{(2)}/kT$ pertaining to C-C imaging, and this ratio is plotted in Fig. 7.

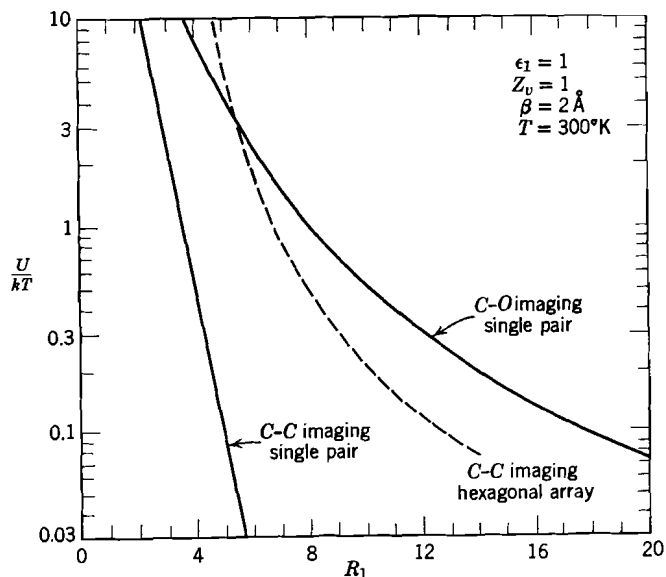


Fig. 7. Normalized single adion energy in the plane of its neighbors, U/kT , vs. $R_1 \equiv r_1/\beta$, the normalized nearest-neighbor distance for a hexagonal array, or the pair separation distance for two isolated adions.

Another way of seeing the diffuse-layer screening in action is to calculate the energy of interaction of two adions imaged in the ESP and OHP and separated by a distance r_1 . Taking $\Gamma = 1$ and $\epsilon_1 = 1$ and making use of the results derived in Appendix I, we obtain for $\exp(-\pi R_1) \ll 1$ the almost exact C-C result

$$U_{\text{pair}}^{(2)}/kT \cong [2/\beta (\text{\AA})]550R_1^{-1/2} \exp(-\pi R_1/2) \quad (23)$$

where T has been set at 300°K. This energy ratio is also plotted in Fig. 7 versus R_1 , and one notes the essentially exponential drop with R_1 . We observe that were there only two adions on the IHP, they would move essentially independently until they approached

each other to within a distance $r_1 \approx 4.5\beta = 9 \text{ \AA}$. At this point the quantity $(U_{\text{pair}}^{(2)}/kT)$ would be about $\frac{1}{2}$. The energy increases rapidly below this distance, and the pair of ions would stringently avoid encounters of r_1 less than about $3.5\beta = 7 \text{ \AA}$, where the energy ratio is somewhat greater than unity and rising precipitously. This statement is true whatever the degree of lattice ordering on the surface. Two adions find it so difficult (at 300°K) to approach each other significantly closer than 7 \AA that we may here neglect such occurrences entirely for C-C conditions. Indeed, we may regard the adions as having a coulombic hard-core diameter, r_c , of about 7 \AA . This is the "hard-core" which is effective in establishing the excluded volume (or area in this surface problem) for the system of adions, even at low coverages. Naturally, an uncharged particle on the surface passes unhindered through this hard core, suffering strong repulsion only in the vicinity of the usual ionic surface, with radius about half of the coulombic radius. These facts may also be stated that *two adions must always have enough room for a water molecule to fit between them when C-C imaging is appropriate*. We note that we may estimate the maximum achievable surface density of ions at ordinary temperature, assuming they all maintain their charge, by the above consideration of the coulombic hard core.* Setting the minimum separation r_1 equal to 3.5β , or about 7 \AA , the maximum allowable surface charge density works out to be about 38 \mu coul/cm^2 , close to that derived from experimental measurements on many electrolyte systems. The fractional surface coverage, θ , at this maximum value would be about $(2\beta/3.5\beta)^2$, or approximately 33%.

* The foregoing argument is satisfactory as it stands for the situation where the particles are wide enough apart that their coulombic hard cores seldom touch. The following development represents a heuristic extrapolation of the concept to the case where the particles are being crowded together and their cores are touching. Our observation that the energy to "compress a hard core," or move particles closer together than r_c , is large does not rule out the possibility of such possible compression if the adsorption energy is large enough. Nonetheless, our estimates indicate that in practice the adsorption free energy will vanish and further ionic adsorption be prevented by the coulombic hard core interaction before such compression can become a large effect. Though exceptions may exist, the concept seems generally to be a useful one.

It is interesting to compare these calculations with the analogous ones for single imaging. For this case we would have for large R_1 that the ratio of lateral pair interaction energy to thermal energy is given by

$$U_{\text{pair}}^0/kT \cong [2/\beta (\text{\AA})]550R_1^{-3} \quad (24)$$

We see from Fig. 7 that not only is this interaction much stronger because of the absence of screening, but it is also much "softer." The variation with R_1 is not as rapid as with the diffuse-layer imaging. Thus, the particle motions become correlated when $R_1 \approx 18$, or $r_1 \approx 36 \text{ \AA}$ (this occurs as an average condition at $q_1 \approx 1.5 \text{ \mu coul/cm}^2$ and $\theta \approx 1.3\%$); yet they can only approach to within distances of about $R_1 \approx R_c \approx 7$, or $r_c \approx 14 \text{ \AA}$ when $\beta = 2 \text{ \AA}$. (This pair separation occurs when $q_1 \approx 10 \text{ \mu coul/cm}^2$ and $\theta \approx 8\%$.)

Based on the foregoing discussion of conducting imaging at the OHP, we may readily understand what is the effect of dielectric imaging there. First of all, if the dielectric imaging is very strong, that is, if $\omega \equiv (\epsilon_s - \epsilon_1)/(\epsilon_s + \epsilon_1) \approx 1$ by virtue of $\epsilon_s \gg 1$ (implying $\epsilon_s \gg \epsilon_1$), then the overall effect of dielectric imaging is identical with conducting imaging. If ω departs somewhat from 1, the result is that the successive nonideal dipole sheets centered at $\pm z_n = 2dn$ are of diminished strength, ω^n . The shielding is not quite as effective as for perfect imaging. As soon as ω departs considerably from unity, we have problems; when ω is considerably smaller than unity, ϵ_1 is comparable with ϵ_s . But for this case it matters very much what we take for ϵ_1 . Polarization in the compact layer plays a greater relative role, and it is no longer a permissible procedure to replace the actual compact-layer polarization with a bogus dielectric constant. Hence, for $\omega < 1$ one really must be prepared to throw out the picture of dielectric imaging based on an ϵ_1 and to start again, taking correct account of the polarization in the inner layer.

It is fortunate in a way that the effect of the dielectric discontinuity near the OHP is the same as the presence of mobile ions in the vicinity of the OHP, that is, to image charges. If it were otherwise, we should have to worry more about the outcome when both of these situations pertained. There might have been, for example, a partial cancellation of the two influences, and we should then have had to be careful in our analysis to determine

the result of these influences. As it is, however, the simultaneous presence of the two reinforcing imaging processes merely increases our confidence that there is indeed an imaging plane more or less on the OHP, and that, even if neither of the processes is sufficient in itself to create perfect imaging, the combination of the two should make perfect imaging a fairly good approximation.

Although the foregoing considerations allow us to be fairly confident of the gross influence of the diffuse layer, we are confronted with a more difficult matter in accurately calculating its effects. We shall now describe some of the complications in the actual physical system which we have glossed over up to this point and which, though not affecting the essential validity of the previous development, do alter the details of the influence of the diffuse layer upon the inner region and the system as a whole.

First, there is actually an interaction between the processes of conductive and dielectric imaging; this must be so, for if the effects were superposable, then it would be possible that the two images produced by the two processes should add to give a net image charge greater in magnitude than that of the object imaged. The simplest way of considering how the two effects actually should add in the first approximation is simply to regard the diffuse-layer ions near the OHP as contributing to the net polarizability of this region of the diffuse layer—and hence to the effective dielectric constant ϵ_s which determines ω . This is consistent with our implicit assumptions when we referred to the reinforcement of the imaging processes, and it agrees with the physically necessary requirement that the presence of the two processes simultaneously can at most cause the OHP to more closely approximate a perfect imaging plane. There is a physical way of understanding why the two effects do not superpose, the images produced by one process being influenced by the presence of the other. Although this physical mechanism is completely contained in the behavior referred to before concerning the "net polarizability," it is well hidden there beneath a lot of relationships which occur in the theory of dielectrics of which the reader would have to be ever cognizant. What occurs is quite easily understood; the presence of strong conductive imaging by the diffuse-layer ions would virtually wipe out the potential variations parallel to the OHP in the diffuse layer itself. Accordingly, the

dielectric polarization would be left with very little to image. Similarly, if dielectric imaging were quite complete, the potential produced at the OHP would be virtually constant even without the assistance of the mobile ions. These ions would no longer be compelled to congregate in bunches over the OHP and indeed would be energetically forbidden from doing so except to the extent necessary to level even more the slight potential variations which remained. These examples merely show that, given one imaging mode at a certain level, the other mode will adjust its level so that the total effect is no more than perfect imaging. The actual division of labor between the two and the degree of perfection actually achieved are matters for a detailed calculation, which will not be discussed here.

There are two related complications which are more troublesome and in fact would have to be taken into account in order to perform the sort of calculation mentioned in the last paragraph. These are the finite thickness of the diffuse-layer ionic sheath and the uncertainty in the position of the dielectric imaging plane. The first of these results from thermal motion of the diffuse-layer ions and involves a length of the order of the Debye shielding distance, λ_D , which may be written for $z_v = 1$ as $(kT\epsilon_s/4\pi c_0 e^2)^{1/2}$, where c_0 is the density of diffuse-layer ions, and the simple inclusion of ϵ_s becomes somewhat ridiculous for the smallest λ_D values. One may use the density in the bulk of the electrolyte to calculate λ_D , or one may argue that the value should be that applying at the OHP. We shall not try to decide the matter here, for if the two concentrations differ by very much one needs really to worry about the diffuse-layer problem from the beginning, including, for example, finite size effects. In any case, the thickness is not zero but varies from hundreds of Angstroms in some situations to perhaps only a few Angstroms in others. Correspondingly, there is an uncertainty about where to place the effective conductive imaging plane (though with the strong potentials set up by the adions we should not insist that this uncertainty is equal to or otherwise simply related to the sheath thickness). For that matter, we are sure that the thermal motion of the diffuse-layer ions, as small as that may be, will to some extent "blur" the images. The extent to which this is liable to occur, as well as the best estimate of the position of the conductive

imaging plane—somewhere on or behind the conventional OHP—is more properly deferred until later in this article. The similar uncertainty in the location and basic pertinence of the dielectric imaging plane is one manifestation of two more fundamental facts. First, as we mentioned at the beginning of the discussion on the diffuse layer, the effective dielectric constant in the diffuse layer most likely varies with distance from the OHP; it presumably ranges from a bulk value down to a possibly considerably smaller and partly saturated value in the midst of the higher ionic concentrations and larger fields very near the OHP. Second, the discreteness of the diffuse-layer dipoles is contrary to the continuum assumed. While this discreteness is of no importance when viewed from far enough away, it does produce a somewhat different potential from that produced by the continuum. This effect is presumably modest, as it tends to be averaged away by motion in the diffuse layer, and by an earlier argument we would expect the deviations induced to fall off with distance z measured from the OHP roughly as $\exp\{-3\pi z/l\}$, where l is a characteristic separation between diffuse-layer dipoles—probably the diameter of a molecule or so. Since the z in this application is almost surely no less than l , we appear now to be discussing an effect which is comfortably unimportant ($\approx e^{-10}$).

To return to the mainstream of our discussion, we have described several effects which might alter the details of the role played by the diffuse layer. They all require for their complete understanding a detailed and complex treatment of the diffuse layer. While several of these matters will be further discussed later in this article, this additional discussion is to a great extent motivated by our duty to give at least some review of all the topics which are in current popularity in this field. Reminding the reader that representing the diffuse-layer effect by imaging is an approximation and that an exact theory requires an *ab initio* theoretical treatment of this complex system, we nonetheless believe that it is a very good, and simply applied, approximation in most circumstances of interest.

6. The Concept of an Inner-Region Dielectric Constant

We have noted several times that the representation of polarization effects within the compact layer by means of a

dielectric constant is a procedure which, though very common throughout the literature, is generally incorrect unless one takes particular pains to determine this quantity from first principles and to avoid extending its application beyond the realm envisioned in its derivation. We shall here amplify this assertion by giving examples of how dielectric constants could be defined for the compact layer and how easily such quantities, once defined, could be falsely applied. Before discussing the compact layer itself, we shall review some of the properties of dielectric polarization in bulk matter with emphasis upon those features peculiar to bulk matter which allow a simple and widely applicable definition of the dielectric constant.

The case generally considered in any discussion of bulk dielectric effects is the following. An external electric field \mathcal{E}_{ext} is developed across a material containing polarizable elements. This field is either constant in magnitude and direction or else varies so slowly (in all directions) over regions containing many discrete polarizable elements that it may be considered constant.* One thereby reduces the problem to that of the behavior of a single macroscopically small, microscopically large region of the material. Under the combined action of the external field and the field produced by the other (polarized) entities, it is next assumed that the objects acquire an electric dipole moment $\mathbf{P} = \alpha \mathcal{E}_{\text{eff}}$, where α is the polarizability of a single entity and is a property of the individual entity, and \mathcal{E}_{eff} is the sum of the external field and the field produced by the other dipoles, \mathcal{E}_r . It is \mathcal{E}_r which contains the effect of the neighboring dipoles of a given dipole. Note that we have already been able to incorporate a great simplification into the picture as a result of the uniformity assumed for \mathcal{E}_{ext} on this scale. All the dipole moments are taken to be precisely the same; similarly all the fields \mathcal{E}_r and \mathcal{E}_{eff} at each polarizable element are the same.

Next one defines the polarization \mathcal{P} as the total dipole moment per unit volume arising from neutral species contained in the region, and again one exploits the microscopic largeness of the macroscopically small region in defining this quantity. The total

* A generalization of the present discussion is to consider fields which vary as $\exp\{\mathbf{i}\mathbf{k} \cdot \mathbf{r}\}$; the resulting dielectric constant is then a function of the wave-vector \mathbf{k} . This description is sometimes called "spatial dispersion."

dipole moment contained in the given region is almost exactly proportional to the volume of the region and independent of the precise location of the boundaries; hence, \mathcal{P} is a well-defined vector—at least to a precision of the order of the ratio between the microscopic spacing between dipoles and the smallest linear dimension of the given region. Next, we set $\mathcal{E}_r = 4\pi S\mathcal{P}$, where S is a constant characteristic of the microscopic structure of the dielectric material, and obtain

$$\mathcal{P} = N_v \alpha \mathcal{E}_{\text{eff}} = (1 - 4\pi N_v \alpha S)^{-1} N_v \alpha \mathcal{E}_{\text{ext}} \quad (25)$$

with N_v the volume density of polarizable elements in the inner region, and α here the polarizability of the polarizable elements.

All that remains in order to find the dielectric constant is to make the observation that the electric field produced by the electric dipoles fluctuates strongly on the microscopic scale; however, if one averages this fluctuating electric field over a microscopically large region,* one is left simply with an average field from these dipoles equal to $-4\pi\mathcal{P}$. Identifying \mathcal{E}_{ext} with the displacement field \mathcal{D} and the sum $\mathcal{E}_{\text{ext}} - 4\pi\mathcal{P}$ with the macroscopic field \mathcal{E} , we find

$$\mathcal{E} = \mathcal{D} - 4\pi N_v \alpha (1 - 4\pi N_v \alpha S)^{-1} \mathcal{D} \quad (26)$$

from whence the dielectric constant, $\epsilon \equiv \mathcal{D}/\mathcal{E}$, is found to be

$$\epsilon = 1 + 4\pi N_v \alpha (1 - 4\pi N_v \alpha S - 4\pi N_v \alpha)^{-1} \quad (27)$$

So defined, the dielectric constant enables us to determine the average electric field existing in the dielectric from a knowledge of the external field alone.

Provided we are not interested in the potential exceedingly close to one of the discrete dipoles, average quantities will be sufficient, since under such conditions the potential seen by any given charge will predominantly arise from the action of the average field over macroscopic distances, and the fluctuation potential associated with the nearest discrete dipoles will be relatively small. Thus, one may usually calculate the interaction between two point charges imbedded in a dielectric material and separated by microscopically large distances simply by

* The same result is of course obtained if the average is taken over precisely one unit cell when the dielectric material is crystalline.

making use of average fields; that is, by incorporating the dielectric constant into the calculation. This is an unexpected bonus, however, for all that was really obtained at the beginning by defining such a quantity was the average field; furthermore, it is clear that if one of the point charges resides in atypically close proximity to one of the discrete dipoles, the fluctuation potential will be relatively large and the interaction between the charges will be moderated by the polarization in a highly specific manner not accounted for by the simple dielectric constant.

To recapitulate, the notion of a dielectric constant naturally arises whenever a microscopically large region containing discrete polarizable elements is subjected to conditions such that all field quantities are very slowly varying over the distances characterizing the microscopic structure of the region. When such conditions obtain, the dielectric constant provides a convenient means of determining average field quantities; however, the significance of such quantities in specific cases depends upon such details of those cases as whether or not special importance is attached to atypical points in the medium by virtue of the particular problem considered. To attempt to extend the concept beyond the limits stated here is hazardous, and each extension must be analyzed as a case in itself. With these thoughts in mind, we are now ready to examine the dielectric constant concept as applied to the compact layer.

It is immediately obvious that the conditions which enabled one to define a useful dielectric constant for bulk matter do not apply to the compact layer; the adion-image fields vary rapidly over the dimensions characterizing the microscopic structure of the compact layer. Furthermore, the distances over which the fields act are not microscopically large. Therefore, the potential at any given point in the compact layer has very little to do with the average fields derivable from a dielectric constant. Nonetheless, provided we exercise some care, we may still define a quantity for the inner layer analogous to a dielectric constant (in that it conveniently accounts for polarization), although its usefulness will not be nearly so great as that of the bulk dielectric constant.

We shall set out to define a dielectric constant for the compact layer in such a way that the effect of polarization upon the average potential, $V(Z)$, is properly accounted for provided $1 < Z < Z_0$.

Once having found this dielectric constant, however, we may only use it in this way. To account for polarization effects upon other quantities, one would have to derive a different dielectric constant appropriate to the quantity considered (not always a possible procedure) rather than simply making use of the same dielectric parameter. This is a reflection of the limited usefulness of the concept itself as applied to this system.

First, we observe that for all Z in the domain $1 < Z \leq Z_0$, the contribution to the average potential from the compact layer polarization is simply $4\pi NP$, where now P is the average normal component of electric dipole moment. Relating N to N_v by $N_v = d^{-1}N$ and defining \mathcal{P} as the normal component of average polarization, we find this contribution may be written $4\pi\mathcal{P}d$. Expressing this result in terms of the average field acting between the ESP and the plane $Z = \text{constant}$, one obtains the result that the polarization produces an average field $-(Z_0/Z)4\pi\mathcal{P}$ between these two planes. As the result depends on Z , we see that a single dielectric constant is insufficient even to account for polarization effects upon the average p.d. between the ESP and an arbitrary plane parallel to it. We shall be content then to consider the "dielectric constant" which determines the total p.d. across the compact layer and shall scrupulously avoid applying this dielectric parameter to the determination of any other quantity. Setting $Z = Z_0$ we find that the average dipole field is $-4\pi\mathcal{P}$, just as for bulk matter.

Again we may set $P = \alpha\mathcal{E}_{\text{eff}}$, where \mathcal{E}_{eff} is now the average normal component of field acting to polarize the entities, but \mathcal{E}_{eff} is not necessarily so simple as it was for bulk matter. Things are not difficult providing there are no adions in the compact layer because for this case the fields acting on all the dipoles are equal, the dipoles themselves are effectively equal, and the external field \mathcal{E}_{ext} is uniform over the whole layer. For this case we may again set

$$\mathcal{E}_{\text{eff}} = \mathcal{E}_{\text{ext}} + 4\pi S\mathcal{P} \quad (28)$$

where S will depend on imaging conditions at the OHP, various structural features of the compact layer, and the type of polarization involved (induced or orientational). Proceeding as for bulk matter, we would obtain an expression for the dielectric constant which is formally identical to that obtained for bulk; of course,

the actual values of N_v and S (as well as α perhaps) would differ for the compact layer from the values appropriate to bulk, so that numerically the dielectric constant would be different. More important than the numerical differences is the fact that this dielectric constant is only applicable to one calculation: finding the average compact-layer potential.

The whole situation is greatly complicated when adions are present in the compact layer; no longer will every dipole see the same field, but the fields will depend upon where the dipoles reside relative to the adions. Correspondingly, no longer will all dipoles have the same effective moment; indeed, as a result of this, no longer will the field \mathcal{E}_r be simply proportional to \mathcal{P} . Thus, for this case \mathcal{E}_{eff} is a very difficult object to determine. There are other problems as well. In particular, the field \mathcal{E}_{ext} is no longer uniform; it acts differently in its roles as a D -field and as a contributor to the production of polarization. Illustrative of this is the fact that for C - C imaging the field contributes nothing to the average compact-layer potential difference, yet it does act upon polarizable matter on the IHP and therefore cannot be ignored as a partner in \mathcal{E}_{eff} . Thus, we find for this case that even the limited type of dielectric constant defined before is unachievable. The average field is no longer proportional to the external field at all. For such situations, it is better to refrain from defining a dielectric constant, instead treating the polarization by more direct means.

Though we might take a hint from the negative results of the last paragraph, we now turn to a consideration of an entirely different type of dielectric constant. We wish to consider to what extent the interaction energy of two adions on the IHP is modified by the presence of polarizable matter in the compact layer. This matter is of extreme interest because of its relevance to such questions as lattice stability under thermal motion, as noted in previous sections. For this purpose, we may set $\psi_e = 0$ with no loss of generality whatever.

Again we shall assume that $\mathbf{P} = \alpha \mathcal{E}_{\text{eff}}$. When the electric fields present are very large and the polarization results from preferential orientation of permanent dipoles, however, this assumption that \mathbf{P} is proportional to \mathcal{E}_{eff} breaks down and the whole situation becomes surprisingly more complex. Under the linear assumption

we may directly determine, formally at least, the change in the energy of interaction between two ions on the IHP as a result of polarization. Let the first ion reside at the origin and the second at \mathbf{r} . The total energy for the two is then written $U = z_0 e \phi(\mathbf{r})$ where $\phi(\mathbf{r})$ is the potential arising from all polarization, the charge at the origin, and all images; it excludes the infinite contribution from the ion itself at \mathbf{r} . Now the potential ϕ is made up of several contributions: that from the images of the charge at \mathbf{r} , that from the charge at the origin and its images, and that from the polarization and its images. The first of these is constant and does not depend upon \mathbf{r} ; we may discard it if we are interested in the interaction energy between the ions. The polarization at any point is the sum of what would be present if only the ion at the origin existed and what would be present if only the ion at \mathbf{r} existed. Since the potential at \mathbf{r} arising from the latter polarization is independent of \mathbf{r} , we may disregard this contribution. Note the utility of the linear assumption. We are left with the following expression for the interaction energy

$$U_{\text{int}} = z_0 e \phi_0(\mathbf{r}) \quad (29)$$

where ϕ_0 is the potential which would exist if the ion at \mathbf{r} were removed and only the ion at the origin, its images, the polarization it sets up, and the images of that polarization were present. The problem of finding the interaction energy between two adions is reduced to that of finding the potential set up by a single adion at the origin along with the resulting polarization and images.

Consider the case of C - C imaging with $\Gamma = 1$. From the results of Appendix I and the asymptotic behavior of the modified Bessel function, $K_0(x) \rightarrow (2x/\pi)^{-1/2} \exp(-x)$, we may roughly approximate the effect of C - C imaging by reducing the potentials and fields which would exist in the absence of imaging by the factor $(4R)^{1/2} \exp(-\pi R/2)$, where $R \equiv r/\beta$ and \mathbf{r} is here the planar distance from the compact-layer source point to the field point on the IHP.* If for simplicity we take $\mathcal{E}_{\text{ext}} = \mathcal{E}_{\text{eff}}$, always a

* Of course, if we reduce the potential by this factor, the field should actually be the sum of two terms; the term we use here and the modified potential times $\{(\pi/2) - 2(4R)^{-1}\}\beta^{-1}$. However, since this is only a rough calculation and it is the exponential factor (contained in both terms) which dominates the behavior we adopt the simpler procedure in the text.

possible approximation for small α , we find for the induced dipole moment at a point r_i from the origin, $P_i \cong \alpha z_v e r_i^{-2} (4R_i)^{1/2} \times \exp(-\pi R_i/2)$, where $R_i \equiv r_i/\beta$.

On the other hand, the effect of a given dipole also falls off exponentially with its distance from the field point for $C-C$ imaging. The overall effect of a given dipole at a given field point therefore involves an exponential factor whose argument contains the sum of the distances from the dipole to the origin and to the field point. These considerations lead us to consider the situation shown in Fig. 8, approximately pertinent for $R_1 = 5$ and $\beta = 2 \text{ \AA}$. The solvent-molecule diameter has been set to $(\frac{3}{2})\beta$, and all entities not shown may be neglected here. We note that only the component of polarization in the plane contributes to the potential on the IHP and hence to the interaction energy.

To avoid a very long and inelegant calculation, since we only wish to roughly establish the dielectric effect here, we simply set the contributions from the first and third row of dipoles equal to that of the middle row of dipoles. Putting all the numbers together we find

$$\begin{aligned} \phi_0 \cong & \frac{1}{2} z_v e \sqrt{20} \exp(-5\pi/2) \\ & + 6\alpha z_v e (13\beta/4)^{-2} (7\beta/4)^{-2} \sqrt{91} \exp(-5\pi/2) \\ & - 6\alpha z_v e (27\beta/4)^{-2} (7\beta/4)^{-2} \sqrt{189} \exp(-27\pi/8) \end{aligned} \quad (30)$$

where ϕ_0 is the potential at the site of the removed positive ion shown dotted in Fig. 8. It will be observed that the relative contributions of those terms we have considered drop very rapidly with the sum of the distances to the field point and to the origin. The first term in the sum is due to the ion at the origin (and its images). The effect of screening is to make the negative term negligible, and the interaction energy is actually increased* by the polarization in this example. The potential ϕ_0 is approximately given by

$$\phi_0 \cong 10^{-4} z_v e \beta^{-1} [3.47 + 6.72J] \quad (31)$$

* Since the self energy has not been included here, the total energy of the system is still lowered by the polarization. As a matter of interest, Fletcher (36) has pointed out the same basic phenomenon we observe here, in connection with the sign of the depolarizing field in a finite cubic lattice (a thin slab) of nonideal dipoles.

where again $J \equiv \alpha/\beta^3$, and the successive dipoles (and their images) considered in the sum for the potential contribute much less than the next most important dipoles—the convergence is of the nature of one more significant figure for every successive set of dipoles considered. For typical values of J , we find that the potential ϕ_0 which determines the interaction between two ions at distance $R_1 = 5$ under $C-C$ conditions may be more than 50% larger than the potential in the absence of polarization. In this case then, the effective dielectric constant which modifies ionic

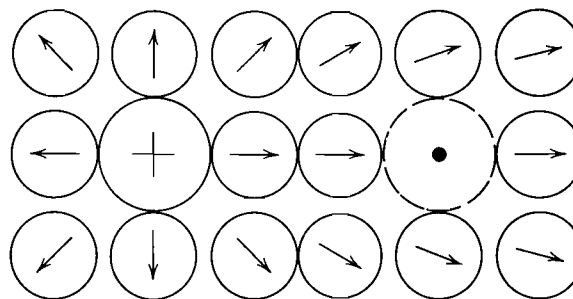


Fig. 8. Schematic diagram illustrating solvent-adion situation used in assessing planar shielding effects.

interaction in the plane may be as small as 0.6 or so for $R_1 = 5$. For smaller J values or larger R_1 , we expect this dielectric constant to increase. (Compare with the Z -dependence noted for our earlier "dielectric constant.") Finally, when R_1 is very large this dielectric constant will be more akin in value to usual macroscopic quantities. Eventually perhaps someone will make a careful calculation to show how the interaction in the plane is modified by polarization including the effects of $\epsilon_{\text{eff}} \neq \epsilon_{\text{ext}}$. This is a very ambitious problem, however, and we must be content with this illustration of how screening and discreteness effects combine here (at small R_1) to produce a "dielectric constant" of the order of and possibly less than unity.

Before ending our discussion of the dielectric constant of the inner region, we wish to point out some interesting properties of orientational polarization in the compact layer. Under most conditions in the double layer, the fields acting normal to the IHP are quite large; large enough to saturate the orientational

polarization. Such saturation always occurs whenever the dimensionless quantity $|\mu\mathcal{E}_{\text{eff}}/3kT|$ appreciably exceeds unity, for under such conditions the average dipole moment, $\langle\mu\rangle$, in the direction of the field is roughly equal to the full magnitude of the permanent dipole moment μ . The contribution of this polarization to the average potential is, under such conditions, slowly varying and not accountable by means of a usual dielectric constant.

On the other hand, for $C-C$ conditions we have seen that, except for the immediate vicinity of an adion, the component of field parallel to the IHP is quite small, certainly very much less than the normal component. When this inequality exists together with the saturation of the orientational polarization, one may readily calculate the component of polarization parallel to the IHP. Since the dipole moment is of magnitude μ aligned in the direction of the vector field, the parallel component must be given by μ times the ratio of \mathcal{E}_{\parallel} to $(\mathcal{E}_{\parallel}^2 + \mathcal{E}_{\perp}^2)^{1/2}$, where the subscripts refer to the parallel and perpendicular components respectively. Under such circumstances, the parallel component of polarization behaves as though it arose from an entity whose polarizability is given, for $\mathcal{E}_{\parallel} \ll \mathcal{E}_{\perp}$, by $\alpha_{\parallel} \sim \mu/\mathcal{E}_{\perp}$. This is clearly less than the low field polarizability, $\alpha_0 \equiv \mu^2/3kT$, by an amount dependent upon how far into saturation the field has taken the dipoles. We may estimate α_{\parallel} most simply by noting that the low field polarizability applies until $|\mu\mathcal{E}_{\text{eff}}/3kT| \ll 1$; the polarization approaches constancy for appreciably larger values of this quantity. Taking the ratio of the "critical field," $3kT/\mu$, to the field \mathcal{E}_{\perp} and multiplying by the low field polarizability gives us a rough estimate of α_{\parallel} : $\alpha_{\parallel} \sim (3kT/\mu\mathcal{E}_{\perp})\alpha_0$. These conditions do not necessarily hold very near an adion or if $\psi_e \cong 0$; the first of these exceptions is discussed somewhat later in this article in connection with solvation of adions in the compact layer.

Two more remarks are pertinent to the question of seriously attempting a dielectric constant calculation for the inner layer. First, if one may disregard parallel components of polarization (because of the absence of adions or because of saturated orientable dipoles being involved), then the $C-C$ imaging situation involves a field \mathcal{E}_{eff} which depends on \mathcal{P} through the parameter

S in a manner quite analogous to what obtains in a crystal lattice; the dipoles in the inner region see image arrays of dipoles quite like those they would see if the whole structure were an infinite crystalline solid. Second, however, if one is interested in the dielectric constant where orientational polarization is involved, one must be extremely careful in making theoretical calculations to be sure that Onsager-type corrections are made in doing the thermal statistics. The point here is that, unlike the case in a solid, the infinite image arrays of dipoles faithfully follow the fluctuations of their masters on the IHP, thereby complicating the evaluation of the probability that a given dipole points in a given direction. The problem is quite difficult, and as far as we know, no one has attempted to treat it properly. However, it is very interesting, and someday such a treatment will be carried out.

7. Complications in the Compact Layer

A. Nonlinearities. Following our qualitative discussion of some of the simplest dielectric effects in the inner region, we now consider briefly some of the complicating features which might prove important in the actual system. The reader is forewarned, however, that these complications have never been considered in any treatment of the double layer thus far published; this discussion represents work which is still to be done.

In the last sections, a relationship often assumed but never derived was that the total energy of the system equals one-half the sum over all real monopole charges (not images or charges in dipoles) of the potential at the site of a monopole (excluding, however, the contribution from the monopole itself) times the charge of the monopole.

$$U = \frac{1}{2} \sum_{\substack{\text{all "real"} \\ \text{charges}}} Q_k \phi(\mathbf{r}_k) \quad (32)$$

Although this relation is widely used, its implications are not always appreciated. The relation appears "simple," yet it conceals a great deal of physics, so much so in fact, that if we start to take a closer look at the equation, our first impulse is to say that it cannot be completely correct. The expression on the right-hand side treats "real" charges completely differently from polarization

charges, the latter being involved only implicitly through their effect upon $\phi(\mathbf{r}_k)$, yet a microscopic view of nature asserts that there is no fundamental difference between the two types of charge. Specifically, it would appear at first that we have neglected the dipole-dipole interactions, for example, in calculating the total energy. Space does not permit a full discussion of all the physics concealed in this expression for energy; an adequate discussion of this is in preparation, and may appear elsewhere. For our present purposes, however, we must present some explanation of what is involved here.

What terms have been apparently neglected in the expression quoted for total electrical energy? The image charges are not included, of course, but we should not be surprised at this because the image charges are fictitious in any case. This is not a completely satisfactory explanation for their exclusion, since the potentials produced by the fictitious images are in fact produced by charges somewhere in the universe. We shall content ourselves with the above explanation, however, and proceed to the question of current interest, i.e., why have the polarization charges been excluded in the summation?

If these charges were included, each dipole would contribute a term $-\frac{1}{2}\mathbf{P} \cdot \mathcal{E}_{\text{eff}}$. We have here assumed that the dipoles are ideal and hence have set quadrupole and higher moments to zero. The factor one-half is introduced to avoid counting pair-wise interactions twice. We have already partially counted the interaction between dipoles and monopoles inasmuch as $\phi(\mathbf{r}_k)$ includes the polarization potential; furthermore, since the term $-\frac{1}{2}\mathbf{P} \cdot \mathcal{E}_{\text{eff}}$ is to be summed (in the proposed addition to the actual energy equation) over all dipoles, the factor one-half will properly do the accounting for distinct pairs. It even accounts for the reduction in interaction energy between charges and images *vis à vis* charges and charges. In summary, it would appear that the extension of the sum in the energy equation to include polarization charges would make everything exactly correct. Yet there is a contribution to the energy which we have neglected, and which under the usual (idealized) conditions will exactly cancel our proposed addition to Eq. 32.

When we consider the energy of a given polarizable element in the field \mathcal{E}_{eff} , we should include the energy of formation of the

dipole, $U_{\text{int}}(\mathbf{P})$. The total energy of that dipole would be

$$U_T = U_{\text{int}}(\mathbf{P}) - \mathbf{P} \cdot \mathcal{E}_{\text{eff}} \quad (33)$$

and the actual value assumed for \mathbf{P} is determined by the condition $\nabla_{\mathbf{P}} U_T = 0$. Thus $\nabla_{\mathbf{P}} U_{\text{int}}(\mathbf{P}) = \mathcal{E}_{\text{eff}}$ is the equation determining the polarization produced by \mathcal{E}_{eff} . Now if we make the linear assumption $\mathbf{P} = \alpha \mathcal{E}_{\text{eff}}$, we may write $\nabla_{\mathbf{P}} U_{\text{int}}(\mathbf{P}) = \alpha^{-1}\mathbf{P}$, from whence it follows that

$$U_{\text{int}}(\mathbf{P}) = \frac{1}{2}\alpha^{-1}\mathbf{P}^2 = \frac{1}{2}\mathbf{P} \cdot \mathcal{E}_{\text{eff}} \quad (34)$$

But this just cancels the term we proposed to add to the sum in Eq. 32, so Eq. 32 is correct after all. Remember, however, that such cancellation depends upon the linear assumption that $\nabla_{\mathbf{P}} \alpha = 0$; that is, that $U_{\text{int}}(\mathbf{P})$ is quadratic in \mathbf{P} . Whenever this condition breaks down, Eq. 32 is no longer correct. (It will be recalled from Section II-6 that other problems arise as well when one leaves the domain of constant α .) Now since the saturation of polarization, or departure from linearity, is more easily achieved for orientational than for electronic polarization, we must show how the foregoing remarks apply to the former type of polarization.

First remark that for the type of polarization just considered, where U_{int} depends upon \mathbf{P} and the equilibrium condition satisfied is that U_T should be a minimum, the entropy of formation of the dipoles is generally zero. Accordingly, all the properties attributed to the energy likewise apply to the free energy: It is (most conveniently) assumed quadratic in \mathbf{P} and is a minimum at given temperature for the equilibrium condition. In the case of orientational polarization, however, it is only the free energy which has these properties. There is in this case no internal energy involved in the formation of the average moment $\langle \mu \rangle$, only entropy. Correspondingly, it is not the energy which is approximately quadratic in \mathbf{P} , but the free energy. Finally (and fortunately for our discussion), the minimum principle satisfied at thermal equilibrium is that of the free energy. The rest of the discussion is exactly the same as before. When the dipoles become saturated, one leaves the linear regime and calculations become more difficult.

The presence of large fields in the compact layer, partially as a result of the "feedback" effects noted earlier, make it likely that

in some cases the nonlinearities introduced by dielectric phenomena alone (we exclude from consideration the nonlinearities of the diffuse layer, or the failure of a simple imaging model to account for that region) may cease to be negligible. The energetics of adsorption as well as motion on the IHP may be significantly altered by this phenomenon, thereby affecting the question of compact layer order as well. It provides an interesting subject for further theoretical study.

B. Solvation. We next consider how some of the foregoing observations apply to the matter of solvation of inner-layer adions. As stated before, the fields acting normal to the IHP are typically quite large enough to saturate the orientable permanent dipoles of a polar solvent. For example, water molecules with permanent dipole moments of 1.85×10^{-18} esu will saturate in fields of the order 10^5 esu, or 2×10^7 V/cm. Such a field is undoubtedly attained within the experimental range. Furthermore, the field parallel to the IHP at the position of a water molecule immediately adjacent to an adion is also of this order of magnitude. Thus, in the absence of the large normal component of field, the solvent molecules immediately surrounding an adion on the IHP would be saturated by the field of that adion. In the presence of the large normal field, the field of the adion only manages to perturb the already saturated surrounding dipoles so that they no longer point directly perpendicular to the IHP. Whether or not this perturbation is small enough to be treated by a linear approximation depends on the actual numbers involved, but we see that, under the conditions applying in the compact layer, the free energy of solvation of adions will exhibit the complexities discussed above. It is therefore of interest to obtain an expression for the free energy of an orientable permanent dipole in the orienting field \mathcal{E}_{eff} .

Proceeding as before, we argue that the equilibrium condition is satisfied whenever

$$\nabla_{\mathbf{P}} F_T = \nabla_{\mathbf{P}} F_{\text{int}}(\mathbf{P}) - \mathcal{E}_{\text{eff}} = 0 \quad (35)$$

where F_T is the free energy of the dipole and F_{int} is its internal free energy. Rewriting slightly and integrating by parts leads to

$$F_{\text{int}} = \mathbf{P} \cdot \mathcal{E}_{\text{eff}} - \int_0^{\mathcal{E}_{\text{eff}}} \mathbf{P}(\mathcal{E}') \cdot d\mathcal{E}' \quad (36)$$

Now if we make use of the classical Langevin result

$$|\mathbf{P}| = \langle \mu \rangle = \mu \{ \coth(\mu |\mathcal{E}_{\text{eff}}|/kT) - (\mu |\mathcal{E}_{\text{eff}}|/kT)^{-1} \} \quad (37)$$

then integration yields

$$F_{\text{int}} = \mu |\mathcal{E}_{\text{eff}}| \{ \coth(\mu |\mathcal{E}_{\text{eff}}|/kT) - (\mu |\mathcal{E}_{\text{eff}}|/kT)^{-1} \} \\ \times [1 + \ln \{ (\mu |\mathcal{E}_{\text{eff}}|/kT)^{-1} \sinh(\mu |\mathcal{E}_{\text{eff}}|/kT) \}] \quad (38)$$

Finally, by adding the energy of interaction $-\mathbf{P} \cdot \mathcal{E}_{\text{eff}}$, we obtain the free energy of the permanent dipole in the orienting field

$$F_T = -kT \ln \{ (\mu |\mathcal{E}_{\text{eff}}|/kT)^{-1} \sinh(\mu |\mathcal{E}_{\text{eff}}|/kT) \} \quad (39)$$

Expanding for small values of the argument gives us the following relationship exactly as anticipated,

$$F_T \doteq -\frac{1}{6} kT (\mu |\mathcal{E}_{\text{eff}}|/kT)^2 = -\frac{1}{2} \langle \mu \rangle |\mathcal{E}_{\text{eff}}| \quad (40)$$

For large values of $|\mu \mathcal{E}_{\text{eff}}/kT|$, the situation of current interest, we find the asymptotic result

$$F_T \doteq -\mu |\mathcal{E}_{\text{eff}}| + kT \ln(2\mu |\mathcal{E}_{\text{eff}}|/kT) \quad (41)$$

The first term is just the asymptotic expression for the energy of the saturated dipole, and the second term follows from the entropy removed upon orientation of the dipole. The first term is the larger of the two for large $|\mathcal{E}_{\text{eff}}|$ (in the ratio of a large number to its logarithm), implying an attractive interaction between the permanent dipole of a water molecule and adions of either sign. Note that, expressed in terms of \mathbf{P} and \mathcal{E}_{eff} , the free energy asymptotically approaches twice the value predicted by the linear (low-field) model.

Though we shall not do so here, the above results should be employed in any adequate classical treatment of adion solvation. The solvation of compact-layer ions and the steric effects accompanying this process is but another example of a process involving polarization of the neutral species which is not adequately representable by means of a dielectric constant.

III. Quantitative Discussion

1. Introduction

In the second section of this article, we have attempted to give a clear account of the principal effects active in determining the

structure and behavior of the compact double layer; at the same time, we have tried to subordinate the arithmetical details involved in actually performing accurate calculations to the more important matter of portraying the principal physical features of the double layer with reasonable fidelity.

In the present part, we turn to somewhat more quantitative matters. We shall herein augment our previous discussion by giving more attention to the quantitative aspects of two previously discussed subjects: the question of order and the role of the diffuse layer. We are still interested primarily in results rather than the methods for obtaining them, however, and it is not until Section IV of this article that we shall become primarily concerned with computational methods.

2. Examining the Question of Order

At this time of writing, the authors are aware of only two serious attempts to evaluate the appropriateness of the hexagonal array model for a system of adsorbed ions. The first of these is by the present authors (88) and titled "Thermal Stability of an Adsorbed Array of Charges in the Einstein Approximation"—hereafter referred to as TSE. The second, the paper by Bell, Mingins, and Levine (8) is "Cell and Hexagonal Lattice Models for Adsorbed Ions in Electrical Double Layer Theory," which will be hereafter referred to as CHM. A somewhat preliminary form of the latter treatment was presented at the Fourth International Conference on Surface-Active Substances (76) and contains most of the principal ideas of the expanded version.

In essence, both treatments parallel the qualitative discussion given earlier. A given ion is considered to move in the field produced by all other ions regarded as fixed at the sites of a hexagonal array. The given ion, which would reside at one of the array sites in the absence of thermal motion is considered to fluctuate about that position at finite temperatures. The central problem within this Einstein-type approximation is to determine the conditions necessary in order that the fluctuations are "small."

The actual criteria used in both TSE and CHM differ in detail somewhat from that discussed earlier in this article. In our earlier discussion, we considered a certain fluctuation in position equal to the distance from point 0 to a' , hence equal to $r_1/\sqrt{3}$. Exploiting

the fact that the activation energy for greater fluctuations than this amount rises very steeply with distance from the "proper" site, we assumed that the crossover between array structure and quasi-random arrangement should occur when the activation energy for such a fluctuation equals kT . In TSE, a somewhat smaller fluctuation was considered; the fluctuation distance was essentially taken to be $(3/4\sqrt{3})r_1$ for reasons which will become clearer later. On the other hand, the fluctuation distance involved in CHM is $(3/16\pi^2)^{1/4}r_1 \cong 0.371r_1$, again for reasons which will emerge in later discussion. We shall refer to these three fluctuations generically as "critical fluctuations." Another slight difference between the criterion in our earlier discussion and the two treatments of interest is in how the critical fluctuation enters the criterion for lattice breakdown. In our earlier discussion we asked when the critical fluctuation requires energy kT . In TSE, however, we ask, "When is the critical fluctuation equal to the actual r.m.s. fluctuation?" Finally, CHM considers the matter by asking, "When does the probability of exceeding the critical fluctuation equal one-third?" As one might expect, the overall criteria for lattice stability employed in TSE, in CHM, and in our earlier discussion are so similar that the results are essentially equivalent, and there is no strong reason for preferring one over another.

Apart from these slight differences, there are additional details in which the TSE and CHM treatments differ. Whereas $C-O$ imaging was treated in TSE, CHM contains a variety of imaging conditions, $C-C$, $C-D$, $O-D$, and $D-D$. A number of useful quantities are tabulated for each case. Second, the CHM treatment approximates the potential $\psi_a(x, y, \beta)$ by a quadratic circularly symmetric potential. Such an approximation strongly overestimates the probability of moderately large fluctuations, particularly along principal lattice directions. The TSE approach, on the other hand, is to calculate the exact r.m.s. fluctuations along particular lines of special interest and then to estimate the r.m.s. fluctuation radius from a knowledge of the fluctuations along the selected directions. This method has the advantage of properly accounting for strong variations, when they occur, from symmetric, parabolic dependence of ψ_a upon x and y , yet it requires an additional step to obtain from the data along the

selected lines the r.m.s. fluctuation radius in the full two-dimensional problem. Such an additional step becomes completely trivial as soon as the circular-symmetry assumption is employed. Finally (most important from the point of view of the final conclusions reached), the numerical values assumed in the TSE and CHM treatments for such quantities as β , γ , and, most critically, ϵ_1 are different. In TSE (applying to the C-O imaging case), the values generally assumed for ϵ_1 for adsorption from a gas or aqueous phase, respectively, were $\epsilon_1 = 2$ and $\epsilon_1 = 6$. On the other hand, the smallest value assumed for ϵ_1 in CHM was 10; data are even quoted for $\epsilon_1 = 15$ and $\epsilon_1 = 28$. In view of our earlier discussion, we now feel that for these purposes, the appropriate dielectric constant must surely be of the order of unity. In summary, the important differences between TSE and CHM are in the more generally applicable imaging assumptions of CHM and the more nearly correct (although probably still excessive) estimates of ϵ_1 in TSE. We next consider these treatments in more detail.

As noted before, the TSE treatment incorporated accurate results for the C-O imaging potential $\psi_a^0(x, y, 1)$ along selected lines to obtain the r.m.s. vibration amplitude along such lines. All distances in this treatment are normalized by $h = (\sqrt{3}r_1/2)$, the altitude of a basic triangle of side r_1 in the hexagonal array. For present purposes, we set the zero of potential at the "proper site" of the given adion on the IHP, taken here to be the origin. Denoting the normalized distance from the origin* along a given line on the IHP by $l \equiv (\text{actual distance})/(\sqrt{3}r_1/2)$, we may write the normalized r.m.s. fluctuation amplitude L according to Boltzmann statistics as

$$L \equiv \langle L^2 \rangle^{1/2} \equiv \left\{ \frac{\int_0^{l_{\max}} l^2 \exp \{ -z_v e \psi_a^0(l) / \epsilon k T \} dl}{\int_0^{l_{\max}} \exp \{ -z_v e \psi_a^0(l) / \epsilon k T \} dl} \right\}^{1/2} \quad (42)$$

The quantity ϵ is here an effective dielectric constant intended to account for polarization effects in the IHP; l_{\max} is the maximum

* In the work cited, not all lines passed through the origin, so a different definition was used for these lines; obviously, such lines are not as interesting as the ones passing through the "proper site."

excursion permitted the given ion along the selected line—it is either infinity or, for lines passing through other charge sites where the potential becomes infinite, equal to the normalized distance from the origin to the nearest such charge site.

What is the relationship between the actual two-dimensional problem and the TSE treatment which only considers one-dimensional motion along various lines? It may appear that because only one-dimensional averaging is carried out, the treatment only applies to a particle constrained to fluctuate along a line. Actually this is not the case; however, the relationship between the one-dimensional averaging and the proper two-dimensional averaging is somewhat subtle. Consider two limiting cases. In the first case, the potential is circularly symmetric, and the normalized fluctuation amplitude is equal for all directions. In this situation $L_2^2 = L_1^2 + L_1^2 = 2L_1^2$, where the subscripts here refer to the dimensionality of the problem considered; that is, L_2 is the r.m.s. amplitude in the two-dimensional problem and L_1 is the corresponding value in the artificial one-dimensional problem actually considered. In this case, which is the "worst" in the sense that all directions are equivalent and particle confinement the least, the relationship is simple; L_2 is obtained from L_1 by multiplication by $\sqrt{2}$. Consider next the opposite extreme where the potential is far from being circularly symmetric and confines the particle motion to a narrow strip about one of six equivalent directed lines. In this case, the particle actually does confine its motion effectively to one-dimensional traversal along the "easy" directions; once on one of the easy lines, it remains there until it passes near the origin, when it can jump to one of the equivalent easy lines. For this case, one would expect L_2 to approximate to L_1 ; this is the "best case". The actual situation lies somewhat between these two extremes. For small excursions about the proper site, the potential approximates to a circularly symmetric one; for large fluctuations, motion directly towards other charges in the lattice is strongly inhibited, fluctuations in these directions are strongly bounded, and the principal contribution to L_2 arises from L_1 calculated along an easy direction, a binary axis of the basic hexagonal array. As seen from Fig. 9, the difference in potential between the easy and hard directions is almost 0.1 V, or about $4kT$, at $l = 0.6$ for $R_1 = 5$, $\beta = 3 \text{ \AA}$, and $\epsilon = 1$. The difference is close to kT for an

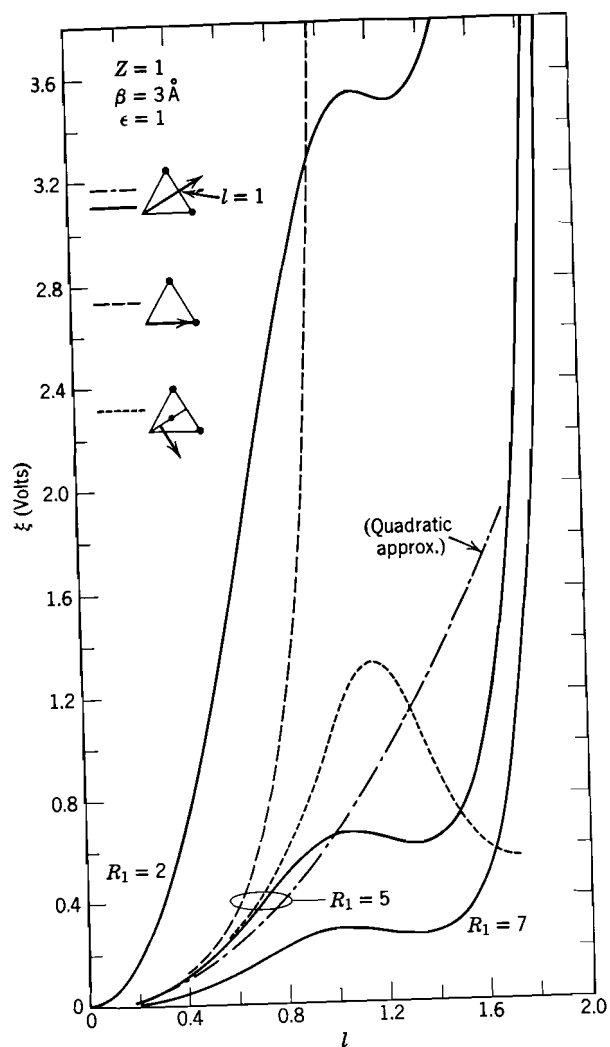


Fig. 9. The quantity $\xi \equiv \psi_a^0(X, Y, 1) - \psi_a^0(0, 0, 1)$ vs. normalized distance, $l \equiv \text{actual distance} / (\sqrt{3}r_1/2)$, measured along the heavy directed lines in the triangle diagrams (88).

l value in the vicinity of 0.5. Since the L_2 value considered critical is also 0.5 in this treatment, the circular symmetry assumption is seen to be fairly good for all fluctuations of interest. (Exactly where one should regard the symmetry assumption as being no longer adequate would, of course, depend on the values of β , ϵ , T , and R_1 as well as imaging conditions.) This serves to justify the relationship actually employed to convert from L_1 to L_2 ; if one can believe that one may carry over this result from the $C-O$ case to the $C-C$ case, this also partially justifies the much simpler and more tractable approach later published by Bell and co-workers in the CHM treatment. One should of course distinguish in principle the question of circular symmetry from that of the quadratic behavior with l of the potential, assumed in CHM. The latter behavior implies the former but is not a necessary consequence of it. Nevertheless, as a practical matter, the two conditions seem to go hand-in-hand. As we shall see later, Bell and co-workers justified their approximation to the potential in an analogous but different way.

When we combine the relation $L_2 \approx \sqrt{2}L_1$ with the TSE criterion for stability, $L_2 < 0.5$, we obtain the stability criterion in terms of L_1

$$\sqrt{\langle \rho^2 \rangle} \equiv hL_1 < (2\sqrt{2})^{-1}h \cong 0.35(\sqrt{3}r_1/2) \cong 0.306r_1 \quad (43)$$

The values obtained for L_1 (along the easy direction) are shown in Fig. 10, where ϵ has been set equal to the (excessively large) value of 6 in obtaining that data. Both the exact results and for comparison the results based on an l^2 approximation to the form of the potential, are shown for the $C-O$ imaging case considered. Also shown for comparison are the $C-D$ imaging results of Bell and co-workers. The data were obtained from the conference paper (76) adjusted to a dielectric constant value of 6, and divided by $\sqrt{2}$ for comparison with the L_1 values obtained in TSE. The greater fluctuations induced by diffuse-layer screening are quite apparent in the results.

When one incorporates the data for L_1 obtained in the TSE treatment into the lattice stability criterion, the results may be expressed in terms of the critical temperature for loss of hexagonal ordering. For $\beta = 3 \text{ \AA}$ and $C-O$ imaging, a lattice with $R_1 = 5$ is

stable up to a temperature of approximately $1760/\epsilon^\circ\text{K}$, while one with $R_1 = 7$ is stable up to about $760/\epsilon^\circ\text{K}$. Since the critical temperature is approximately quadratic in β , the above data imply that for $\beta = 2 \text{ \AA}$, the critical temperature for a lattice with

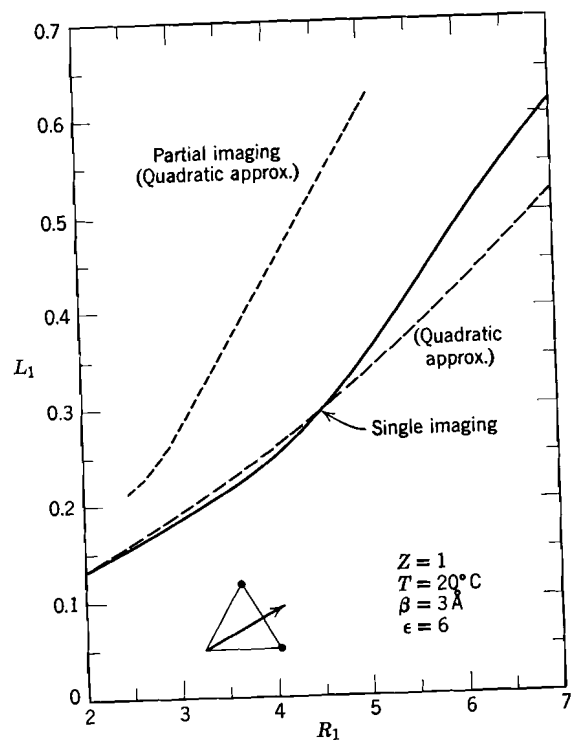


Fig. 10. The normalized r.m.s. vibration amplitude $L_1 \equiv [4(\bar{X}^2 + \bar{Y}^2)/3R_1^2]^{1/2}$ vs. $R_1 \equiv r_1/\beta$ (88).

$R_1 = 7.5$ is about $785/\epsilon^\circ\text{K}$, while for $R_1 = 10.5$ the critical temperature is about $338/\epsilon^\circ\text{K}$, somewhat above room temperature for $\epsilon = 1$. We would therefore expect the hexagonal lattice to be stable at room temperature provided $R_1 \leq 11$, according to TSE. This conclusion, which only applies in the $C-O$ situation, is in substantial agreement with our earlier discussion of lattice stability in the $C-O$ regime.

Unfortunately, no treatment along the lines of TSE has been published heretofore for the $C-C$ and $C-D$ situations. Accordingly, the only source of prior calculations pertinent to these cases is the treatment of CHM. Still, the approximations made there are likely to be quite adequate, and so with more likely values for the dielectric constant, this work should be a fairly reliable guide to the lattice stability situation in the electrolyte double layer, where single imaging seems inappropriate. It is therefore of great interest to examine this work in somewhat greater detail.

TABLE III
Results of the CHM Treatment for the $C-C$ Case

$N^{-1} (\text{\AA}^2)$	$r_1 (\text{\AA})$	R_1	$\lambda' (\epsilon = 1)$	$\sqrt{\langle \rho^2 \rangle} (\text{\AA})$	L_2
50	7.6	2.5	243	1.3	0.20
70	9.0	3.0	108	1.9	0.24
100	10.75	3.6	46	2.9	0.31
200	15.2	5.1	7.5	7.3	0.55

As we have mentioned, the CHM treatment involves approximating the potential energy variation on the IHP in the vicinity of the origin by a parabola of revolution: $z_0 e \psi_a \cong \lambda' \rho^2 + \text{constant}$, where λ' is a parameter which is obtained by expanding the accurate potential expression near the origin. In carrying out this calculation, the direct image summation method was employed by Bell and co-workers, and results were compared which involved truncation after 30 and 40 terms in the image series. In all cases, the 90 nearest neighbors and their images were included. In Table III we give results for λ' taken from the CHM treatment for $C-C$ imaging, modified here by taking $\epsilon = 1$ rather than 15. The value of β is 3 \AA .

There is a particular utility to the parabolic approximation used in CHM. When the potential varies quadratically with distance ρ from the origin, the integrals involved in the theory may be carried out analytically. The result is that we recover the equipartition result applying to quadratic contributors to the energy. Indeed, the expression for r.m.s. fluctuation simplifies to the result $(\langle \rho^2 \rangle)^{1/2} = (kT/\lambda')^{1/2}$. In the last two columns of Table III we show the normalized and unnormalized r.m.s. fluctuation amplitude following from the CHM treatment for

C-C imaging. Thus, we see from a comparison of the critical r_1 value implied by Table III (a little less than 15.2 Å) with our earlier estimate (about 14 Å) that the major difference between the CHM treatment and that contained earlier in this article is primarily not so much one of principle as what value of dielectric constant to use in the present context. The difference in viewpoint on this one matter is sufficient to cause strikingly different appraisals by the present authors *vis à vis* Bell et al. concerning the domain of validity of the hexagonal model. The CHM treatment actually considers several quantities other than the ones we have discussed here; these are all associated with the cell concept employed in that treatment, and it is most interesting to consider some of the features of this approach.

The CHM treatment invokes a concept familiar in solid state physics, that of the proximity cell.* By definition, the proximity cell associated with any given hexagonal lattice site is the locus of all points on the IHP closer to that lattice site than to any other lattice site. From its definition, it is clear that the proximity cells surrounding each lattice point are hexagons and completely fill the surface (except for a set of measure zero) like a pattern of tiles. The area of each proximity cell is equal to the average area of surface available per adion, and hence is equal to the reciprocal of the adion surface density N . One of the basic assumptions of the CHM treatment is that all the ions, including the given ion, are confined to the interiors of the proximity cells associated with their respective proper sites. We believe that there is no good reason for making such an assumption: first, because as we shall explicitly see later, the actual particle array does not maintain spatial correlation over indefinite distances (unlike a three-dimensional solid), and the hexagonal ordering is therefore only local (88); second, since each particle is not bound to a true fixed hexagonal site determined by the boundaries of the array and the remote particles as well as the near neighbors, particle motion eventually can transport a given particle indefinitely far from its original neighbors. This latter process can occur even though the local surroundings of a particle remain hexagonal during most of the time; nevertheless, the identity of the neighbors will have changed.

* In solid state physics, the term used is Wigner-Seitz cell.

Because the hexagonal boundary of the proximity cell is inconvenient in performing calculations, Bell and co-workers borrow another trick from solid state physics, this time originated by Debye in his theory of specific heats and later more explicitly employed by Wigner and Seitz to calculate approximate wave functions in solids. The hexagonal proximity cell is replaced by a circular region centered at the lattice site and having the same area as the true cell. The radius, r_M , of this circular cell is clearly $(\pi N)^{-1/2}$, or $r_M = (\sqrt{3}/2\pi)^{1/2} r_1 \equiv r_0$; it plays the same role in the statistical integrals as did l_{\max} in the TSE treatment. Clearly, from its definition, the quantity l_{\max} represents a true limit to the particle motion for the situation considered, whereas r_M represents an artificially imposed restriction. The use of r_M rather than l_{\max} has the effect of underestimating the magnitude of fluctuations by constraining the particles to the interiors of their cells. On the other hand, the error made is quite small unless there is significant probability for fluctuations larger than r_M ; when this situation occurs the fluctuations have broken down the lattice structure in any case and the whole calculation is pointless. As a practical matter then, the use made of r_M is permissible provided one does not apply the calculation in the regime where the Einstein model itself is nonsense, the quasi-random regime. Since the treatment is only intended to demonstrate approximately where the hexagonal lattice begins to break down and not the properties of the system after that disorganization has been significantly accomplished, logical consistency is maintained.

Next, the CHM treatment defines a critical fluctuation radius equal to $(2)^{-1/2} r_M$. This radius has the property of dividing the circular cell into two equal-area halves. Bell and co-workers finally assert that the lattice structure will break down when the probability of the ion's occupying the outer half (the annular ring) is just greater than one-half the probability of occupying the inner half (the interior of the circle of radius $r_M/\sqrt{2}$). Defining the ratio of the probabilities of occupation as \hat{p} (termed "p" in CHM), we have $\hat{p} \equiv (\text{probability of occupying outer half})/(\text{probability of occupying inner half})$. The CHM criterion for lattice breakdown is then $\hat{p} > \frac{1}{2}$. Actually, the probability of exceeding the critical fluctuation radius is, in terms of \hat{p} , equal to $\hat{p}(1 + \hat{p})^{-1}$. Thus, the CHM criterion is somewhat more stringent than it first might

appear and perhaps more stringent than intended. The probability for exceeding the critical fluctuation must be greater than $\frac{1}{2}(1 + \frac{1}{2})^{-1}$, or $\frac{1}{3}$.

Finally, Bell et al. use a peculiar procedure to test the validity of their parabolic approximation. They calculate the potential at various points on the IHP arising only from the six nearest neighbors, excluding the contributions from images. They then compare this potential with the value obtained from their parabolic approximation at various points. They conclude from the fact that agreement is fairly good within most of the proximity cell (whose boundary is the inner hexagon in Fig. 11), that the parabolic

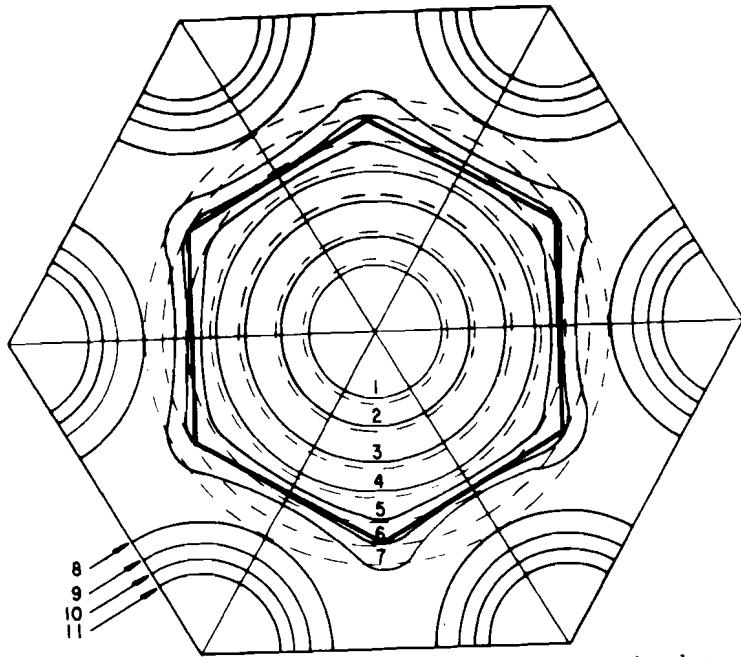


Fig. 11. Contours of equal electrostatic energy of interaction between a mobile ion and its six nearest neighbors (without images) in the region between the central lattice point and the six nearest lattice points. Full curves are accurate energy contours; dashed curves are energy contours following from parabolic approximation. The energy of interaction at the center is $6z_0^2 e^2 / \epsilon_1 r_1$ and the numbers correspond respectively to (1) 6.02, (2) 6.1, (3) 6.2, (4) 6.3, (5) 6.4, (6) 6.5, (7) 6.6, (8) 7.0, (9) 7.5, (10) 8.0, (11) 8.5 in units of $z_0^2 e^2 / \epsilon_1 r_1$. The heavy hexagon shows the boundary of the central proximity cell (8,76).

approximation likewise applies to the full $C-C$ problem. Unfortunately, we cannot agree with Bell and his co-workers that this argument is a cogent one. The effect of imaging is to alter strikingly the potential variation in the plane as we have already seen (refer also to Section V). For example, if one computes the actual $C-C$ potentials for a hexagonal array with $R_1 = 5$ at the points c' and a' , these (normalized) potentials are respectively 0.0177 and 0.0395 higher than that at point 0. Since the distances of these two points from the origin are in the ratio of 1:2, the potentials relative to the origin should be in the ratio of 1:4 if the parabolic approximation is valid. Instead their ratio is 1:2.23, and if an exponent is derived from this, one finds that the average power law applying from the origin to a proximity cell vertex is $\psi(\rho) = A_1 + A_2 \rho^{1.16}$, where A_1 and A_2 are constants. This points up the desirability of a closer check on the CHM treatment.

As a short digression, we remark that there is a much simpler method of determining the parameter λ' than that used by Bell et al. From Laplace's equation as it pertains to a point on a symmetry line parallel to the z axis, we may write immediately

$$\psi(\rho, z) \cong \psi(0, z) - \frac{1}{4} [\partial^2 \psi(0, z) / \partial z^2] \rho^2 \quad (44)$$

where ρ is the distance of the field point from the symmetry line, and thus the argument "zero" in ψ on the right-hand side designates that the quantity is to be evaluated on the line of symmetry. This equation, essentially a recipe for λ' , is more general than any recipe applying only at the IHP or on the line through 0. It applies for any z and on any axis of n -fold rotational symmetry,* the only place where such a parabolic behavior may apply. Its particular advantage lies in the relative simplicity of calculating values of ψ on lines of symmetry as compared with calculating ψ at a general point. Things are particularly simple if we retain only the leading term in the separated form of the general solution of Laplace's equation under $C-C$ imaging conditions. The leading term has a z -dependence given by $\sin(\pi z/d)$, whence $\partial^2 \psi / \partial z^2 = -(\pi/d)^2 \psi$. Introducing this approximation into Eq. 44 yields the

* We exclude the trivial case $n = 1$; for $n = 2$, λ' depends on direction, and our formula gives the average value.

beautifully simple

$$\psi(\hat{\rho}, z) \cong \psi(0, z) \{1 + (\pi\hat{\rho}/2d)^2\} \quad (45)$$

From this result it follows that $\lambda' \cong (\pi/2d)^2 z_0 e \psi(0, z)$.

To conclude this section on lattice stability, we shall briefly point out the interesting possibilities for applying another type of basic approximation rather than the Einstein model. In the Einstein model, the different ions were considered to move independently in the potential provided, on the average, by the other ions. For small motions of the ions, we even ignore the small effect upon the time-average local potentials of the smearing out of all the ions into small neighborhoods of their proper sites. In a three-dimensional problem, we should have argued that since the slight smearing is almost spherically symmetric, there will be no effect anyway. In the present system we are not so fortunate, for the potential arising from a small disk of charge is only approximately equal to the potential obtaining when all such charge is regarded as concentrated at the center. Furthermore, the screening effect of the diffuse layer will cause the approximation to be even poorer. Nonetheless, being a bit lazy, we prefer to argue that for small enough fluctuations, the alterations brought about by this effect will be negligible, that it is a "higher-order effect." This is by no means an unprecedented approach—it is not necessarily all bad, it simply has its limitations.

Rather than embark upon a laborious program for correcting the "small" errors in the Einstein model, it might be just as easy to employ another approach which to some extent takes into account the correlations in particle motions as well as the simultaneity of their motions. This approach is the phonon picture, harmonic approximation, or normal-mode method (14, 109, 110, 132). What it involves is a solution of the coupled equations of motion for small displacements; it generally describes the vector displacement directions and frequencies versus wave-vector \mathbf{k} for wave disturbances proportional to $\exp i\{\mathbf{k} \cdot \mathbf{r}\}$. At thermal equilibrium, the energy contained in each mode is determined from an Einstein-Bose distribution, and for all modes for which the circular frequency ω is much less than kT/h , the equipartition principle applies. The energy in each such mode is kT .

Consider such modes, which can be analyzed classically.

The total energy contained in a mode will be given by $E_i = \frac{1}{2} N_0 m \omega_i^2 |A_i|^2$, where $m \equiv$ the mass of each particle, $N_0 \equiv$ total number of particles in the system, $\omega_i \equiv$ circular frequency of the mode, and $A_i \equiv$ complex amplitude of the mode. The equipartition principle tells us that $|A_i|^2 = 2kT/N_0 m \omega_i^2$. Given this fact, the frequencies $\{\omega_i\}$, and the reasonable assumption that the phases of the different modes are uncorrelated, one can in principle determine many thermal-equilibrium expectation values for various quantities of interest. We shall not say much more about this here, but we are presently working along this vein and hope to present a detailed treatment in the future. For the present, we shall merely illustrate some particular consequences of the phonon approach.

Let us ask what is the mean-square fluctuation in the position of the particle whose proper site is the origin according to the phonon picture. Each mode contributes its A_i to the displacement; the expectation value for the square of the particle displacement is therefore

$$\langle \rho^2 \rangle = \sum_i \sum_j \langle A_i A_j^* \rangle = \sum_i \langle |A_i|^2 \rangle \quad (46)$$

the sums being over modes and the expectation values for cross-terms, $\langle A_i A_j^* \rangle$ with $i \neq j$, vanishing by the random-phase assumption. We next consider the contribution to $\langle \rho^2 \rangle$ from the "acoustic branch," modes for which $\omega = S\kappa$, where S is the speed of the wave with wave-number κ . We find

$$\langle \rho^2 \rangle = \sum_i 2kT/N_0 m \omega_i^2 = (2kT/N_0 m S^2) \sum_i \kappa_i^{-2} \quad (47)$$

Now the number of acoustic modes with wave number between κ and $\kappa + d\kappa$ will be proportional to N_0 and to κ : something like $(2\pi N)^{-1} N_0 \kappa d\kappa$, where N is the surface density of particles. Changing the sum to an integral then yields

$$\langle \rho^2 \rangle = (kT/\pi m N S^2) \int_0^{\kappa_{\max}} \kappa^{-1} d\kappa \quad (48)$$

where actually we are not interested now in the factor outside the integral but only in the form of the integral. The quantity κ_{\max} is determined from the microscopic structure of the system; this does not interest us here either. All that we are concerned with here is the logarithmic divergence of the integral coming from the lower

end of integration (where our expression for ω applies). There is no way of arguing the lower limit of integration effectively away from zero provided we are dealing with a truly macroscopic system. The prediction is unequivocal. The long wavelength types of collective motion contribute a divergent amount to the thermal motion of a given ion away from its proper site. This would not have occurred in a three-dimensional system, where the number of modes in the wave number range $d\kappa$ about κ is proportional to κ^2 , but here we are definitely stuck with the divergence.

But what is the physical meaning of such powerful long-wavelength oscillations? Such motions merely translate large sections of surface relative to other very remote sections of surface without significantly affecting the relative positions of closer neighboring particles. Hence, these modes do not affect the local environment of a particle even though they do allow it (and its neighbors) to work its way through the large collection of particles in a Brownian motion fashion: many "microcrystals" moving relative to each other, diffusing away from their starting points, occasionally exchanging member particles where their (fuzzy) boundaries meet, but each one a microcosmos, containing whatever internal order in its constituent particles is allowed by the amplitude of the short-wavelength modes, which, of course, do not contribute any divergences (88). Such is our physical picture of the two-dimensional system we treat, this picture obtained in the most painless way from the phonon method.

3. Diffuse-Layer Screening

In the previous sections, we have repeatedly been concerned with the screening effects the diffuse layer provides, both from dielectric imaging and from the effects of mobile ions near the OHP. In the present section, we examine a few aspects of such screening which did not seem appropriate to include in our earlier discussion. First, we will consider the effect upon screening of $\Gamma \neq 1$. Next, we examine the restrictions on the validity of the Poisson-Boltzmann equation (23,55), in connection with the statistical treatments of the diffuse layer. Finally, we shall briefly discuss the usual sort of approximations involved in such statistical treatments. The discussion of the diffuse layer will be brief, first

because this article is really concerned primarily with the compact layer, and second because the usual approximations seem to us to be so unphysical and inappropriate that the subject itself is not one of our favorites.

We have already pointed out that for given d , the combined causes leading to diffuse-layer screening have their maximum effect for $\Gamma = 1$ and for $C-C$ imaging are invariant under the interchange $\beta \leftrightarrow \gamma$. Therefore, in the preceding discussion where the choice $\beta = \gamma$, or $\Gamma = 1$, was made the diffuse-layer screening effects were at their maximum, particularly significant with regard to lattice stability. What we now consider is how the screening effects depend on γ for given β .

It is most convenient to return to the matter of the interaction energy between two adions separated by the distance r_1 and conductively imaged both by the ESP and by the OHP. We shall take $\epsilon_1 = 1$ for our present discussion. Using the results of Appendix I, we have calculated the normalized interaction U/kT as a function of r_1 for various values of γ , $T = 300^\circ\text{K}$ and $\beta = 2 \text{ \AA}$. (The interaction energy is proportional to β^{-1} for given $R_1 = r_1/\beta$ and Γ , so the conversion to another temperature or β value may be easily accomplished.) As anticipated, the approximately exponential drop in interaction energy with particle separation is characterized by a "relaxation length," or characteristic screening distance of the order $2d/\pi$. Hence as γ is increased, the slope of $\ln(U/kT)$ vs. R_1 decreases in absolute value as anticipated. An interesting consequence of this behavior is that for larger and larger values of Γ the critical value of R_1 , termed here R_c , at which U/kT becomes unity is shifted upwards. Based on our earlier discussion of U/kT for $C-O$ imaging, we would anticipate that as $\Gamma \rightarrow \infty$, the value of R_c should approach the $C-O$ result: $R_c \rightarrow 8.2$. The results for R_c summarized in Table IV seem to verify this limiting behavior.

In Table IV we have also shown values of the function $G(\Gamma) \equiv R_c/3.6$, which is the ratio of R_c for a general value of Γ to that for $\Gamma = 1$. It should be a reasonable approximation to obtain r.m.s. fluctuation distances, crossover values of R_1 , coulombic hard-core diameters, and the like for $\Gamma \neq 1$ simply by multiplying the appropriate $\Gamma = 1$ value by the function $G(\Gamma)$. Note that the value of R_c for $\Gamma = 1$ differs slightly from that used elsewhere in

this article; the present value, $R_c = 3.6$, is the more accurate. Because of the possible usefulness of $G(\Gamma)$, we have also obtained a Chebychev rational function fit to the tabular data with the result

$$G(\Gamma) \cong 2.28 - \frac{117 + 0.24\Gamma}{65.4 + 10.8\Gamma + \Gamma^2} \quad (49)$$

Such a function will prove particularly significant for any situation where the effective imaging plane differs appreciably from the conventionally defined OHP.

TABLE IV
Effect of Γ upon Screening

Γ	R_c	$G(\Gamma)$	Γ	R_c	$G(\Gamma)$
$\frac{1}{2}$	2.7	0.75	3	5.6	1.56
1	3.6	1.0	6	6.93	1.93
$1\frac{1}{2}$	4.25	1.18	12	7.75	2.15
2	4.8	1.33	24	8.0	2.22
$2\frac{1}{2}$	5.25	1.46	∞	8.2	2.28

Much of the theory of the diffuse layer has invoked the Poisson-Boltzmann equation (13,16,37,62,63,67,68,71,78,116,120,122,129,131), so we will now examine briefly the approximations inherent in such an equation and attempt to assess its validity in describing the diffuse layer in the vicinity of adsorbed charges on the IHP. Much of our discussion here is directly analogous to that concerning the concept of a dielectric constant.

In using the Poisson-Boltzmann equation, one first ignores discreteness of charge in the statistical assemblage of particles, approximating the actual particle distributions in that assemblage by continuous smoothly varying functions. For positive ions the spatial distribution function may be written $\rho_+(\mathbf{r})$; for negative ions, $\rho_-(\mathbf{r})$. Thus, in this section ρ denotes a particle number density, not a distance. The charge distribution is therefore taken to be the smoothly varying function $e\rho_+(\mathbf{r}) - e\rho_-(\mathbf{r})$, where for convenience we consider only a uni-univalent electrolyte with $|z_v| = 1$. Note that although we still may allow for the presence of discrete charged particles, such as adions, which are not regarded

as part of the present statistical assemblage, the diffuse-layer ions are smoothed out into a continuous distribution. The smoothed electrical potential therefore obeys the equation

$$\nabla^2\psi = (4\pi e/\epsilon_s)[\rho_-(\mathbf{r}) - \rho_+(\mathbf{r})] \quad (50)$$

The next step is to assert that the distributions obey the Boltzmann law, which we write approximately in a form consistent with our smoothed potential

$$\rho_{\pm} = \rho_0 \exp \{ \mp e\psi(\mathbf{r})/kT \} \quad (51)$$

where we have defined ρ_0 to be the density of either species at a point where the potential vanishes, taken here to be the remote bulk of the electrolyte.

On combining the two equations, one finds the usual result,

$$\nabla^2\psi(\mathbf{r}) = (8\pi\rho_0 e/\epsilon_s) \sinh \{ e\psi(\mathbf{r})/kT \} \quad (52)$$

This equation is so often employed as the starting point for statistical theories of the diffuse layer that it seems almost heretical to remark its approximate character. Nonetheless, there are clearly several assumptions* involved if the Poisson-Boltzmann equation is to adequately describe the system.

First, if "local field corrections," or "fluctuation potentials" as they are sometimes called, are to be unimportant, we require that the potential at \mathbf{r} arise predominantly from those charges other than the closest neighbors. If this condition were not fulfilled, then the actual potential at \mathbf{r} would have very little to do with $\rho_{\pm}(\mathbf{r})$ but would mainly involve the detailed locations of the close neighbors to \mathbf{r} . Since the actual potential at \mathbf{r} and not some sort of smoothed ψ is what properly enters into the Boltzmann expression, we clearly require that over most of a microscopically large neighborhood of \mathbf{r} , the actual potential should not fluctuate by an amount significant compared with (kT/e) if the Poisson-Boltzmann equation is to hold. From this restriction, we obtain two necessary conditions. Since the fluctuation potential is at least $e\rho^{1/3}/\epsilon_s$, where ρ is the larger of ρ_+ and ρ_- , we find that ρ_{\pm} must nowhere exceed the value implied by the inequality $(e^2 \rho^{1/3}/kT\epsilon_s) \ll 1$.

* We will allow here the assumption of a well-defined dielectric constant ϵ_s , inasmuch as this type of approximation has been flogged enough herein already.

Introducing the concept of a local Debye length

$$\lambda_D(\mathbf{r}) \equiv (kT\epsilon_s/4\pi e^2)^{1/2}\{|\rho_+| + |\rho_-|\}^{-1/2} \quad (53)$$

we may rewrite the above inequality in the form $[r_1/\lambda_D(\mathbf{r})] \ll 1$ where r_1 is here the mean separation distance between diffuse-layer ions. The Debye sphere of radius $\lambda_D(\mathbf{r})$ must everywhere contain many ions. The second necessary condition follows from the condition for validity of the Boltzmann statistics, that ψ should be essentially constant over a microscopically large region, a region containing many particles. We have that $\rho^{-1/3} |\nabla\psi| \ll kT/e$. However, ψ includes the effects of external charges; so specializing to the case of a single adsorbed adion imaged in the ESP, we would have $\psi_{\text{ext}}(\mathbf{r}) \cong 2z_0 e\beta z/\epsilon_s r^3$, where the origin is at the ESP on the line connecting the adion with its image. (Note that we do not consider the effect of diffuse-layer ions here; there is no need to do so, since we are only determining roughly the rapidity of variation of ψ near an adion, and the effect of the diffuse layer is to increase the rate of such variation in any case.) We find that

$$|\nabla\psi| = 2|z_0| e\beta(1 + 3z^2/r^2)^{1/2}/\epsilon_s r^3 \cong 3|z_0| e\beta/\epsilon_s r^3 \quad (54)$$

Finally, our necessary condition for this case becomes

$$(3|z_0| e^2\beta r_1/\epsilon_s r^3 kT) \ll 1 \quad (55)$$

where the meaning of r_1 here is the same as just above. Again using the concept of a local Debye length, this time evaluated in the vicinity of the adsorbed ion, we find that in order for the Poisson-Boltzmann equation to apply it is necessary that we consider no values of \mathbf{r} smaller than those satisfying the inequality $r^3 \gg \beta r_1^2 (r_1/\lambda_D)^2$. Finally, the maximum density of ions must not be so large that short-range forces become important.

When all of the foregoing conditions are satisfied, the Poisson-Boltzmann equation approaches exactitude. Unfortunately, in the vicinity of the OHP, particularly near an adsorbed ion, these conditions fail very badly in almost every case of interest, thereby vitiating all theories based on this approach in this regime.

In spite of the limitations of the Poisson-Boltzmann approach for our present system, we go on to consider a popular approximate method of solving this equation when an infinitesimal perturbation is applied. The method is useful when it is applicable; again, because the actual "perturbations" involved near adsorbed

ions happen to be quite large (we leave this for the reader to verify), the method seems inapplicable here, even if the Poisson-Boltzmann equation itself were a good approximation.

The essence of Loeb's linearization method (77,78,129) consists in the following. Suppose we have found a solution to a Poisson-Boltzmann problem which we designate by a superscript 0. That is,

$$\rho_{\pm}^0 = \rho_0 \exp\{\mp e\psi^0(\mathbf{r})/kT\} \quad (56)$$

$$\nabla^2\psi^0 = -(4\pi e/\epsilon_s)\{\rho_+^0(\mathbf{r}) - \rho_-^0(\mathbf{r})\} \quad (57)$$

What will occur if we change ψ by an infinitesimal amount by bringing up* an external charge? The potential ψ will become $\psi^0 + \delta\psi$, the particle densities will become $\rho_{\pm}^0 + \delta\rho_{\pm}$, and presumably the Poisson-Boltzmann equation will still apply to the modified quantities.

On writing $\rho_{\pm}^0 + \delta\rho_{\pm} = \rho_0 \exp\{\mp e[\psi^0(\mathbf{r}) + \delta\psi(\mathbf{r})]/kT\}$ and expanding for $|e\delta\psi/kT| \ll 1$, one obtains

$$\rho_{\pm}^0 + \delta\rho_{\pm} \cong \rho_0 \exp\{\mp e\psi^0(\mathbf{r})/kT\}\{1 \mp e\delta\psi/kT\} \quad (58)$$

therefore

$$\begin{aligned} \delta\rho_{\pm} &\cong \mp \rho_0 \exp\{\mp e\psi^0(\mathbf{r})/kT\} e\delta\psi(\mathbf{r})/kT \\ &= \mp e\rho_{\pm}^0 \delta\psi(\mathbf{r})/kT \end{aligned} \quad (59)$$

The linearity of the Poisson equation gives

$$\nabla^2(\delta\psi) = (-4\pi e/\epsilon_s)\{\delta\rho_+(\mathbf{r}) - \delta\rho_-(\mathbf{r})\} \quad (60)$$

Combining these equations leads to an equation for the perturbation potential

$$\nabla^2(\delta\psi) = (4\pi e^2/\epsilon_s kT)\{\rho_+^0(\mathbf{r}) + \rho_-^0(\mathbf{r})\} \delta\psi \quad (61)$$

It is readily seen that in terms of the local Debye length, this equation may also be written $\nabla^2(\delta\psi) = \lambda_D^{-2}(\mathbf{r}) \delta\psi$, clearly exhibiting the perturbation approach from which it was obtained.

We next mention another type of perturbation procedure favored by some (17,121), but which in its application here generally suffers from the same drawbacks. The typical expansion parameters are not small, but often much greater than unity.

* For simplicity, we only consider regions in the system where the external charge density vanishes; the approach is not restricted to this, however.

The approach in question is commonly known as the cluster expansion method, was introduced by Ursel, Yvon, Mayer, and others, and represents a brick in the rapidly growing edifice of modern statistical mechanics. There are several related computational techniques in this field, and each technique has its own set of boring (but useful) theorems, graphical representations, and proponents. The general outlook for the growth in our ability to do the bookkeeping and arithmetic associated with many-body systems is very hopeful. However, there is always the danger that some of us will learn the arithmetic and the formalism for performing the bookkeeping, and give insufficient attention to the physics of the situation, the validity of the approximations, etc. This is a temptation which is hardest to resist when the formalism itself has a certain beauty and the investigator the sophistication to appreciate it.

The cluster expansion method relies upon the fact that the partition function \mathcal{Z} involves the pairwise interactions U_{ij} between particles i and j in the following manner

$$\begin{aligned}\mathcal{Z} &= \sum_{\substack{\text{All system} \\ \text{configurations} \\ \text{(ASC)}}} \exp \{-U_{\text{total}}/kT\} \\ &= \sum_{\text{ASC}} \exp \left\{ -\frac{1}{kT} \sum_{(i<j)} U_{ij} \right\}\end{aligned}\quad (62)$$

One defines the Mayer f -bond f_{ij} according to the equation

$$f_{ij} \equiv \exp \{-U_{ij}/kT\} - 1 \quad (63)$$

from whence we find

$$\mathcal{Z} = \sum_{\substack{\text{ASC} \\ (i<j)}} \prod_{i,j} (1 + f_{ij}) = \int d^3r_1 \int d^3r_2 \dots \int d^3r_N \prod_{\substack{i,j \\ (i<j)}} (1 + f_{ij}) \quad (64)$$

Now the cluster expansion procedure extracts out of the product of $N(N-1)/2$ factors all of those terms containing zero, one, two, three, etc., f -bonds. All but a few of the integrations may be carried out for these early terms in the expansion (yielding system volume raised to a power) and one is left with "simple" integrals

to do, involving the interactions between only a few particles. The method is particularly suitable for short-range forces. One notes that $|f_{ij}|$ is guaranteed to be less than unity, so there is no great problem there. Occasionally the method is used in conjunction with approximations to f_{ij} , however, and then the expansion obtained may actually be in terms of a large parameter. For example a possible but hazardous procedure is to replace the proper definition of the f -bond by the linearized approximation $f_{ij} \cong -U_{ij}/kT$ valid for $|U_{ij}| \ll kT$. This is most dangerous for strong long-range interactions such as the Coulomb interaction $U_{\text{int}} - (U_{\text{int}}/kT)$ is roughly $500r^{-1}$ for two charges separated by distance r (in Angstroms) at 300°K with $\epsilon = 1$; for $\epsilon = 80$, the quantity U_{int}/kT is greater than unity for all $r < 6.25 \text{ \AA}$. In any given problem, one must naturally consider the strength of the interactions, including the moderating effects present, before making approximations of this kind. Finally, it sometimes happens that the basic cluster expansion is very slow to converge, even without making the linearized approximation. This occurs whenever f_{ij} drops off so slowly with particle separation (as a result of a long-range interaction) that for the first terms in the cluster expansion the growing number of equivalent permutations (among the ij indices involved in a product of f -bonds) dominates, and the magnitudes of successive terms may at first actually increase. This behavior is similar to what occurs when a large number L is considered in the series expansion of $e^L = 1 + L + (2!)^{-1}L^2 + (3!)^{-1}L^3 + \dots$. Under such circumstances the cluster expansion method becomes difficult to apply in a meaningful way.

To close this section on the diffuse layer, we give a crude derivation (using the foregoing types of approximations which we do not believe in) of the effective plane modification presumably first calculated by Levine, Mingins, and Bell (77). The present derivation is our own; it is so crude that we feel compelled to claim it lest Levine and co-workers or some other innocent persons be unjustly associated with it. Still, we believe that the present derivation contains most of the basic ingredients contained in the other more carefully prepared treatments.

Consider a single adion on the IHP and for simplicity consider the ESP as nonimaging. Let the ion charge density (not number density) in the diffuse layer be given by $\rho(\mathbf{r})$. Now assume that

$\rho(\mathbf{r})$ is approximately of the form

$$\rho(\mathbf{r}) = -e\chi(x, y, z)f(z) \quad (65)$$

where $-e\chi(x, y, z)$ is the surface charge density which would be induced on a perfect conductor by a charge e at the point $(0, 0, -\gamma)$; the origin is taken here as lying on the OHP. Under such circumstances, each plane slab of the diffuse layer of thickness dz acts like a metal conductor, except that the images produced are not of the usual full magnitude. The total potential is evidently

$$\begin{aligned} \phi = & e\{x^2 + y^2 + (z + \gamma)^2\}^{-1/2} \\ & - e\{x^2 + y^2 + (z + \gamma)^2\}^{-1/2} \int_0^z f(\zeta) d\zeta \\ & - e \int_z^\infty d\zeta f(\zeta) \{ [2\zeta + \gamma - z]^2 + x^2 + y^2 \}^{-1/2} \end{aligned} \quad (66)$$

Using the fact that

$$\int_0^\infty f(z) dz = 1$$

we rewrite Eq. 66 as

$$\begin{aligned} \phi = & e \int_z^\infty f(\zeta) d\zeta \{ [x^2 + y^2 + (z + \gamma)^2]^{-1/2} \\ & - [x^2 + y^2 + (2\zeta + \gamma - z)^2]^{-1/2} \} \end{aligned} \quad (67)$$

Specializing to the case $x = y = 0$ and expanding for large γ , we obtain the simple approximation

$$\phi \cong 2e\gamma^{-2} \int_z^\infty d\zeta f(\zeta) (\zeta - z) \quad (68)$$

But since $\chi(0, 0, z) = [2\pi(\gamma + z)^2]^{-1}$ and the charge density obtained from linearizing the Poisson-Boltzmann equation is $\rho \cong -2c_0e^2\phi/kT$, where c_0 is the bulk ionic concentration, we obtain

$$f(z) \cong [4\pi c_0 e(\gamma + z)^2/kT] \phi \quad (69)$$

On inserting our expression for ϕ , we find the integral equation

$$f(z) = (8\pi c_0 e^2/kT)(1 + 2z/\gamma) \int_z^\infty d\zeta (\zeta - z) f(\zeta) \quad (70)$$

But

$$\int_z^\infty d\zeta (\zeta - z) f(\zeta) \equiv \int_\infty^z d\zeta' \int_\infty^{\zeta'} d\zeta'' f(\zeta'') \quad (71)$$

therefore by neglecting $2z$ compared with γ , consistent with our earlier approximation, we are able to write down a very simple differential equation for f

$$(kT/8\pi c_0 e^2)(\partial^2 f/\partial z^2) = f(z) \quad (72)$$

from whence it follows that

$$f(z) = \lambda_D^{-1} \exp(-z/\lambda_D) \quad (73)$$

where λ_D is here the bulk Debye length. The average plane of the induced charge thus lies a distance λ_D behind the OHP. Within our approximations, to the left of the OHP the total potential is

$$\phi \cong e\{x^2 + y^2 + (z + \gamma)^2\}^{-1/2} - e\{x^2 + y^2 + (z - 2\lambda_D)^2\}^{-1/2} \quad (74)$$

This essentially represents the modification in the effective position of the imaging plane derived by Levine et al. The only real difference between our result and that of Levine and co-workers is that in the latter work the Debye length which is involved is evaluated at a point in the diffuse layer where the potential reaches a certain finite value. In view of the approximations involved in the approach, this distinction is not likely to be of practical significance.

IV. Methodology

1. Some Exact Array Methods

In the discussion up until now, we have suggested that provided the arrangement of adions on the IHP is known and the actions of the electrode and diffuse layer is representable by some type of imaging at the ESP and on or near the OHP, the determination of the local potential becomes simply a matter of arithmetic. While this may be true, the arithmetical problem of computing such potentials is a practical matter of some difficulty. Several procedures have evolved for performing such calculations readily, and we here present the most widely used methods in just enough detail that the reader may recognize possible applications to other problems as they arise. References 86 and 126 contain useful reviews of the subject.

The least useful method of all, generally speaking, is to perform the unmodified array sums coming out of the image treatment. These sums too often converge so slowly that accurate results are difficult to obtain even with the aid of large digital computers. The simplest array sum to perform, it would appear, would be the expression for the field at point 0 arising from an array of adions singly imaged in a conducting electrode, considered to form with their images an ideal dipole array. Yet, the first evaluation of this quantity seems to have been by Topping (125), who employed analytical methods based on formulae of Lennard-Jones and Ingham applying to the generalized zeta-functions of Epstein. According to Topping, the field at a vacancy site in an otherwise complete hexagonal array of dipoles, each of moment P , is given by $\mathcal{E} \cong -11.034176Pr_1^{-3}$. In Section IV-2 of this paper, we shall see how knowledge of this exact but rather limited result is of great assistance in developing approximate methods for computing potentials in a much wider class of imaging situations and for other than ideal dipole arrays.

We shall be discussing methods of obtaining potentials for $C-C$ and $C-D$ imaging. Before doing so, it is necessary to point out a somewhat troublesome distinction between the discrete adion-image potentials appropriate in the $C-C$ case and the potentials appropriate for $C-D$ imaging in the limiting case $\epsilon_s \rightarrow \infty$. We have already remarked that given the arrangement of adions on the IHP and the mean charge density q on the ESP, the total potential $\psi = \psi_a + \psi_e$ is the same for $C-C$ imaging as it is for the $C-D$ case with $\epsilon_s \rightarrow \infty$. On the other hand, we have seen that the condition $\psi_e = 0$ for $C-C$ imaging obtains when q and q_1 are related by $q + \lambda q_1 = 0$; in contrast, the $\psi_e = 0$ condition is met under $C-D$ imaging when $q + q_1 = 0$. Thus the ψ_a potentials for $C-C$ and $C-D$ imaging, though both referring to the potentials produced by the adions and the infinite set of images, equal the total potential under different ESP charge conditions. Put another way, if the ESP is grounded and the OHP is the surface of a dielectric whose dielectric constant is as large as we please, the surface charge density on the ESP is just the negative of q_1 provided there is no free charge on the dielectric surface. This is a description of the conditions pertaining under $C-D$ imaging conditions when $\psi = \psi_a$. If instead of a dielectric, a perfect

grounded conductor is substituted, charge will flow between the two conductors such that only the fraction γ/d of the charge $-q_1$ will remain on the ESP; the remainder will reside on the OHP. Under these new circumstances $\psi = \psi_a$ again, and we have $C-C$ imaging. To distinguish these two different ψ_a potentials, we shall refer to the $C-C$ imaging ψ_a with a superscript two, thus $\psi_a^{(2)}$; similarly, the $\omega = 1$ $C-D$ ψ_a will be designated $\psi_a^{(1)}$. The relation between the two is readily obtained in a number of ways with the result (91)

$$\psi_a^{(2)}(x, y, z) = \psi_a^{(1)}(x, y, z) - 4\pi q_1(1 + \Gamma)^{-1}z \quad (75)$$

In normalized form this relation becomes

$$\Psi_a^{(2)} = \Psi_a^{(1)} - Z/Z_0 \quad (76)$$

Now which of the two potentials one obtains if he sets the $C-D$ imaging parameter $\omega \equiv (\epsilon_s - \epsilon_1)/(\epsilon_s + \epsilon_1)$ directly equal to unity, rather than taking the limit $\omega \rightarrow 1$, depends upon how the calculation is carried out. It turns out that the series we shall develop for the $C-D$ imaging case are only conditionally convergent at $\omega = 1$; however, the particular grouping of terms actually employed will always give $\psi_a^{(1)}$, even for $\omega \equiv 1$. Physically a dielectric, no matter how strong, is fundamentally different from an ideal conductor; only the latter has mobile free charge on its surface, and the boundary conditions applying at the surface of a dielectric of arbitrary strength are different from those applying at a conductor. But the important thing to know here is not just why $\psi_a^{(1)}$ and $\psi_a^{(2)}$ should differ, but which of the two our equations are producing at any given time. It would be disastrous to combine $\psi_a^{(1)}$ with a $\psi_e \equiv -4\pi(q + \lambda q_1)z$ to get a total ψ , for example; this is the reason we tossed in the "extra" uniform field part in Eq. 22 early in this article.

The method of calculating $C-C$, $C-D$, and $D-D$ potentials which seems most popular, particularly among the Russian workers (60,71,131), is what we shall term the Green's function approach (GFA). In the GFA one first determines in some manner or other an expression for the potential everywhere due to a single unit charge on the IHP; this potential is required to be an actual solution to the problem in the sense that all boundary

conditions are satisfied, yet we must not write this solution in the form of an infinite-image sum. The last restriction is simply to avoid arriving back at our starting point, an infinite-image array triple summation. We have already employed this single charge solution, or Green's function, for the $C-C$ case. It is the solution derived in Appendix I; it still involves a single summation, but the summation is now a rapidly convergent one and generally may be truncated after the first few terms.* The actual array potential is then obtained from a further two-dimensional sum. Thus, if the Green's function evaluated at \mathbf{r} is designated $\mathcal{G}(\mathbf{r}, \mathbf{r}')$, where the charge is placed at \mathbf{r}' , then for an array of charges whose positions on the IHP are the set $\{\mathbf{r}'_{mn}\}$, the discrete potential is

$$\psi_a^{(2)}(\mathbf{r}) = z_a e \sum_m \sum_n \mathcal{G}(\mathbf{r}, \mathbf{r}'_{mn}) \quad (77)$$

In our $C-C$ imaging case, Appendix I gives

$$\mathcal{G}(\mathbf{r}, \mathbf{r}'_{mn}) = 4d^{-1} \sum_{p=1}^{\infty} \sin\left(\frac{\pi p}{1+\Gamma}\right) \sin(\pi d^{-1} p z) K_0(\pi d^{-1} p \rho_{mn}) \quad (78)$$

where

$$\rho_{mn} \equiv \{(x - x'_{mn})^2 + (y - y'_{mn})^2\}^{1/2} \quad (79)$$

$$\mathbf{r} \equiv (x, y, z) \quad (80)$$

and

$$\mathbf{r}'_{mn} \equiv (x'_{mn}, y'_{mn}, \beta) \quad (81)$$

The GFA would be unattractive were it not for the fact that the remaining sum over the two-dimensional array may generally be truncated after a few terms as a result of screened behavior of \mathcal{G} ; that is, \mathcal{G} rapidly approaches zero for large ρ . One has reduced the problem to that of evaluating a triple sum, rapidly convergent in all indices of summation.

The GFA applied to the $C-D$ case is less attractive from the point of view of actually performing computations. The problem lies, of course, in the less convenient form of the Green's function. It is now a Fourier-Bessel integral rather than a discrete sum, and

* The only way to fully appreciate the improvement over the direct image sequence is to attempt a hand calculation of the potential using both the image series and the Green's function series.

is given by

$$\begin{aligned} \mathcal{G}(\mathbf{r}, \mathbf{r}'_{mn}) = & - \int_0^{\infty} d\lambda J_0(\lambda \rho_{mn}) \{ [\omega - \exp(2\lambda d)]^{-1} \\ & \times [\{\omega - \exp(2\lambda \gamma)\} \exp\{-\lambda(z - \beta)\} \\ & + \omega [1 - \exp(2\lambda \beta)] \exp\{\lambda(z - \beta)\}] \\ & - \exp\{-\lambda|z - \beta|\} \} \end{aligned} \quad (82)$$

Since the Green's function must still be summed over m and n , it is questionable how much has been accomplished by this approach.*

An easily applied method of computation pertinent to the regular lattice structures for the $C-C$ imaging case, which has been employed by the present authors, derives from the Ewald method for calculating lattice sums in crystals (35). This useful method was placed in a broader, more general perspective by Nijboer and de Wette (99) and stimulated by their work several generalizations have recently appeared, notably by Adler (1) Grant (54), and the present authors (5). The basic approach involved in the generalized Ewald method (GEM) is described below.

First one writes the sum to be evaluated,

$$S \equiv \sum_{\mathbf{k}} f(\mathbf{R}_{\mathbf{k}})$$

in the form

$$S = \sum_{\mathbf{k}} f(\mathbf{R}_{\mathbf{k}}) \Phi(\mathbf{R}_{\mathbf{k}}, s) + \sum_{\mathbf{k}} f(\mathbf{R}_{\mathbf{k}}) \{1 - \Phi(\mathbf{R}_{\mathbf{k}}, s)\} \quad (83)$$

where the sums are over the three-dimensional regular lattice points $\{\mathbf{R}_{\mathbf{k}}\}$, and the function Φ is chosen so as to make the second sum converge rapidly; this function may depend on a parameter s which is chosen conveniently. The remaining problem is to evaluate the first sum, which still converges slowly.

This may readily be accomplished with the aid of a three-dimensional analog to the Poisson summation formula. Writing the Fourier transform of $f(\mathbf{R}) \Phi(\mathbf{R}, s)$

$$G(\boldsymbol{\lambda}, s) \equiv \int d^3 R f(\mathbf{R}) \Phi(\mathbf{R}, s) \exp\{2\pi i \boldsymbol{\lambda} \cdot \mathbf{R}\} \quad (84)$$

this analog reads

$$\sum_{\mathbf{k}} f(\mathbf{R}_{\mathbf{k}}) \Phi(\mathbf{R}_{\mathbf{k}}, s) = |\mathbf{a}_1 \cdot \mathbf{a}_2 \times \mathbf{a}_3|^{-1} \sum_{\mathbf{k}} G(\boldsymbol{\lambda}_{\mathbf{k}}, s) \quad (85)$$

* Notice, however, that in principle the GFA may be applied even when the adions do not form a regular lattice, hence its popularity in statistical theory.

where the vectors $\{\lambda_k\}$ are the reciprocal lattice vectors and $\mathbf{a}_1, \mathbf{a}_2,$ and \mathbf{a}_3 are the basic lattice vectors of the actual array. In terms of the \mathbf{a} vectors

$$\lambda_k \equiv |\mathbf{a}_1 \cdot \mathbf{a}_2 \times \mathbf{a}_3|^{-1} \{k_1 \mathbf{a}_2 \times \mathbf{a}_3 + k_2 \mathbf{a}_3 \times \mathbf{a}_1 + k_3 \mathbf{a}_1 \times \mathbf{a}_2\} \quad (86)$$

where $k_1, k_2,$ and k_3 are integers.

Finally, one chooses s such that the convergence of

$$\sum_k f(\mathbf{R}_k) \{1 - \Phi(\mathbf{R}_k, s)\}$$

as well as

$$|\mathbf{a}_1 \cdot \mathbf{a}_2 \times \mathbf{a}_3|^{-1} \sum_k G(\lambda_k, s)$$

is rapid.

We have applied these steps to find the potential arising from a hexagonal array of ions under $C-C$ imaging conditions omitting the effect of the ion on the line through the origin but for reasons of convenience retaining the effect of its images. The function Φ was chosen to be the error function. After considerable manipulation and choosing the origin of coordinates at the missing adion site, the result is the following (5).

$$\begin{aligned} \phi_a(\mathbf{r}) = & I_1(\mathbf{r}, s) - z_v e \left| (1 + \Gamma)^{-1} \mathbf{a}_3 + \mathbf{r} \right|^{-1} \\ & + z_v e \sum_k \left\{ \frac{\operatorname{erfc}(\pi^{1/2} s^{-1} |\mathbf{R}_k - \mathbf{r}|)}{|\mathbf{R}_k - \mathbf{r}|} \right. \\ & \left. - \frac{\operatorname{erfc}(\pi^{1/2} s^{-1} |\mathbf{R}_k - (1 + \Gamma)^{-1} \mathbf{a}_3 - \mathbf{r}|)}{|\mathbf{R}_k - (1 + \Gamma)^{-1} \mathbf{a}_3 - \mathbf{r}|} \right\} \quad (87) \end{aligned}$$

where the summation excludes the point at the origin, the vector \mathbf{a}_3 lies in the z direction and is of length $2d$, and

$$\operatorname{erfc}(x) \equiv 1 - \operatorname{erf}(x) \equiv 1 - 2\pi^{-1/2} \int_0^x \exp(-t^2) dt \quad (88)$$

The quantity I_1 is evaluated by taking Fourier transforms

$$\begin{aligned} I_1(\mathbf{r}, s) = & \frac{1}{3} z_v e d^{-1} \sqrt{3} \sum_k \pi^{-1} |\lambda_k|^{-2} \exp\{-\pi s^2 |\lambda_k|^2\} \\ & \times \{ \exp\{-2\pi i \lambda_k \cdot \mathbf{r}\} \\ & - \exp\{-2\pi i \lambda_k \cdot [\mathbf{r} + (1 + \Gamma)^{-1} \mathbf{a}_3]\} \} \\ & - \pi^{-1/2} z_v e \left[|\mathbf{r}|^{-1} \gamma\left(\frac{1}{2}, \pi s^{-2} |\mathbf{r}|^2\right) \right. \\ & \left. - \frac{\gamma\left(\frac{1}{2}, \pi s^{-2} |\mathbf{r} + (1 + \Gamma)^{-1} \mathbf{a}_3|^2\right)}{|\mathbf{r} + (1 + \Gamma)^{-1} \mathbf{a}_3|} \right] \quad (89) \end{aligned}$$

Again the sum excludes the point at the origin; the γ -function in general is related to the incomplete Γ -function: $\gamma(n, x) \equiv \Gamma(n) - \Gamma(n, x)$; for $n = \frac{1}{2}$, $\gamma(\frac{1}{2}, x^2) \equiv \pi^{1/2} \operatorname{erf}(x)$.

Having come so far, the work is not finished, as one still requires convenient expressions for the vector dot products and cross products which occur. This is a matter too boring to discuss here, and the reader is referred to the original literature.

Having found ϕ_a in order to find ψ_a , one must still subtract out the effect of the line of images through the origin. There are special means of doing this in terms of ψ -functions for special choices of \mathbf{r} ; however, in general we may make use of the Green's function discussed earlier to effect this subtraction, provided we are careful to note that the Green's function includes the potential of an ion at the origin. As a practical matter, more heroic efforts may be needed in determining ψ_a from ϕ_a very near the missing adion but not on the normal line through its site. Again, such details are inappropriate to consider here.

As we shall see, the $C-D$ imaging case is most easily treated by summing $C-O$ imaging results, therefore we next consider exact methods for computing $C-O$ imaging potentials.

Although the GEM with certain modifications is applicable to the case of $C-O$ imaging, we have found that the best technique for this case is one described for other series by van der Hoff and Benson (127), presumably originated by Mackenzie (93), which is based on Jacobi's imaginary transformation for theta-functions. The method converges most rapidly for $R_1 \rightarrow 0$ and results in an almost closed form expression for the potential, with the remaining summations contributing small amounts generally. The basic ingredients of the method, denoted here as the MHB method, are described below (6,86).

First, one writes all inverse powers of distances, which occur in the image sum for potential, in terms of an integral by means of the identity

$$x^{-n} \equiv \frac{1}{\Gamma(n)} \int_0^\infty t^{n-1} \exp(-xt) dt \quad (90)$$

which follows from the definition of the Γ -function. The number n is typically one-half, and x is here the square of the distance between the field point and a given source point (adion or image).

The next MHB identity which one finds handy if he is alert to the opportunities present is

$$\sum_{m=-\infty}^{\infty} \exp\{-(m+a)^2 t\} \equiv (\pi/t)^{1/2} \sum_{m=-\infty}^{\infty} \exp\{-\pi^2 m^2/t\} \cos(2\pi am) \quad (91)$$

This quantity will come from the factor $\exp(-xt)$ in the integral, and one will be left with something akin to

$$\sum_{m=-\infty}^{\infty} \frac{\pi^{1/2}}{\Gamma(n)} \int_0^{\infty} t^{n-3/2} \exp\left\{-k^2 t - \frac{\pi^2 m^2}{t}\right\} dt$$

where additional factors independent of t may appear.

Third, one exploits the fact that the integral is expressible in closed form; it involves the ubiquitous modified Bessel functions of the third kind. In particular

$$\int_0^{\infty} t^{n-3/2} \exp\left\{-k^2 t - \frac{\pi^2 m^2}{t}\right\} dt \equiv 2 \left(\frac{\pi |m|}{k}\right)^{n-1/2} K_{n-1/2}(2\pi k |m|) \quad (92)$$

Finally, one performs the summations; one of the original indices of summation remains, and the other summation has been accelerated by the transformation effected by the MHB. Again the double sum remaining is rapidly convergent in both indices. The "almost closed form" of the expression for potential is associated with the single sum over the leading term ($m=0$) of the transformed series. Generally, some care is required to evaluate this leading term, taking proper limits and that sort of thing; however, the final result is well worth the effort. With this road map we now exhibit in greater detail how the MHB has been used to find the potential $\psi_{aic}(\mathbf{r})$ arising from a complete lattice of adions singly imaged in the ESP. It is of course a trivial matter to relate this to the incomplete lattice potential ψ_a .

If we place the origin of coordinates on the ESP as is the usual convention in this article and express the adion-image summation in rectangular coordinates we may write

$$\psi_{aic}(\mathbf{r}) = z_v e \beta^{-1} \sum_{l=-\infty}^{\infty} \sum_{m=-\infty}^{\infty} [S_0^- - S_0^+ + S_1^- - S_1^+] \quad (93)$$

where

$$S_r^{\pm} \equiv \left[\left(\frac{X}{R_1} - l - \frac{r}{2} \right)^2 + \left(\frac{Y}{R_1} - \sqrt{3}m - \frac{\sqrt{3}}{2}r \right)^2 + \left(\frac{Z \pm 1}{R_1} \right)^2 \right]^{-1/2} \quad (94)$$

If we define $P_r^{\pm} \equiv [S_r^{\pm}]^{-2}$, then the expression for ψ_{aic} involves $(P_r^{\pm})^{-1/2}$ and we may use the first of our identities

$$\psi_{aic}(\mathbf{r}) = \pi^{-1/2} r_1^{-1} z_v e \sum_{l=-\infty}^{\infty} \sum_{m=-\infty}^{\infty} \left\{ \int_0^{\infty} [\exp(-P_0^- t) - \exp(-P_0^+ t)] \right. \\ \left. + \exp(-P_1^- t) - \exp(-P_1^+ t)] t^{-1/2} dt \right\} \quad (95)$$

We next perform the summation over l only by factoring out of the exponentials that part which is independent of l and employing the second of the identities. This yields

$$\psi_{aic}(\mathbf{r}) = z_v e r_1^{-1} \sum_{m=-\infty}^{\infty} \sum_{s=-\infty}^{\infty} \int_0^{\infty} \{ \exp(-V_0^-) - \exp(-V_0^+) \\ + (-1)^s [\exp(-V_1^-) - \exp(-V_1^+)] \} t^{-1} \cos\left(2\pi s \frac{X}{R_1}\right) dt \quad (96)$$

where

$$V_r^{\pm} \equiv \left[\left(\frac{Y}{R_1} - \sqrt{3}m - \frac{\sqrt{3}}{2}r \right)^2 + \left(\frac{Z \pm 1}{R_1} \right)^2 \right] t - \frac{\pi^2 s^2}{t} \quad (97)$$

Next, we use the third identity to evaluate the integral, and obtain

$$\psi_{aic}(\mathbf{r}) = 2 z_v e r_1^{-1} \sum_{m=-\infty}^{\infty} \sum_{s=-\infty}^{\infty} \{ K_0(T_{m0}^-) - K_0(T_{m0}^+) \\ + (-1)^s [K_0(T_{m1}^-) - K_0(T_{m1}^+)] \} \cos\left(2\pi s \frac{X}{R_1}\right) \quad (98)$$

where

$$T_{mr}^{\pm} \equiv 2\pi |s| \{ [\sqrt{3}(m + \frac{1}{2}r) - R_1^{-1}Y]^2 + [R_1^{-1}(Z \pm 1)]^2 \}^{1/2} \quad (99)$$

If one now evaluates the $s=0$ terms by taking limits, it is possible

to rewrite ψ_{aic} in the form

$$\psi_{aic}(\mathbf{r}) = 4z_v e\tau_1^{-1} \left\{ \sum_{m=-\infty}^{\infty} \sum_{s=1}^{\infty} \cos\left(2\pi s \frac{X}{R_1}\right) \{K_0(T_{m0}^-) - K_0(T_{m0}^+)\} \right. \\ \left. + (-1)^s [K_0(T_{m1}^-) - K_0(T_{m1}^+)] \right\} + \frac{1}{2} \sum_{m=-\infty}^{\infty} \ln \left\{ \frac{T_{m0}^+ T_{m1}^+}{T_{m0}^- T_{m1}^-} \right\} \quad (100)$$

The final single summation may be expressed in closed form as

$$2z_v e\tau_1^{-1} \sum_{m=-\infty}^{\infty} \ln \left\{ \frac{T_{m0}^+ T_{m1}^+}{T_{m0}^- T_{m1}^-} \right\} \\ = z_v e\tau_1^{-1} \ln \left\{ \frac{\cosh\{4\pi(Z+1)/R_1\sqrt{3}\} - \cos(4\pi Y/R_1\sqrt{3})}{\cosh\{4\pi(Z-1)/R_1\sqrt{3}\} - \cos(4\pi Y/R_1\sqrt{3})} \right\} \quad (101)$$

The above expression is the MHB closed form part of ψ_{aic} which generally dominates; it only applies for $Z \neq 1$ when $Y = 0$, and special procedures are necessary to transform the result to a form useable for $Z = 1 = Y = 0$. These procedures merely involve taking several limits, and will be allowed to rest undisturbed in reference 6, where the interested reader may find them detailed.

Finally, we consider the case of $C-D$ imaging. It should be abundantly clear from an examination of Fig. 1 of reference 91 that the potential ψ_a applying in the $C-D$ regime is expressible in terms of a superposition of $C-O$ potentials. This type of superposition was also employed qualitatively by Grahame in his treatment (52) of $C-C$ imaging. The present superposition must take the diminishing dipole moment magnitudes into account. In particular, in the inner region, the infinite set of apparent nonideal dipole arrays lying about the planes $z = \pm 2nd$ produces the potential

$$\sum_{n=1}^{\infty} \omega^n \{ \psi_a^0(x, y, z + 2nd) - \psi_a^0(x, y, 2nd - z) \}$$

The real adions and their direct images produce the potential $\psi_a^0(x, y, z)$; hence the total ψ_a potential is given by

$$\psi_a(x, y, z) = \psi_a^0(x, y, z) \\ + \sum_{n=1}^{\infty} \omega^n \{ \psi_a^0(x, y, z + 2nd) - \psi_a^0(x, y, 2nd - z) \} \quad (102)$$

If one has an adequate method of obtaining ψ_a^0 , the $C-O$ potential for a lattice with a single vacancy, then one may readily determine the $C-D$ potential. But of course we have just described a method of determining ψ_{aic} , from which ψ_a^0 is obtained trivially by subtracting out the potential due to a single adion and its image. Therefore, the MHB method provides us with the solution for the $C-D$ case as well as the $C-O$. (As a matter of interest, note that the potentials ψ_{aic} could be used in the $C-D$ summation and the line of images of the missing adion itself subtracted out of the final answer in one step by use of the $C-D$ Green's function.)

To complete our $C-D$ imaging discussion we note from Fig. 2 of reference 91 that in the region $z \geq d$, the potential ψ_a is simply due to the "apparent nonideal dipole arrays." Thus, in this region

$$\psi_a(x, y, z) = (\eta\epsilon_1/\epsilon_s) \sum_{n=0}^{\infty} \omega^n \psi_a^0(x, y, z + 2nd) \quad (103)$$

where $\eta\epsilon_1/\epsilon_s \equiv 1 - \omega$.

To complete this section on exact methods, we merely remark that there are always certain inelegant procedures available for exact computation when all the clever methods have failed. We may always perform an unmodified sum for awhile and approximate the remainder by an integral, for example. This method is somewhat related to certain approximation techniques discussed in the next section. Another approach is to modify the terms in the series by a convergence factor, calculate the sum for several values of the parameter involved in this factor, and extrapolate through the range where the sum becomes slowly convergent again, all the way to where the convergence factor becomes unity. Such extrapolations are often long, and one frequently needs recourse to an extrapolation aid such as the ϵ -algorithm (83) in order to carry it through. Such methods as these last described may not be as elegant as some, but for some future problems we may need to depend on them nonetheless.

2. Approximate Methods

The first part of this section will be concerned with approximate methods of calculating potentials arising from fixed, known distributions of ions. For several cases of prime interest in the

electrolyte situation, the methods discussed later in this section are much superior to those first discussed, and therefore, the initial discussion will be relatively brief.

One way of evaluating a lattice sum is just to numerically sum the terms of the original series until the remainder becomes negligible. This method is unavailable for the triply infinite series of the hexagonal-array $C-C$ imaging situation. The series is only conditionally convergent, and many millions of terms would be required to be summed with very great accuracy (in the proper sequence) before the remainder could be neglected for R_1 values of interest. In this case, then, the methods discussed in the preceding section of transforming a series to one of more rapid convergence are essential if accurate numerical values are required (5).

Grahame (52) has applied the direct summation method for single imaging, where the series involved is only doubly infinite. His results are approximately 4% too small in magnitude, showing that summation was ended too soon.

Another method, which has been widely applied both for single imaging (45,119,123) and for NaCl-type solids (126,127), is that of direct summation of the first few terms of the series in question, then the approximation of the remaining terms by an integral. This method thus smears out the charges whose contribution is replaced by the integral. Although this approach should be capable of good accuracy, it has sometimes led to rather poor correspondence between accurate and approximate results (6).

Stigter (119) has applied the above method to find the potential at point 0 and $Z = 1$ for a plane hexagonal array of charges. He first divided the array into equivalent charge groups by means of a series of concentric circles centered at 0. Each circular annulus contained only charges of equal distance from 0. Stigter then compared the results obtained for the contribution of successively distant groups of equivalent neighbors calculated by direct summation and by integration. The normalized results, written as (exact, smeared), found were (10.39, 13.20), (5.20, 5.47), (7.86, 7.73), and (5.77, 5.93) for the first 6, next 6, next 12, and next 12 equivalent charges. We see that there still remains almost a 3% error between the discrete and smeared results for the last group. Further, the error in the last group is nearly twice as large as that

present between the two results for the preceding group. Nevertheless, Stigter concluded that sufficient accuracy could be obtained by summing only the contributions from the first six (nearest) neighbors, then accounting for the rest of the charges by smearing and integration. Had a nonideal dipole single-image situation been appropriate, much better results could have been obtained from this general procedure, as we shall see.

Since the simplest way to calculate potentials and fields for $\omega \neq 0$ is to make use of $\omega = 0$ single-imaging results, as we have demonstrated in Section IV-1, it is important to have available as simple methods as possible for calculating the underlying single imaging quantities needed when $\omega \neq 0$. In the general case of X, Y, Z arbitrary, the complicated exact $\omega = 0$ results discussed in Section IV-1 must be used for hexagonal-array calculations. When $\xi \gg 1$, the series contributions become negligible, however, and only an easily handled closed form expression remains. Further, for $X = Y = 0$ (point 0) or point a and a few other high symmetry positions, a much simpler and approximate, but highly accurate, approach may be used which applies for all ξ .

The approximate method is based on Grahame's (52) pioneering cutoff approach but extends it considerably. Grahame considered a single-imaging situation such as that of Fig. 26*b*; i.e., $O-C$ imaging. For convenience, we shall instead illustrate the approach using imaging at a conducting ESP, $C-O$ imaging. Grahame replaced the discrete planar distributions of nonpolarizable adions and their images by smeared uniform charge sheets, each containing a colinear, circular, charge-free hole having its center on the line through 0. His method is thus a degenerate form of the summation-integration approach already discussed. He used a hole radius, r_0 , associated with the average circular area available to a single charge. Throughout this article, we shall use r_0 , and $R_0 \equiv r_0/\beta$ for this Grahame radius, which necessarily satisfies the relation $\pi r_0^2 N = 1$. We may also write $q_1 \cong 510 z_0 r_0^{-2}$ when q_1 is expressed in $\mu\text{coul}/\text{cm}^2$ and r_0 in Angstroms. We shall frequently use the hexagonal-array nearest-neighbor distance, r_1 , as a convenient measure of q_1 even in situations where a rigid array is not appropriate. Then $r_0 = (\sqrt{3}/2\pi)^{1/2} r_1 \cong 0.5250376 r_1$, and $q_1 \cong 1850 z_0 r_1^{-2}$ with q_1 in $\mu\text{coul}/\text{cm}^2$ and r_1 in Angstroms.

Although the Grahame model takes discreteness into account to some extent, its applicability to a real situation needs establishing. Grahame himself pointed out the way to do this by comparing cutoff model predictions with those of a hexagonal array. As we shall see later, his treatment was approximate and incorrect in part but his general idea was correct. In most of the work of Levine and his associates, the Grahame cutoff model has been used without adequate examination of its applicability and sometimes without reference to Grahame. Recently, however, Levine, Mingins, and Bell (77) have examined the applicability of the model to some extent, and generalized it in a semiquantitative way. This work will be discussed at some length in Section V-2-D.

The present authors (90-92) have followed Grahame's lead and shown in detail some of the deficiencies of the ordinary cutoff model and how it may be modified to yield hexagonal-array potentials and fields with high accuracy and concomitant ease of calculation. Consider a cutoff model with two parallel circular areas of the same but arbitrary radius, r_b . It is easy to show by integration that when $q = -q_1$, one obtains

$$\Psi_a^0(Z, R_b) = \frac{1}{2} \{ [R_b^2 + (Z + 1)^2]^{1/2} - [R_b^2 + (Z - 1)^2]^{1/2} \} \quad (104)$$

where the superscript 0 again denotes single imaging, $\Psi_a^0 \equiv \psi_a^0/\psi_\infty$, $R_b \equiv r_b/\beta$, and $Z \equiv z/\beta$ is measured from the imaging ESP as usual. This result applies to a nonideal dipole situation; of course the equation will still apply when one array of charges is not made up of images but of real charges. It is also useful to consider the transformation of Eq. 104 which takes place when the nonideal dipoles formed by an adion and its image become ideal dipoles. To effect this change, let $\beta \rightarrow 0$ and $R_b \rightarrow \infty$ but hold the dipole moment, $\mu \equiv 2z_0 e \beta$, constant. Then ψ_∞ , originally $4\pi z_0 c N \beta / \epsilon_1$, becomes $2\pi N \mu / \epsilon_1$, and Eq. 104 transforms to

$$\Psi_a^0(z, r_1) = [1 + (r_b/z)^2]^{-1/2} \quad (105)$$

We have termed the use of a cutoff model with a disposable r_b , not necessarily equal to r_0 , the modified cutoff approach (90,91). Let us now see what form the modifications take for a rigid hexagonal array of nonideal (and ideal) dipoles. Let us write $p(\xi) \equiv r_b/r_1$, where $\xi \equiv z/r_1$, equal to Z/R_1 when $\beta \neq 0$. For

numerous values of ξ and R_1 , we have used (90) our accurate hexagonal-array single-imaging results (6) to calculate the function $p(\xi, R_1)$, usually abbreviated here as $p(\xi)$ or even p , which allows the above cutoff formulas with r_b replaced by $p(\xi)r_1$ to yield highly accurate hexagonal lattice potentials. Some of the

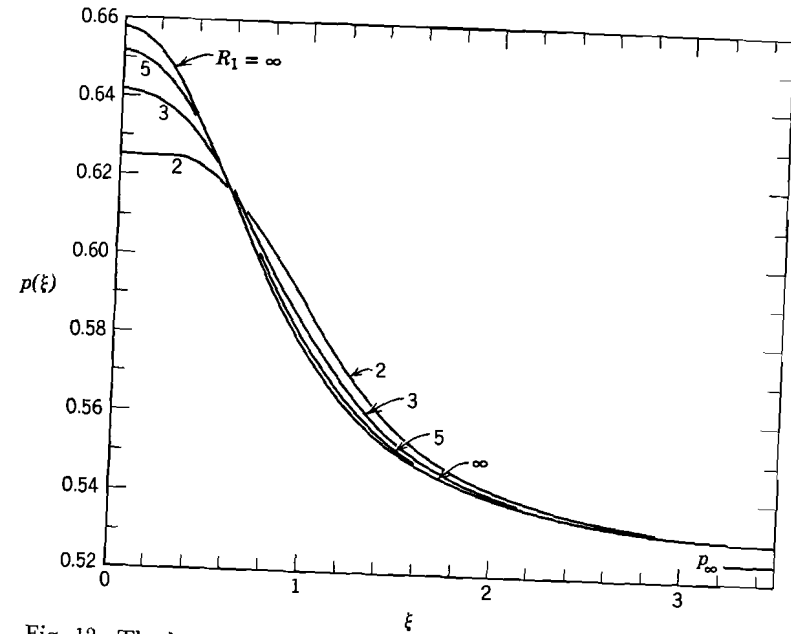


Fig. 12. The hexagonal array function $p(\xi) \equiv r_b/r_1$ for $R_1 = 2, 3, 5$, and ∞ (ideal dipoles) plotted with an expanded ordinate scale (90).

results of such calculations are illustrated in Fig. 12. The smallest possible value of r_1 , r_{1m} , enforced by the steric hard-core repulsion between ions, is usually approximately an ionic diameter.

Note the expanded ordinate scale of Fig. 12. Evidently, $p(\xi)$ need not vary over a very wide scale to allow the modified cutoff formulas to yield hexagonal-array results. Further, the variation with R_1 is even much less than that with ξ . The $R_1 = \infty$ curve is for ideal dipoles; the $p(\xi)$ shown enters Eq. 105 through $(r_b/z) \equiv (r_1/z)p(\xi) = \xi^{-1}p(\xi)$. The smallest value of p is $p_\infty \equiv r_0/r_1 = (\sqrt{3}/2\pi)^{1/2} \cong 0.525$, which follows from Grahame's choice for r_0 .

This value is only appropriate when $\xi \rightarrow \infty$ (hence the subscript for p), a condition of practical importance only when $z \gg r_1$. But when $z \gg r_1$, $\Psi_a \cong 1$; thus, the original Grahame value, p_∞ , is hardly ever needed when dealing with a hexagonal array. In contradistinction, the $\xi \rightarrow 0$ limiting value of the ideal dipole curve, $p_0 = 4\pi/\sqrt{3}\sigma \cong 0.6575206$, turns out to be quite appropriate since many actual double-layer situations may be well approximated by the ideal dipole limit. Here, the quantity $\sigma \cong 11.0341754$ is the Topping lattice sum (125,127) given by $\sigma = r_1^3 \sum_i r_i^{-3}$. The distance r_i is that between the i th point in a fixed plane hexagonal array of nearest-neighbor distance r_1 and point 0 of the lattice. The index i ranges over all points in the infinite array but 0.

In the present article, we omit much discussion of field calculations. It should be mentioned, however, that the original paper (90) discusses how hexagonal-array fields may be obtained from the modified cutoff approach using $p(\xi)$ and its logarithmic derivative $-F \equiv d \ln p(\xi)/d \ln \xi$. Further, when it is desired to simplify the calculation of Ψ_a^0 by ignoring the variation of p completely, the earlier work gives best least-squares values of p to use in various situations. A best choice for all ξ and R_1 combinations of experimental interest is 0.607, not very far from p_0 . Although the curves of Fig. 12 should yield sufficiently accurate values of $p(\xi)$ for most calculations, occasions arise when greater accuracy is needed. We have, therefore, published (90,91) a number of rational function approximations of the Chebyshev type to $p(\xi)$ and $F(\xi)$ for several fixed values of R_1 (ξ variable) and for $Z = 1$ (R_1 variable). These provide even greater accuracy in single image calculations when needed.

The curves of Fig. 12 need not extend beyond $\xi = 3.5$ because for larger values exceedingly accurate closed-form expressions for the point 0 may be derived from the exact single-image results (6). These expressions are (90)

$$\Psi_a^0(Z, R_1) \cong 1 - (\sqrt{3}/4\pi)[R_1^2/(Z^2 - 1)] \quad (106)$$

and

$$\Psi_a^0(z, r_1) \cong 1 - (\sqrt{3}/4\pi)\xi^{-2} \quad (107)$$

for nonideal and ideal dipoles, respectively. They hold to within one part in 10^7 or 10^8 for $Z \cong 1 + 3R_1$ in the nonideal case and

for $\xi \approx 3$ for ideal dipoles and are even more accurate for larger ξ values.

We have seen how the cutoff approach may be modified to deal with a rigid hexagonal array. It turns out that its applicability may be extended even beyond the hexagonal-array regime. We have stated elsewhere (90,92) and show explicitly in Appendix II that the mean distance, $\langle r_1 \rangle$, of nearest neighbors for a random array without interactions between the discrete elements of the array is $(4N)^{-1/2}$. If we set $\langle r_1 \rangle = r_b$ for such an array, then the corresponding p is approximately 0.465, even smaller than p_∞ . We do not expect to see such behavior, however, even at the highest possible temperatures because of the hard-core repulsion between adions. In the high-temperature limit (abbreviated HTL) situation, the nearest distance of approach of adsorbed ions will be r_{1m} . Let us consider identical, spherical adions with charge centroids at the sphere centers. The presence of a given adion at point d then ensures that the charge centroids of neighboring adions remain on or outside a circle of radius r_{1m} centered on d . Further, at high temperatures, the planar motion of the adsorbed charges may be considered quasi-random; the discrete charge will be smeared, or space averaged, over the time required for a measurement. Notice now, however, that we have just described the physical conditions of a cutoff model with $r_b \equiv r_{1m}$. Thus, in the HTL, the cutoff model with $r_b = r_{1m}$ should be fully applicable, not approximate (92). Observe that with this value of r_b and $Z = 1$, the cutoff Eq. 104 reduces to the expression already given for this case, Eq. 6.

If a fully close-packed adion array could be achieved, it would be hexagonal with $r_1 = r_{1m}$. The corresponding value of r_b would, however, be $p(\xi_m)r_{1m}$ here, where $\xi_m \equiv z/r_{1m}$. We have taken this full monolayer condition to correspond to $\theta = 1$. We may therefore write $\theta \equiv |q_1/q_{1\max}| \equiv (r_{1m}/r_1)^2$, or $(R_{1m}/R_1)^2$ for nonideal dipoles. As we have seen, however, the $\theta = 1$ limit will not usually be reached in an electrolyte adsorption situation because of Coulomb repulsion between adions. The earlier discussion shows that such repulsion leads to a coulombic hard core of diameter r_c . Although r_c varies with temperature, reducing to r_{1m} in the HTL if $r_c > r_{1m}$ at low temperatures, and with ESP and OHP shielding conditions as well, it is a useful concept.

If $r_c > r_{1m}$, as seems to be the case except for the largest ions under $C-C$ imaging, then the maximum possible value of θ at a given temperature will be about $(r_{1m}/r_c)^2$. If one tries to increase N beyond this limit, breakdown and discharge will occur and the electrode will not remain blocking to charges.

At ordinary temperatures and closest enforceable packing, the adion array will be essentially hexagonal with r_1 equal to the larger of r_{1m} and r_c . We shall assume r_c the larger from now on. As we have seen, as N decreases at constant temperature from that corresponding to r_c , a value will be reached where hexagonal structure begins to disappear. Then occurs a transition region where long-range coulombic interactions still remain of some importance. Finally, even smaller N or $|q_1|$ leads on to the quasi-random region, which we shall term the low-density limit (LDL) regime. In this region, the widely separated adions move essentially independently except for the short-range coulomb interactions represented by r_c which come into play when two charges happen to approach one another closely. We see that this situation may also be represented, essentially exactly, with a cutoff model for which $r_b \equiv r_c$. We qualify the word "exactly" here because there is a certain arbitrariness in the definition of r_c . The ESP-OHP shielded coulombic hard core is not as hard as the steric one; that is, the coulombic two-particle interaction energy is not as rapidly increasing a function of interparticle distance as is the steric interaction. It thus becomes somewhat a matter of what definition one wishes to use to define a useful r_c .

The foregoing results for $R_b(R_1)$ are illustrated in Fig. 13. We have elected to portray a $C-C$ imaging situation since we believe this is approximately the condition which will obtain in the electrolyte inner layer, especially at high solute concentrations. As we have seen, $C-C$ imaging is physically equivalent, as far as the overall potential conditions are concerned, to $C-D$ imaging with $\omega = 1$, a situation which can be treated using a summation of $\omega = 0$ results. We use the value $\beta = 2 \text{ \AA}$, reasonable for KI, have taken $\gamma = \beta$, and have employed the value $R_c = 3.5$ calculated for $C-C$ imaging in Section II. The R_1 values at the two boundaries of the transition region are also taken from the results in Section II and are therefore somewhat uncertain as well but are quite adequate for illustrative purposes. The $R_1 = 7$ value is that which

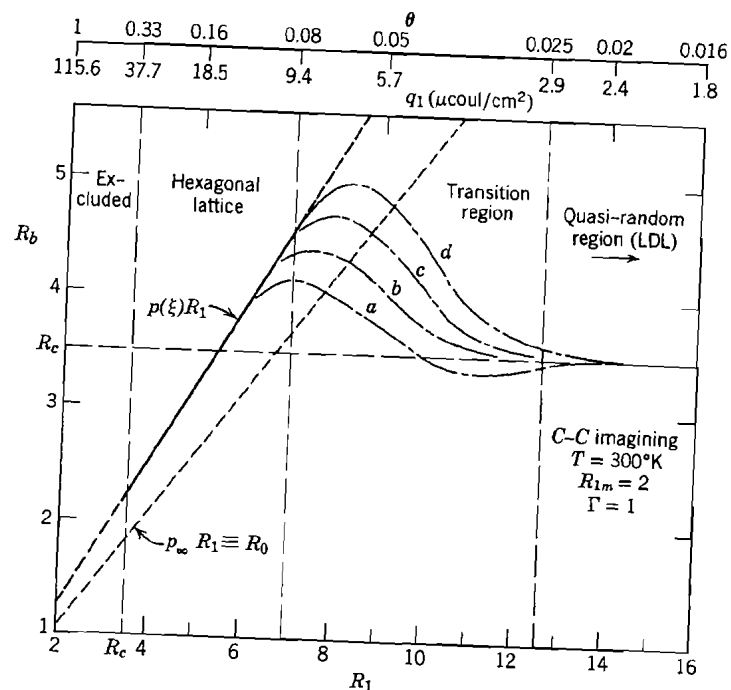


Fig. 13. The modified cutoff approach parameter R_b vs. R_1 for $C-C$ imaging and the plane $Z = 1$. Scales of q_1 and θ are also shown, appropriate for $\beta = 2 \text{ \AA}$ and $z_v = 1$. The dotted line shows the behavior of R_0 , the ordinary Grahame cutoff parameter.

makes the U/kT of Eq. 20 equal two. (U/kT is essentially unity at $R_1 = 7$ when it is calculated more accurately for this case; see Fig. 7.) This crossover value of R_1 , where the hexagonal array begins to go, is somewhat fuzzy; we believe, however, that the value is accurate to within about ± 0.5 . For R_1 values somewhat smaller than 7, there will be a good hexagonal array; for values somewhat greater than 7, the array will be poor.

The R_1 value of 12.6, where the LDL regime begins, is the most uncertain of all. It is the value of R_1 which corresponds to $U/kT \cong 0.1$ using the proper curve of Fig. 7. Actually, the array will be nearly random here, not hexagonal, but the hexagonal array result should give a much closer estimate, nevertheless, of

the transition value of R_1 than should the two-ion result of Eq. 23 which neglects the moderating effect of the other charges (and their images) present at the IHP. For comparison with the R_1 values of 3.5, 7, and 12.6 used in Fig. 13 for the C-C case, had we considered single imaging instead the corresponding R_1 's would have been approximately 7, 15, and 32.

At the top of the figure, a q_1 scale has been added appropriate for $\beta = 2 \text{ \AA}$ and $z_v = 1$. The corresponding θ scale is also shown and indicates that the hexagonal regime covers the largest part of the adsorption range of interest. Note the rather good correspondence of the $q_{1 \text{ max}}$ value of $37.7 \text{ \mu coul/cm}^2$ with the maximum $|q_1|$ of $42.61 \text{ \mu coul/cm}^2$ found from experiments on 1N KI by Grahame (51).

In Fig. 13 the dash-solid-dash line gives the value of $R_b \equiv p(\xi)R_1$ appropriate for a rigid hexagonal array. Since $Z = 1$ here, $\xi = R_1^{-1}$. We have taken $R_{1m} = 2$; since $R_c = 3.5$ at the temperature shown, the minimum value of R_b will be R_c and the lower dashed part of the $p(\xi)R_1$ line is largely beyond that experimentally possible. Similarly, the upper dashed line is within the transition region where the hexagonal $p(\xi)R_1$ should no longer apply well. It is interesting that the full $p(\xi)R_1$ curve is almost exactly a straight line. Although $p(\xi)$ varies here from about 0.62 to about 0.653 as R_1 varies from 2 to 10, the variation is very nearly of the form $p(\xi) = a - b\xi$, where a and b are independent of ξ . It thus follows that over the range shown $R_1 p(\xi) \cong aR_1 - b$, the linear dependence evident.

We have set $R_b = R_c$ in the LDL region and have shown four possible dash-dot lines joining the $p(\xi)R_1$ curve of the hexagonal region with the limiting value R_c . Since no theory presently exists which can take us very far into the transition region from either side, we are forced to join the regions of known R_b behavior by guessed interpolation curves. For the values of R_1 shown defining the transition region boundaries, we believe that curve b is most plausible. Certainly for these R_1 values and $R_c = 3.5$ there is a very high probability, we believe, of a peak in R_b exceeding the limiting value R_c . On the other hand, had R_c been considerably larger, raising the horizontal R_c line, or had the right hexagonal region boundary occurred at a smaller R_1 value, there might very well not have been a peak but only a monotonic

rise in R_b from $p(R_c^{-1})R_c$ to R_c as R_1 increased from R_c . Nevertheless, we believe that our value of R_c and the transition region boundary R_1 values are sufficiently accurate for the case considered that there will be a peak in this situation. Since Ψ_a^0 at fixed Z decreases as R_b increases, the presence of a peak in R_b leads to a minimum in Ψ_a^0 .

If we assume that the curve for R_b in Fig. 13 which involves the choice b is a good approximation to the actual dependence of R_b on R_1 or $|q_1|$, of what use is it? Since it was constructed for a C-C imaging case, it may be used in Eq. 102 with $\omega = 1$ to calculate $\psi_a(Z, R_1)$, equal to $\psi_a^{(1)}(Z, R_1)$ here, for infinite imaging. The series requires different effective values of Z at constant R_1 ; thus, different known values of ξ will also be involved in the $p(\xi)R_1$ hexagonal lattice part of R_b . There will probably also be some (unknown) changes with effective ξ in at least part of the curve spanning the transition region as well. Thus, as we shall see later, we can calculate accurate Ψ_a curves for the hexagonal array region of the C-C case. Accurate values of $\Psi_a(Z, R_c)$ may also be obtained in the LDL regime when R_c is known, but current uncertainty in R_b values in the transition region precludes accurate potential calculations there. Note that R_b curves like those of Fig. 13 are required for Ψ_a calculations for every value of ω of interest and that R_c and the transition region boundary R_1 values will all be functions of ω (and of any ionic shielding as well when $\omega < 1$).

The line $p_\infty R_1 \equiv R_0$ is shown dotted in Fig. 13. Notice that it differs appreciably from $p(\xi)R_1$ and greatly from the likely full R_b curve. In the region where $R_0 < R_b$, the use of the Grahame R_0 will result in an overestimate of Ψ_a^0 and *vice versa mutatis mutandis*. In the transition and LDL regions where R_0 may exceed R_b very appreciably, the use of R_0 will result in a great error in Ψ_a^0 . In most of their work (75 and earlier references given therein) Levine and co-workers have, however, used R_0 in these disordered array regions, assuming that the cutoff model with $R_b = R_0$ will allow thermal disordering effects to be taken into account somewhat, if only in a temperature independent way. Although we see that this approximation is indeed somewhat better than the use of a fixed hexagonal array in these regions, since $R_0 < p(\xi)R_1$ there, it remains a very poor approach. In fact, it has been shown

above that only when $\xi \rightarrow \infty$ does $p(\xi) \rightarrow p_\infty$ and $R_b \rightarrow R_0$. At fixed Z , however, this corresponds to $R_1 \rightarrow 0$, the opposite end of the R_1 region from that considered by Levine and co-workers.

Finally, the nondegenerate cutoff model, or summation-integration method, may be used quite conveniently to obtain approximate values of hexagonal array potentials and fields at high symmetry points other than 0. Suppose we wish the potential at point a of Fig. 5, i.e., for a complete hexagonal lattice. Since there are three symmetrically situated nearest charges, we may obtain the potential at a by calculating the cutoff potential with a circle of radius r_f , where $\pi r_f^2 N = 3$, then adding to the result the potential at a arising from the three neighboring charges and their images. The larger the circle of removed charge (and hence the more charges taken into account in a discrete fashion), the more accurate will the potential calculated by this method be. As an example, for $R_1 = 5$ and $R_f \equiv r_f/\beta = \sqrt{3} p_\infty R_1$, the relation appropriate for point a , the above method yields for this point and $Z = 1$, $\Psi_a^0 \cong 0.529$ as compared with the accurate value of 0.5193.

V. Discussion of Results: Nonpolarizable Adions

1. Local Potentials

A. Single Imaging. The discussion herein on local potentials starts with the simplest case and progresses through more complicated situations. Therefore, it cannot, perforce, follow the historical development in proper order. Field variation will not be examined in detail but does appear in some of the basic papers (6,60,61). We shall first be concerned with $C-O$ imaging (6) produced by perfect conductive imaging of an array of discrete monopoles in the electrode. All effect of the diffuse layer is ignored; thus, the dielectric constant in the diffuse region, ϵ_s , is taken equal to ϵ_1 and there is no specific OHP. The situation is therefore not very close to that usual in a real electrolyte double layer but does provide a useful limiting case for comparing with more complicated situations. Further, it is close to the actual situation expected for adsorption of low polarizability ions from a gas phase.

The zero of local potential is taken at the imaging plane. No potential variation thus appears for $Z < 0$. Were the images real, however, there would be variation in this region. The present results may easily be extended to the situation of two matched arrays of real charge of opposite sign, as in Fig. 6, by extending potential curves into the $-Z$ region in an antisymmetric fashion. Thus, $\psi(-Z)/\psi_\infty = -\psi(Z)/\psi_\infty$. We shall initially be concerned only with the potential variation perpendicular to the ESP along a line through point 0 of Fig. 5, the position of a removed adion in a hexagonal array, or the center of the circular disk of removed charge in the cutoff model. In this case, $X = Y = 0$.

Figure 14 shows a comparison of normalized average and local potential variation in the Z direction for a fixed, hexagonal array of adions for the value $R_1 = 10$, which corresponds to the low coverage $\theta = 0.04$, assuming $R_{1m} = 2$. The average potential may be expressed as

$$V(Z) = -V_\infty [Z(q/q_1) + (Z-1)u_0(Z-1)] \quad (108)$$

where $u_0(<0) \equiv 0$ and $u_0(>0) \equiv 1$. The top curves are pertinent when $q = -q_1$ and thus show the discrete charge and image contributions to the normalized potential: $\psi(Z) \equiv \psi_a(Z)$. Compare the qualitative curves of Fig. 6 starting at the center and progressing to the right. The uniform D field contribution, $\psi_e(Z)$, equal to $-V_\infty Z[1 + (q/q_1)]$ in the present single imaging case, enters also in the $q = 0$ bottom curves and greatly changes their character. Note that the ϵ appearing on this and later figures is ϵ_1 , the inner-layer dielectric constant. The $\psi(Z)/\psi_\infty$ curve in Fig. 14b is almost but not quite a straight line, and there will be more and more curvature as R_1 decreases.

Figure 15 presents results for the actual potential variation for three pairs of associated q, q_1 values. The q_1 values appropriate at each q correspond to small, medium, and maximum anion adsorption derived from Grahame's (51) 1N KI data and analysis. Further, the curve denoted $\psi_i(Z) (\equiv \psi(Z) + \phi_{iZ})$ includes the contribution to the local potential arising from the image of a given adsorbed anion, $\phi_{iZ} \equiv -z_v e / 2\epsilon_1 \beta Z$. This image contribution, of course, becomes more and more important the closer and closer to the imaging plane an adion moves. Of course, the adion

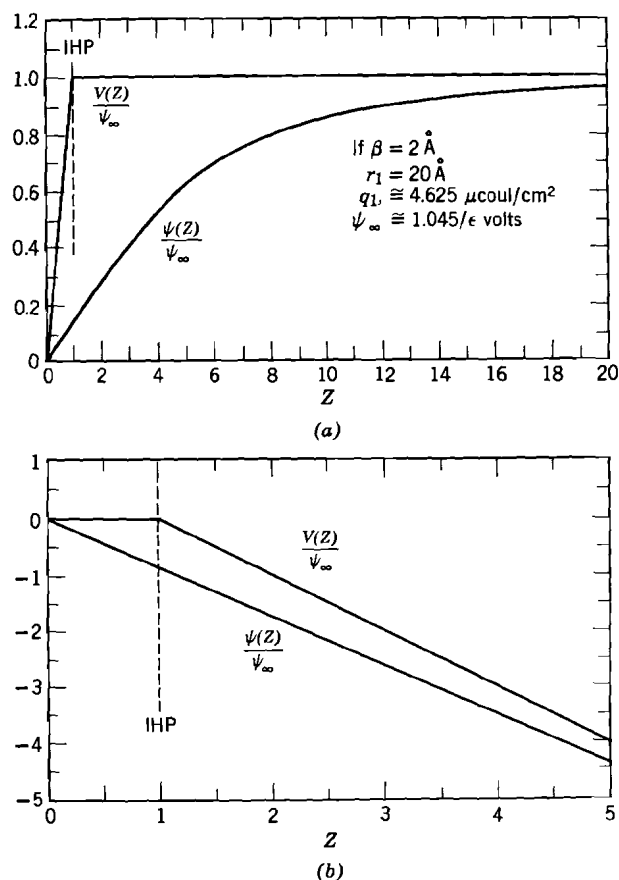


Fig. 14. Dependence of normalized average and local potentials on $Z \equiv z/\beta$ for a hexagonal array with $R_1 = 10$ and for (a) $q = -q_1$, and (b) $q = 0$ (6).

actually moves no closer than the IHP; thus, those parts of the $\psi_i(Z)$ curves lying at $Z < 1$ are not of physical significance. Note that for convenience $\epsilon \equiv \epsilon_1$ has been taken as unity in Fig. 15. The potentials given there should, therefore, be reduced by a factor arising from polarization effects. At position 0 in the IHP, there is a field (including the image contribution) of about $-8 \times 10^7/\epsilon_1 \text{ V/cm}$ urging anions away from the IHP for the conditions of Fig. 15a. The actual small adsorption present would, therefore,

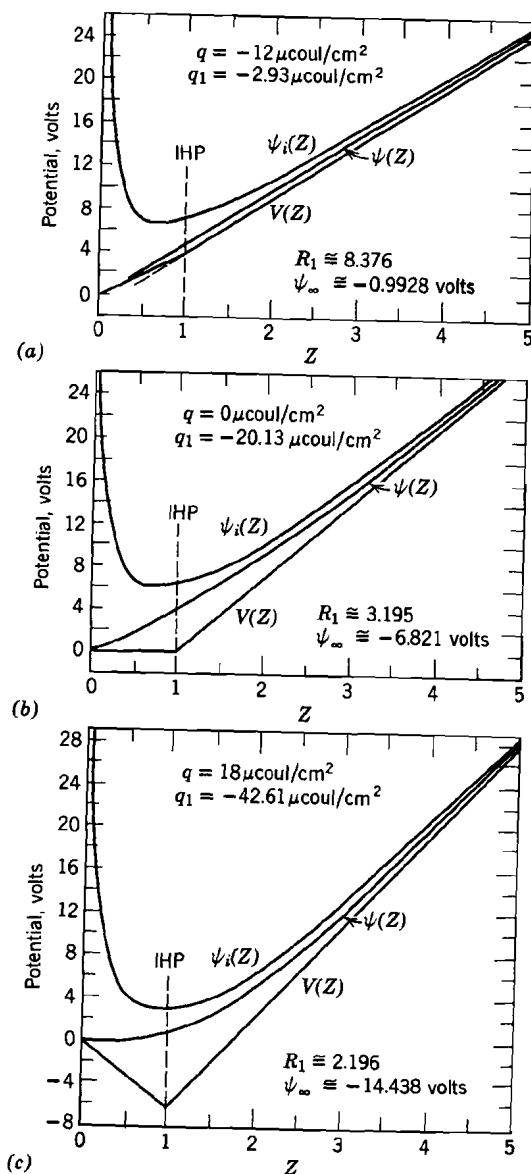


Fig. 15. Variation of several potentials with Z for $\epsilon_1 = 1$ and $\beta = 3 \text{ \AA}$ and three different sets of $q_1(q)$ values associated with Grahame's (51) 1.0N KI results (6).

arise from overriding specific, "chemical" forces if the present model were actually completely applicable. The field is about $-7 \times 10^7/\epsilon_1$ V/cm and $+5 \times 10^6/\epsilon_1$ V/cm for the situations in *b* and *c* respectively, showing that the field behavior at the IHP is indeed consonant with increased adsorption as one goes from *a* to *c*.

The value $\beta = 3 \text{ \AA}$ used in Fig. 15 has been extensively used by Levine et al. (8,75,77) but seems inconsistent with Grahame's 1*N* KI data. The value $|q_1| = 42.61 \mu\text{coul}/\text{cm}^2$, the largest derived from the data, leads when $\beta = 3 \text{ \AA}$ to $R_1 \cong 2.196$, overly close to the limiting value of about 2. These figures, in fact, correspond to $\theta_{\text{max}} \cong 0.83$. It therefore seems necessary that β be somewhat less than 3 \AA . If one takes $\beta = 2 \text{ \AA}$, the smallest value likely for an anion such as I^- , the q_1 value in *c*, the maximum $|q_1|$ observed, leads instead to $R_1 \cong 3.294$, corresponding, for $R_{1m} = 2$, to $\theta \cong 0.37$, a plausible value.

Figure 16 illustrates the dependence of the normalized local potential, as in Fig. 14, upon *Z* for a variety of R_1 values in the grounded electrode case, $q = -q_1$. It is of considerable interest that these curves almost coincide when the variable $\xi \equiv z/r_1 \equiv Z/R_1$ is used instead of *Z*. Figure 17 illustrates important limiting conditions using this variable. The $R_1 = 2$ curve represents the smallest R_1 value that generally needs to be considered. The $R_1 = \infty$ curve is that for an array of discrete ideal dipoles, the limit of nonideal dipoles of charge-image separation 2β when $\beta \rightarrow 0$. The near coincidence of the two limiting curves means that for many purposes, either a distinction between ideal and nonideal dipoles need not be made or all nonideal dipole normalized potential curves may be calculated versus ξ using an intermediate value of R_1 , say $R_1 = 4$ or 5, provided the actual R_1 value is used in obtaining *Z* from ξ .

What happens to the single-image local potential when either r_1 becomes so large at fixed temperature that a rigid hexagonal array no longer exists (the LDL) or the array disappears because at fixed r_1 the temperature is too high to allow a reasonably stable regular array (the HTL)? We have already seen that in the HTL, where the cutoff model is fully appropriate, $p \rightarrow r_{1m}/r_1$. Then in the nonideal dipole case $pR_1 \rightarrow R_{1m}$, while for ideal dipoles $p/\xi \rightarrow r_{1m}/z$. In neither case does the normalized potential depend

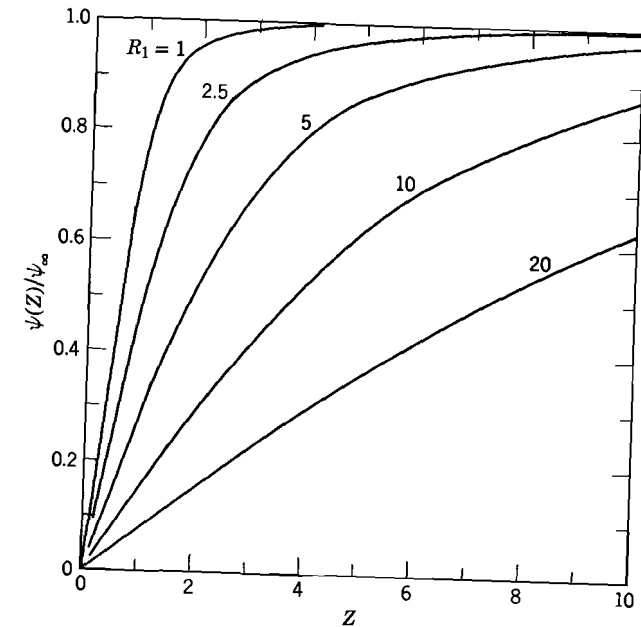


Fig. 16. Dependence of normalized local potential for a hexagonal array on *Z* for $q = -q_1$ and a variety of R_1 values (6).

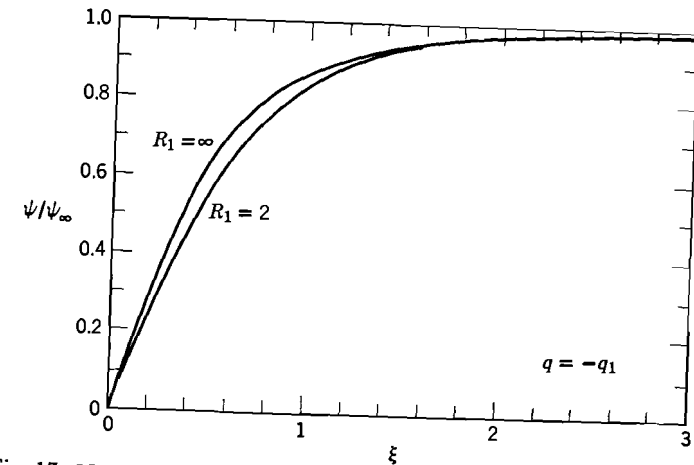


Fig. 17. Normalized local potential for a hexagonal array vs. $\xi \equiv z/r_1$ for $R_1 = 2$ and ∞ (ideal dipoles) (90).

on r_1 itself in this limit. Let us therefore introduce the new normalized distance variable $\xi_m = z/r_{1m}$ (or Z/R_{1m} for nonideal dipoles), analogous to $\xi = z/r_1$. Then, for the HTL we may write, when $q = -q_1$

$$\psi_i(Z)/\psi_\infty = [1 + \xi_m^{-2}]^{-1/2} \quad (109)$$

$$\psi_n(Z)/\psi_\infty = \frac{1}{2}[\{R_{1m}^2 + (Z + 1)^2\}^{1/2} - \{R_{1m}^2 + (Z - 1)^2\}^{1/2}] \quad (110)$$

where the i and n subscripts here denote ideal and nonideal, respectively.

Figure 18 illustrates the predictions of the above formulas. Also plotted is the ordinary nonideal-dipole curve for $R_1 = 3$. It is included not because it is theoretically appropriate for the HTL case but because when the $R_1 = 3$ normalized potential is plotted versus $\xi_m = Z/2$, it lies, as shown, surprisingly close to the very differently calculated HTL curves. We have not included a $R_{1m} = 4$ curve in Fig. 18 because it falls between the ideal and

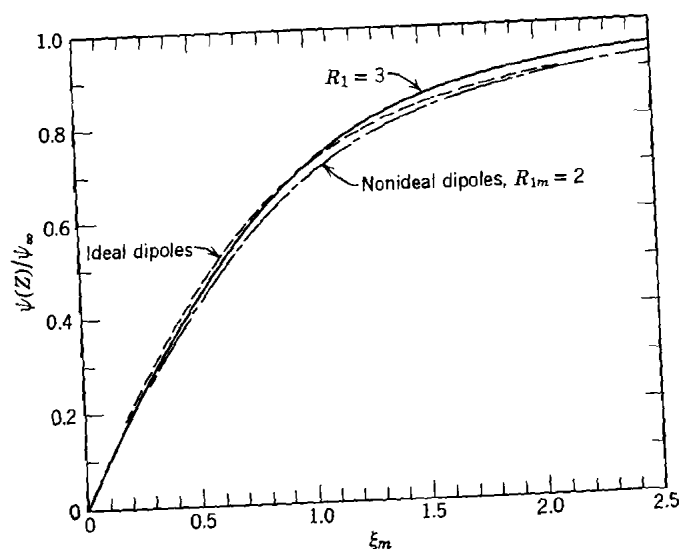


Fig. 18. Normalized local potential under HTL conditions vs. $\xi_m \equiv z/r_{1m}$ with $q = -q_1$ for ideal and nonideal dipole ($R_{1m} = 2$) situations. The fixed hexagonal lattice $R_1 = 3$ curve is included for comparison.

nonideal curves, and, in fact, lies very close to the ideal-dipole curve throughout. As $R_{1m} \rightarrow \infty$, the ideal dipole curve is approached uniformly. Further, as the figure shows, the relative difference between the ideal and nonideal curves decreases towards zero as ξ_m or Z increases at fixed R_{1m} .

Although the adion array may also become virtually random at low coverage and fixed temperature, the minimum average distance of approach between adions, r_c , will be somewhat larger, as we have seen, than the steric limit, r_{1m} , because of "hard-core" Coulomb repulsion effects. The above HTL cutoff model results therefore apply as well in the LDL case with R_{1m} replaced by $R_c = r_c/\beta$ and ξ_m by $\xi_c = z/r_c$. Since $R_c > R_{1m}$, the ideal dipole curve will usually be a good approximation to the actual situation in this case. Note that at constant temperature the curves of Fig. 17 will apply well for sufficiently large θ while those of Fig. 18 must apply for sufficiently small θ that the adion distribution is essentially random. There is, as yet, no accurate interpolation theory available to cover the intermediate range of θ 's between these values. Further work should fill this lacuna.

Next, we shall consider variation of the normalized potential (including all image contributions) for a complete, fixed, hexagonal array and compare, where appropriate, with corresponding results for an array with an adion (and its image) at $X = Y = 0$ missing. In all the succeeding single-image curves we shall take $q = -q_1$. Figure 19 shows the variation of normalized potential with R_1 at various points (see Fig. 5) located in the IHP. The closer one is to a charge, of course, the less rapid the decrease of normalized potential with R_1 . The curve marked 0 corresponds to the incomplete array and is appreciably different from the others because of the larger distance (r_1) from point 0 in the plane $Z = 1$ to a neighboring charge.

The R_1 scale of Fig. 19 probably extends to somewhat larger values of R_1 than are likely to be associated with a good hexagonal lattice, the structure for which the curves were actually calculated. At extreme values of R_1 , probably considerably larger than those illustrated, LDL behavior will be appropriate for adion adsorption from either a gas or electrolyte. Equation 110 with R_{1m} replaced by R_c shows that in this case the conditions $Z = 1$ and $R_c = 4$, for example, lead for point 0 to $\psi_n(1)/\psi_\infty \cong 0.236$.

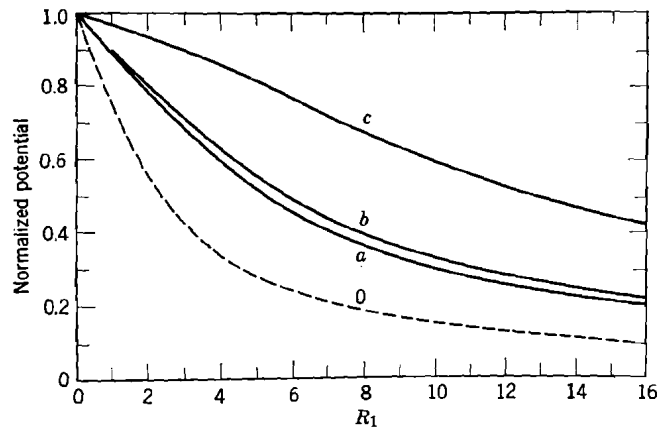


Fig. 19. Normalized local potential for a fixed, complete hexagonal array vs. R_1 for $Z = 1$ and $q = -q_1$ and various array positions denoted by the letters (6).

Since this value is somewhat larger than those achieved by $R_1 \cong 15$ for the point 0 hexagonal model curve, it appears that the actual normalized potential curve for point 0 may reach a minimum as R_1 increases, then increase to $\cong 0.24$ and remain constant for larger R_1 . Since ψ_∞ decreases as R_1^{-2} , the actual potential, ψ_n , will continuously decrease as R_1 increases. In the HTL or LDL situations, the distinction between points a , b and c disappears. For the HTL case where $R_{1m} \cong 2$, $\psi_n(1)/\psi_\infty \cong \sqrt{2} - 1 \cong 0.414$, an even larger limiting value.

Figure 20 illustrates the variation with normalized distance ξ of the normalized potential for lines perpendicular to the ESP through the indicated points in the array. With the ξ distance variable used, there is very little difference in the $R_1 = 5$ and $R_1 = 10$ curves. The short vertical lines on the curves indicate the position of the IHP.

Let us next examine potential variation in $Z = \text{constant}$ planes. Figure 21 shows such variation along the line from d to b of Fig. 5 for $Z = 1$ and 2. Since the potential is identically zero for $Z = 0$, we have shown instead the normalized field variation in this plane. For these field curves, we have normalized with $E_\infty \equiv -4\pi q_1/\epsilon_1$. The normalized distance L_1 is defined as

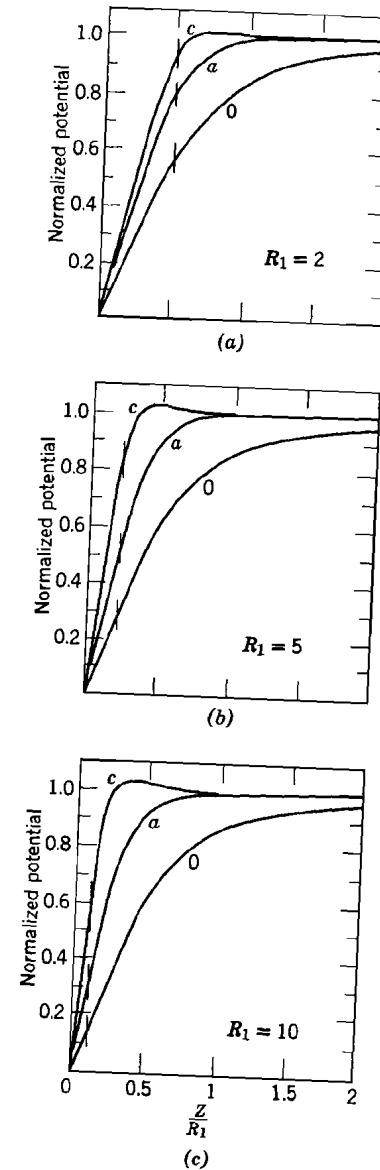


Fig. 20. Variation of hexagonal array normalized potential with $Z/R_1 \equiv \xi$ for $q = -q_1$ and three R_1 values (6).

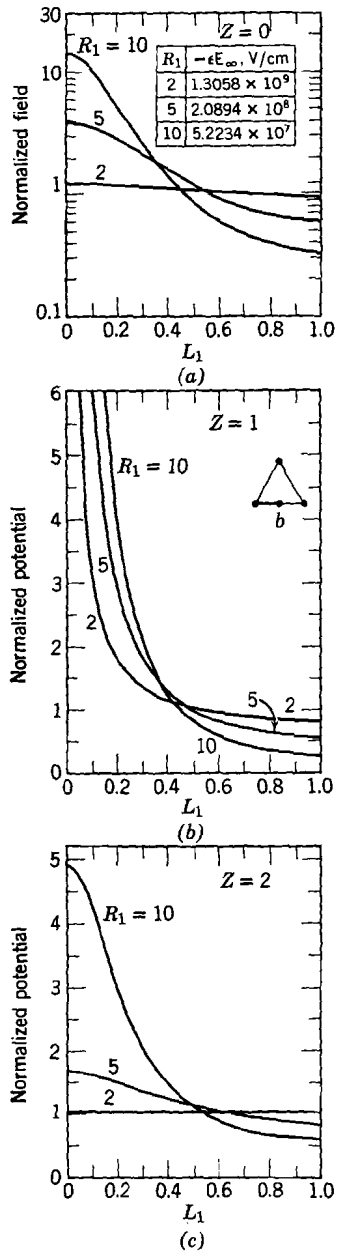


Fig. 21. Variation of hexagonal array normalized field and potential for various R_1 and Z values along the heavy line in the plane shown on the triangle of (b). $L_1 \equiv 2X/R_1$ (6).

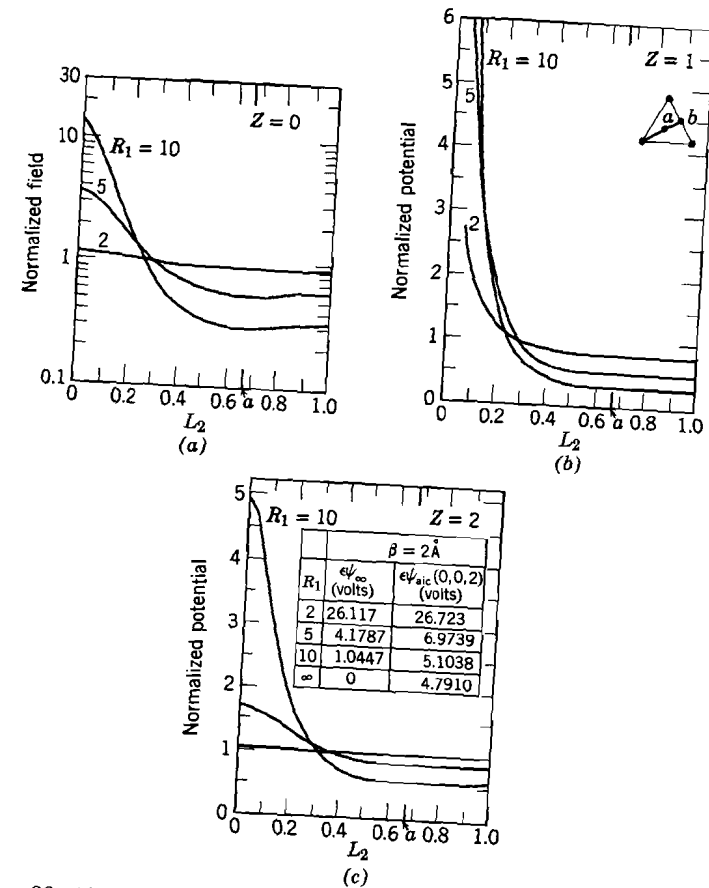


Fig. 22. Variation of hexagonal array normalized field and potential for various R_1 and Z values along the heavy line in the plane shown on the triangle of (b). $L_2 \equiv 4X/3R_1$ (6).

$2X/R_1$. Thus, $L_1 = 1$ corresponds to point b . The potential variation is symmetric around this point.

Similar curves appear in Fig. 22 except that here the planar line along which variation is calculated is that defined by $dcab$ of Fig. 5. Since $L_2 \equiv 4X/3R_1$, $L_2 = 1$ again corresponds to point b . These curves are not very different from those of Fig. 21 except that there is a shallow minimum at point a , as indicated on the abscissae scales. The table in Section III shows some values of

$\epsilon \equiv \epsilon_1$ times the full array potential at $X = Y = 0$ and $Z = 2$. The $R_1 = \infty$ value is just that arising from a single positive charge (valence unity) at $(0,0,1)$ and its image at $(0,0,-1)$. The present results all apply to $O-C$ imaging as well as $C-O$, of course. Further single-imaging potential curves appear in the next section for comparison with results calculated for other imaging conditions.

B. Other Imaging Conditions. As we shall see in a later section, there has been much more work on micropotential calculation in complicated imaging situations than on variation of local potential under such conditions. Krylov (60,61) seems to have been the first to publish an explicit expression for $\psi_i(Z)$ pertaining for the following types of hexagonal-lattice imaging: $C-C$, $O-C$, and $D-C$ ($\omega = -1$ only). In this work Krylov approximated the diffuse layer as an equipotential plane lying at $z = \beta + \gamma$ (i.e., $Z = Z_0$).

Krylov uses the dielectric imaging parameter

$$\omega \equiv (\epsilon_0 - \epsilon_1)/(\epsilon_0 + \epsilon_1)$$

introduced by Levich and Krylov (69) in an earlier micropotential paper. The condition $\omega = 1$ is implicitly taken as $C-C$ imaging, not $D-C$ with $\epsilon_0 = \infty$. As we have seen earlier, an interesting distinction may be drawn between these two cases. Further, whenever $\omega < 1$, Krylov implicitly considers only an uncharged dielectric-solution boundary at the ESP and a charge $q = -q_1$ on the equipotential OHP. He assumes a complete hexagonal lattice and calculates $\psi_{02} - \psi_i(Z)$ for $0 \leq Z < Z_0$. His expression for this potential difference may be divided into three parts: a constant field potential ψ_c ; a part arising from a line of images which is only nonzero for points on the line $X = Y = 0$ passing through point d of Fig. 5; and, for the cases $\omega = \pm 1$, the complicated triply infinite sum of modified Bessel functions we have already discussed in connection with the GFA. As we have mentioned before, the GFA is not at all attractive for $\omega \neq 1$, involving as it does complicated integrals of Bessel functions; accordingly, for $|\omega| \neq 1$ Krylov reverts to the unmodified adion image summations but carries out calculations only for $\omega = 0$.

In view of the above assumptions and restrictions, Krylov's ψ_c becomes

$$\psi_c = -V_\infty \delta_{1\omega} [\lambda + (q/q_1)] [Z - Z_0] \quad (111)$$

which is only nonzero when $\omega = 1$, for which the Kronecker $\delta_{1\omega} = 1$. This agrees with Krylov's implicit choice of $q = -q_1$ when $\omega \neq 1$. For further reference, it is useful to give an expression for $\psi_c(Z)$ here which applies generally both for $C-C$, $C-D$, and $C-O$ (and $D-C$ and $O-C$) imaging. Taking the zero of potential at $Z = 0$ as usual, we find

$$\psi_c(Z) = -V_\infty Z [1 + (q/q_1) + (\lambda - 1) \delta_{cx}] \quad (112)$$

where $\delta_{cc} \equiv 1$ and $\delta_{cx} \equiv 0$ for $x \neq c$. It will be seen that this more general result agrees with Eq. 111 when it is remembered that the latter is written for zero potential at the OHP rather than at the ESP and applies when $\omega \neq 1$ only for $q = -q_1$. The $q = -q_1$ condition is almost always appropriate when the ESP is nonconducting (e.g., $D-C$ or $O-C$ imaging), but it is not necessarily appropriate for the $C-D$ imaging or the $C-O$ imaging of Section V-I-A.

Probably because of the very considerable difficulty in evaluating his triple series, Krylov does not present many calculated curves of potential variation. Those that he did publish are shown in Figs. 23 and 24. These results were calculated with the specific choices $q = 0$ for $\omega = 1$ ($C-C$ imaging) and $q = -q_1$ for $\omega \neq 1$. The lengths β and γ were taken as equal ($\Gamma = 1$). The $\theta \equiv (2/R_1)^2$ values shown are (implicitly) based on the usual value $R_{1m} = 2$ and correspond to choices of $R_1 = 4$ and 20. Figure 23 shows the variation of normalized potential perpendicular to the plane along a line through point a of Fig. 5. The normalizing potential is ψ_∞ for all the conditions considered. The normalized abscissa scale extends from the ESP at the left to the IHP at the center and to the OHP at the right. Note the increased curvature of the curves as one goes from $\omega = 1$ to 0 to -1 and from $\theta = 1\%$ (not a condition under which a $z_v = 1$ hexagonal electrolyte double-layer array could be stable at room temperature for any ω) to $\theta = 25\%$. The $\omega = -1$ case corresponds roughly to an air-solution interface. For example, if $\epsilon_0 = 1$ and $\epsilon_1 = 6$, $\omega \cong -0.71$. A table containing a few values of normalized potential for the perpendicular line through point d is also included by Krylov.

Finally, Fig. 24 illustrates the variation of normalized potential in the plane $Z = 0.5$, a strange choice since adions do not move

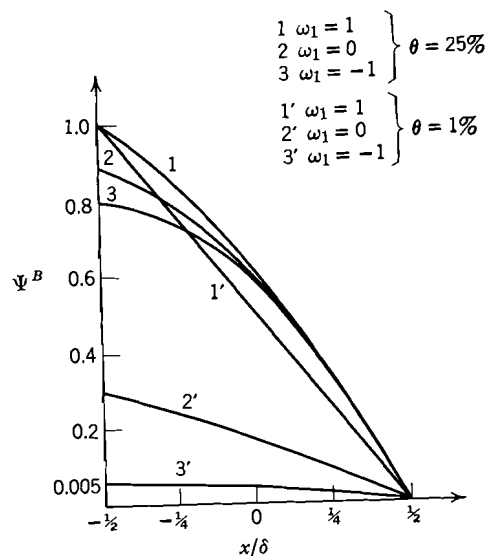


Fig. 23. Variation of hexagonal array normalized local potential with position along a line through point a of a complete lattice for $\Gamma = 1$ and various imaging conditions. Here x/δ is equal to our $(Z - 1)/2$ and ω_1 to our ω . The zero of potential is taken at the OHP (60,61).

into this plane. The variation is that along the line connecting points A (our d) to B (our a). Notice that although none of the curves quite reaches zero at a , the variation in the plane is of considerable magnitude. The $\omega = 0$ curves here are in general agreement with those presented in Section V-1-A. (remember the different positions of zero potential chosen) but cannot be quantitatively compared with them because neither $R_1 = 20$ nor $R_1 = 4$ was a chosen value there. The value of normalized potential for $Z = 1$ and $R_1 = 4$ taken from curve a of Fig. 19 of Section V-1-A and the present $\omega = 0$, $\theta = 25\%$ curve of Fig. 23 agree very well, however. A complicated but very rapidly convergent (except for $R_1 < 2$) triple series for the discreteness potential contribution, $\psi_a^{(2)}(X, Y, Z)$ in the $C-C$ case, was presented by the authors (5) but only used to calculate micro-potentials, not local potentials.

Using a method involving only a single, rapidly convergent series and expressions for $C-O$ single-imaging potentials (which

can be readily calculated from the modified cutoff approximation at small ξ and from very accurate limiting expressions for appreciable ξ), we have recently investigated the hexagonal lattice $C-D$ imaging situation in considerable detail (91). The quantity ω was defined as $(\epsilon_2 - \epsilon_1)/(\epsilon_2 + \epsilon_1)$ and ϵ_2 was taken either as ϵ_s ($C-D$ imaging) or ϵ_0 ($D-C$ imaging). In view of the relationship given in Eq. 75, the results also include $C-C$ imaging. Figure 25 illustrates potential variation results obtained for the complete range of ω , for $q = -q_1$, $R_1 = 5$, and three values of Γ probably encompassing the range of Γ likely in most electrolyte situations. Here the normalized potential ψ^N is $\psi(Z)/\psi_\infty$ and pertains to the usual line through point 0. The normalized distance $\xi \equiv Z/R_1$ is again employed for the abscissa scale. Although only incomplete

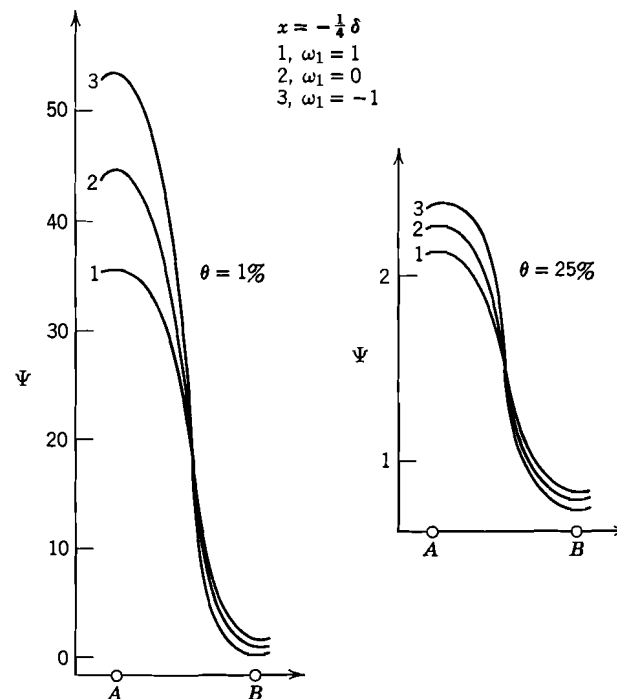


Fig. 24. Variation of hexagonal array normalized local potential with position along the line between points A and B (our d and a , respectively) in the plane $Z = \frac{1}{2}$ for $\Gamma = 1$ and various imaging conditions (60,61).

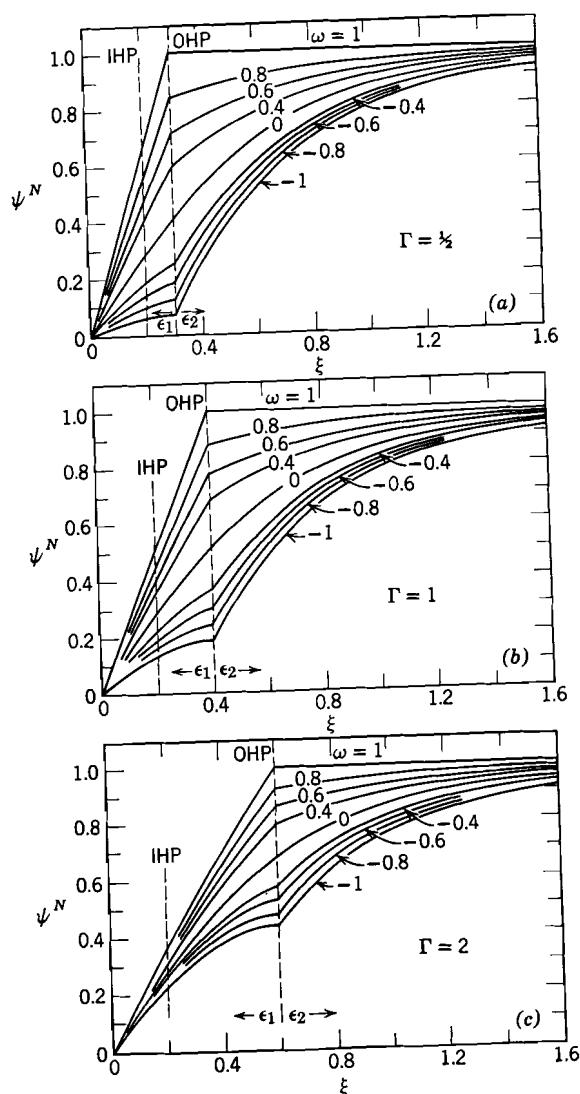


Fig. 25. Hexagonal array normalized potential vs. $\xi \equiv Z/R_1$ for $q = -q_1$, $R_1 = 5$, several Γ values, and the complete range of ω (91).

array potentials, particularly useful in discussing the micro-potential, were calculated, the paper discusses how potentials for any X and Y and an incomplete or complete array can be obtained with much less work than needed using any previous methods. Further, the method is sufficiently general to apply to any cutoff model as well as the hexagonal array. It may therefore be used to investigate HTL and LDL conditions for any pertinent ω .

As Fig. 25 indicates, there is a discontinuity in field (but not displacement) at the OHP ($\epsilon_2 \equiv \epsilon_s$) or ESP ($\epsilon_2 \equiv \epsilon_0$) for all ω values but zero. Further, a larger and larger proportion of ψ_∞ occurs outside the inner region the more ω departs from unity. When $\epsilon_2 \equiv \epsilon_s$ and $C-D$ imaging is considered, the largest likely value of ϵ_s in an aqueous solution is about 80, leading, with $\epsilon_1 = 6$, to $\omega \cong 0.86$. Even this large a value of ω does not give a very close approximation to $\omega = 1$ behavior, but one should remember that $C-D$ imaging alone ignores the shielding arising from mobile diffuse-layer ions and is therefore applicable only at low solute concentrations unless $\Gamma \gg 1$.

2. Micropotentials

A. Early Work. The first attempt to explicitly calculate the work of adsorption (or, equivalently, the micropotential) for a discrete electrolyte double-layer system was that of Esin and Shikov (34). Their model, illustrated in Fig. 26a, applies only for $q = 0$ and corresponds to the $O-O$ case of Table I. They consider that rigidly associated with each adion located at the IHP there is a counterion at the OHP. Each such ion pair thus forms a finite-separation dipole, and Esin and Shikov assume an infinite, hexagonal plane array of such dipoles. Although they devote some attention to the effect of thermal motion, their main calculations assume a rigid array. Even though we have seen that this approximation can be a good one under many conditions of interest, the additional approximations of neglecting the effect of the electrode and subsuming all diffuse-layer effects in rigidly associated counterions are inadequate under almost all conditions.

Esin and Shikov essentially calculate the p.d. $\psi_{0p} \equiv \psi_0 - \psi_p$ between points at the centers of the dotted circles marked 0 and p of Fig. 26a. Let the average p.d. produced by the entire dipole

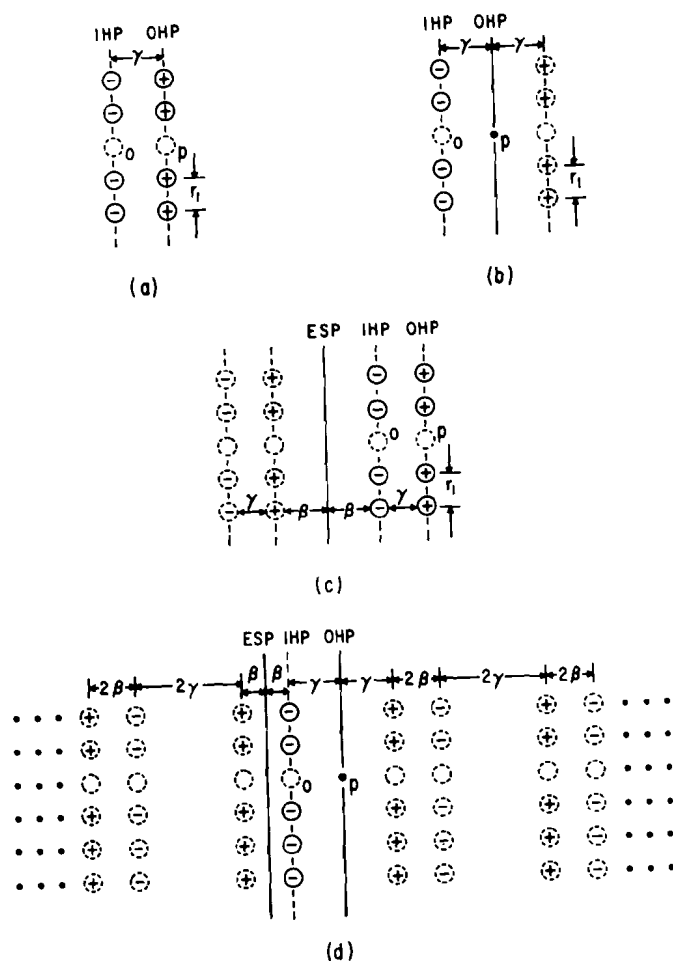


Fig. 26. Discrete charge models for early micropotential calculations. Image charges are shown dotted and the p.d. of interest is that between points 0 and p .

layer be V_0 . This is the drop across it if all charges were smeared; it is also the p.d. across a discrete array between two points at distances from the array large compared to r_1 (see also Fig. 6). This p.d. is given by

$$V_0 = 4\pi\gamma q_1/\epsilon_1 \equiv \Gamma V_\infty \quad (113)$$

where as usual ϵ_1 is intended to account for the dielectric constant contributions arising from solvent molecules in the inner layer and possibly also those arising from adion polarizability. The quantity V_0 is not quite logically equivalent to the V_∞ introduced earlier. For V_∞ , layer spacing was 2β rather than the present γ , and half of the layer was composed of images. The p.d. sought in that case was measured from the center of the array to "infinity." These differences so compensate that V_∞ is, however, just the above V_0 with γ changed to β .

We have earlier introduced the normalized distance $R_1 \equiv r_1/\beta$ appropriate for an array of adions and their images a distance 2β away. Here, the adion-counterion separation is γ , so it is convenient to redefine R_1 for the present situation as $2r_1/\gamma$, structurally the same quantity. We may now express the basic Esin-Shikov result as

$$\Lambda \equiv \psi_{0p}/V_0 = 0.74\gamma/r_1 = 1.48R_1^{-1} \quad (114)$$

Note that the effective dielectric constant ϵ_1 has cancelled out in this ratio.

In their actual calculation of the ratio Λ , Esin and Shikov tacitly assume ideal dipoles rather than charge pairs a distance γ apart. Their method is thus logically correct only in the associated limits $\gamma \rightarrow 0$, $R_1 \rightarrow \infty$, and $\xi \rightarrow 0$. In addition, not knowing of Topping's earlier accurate calculation of the sum σ , Esin and Shikov established the following bounds to it (termed K_3 by them) by partial summation: $10.8 < \sigma < 11.1$. Unfortunately, they actually used 10.8 in their calculations rather than their upper limit, which is close to the more exact Topping-van der Hoff and Benson (127) value $\sigma \cong 11.0341754$. When this value is employed, one finds that the proper $R_1 \rightarrow \infty$ limiting behavior of Λ in the present situation is

$$\Lambda = (p_0 R_1)^{-1} \cong 1.5209 R_1^{-1} \quad (115)$$

This may be compared with the result of the approximate analysis given earlier in Eq. 7.

Equation 115 is represented by the bottom straight line in Fig. 27. We shall explain the other curves subsequently. At this point, we only remark that the bottom dotted line marked $B = \infty$ is the accurate solution of the Esin-Shikov problem without the

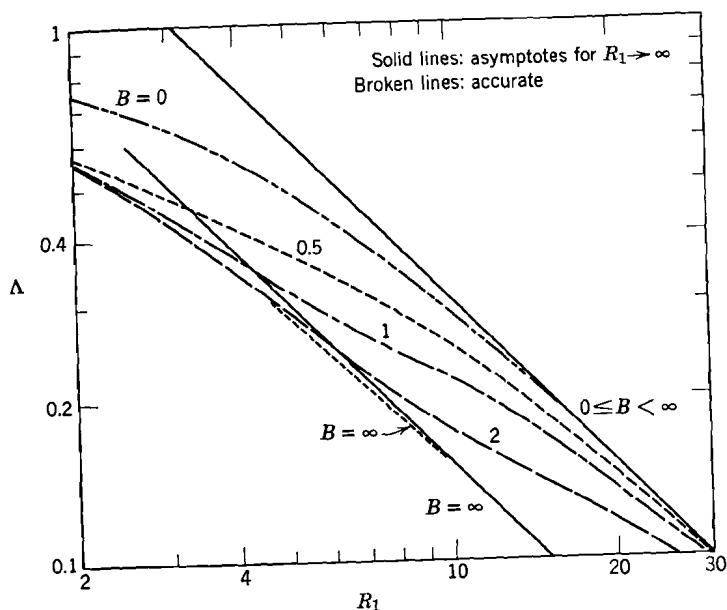


Fig. 27. The micropotential quantity $\Delta \equiv \psi_{0p}/V_0$ vs. R_1 for various situations and values of $B \equiv \beta/\gamma$.

approximation of ideal dipoles. It was obtained using our highly accurate modified cutoff method for hexagonal arrays.

Figure 27 illustrates that the asymptotic law of Eq. 115 is reasonably accurate for $R_1 \gtrsim 8$. For R_1 as small as 3, however, where a rigid hexagonal lattice is an excellent approximation, the results of the asymptotic line are about 18% high. When Esin and Shikov compared their result, Eq. 114, with the Esin-Markov experimental findings, they obtained a value of γ/r_1 corresponding to $R_1 \cong 2.6$, a result they considered to correspond to an improbably high adion surface coverage density. For example, with $\gamma = 2 \text{ \AA}$, $|q_1| \cong 280 \text{ } \mu\text{coul/cm}^2$, much too high a value. The same data lead to an even larger value of $|q_1|$ when the accurate nonideal dipole treatment is used.

Esin and Shikov ascribed the failure of their treatment to explain the Esin-Markov results entirely to their neglect of thermal effects. More important, we believe, is the general crudeness of the model used, which neglects the effect of the

electrode, oversimplifies the effects of the diffuse layer, smears out discrete dielectric constant contributions in the inner region, and treats nonideal dipoles as ideal. In spite of these deficiencies, which are easy to see in retrospect, the Esin-Shikov treatment was a pioneering attack on the problem of discreteness effects in the double layer.

Ershler's (32) treatment is strongly founded on that of Esin and Shikov but makes a number of valuable modifications. The three different models considered by Ershler are illustrated in Fig. 26*b*, *c* and *d*, where the circles denoting image charges are shown dotted.

The model of Fig. 26*b* is based on imaging of adions in the diffuse layer. As Ershler points out, the regular array of counterions at the OHP assumed by Esin and Shikov will be disorganized by thermal motion and, if the concentration is sufficiently high, the charge in the diffuse layer may be well approximated as all lying in the OHP. The resulting imaging of the adions is of the *O-C* type of Table I. This conductive single imaging in the OHP (rather than in the electrode) should be distinguished from the different, perfectly polarizable ($\epsilon_s = \infty$) dielectric imaging (*O-D*) with which it might possibly be confused. In the latter case, there would be no real charge at the OHP.

For the model of Fig. 26*b*, Ershler obtains the result

$$\Delta = 0.74(2\gamma/r_1) = 2.96R_1^{-1} \quad (116)$$

We have maintained here and will continue to maintain the meaning of γ as the distance between IHP and OHP. In the present case, it is only half the distance between charge layers, whereas it was the full distance in the Esin-Shikov model. Nevertheless, it is convenient to retain the same definition, $R_1 \equiv 2r_1/\gamma$, in the two cases, allowing direct comparison between them.

The result of Eq. 116 arises because both ψ_{0p} and the average p.d., here identified with the quantity V_∞ defined earlier (with β replaced by γ), are measured only over half the distance between charge layers, since one of them is here composed of image charges. Thus Eq. 116 is fully equivalent to Eq. 114, since 2γ here measures the distance between layers which was given by γ in the Esin-Shikov treatment. Numerically also, the actual layer separation is, in the present case, twice that in the former. The

use of the more accurate value of σ changes the factor 2.96 to 3.0418. On employing this number and $\gamma = 2 \text{ \AA}$ as before, the Esin-Markov results lead to $|q_1| \cong 70 \text{ \mu coul/cm}^2$, still considerably too large a value but much closer to a reasonable result than before. The nonideal dipole curve for this model is that marked $B = 0$ in the figure. The derivation of this result will be discussed later. Since it lies below the asymptotic solid straight line, accurate treatment of the model does not improve agreement between theory and experiment.

In order for calculations taking some discreteness into account to explain the Esin-Markov effect, it is necessary for Λ to be larger, for reasonable values of β and γ , than predicted by the last two models. Ershler's next attempt [Fig. 26c] reverted back to the real charge pairs of the Esin-Shikov model. He added conductive imaging in the ESP of the nonideal dipoles formed by these charges. This, then, is single imaging of nonideal dipoles rather than single charges, but Ershler actually again treats them as ideal dipoles. Ershler shows that, in this limit, the asymptotic result is again given by Eq. 114 and is independent, in the limit, of β . Thus, this calculation also cannot explain the Esin-Markov effect.

When the dipoles and their images in the metal are no longer treated as ideal, it is of interest to examine the resulting curves for Λ , which will, in this case, depend on $B \equiv \beta/\gamma$ as well as R_1 . To do so, we shall use the modified cutoff model. For the present model with conductive single imaging of nonideal dipoles, it leads directly to the following expression

$$\begin{aligned} \Lambda = & \left(\frac{R_1}{4}\right) \left[2\left\{ \left[p(R_1^{-1}) \right]^2 + (2R_1^{-1})^2 \right\}^{1/2} - p(R_1^{-1}) \right] \\ & + \left[\left\{ p\left(\frac{4B+1}{R_1}\right) \right\}^2 + (4BR_1^{-1})^2 \right]^{1/2} \\ & - \left[\left\{ p\left(\frac{4B+1}{R_1}\right) \right\}^2 + \left(\frac{4B+2}{R_1}\right)^2 \right]^{1/2} \\ & - \left[\left\{ p\left(\frac{4B+3}{R_1}\right) \right\}^2 + \left(\frac{4B+2}{R_1}\right)^2 \right]^{1/2} \\ & + \left[\left\{ p\left(\frac{4B+3}{R_1}\right) \right\}^2 + \left(\frac{4B+4}{R_1}\right)^2 \right]^{1/2} \end{aligned} \quad (117)$$

The first term in curly brackets arises from the right dipole layer and the remaining square-root terms all originate from the left (image) layer. This expression involves the nearly constant function $p(\xi)$ introduced earlier for fixed hexagonal arrays.

The broken-line curves of Fig. 27 illustrate results calculated from Eq. 117 for several values of B . In these calculations, $p(\xi)$ was obtained from a 2-2 rational function approximant in order to yield high accuracy. It was found, however, that for this particular expression for Λ , the $\xi = 0 (R_1 \rightarrow \infty)$ value of p , $p_0 \cong 0.6575206$, yielded results within 3% of the accurate ones for all B values shown over the range $2 \leq R_1 \leq 30$. It may, therefore, be used in practical calculations of this type with a great gain of simplicity and insignificant loss of accuracy. Note that all the broken-line curves go to unity as $R_1 \rightarrow 0$.

The $B = \infty$ broken-line curve was calculated from Eq. 117. In this case, imaging disappears and the model reduces to that of Fig. 26a for a single nonideal dipole array of real charges. Note that the $B \rightarrow \infty$ limit must be taken before the $R_1 \rightarrow \infty$ (ideal dipoles) limit used in obtaining the bottom straight line. Thus, the $B = \infty$ broken line is asymptotic to the bottom straight line, while all finite B curves are asymptotic to the top solid line. It is evident that no distinction need be made between the $B = 2$ and $B = \infty$ curves when $R_1 \leq 4$. Since all the B curves lie below the top solid line, the accurate treatment does not lead to a better explanation of the Esin-Markov effect.

The $B = 0$ curve of Fig. 26c is of special interest because when $\beta = 0$ the central $(-q_1) - (q_1)$ dipole charges coalesce and vanish. The model then becomes essentially equivalent to that of Fig. 26b (separation of charge layers 2γ). An excellent internal check on the accuracy of the results is afforded by the recognition that the $B = 0$ curve can be derived from the $B = \infty$ curve by picking a given R_1 , finding the point on the $B = \infty$ curve at $R_1/2$ (because when $\gamma \rightarrow 2\gamma$, $R_1 \rightarrow R_1/2$) and then moving this point back to the line defined by the original R_1 choice. This is equivalent, of course, to moving a given point on the $B = \infty$ curve horizontally to the right by a factor of 2. We find very close agreement between the curves when this process is carried out even though the actual $B = \infty$ curve was calculated with only the first part of Eq. 117 and the $B = 0$ curve with the entire

formula involving $p(\xi)$'s with several different values of ξ . This agreement, of course, establishes a complicated relationship among the $p(\xi)$'s, since it is possible to set equal the Λ formula for given R_1 and $B = \infty$ with the more complex Λ formula for $B = 0$ and R_1 half the $B = \infty R_1$ value.

The last Ershler model, Fig. 26*d*, corresponds to the infinite imaging, C-C case of Table 1. Ershler does not really treat this case as an infinite imaging problem, however. Instead, by a judicious averaging of results obtained from some of his earlier models, he obtains

$$\Lambda = 0.5[1 + 0.37(\gamma/r_1)] = 0.5[1 + 0.74R_1^{-1}] \quad (118)$$

This result, like the earlier ones, was taken to apply only for $q = 0$ and is appropriate only for $\beta = \gamma$. If we use $\gamma = 2 \text{ \AA}$ and the Esin-Markov result $\Lambda \cong 0.58$, we find from Eq. 118 that $R_1 \cong 4.6$ and $|q_1| \cong 86 \text{ \mu coul/cm}^2$. The $|q_1|$ value is still too large; for it to be as small as 30 \mu coul/cm^2 , γ must be about 3.4 \AA , probably too large a value.

Ershler used his result in a simple isotherm to explain the Esin-Markov results. (See Section II-2.) Although he obtained reasonably good agreement with experiment, he took $\gamma/r_1 < 0.1$, probably too small over much of the experimental range, and of course, made the specific and not necessarily accurate assumption $\gamma = \beta$. These approximations, taken together with most of those discussed in connection with the Esin-Shikov calculations, make Ershler's agreement with experiment quite suspect. Such agreement may also arise from the use of an inadequate isotherm. In spite of these strictures, the Ershler treatment was a long step forward, and, in particular, provided the seed for the flowering of the modern single- and infinite-imaging treatments.

Grahame (52) was next to carry out significant discreteness calculations. He first considered a single-imaging situation with discrete charge layer separation of $\delta \equiv 2\gamma$, as in Fig. 26*b*. In this work, Grahame compared results of his cutoff treatment with p.d. results obtained by directly summing the contributions from a finite number of hexagonally arranged ions and their images in the diffuse layer. For the cutoff model, he used the value $p = p_\infty \cong 0.5250376$, which we have seen is only appropriate for a fixed hexagonal lattice when $\xi \rightarrow \infty$ (since we are presently dealing

with imaging in the diffuse layer, $\xi \rightarrow \infty$ is equivalent to $r_1 \rightarrow 0$ and/or distance measured from the imaging plane at $z = d$ approaching "infinity"). By comparing ψ_{0p} values obtained from the cut-off and summation methods, Grahame found that as $R_1 \equiv 2r_1/\gamma$ became sufficiently large, the summation result approached about 0.805 of the cutoff prediction.

Now in the limit $R_1 \rightarrow \infty$, ideal dipole results should be obtained. In this limit ($\xi \rightarrow 0$), the appropriate p is not p_∞ but that of Topping: $p = p_0 \cong 0.6575206$. The ratio p_∞/p_0 is about 0.7985, close to Grahame's value of 0.805. Part of the difference arises because it has been shown (6) that Grahame's direct summation results for ψ_{0p} are about 4% too small.

Grahame did not recognize that in order to employ the cutoff approach to yield accurate values of ψ_{0p} , one should use (90) p_0 for $R_1 \rightarrow \infty$ and p_∞ for $R_1 \rightarrow 0$. He instead used p_∞ throughout, and, for reasonably small γ , merely multiplied the p_∞ cutoff ψ_{0p} result by 0.805. Except for the minor difference between 0.805 and 0.7985, this procedure should be valid for sufficiently small γ/r_1 that only the first-order expansion term in the cutoff model (involving γ/r_1) be significant. Grahame expanded to second order, however, and obtained

$$\begin{aligned} \Lambda &\cong 3.064R_1^{-1} - (3.5465R_1^{-1})^3 \\ &\cong 3.064R_1^{-1} - 44.61R_1^{-3} \end{aligned} \quad (119)$$

Expansion to second order of the cutoff expression for ψ_{0p} using $p = p_0$ actually leads for $R_1 \gg 3$ to

$$\begin{aligned} \Lambda &\cong 3.0418R_1^{-1} - (3.0418R_1^{-1})^3 \\ &\cong 3.0418R_1^{-1} - 28.144R_1^{-3} \end{aligned} \quad (120)$$

Grahame's result is quite close for the number in the first-order term, but his second-order term is too large and needs to be multiplied by the factor $(0.7985)^3/0.805$. Grahame would have obtained nearly the correct second-order term also had he applied his factor 0.805 twice more to it instead of using this factor only to multiply the $p = p_\infty$ cutoff expression for ψ_{0p} . Actually, the second-order term should not be given anyway because by the time R_1 is sufficiently small that the second-order term becomes a significant fraction of the first-order one, $p(\xi)$ itself can no longer be accurately approximated by p_0 .

Grahame also carried out a semiquantitative calculation of the $C-C$ infinite imaging situation. His treatment, while seminal, contained several errors (6) and even though some of them compensated for others, he arrived at the result (see Fig. 26*d*)

$$\Lambda = \psi_{0p}/\psi_{\infty} = \psi_{12}/V_{02} = \lambda \equiv \gamma/(\beta + \gamma) \quad (121)$$

supposed to hold exactly for all q and q_1 combinations. This result corresponds to the assumption of a constant field in the inner region. It actually neglects the direct contribution to ψ_{12} from the discrete adions themselves and implies $\psi_{12} = V_{12}$. Thus, the potential varies linearly across the inner region and V_{12} is reduced from V_{02} by just the proper distance ratio λ .

When $q = 0$ and R_1 is sufficiently large, we shall see later that an exact treatment of this problem (5) shows that Eq. 121 is indeed a good approximation. On the other hand, the constant field approximation may be very poor for q and q_1 values found experimentally with, for example, 1.0N KI in water. Then Eq. 121 becomes a poor approximation. We will now revert to the more usual definition, $R_1 \equiv r_1/\beta$.

B. Conductive-Conductive Imaging. The first exact treatment of a simplified double-layer model taking discreteness of charge in the inner layer into account seems to be that of Levich, Kir'yanov, and Filinovsky (70), presented at a symposium honoring David Grahame in 1960. An almost identical paper by Levich, Kir'yanov, and Krylov (71) appeared a few months later. Besides the replacement of Filinovsky, the only important change in the published version is that the original conclusion of "insufficiently close agreement" between some of the theoretical results and known experimental data is converted to "quite close agreement." Can we conclude that Filinovsky was cautious and Krylov optimistic? Insufficient results are presented in the paper, unfortunately, to allow one to answer this question readily.

The Levich et al. calculation deals with the $C-C$ infinite imaging case for an infinite fixed, plane hexagonal lattice of adions. An inner-region dielectric constant is introduced and a general analytic expression for ψ_{12} is quoted. Few details of the calculation are included, but the authors seem to use the GFA Fourier-Bessel integral technique (115) which finally leads to a triply infinite sum of modified Bessel functions of the third kind.

This series is difficult to evaluate and no numerical results for ψ_{12} or $\Lambda \equiv \psi_{12}/V_{02}$ were given. Although it is thus difficult to check the correctness of their series against later accurate values of Λ calculated by simpler methods (see later discussion), the authors reached the Ershler-Grahame conclusion that $\Lambda \cong \lambda$ for adion surface coverages of 25–30%, corresponding, they believe, to the maximum found experimentally.

For the $C-C$ case, where the deviation in linearity of the potential may indeed be small, it is convenient to introduce the quantity Δ through

$$\Lambda \equiv \psi_{12}/V_{02} \equiv \lambda[1 + \Delta] \quad (122)$$

where Δ measures the relative deviation from linearity. The potential difference ψ_{12} is made up of a uniform D field part, $\psi_e(1) - \psi_e(Z_0)$, and a part arising from the discrete adions themselves: $\psi_a(1) - \psi_a(Z_0) = \psi_a(1) \equiv \psi_a^{(2)}(1)$, in the present case. On noting that $\psi_e(1) - \psi_e(Z_0) = \lambda V_{02} \equiv \Gamma V_{\infty}(\lambda + (q/q_1))$, we obtain

$$\Delta = \psi_a^{(2)}(1)/\lambda V_{02} \quad (123)$$

The various Russian writers have usually expressed the deviation from linearity in a slightly different fashion. They write, for $\omega = 1$

$$\psi_{12} \equiv \lambda V_{02} + \alpha \Gamma V_{\infty} \quad (124)$$

from which it readily follows that

$$\alpha \equiv B\Psi_a^{(2)}(1) = [\lambda + (q/q_1)]\Delta \quad (125)$$

where $\Psi_a^{(2)}(1) \equiv \psi_a^{(2)}(1)/\psi_{\infty}$. Note that this α has nothing to do with the polarizability α used earlier. When $q = 0$, let $\Delta \equiv \Delta_0$ and when $\gamma = \beta$ define $\Delta \equiv \Delta^0$. Most authors have dealt primarily with the combined case, for which $\Delta = \Delta_0^0$ and $\alpha = 0.5\Delta_0^0$.

We now see that the Levich et al. conclusion $\Lambda \cong \lambda$ is equivalent to neglecting Δ compared to unity or, equivalently, the term involving α , at least when $q = 0$. For $\theta = 0.30$, $R_{1m} = 2$, $\beta = \gamma = 2 \text{ \AA}$, we find $r_1 \cong 7.3 \text{ \AA}$ and work to be discussed later yields $\Delta_0^0 \cong 0.04$ for the hexagonal-array situation, not entirely negligible but nearly so.

The next significant work on $C-C$ imaging was that of Levine et al. (75) who used the Grahame cutoff model with Grahame's constant p value, p_{∞} . The micropotential $\psi_{1\infty}$ was written as

$V_{1\infty} + \phi''_\beta$, where ϕ''_β is a self-atmosphere perturbation potential. Since ϕ''_β is written as $\phi_1(0,0)$ by Levine in later work (77), we shall here denote this quantity by ϕ_1 . We may write

$$\psi_{12} \equiv V_{12} + \phi_1 = \Gamma\psi_\infty[1 + (q/q_1)] + \phi_1 \quad (126)$$

showing how ψ_{12} differs from the average value V_{12} . Further, Levine et al. (75) introduce the quantity g through

$$\phi_1 \equiv -\lambda\psi_\infty g \quad (127)$$

and write g as $g_\phi(r_\beta)$ in later work (77). We shall use the simple g designation.

On comparing Eqs. 122, 123, and 126, one readily discovers that

$$\phi_1 = \psi_a^{(2)}(1) - \lambda V_\infty \quad (128)$$

and

$$g \equiv 1 - \lambda^{-1}\Psi_a^{(2)}(1) \quad (129)$$

We may also write

$$\Delta = [1 - g][\Gamma + Z_0(q/q_1)]^{-1} \quad (130)$$

and

$$\alpha = \lambda[1 - g] \quad (131)$$

Note that when $q = 0$ and $\gamma = \beta$, $\Delta \equiv \Delta_0^0 = 2\alpha = 1 - g$. Since Δ_0^0 varies from 1 to 0 as R_1 changes from 0 to ∞ , g will correspondingly change from 0 to 1 in this case. Since they are almost exclusively concerned with ϕ_1 and g , Levine et al. do not generally specify q when they deal with q_1 . Nevertheless, q and q_1 cannot really be separated and should be considered together. The above relations show how terms involving q enter the various equations when q is arbitrary and is not necessarily taken as zero.

In order to treat the $C-C$ case with the restriction $\beta = \gamma$, Levine et al. (75) summed an infinite number of cutoff model single-image potentials in a way which follows directly from Grahame's (52) more qualitative treatment of $C-C$ imaging. After applying the Poisson summation formula, they obtained a result which may be written

$$\Delta_0^0 = (8\tau/\pi) \sum_{m=1}^{\infty} (2m-1)^{-1} K_1[(2m-1)\pi\tau] \quad (132)$$

where K_1 is a modified Bessel function of the third kind and $\tau \equiv \tau_0/d \equiv p_\infty R_1/2$. Thus, $R_1 \cong 3.8093\tau$, and $R_1 \cong 0.6349 \times 10^8 r_0$ when $\beta = 3 \text{ \AA}$. For $R_1 \gg 5$, it is a reasonably good approximation to retain only the first term in the series and replace K_1 by its asymptotic expansion. One then obtains

$$\Delta_0^0 \cong (4/\pi)(p_\infty R_1)^{1/2} \exp[-\pi p_\infty R_1/2] \quad (133)$$

where $(\pi p_\infty/2) \cong 0.8247$. Thus, for $R_1 \gg 5$, the linearity parameter Δ_0^0 rapidly decreases and soon becomes negligibly small. No numerical values of g (or Δ_0^0) vs. τ or R_1 were given by Levine et al. It should be stressed that the above results for Δ_0^0 apply for a cutoff approximation only, not for a hexagonal array; thus, $R_1 \equiv (r_0/p_\infty\beta)$ is just a normalized distance measure, not a hexagonal nearest-neighbor distance, in this case. The constant- p cutoff approximation smears out much but not all of the discreteness contributions to the potential. It is not possible to use Levine's method for a hexagonal lattice approach to $C-C$ imaging because p must vary with ξ in this case. Each term in the original series then requires a different p , since each pertains to an image plane at a different Z , and the Poisson summation formula is inapplicable.

On the other hand, since p is independent of Z in either the HTL or LDL situation, the above limitation does not apply in these cases. The Levine series and its asymptotic approximation will, therefore, apply for these conditions if we replace r_0 by r_{1m} or r_c , p_∞ by R_{1m}/R_1 or R_c/R_1 , and τ by $R_{1m}/2$ or $R_c/2$ for the HTL and LDL cases, respectively. For example, the choices $R_c = 2, 4$, and 7 in Eq. 132 with $R_c/2$ replacing τ lead to $\Delta_0^0 \cong 0.087, 5 \times 10^{-3}$, and 6×10^{-5} , respectively. These results indicate virtual linearity of the local potential for $0 \leq Z \leq Z_0$ when $R_c \gg 4$ in the LDL case. Note that they are independent of R_1 provided the latter is sufficiently large that the LDL condition is indeed appropriate.

In 1962, Levich and Krylov (69) gave new expressions for the hexagonal lattice micropotential ($|\omega| = 1$) pertaining when $\beta = \gamma$. No numerical results for ψ_{12} or α were given, possibly because complicated triply-infinite series were involved, but the series were, in fact, used to derive curves to compare (for $\omega = \pm 1$) with data illustrating the Esin-Markov effect. Using a Henry

(Boltzmann) isotherm, Levich and Krylov achieved qualitative agreement with experiment provided they allowed γ to vary from 0.847 Å to 0.780 Å over the experimental range of V_{02} from zero to maximum $|V_{02}|$ in the $\omega = 1$ case and from 2.112 Å to 1.860 Å in the $\omega = -1$ case. Further, in these cases ϵ_1 varied as well from 14.11 to 13.00 and 28.16 to 24.80, respectively. The use by Levich and Krylov of an overly simple isotherm, the choice $\beta = \gamma$, and probably unjustified magnitudes and variation of γ and ϵ_1 all combine to render the qualitative agreement found of little if any significance in our opinion.

Later, Krylov and Levich (64) applied their results to a consideration of surface tension for $\omega = \pm 1$. Calculations using hexagonal and cutoff ($p = p_\infty$) models were compared, and it was found that interaction between adsorbed charges led to an increase in surface tension with increased coverage. The cutoff increases were somewhat smaller than those following from the fixed hexagonal lattice situation. Further, the changes were greater for $\omega = -1$ than for $\omega = 1$.

The hexagonal array model was next used by the present authors (5) to treat the $C-C$ imaging case. A modification of the Ewald method was employed to yield a rapidly convergent triply infinite series for $\psi_a^{(2)}(1)$, and many curves of Δ vs. r_1 or R_1 were presented. This work was not restricted to the conditions $q = 0$ and $\beta = \gamma$. Figure 28 illustrates, however, the results obtained for this simplified case. The cutoff model curves, shown dashed, were calculated using Eq. 132. It is clear that in the range of possible r_1 values, from perhaps $r_1 = 5$ or 6 Å on, Δ_0^0 is small and decreases almost exponentially with increasing r_1 . For large r_1 , there is substantial difference between the hexagonal and cutoff curves but such difference is of little or no significance in this region where Δ_0^0 is too small anyway to be important.

To illustrate the $\beta \neq \gamma$, $q \neq 0$ case, we include Fig. 29 which uses Grahame's $1N$ KI q_1, q results (51). Here $z_v = -1$, and the Δ_0 curve shows the behavior if q were zero for each q_1 value. When corresponding q_1 and q values are used, the Δ curve given is obtained. It has a pole at the point where V_{02} changes sign. We thus see that when experimentally derived pairs of q and q_1 values are used, ψ_{12} may be far from the proportion λ of V_{02} . Nevertheless, $\Psi_a^{(2)}(1)$ may actually be quite small over the entire

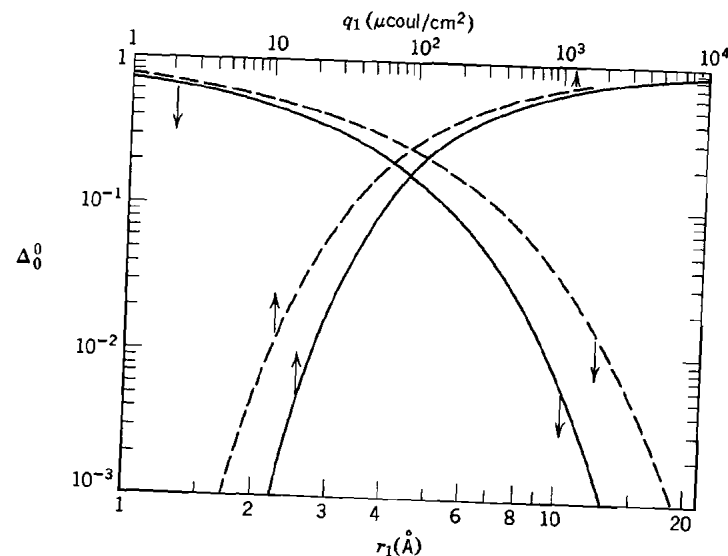


Fig. 28. Dependence of the $C-C$ imaging, $\Gamma = 1$, $q = 0$ linearity deviation parameter Δ_0^0 on r_1 and q_1 for $\beta = \gamma = 2$ Å and $z_v = 1$. Solid lines: fixed hexagonal array; dashed lines: ordinary cutoff model (5).

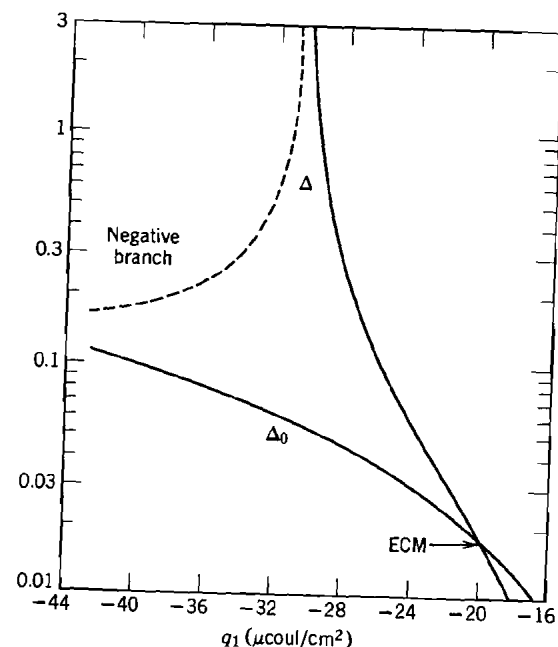


Fig. 29. Dependence of the $C-C$ imaging linearity deviation parameters Δ_0 and Δ on q_1 for $\beta = 3$ Å, $\gamma = 1$ Å, using Grahame's (51) $1N$ KI q and q_1 results (5).

range of q_1 . For example, at $q_1 = -42.61 \mu\text{coul/cm}^2$, $r_1 \cong 6.59 \text{ \AA}$. When $B = 3$, we then find that the hexagonal Δ_0 is approximately 0.09. Since $\Delta_0 \equiv \Psi_a^{(2)}(1)/\lambda\Gamma$, we obtain in this case $\Psi_a^{(2)}(1) \cong 0.0075$. On the other hand, the corresponding

$$\Psi_a^{(1)}(1) \equiv \Psi_a^{(2)}(1) + \lambda B$$

is approximately 0.7575. This value is close to the fraction $B\lambda \equiv 1 - \lambda = 0.75$ which the local potential $\psi_a^{(1)}(1)$ should be of ψ_∞ for $\omega = 1$ in the $q = -q_1$ case (see Fig. 37) provided the potential variation is linear.

It is of interest to show how $\Psi(1) \equiv \psi(1)/\psi_\infty$ may be readily obtained from published $C-C$ and $\omega = 1$ values of Δ_0 for $q \neq 0$ and $\beta = \gamma$. Since $\Psi(1) \equiv \Psi_a^{(1)}(1) + \{\psi_e(1)/\psi_\infty\}$, we may use the above relation between $\Psi_a^{(1)}(1)$ and $\Psi_a^{(2)}(1)$ plus the identity $\Psi_a^{(2)}(1) \equiv \lambda\Gamma\Delta_0$ to obtain

$$\Psi_a^{(1)}(1) = \lambda[\Gamma\Delta_0 + B] \quad (134)$$

and

$$\Psi(1) = Z_0^{-1}[\Gamma^2\Delta_0 - \Gamma\{1 + (q/q_1)\} - (q/q_1)] \quad (135)$$

This result of course only applies for $C-C$ imaging or for $C-D$ with $\omega = 1$. In the above KI case with $B = 3$, $q = 18 \mu\text{coul/cm}^2$ when $q_1 = -42.61 \mu\text{coul/cm}^2$. The quantity $\psi_e(1)/\psi_\infty$ then turns out to be about -0.578 . Thus, $\Psi(1)$ itself is about 0.18 in this case. In the single imaging case, $\Psi(1)$ is much smaller, less than 0.01, since most of the potential variation lies beyond the IHP for this situation.

Next, Krylov (61) extended some of his earlier results and calculated values of α for the $\beta = \gamma$ case. His results are shown in Fig. 30 and compare the hexagonal lattice and ordinary cutoff model predictions for α for both $\omega = 1$ (α_1 scale) and $\omega = -1$ (α_2 scale). Note that for $\omega = 1$ and $\beta = \gamma$, $\alpha \equiv \alpha_1 = \Delta_0^0/2$. The abscissa scale measure, δ/r_0 , equals $2\beta/r_1 \equiv 2/R_1$ in our notation. For the choice $R_{1m} = 2$, δ/r_0 thus also equals $\sqrt{\theta}$. We have compared some $2\alpha_1$ values with the corresponding hexagonal and cutoff values of Δ_0^0 shown in Fig. 28 and find good agreement even though the methods of calculation differed tremendously. The $\omega = -1$ results for α_2 will be discussed later along with more $C-C$ and $\omega = 1$ imaging results included under partial imaging.

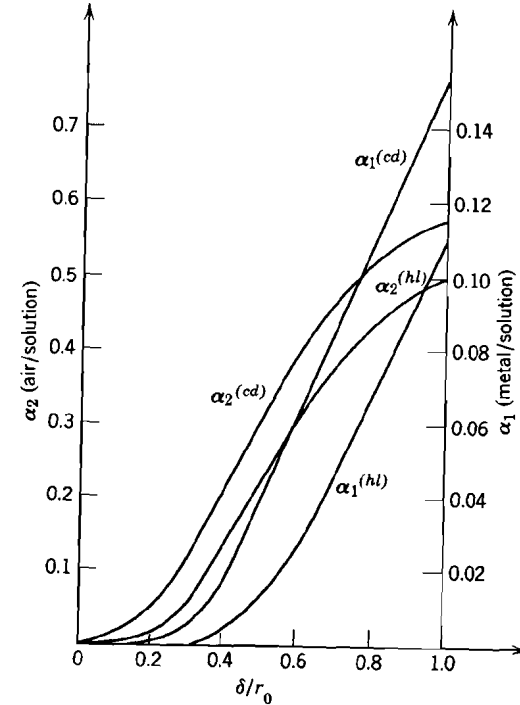


Fig. 30. Dependence of the Krylov discreteness parameter α ($\alpha \equiv \alpha_1$ for $C-C$ imaging; $\alpha \equiv \alpha_2$ for $\omega = -1$) upon $\delta/r_0 \equiv 2/R_1$. Here, curves marked "hl" refer to a hexagonal array and those marked "cd" to the ordinary Grahame cutoff model (61).

Finally, it should be mentioned that Levine et al. (77) have recently given an expression for the $C-C$ quantity g , for β not necessarily equal to γ , which involves three separate singly infinite series. It was derived using the ordinary cutoff model with an arbitrary r_0 , denoted r_β . Thus, this expression may be used in the HTL and LDL situations as well as in the ordinary Grahame case for which $r_\beta = r_0$ and $p = p_\infty$.

Although no curves of g vs. $\tau \equiv r_\beta/d$ are given by Levine et al., they do present some numerical values of $(1 - g)$ for six τ 's lying between $\tau = 1$ and 2 for $\beta = 3 \text{ \AA}$ and $\gamma = 1$ and 2 \AA . When plotted, one finds that in both cases $(1 - g)$ is very nearly proportional to $\exp(-2.85\tau)$.

C. Single Imaging. Let us first consider $C-O$ imaging with a conducting electrode. All imaging effects of the diffuse layer are thus necessarily neglected, valid if $\epsilon_s = \epsilon_1$ and the solute concentration is very low. There is good reason why the micropotential ψ_{12} rather than $\psi_{1\infty}$ should be considered in this case. When $q \neq -q_1$, the uniform field potential

$$\psi_e(Z) = -\psi_\infty Z[1 + (q/q_1)] \quad (136)$$

is nonzero and is of infinite magnitude when $Z = \infty$. Thus, it is preferable to consider the theoretical p.d. ψ_{12} and, when pertinent, add to it the actual small p.d. across the diffuse layer $\psi_{2\infty}$ (or $V_{2\infty}$) derived from experimental results.

We may now write

$$\begin{aligned} \psi_{12} &= \psi_a(1) - \psi_a(Z_0) + \psi_e(1) - \psi_e(Z_0) \\ &= \psi_{a1Z_0} + \Gamma\psi_\infty[1 + (q/q_1)] \end{aligned} \quad (137)$$

where $\psi_{a1Z_0} \equiv \psi_a(1) - \psi_a(Z_0)$. It then follows that

$$\begin{aligned} \Lambda &\equiv \frac{\psi_{12}}{V_{02}} \equiv \lambda(1 + \Delta) \\ &= \frac{\Gamma[1 + (q/q_1)] + \Delta\Psi_a}{\Gamma + Z_0(q/q_1)} \end{aligned} \quad (138)$$

where $\Delta\Psi_a \equiv \psi_{a1Z_0}/\psi_\infty$. The quantity Δ may now be written

$$\Delta = \frac{1 + (1 + B)\Delta\Psi_a}{\Gamma + Z_0(q/q_1)} \quad (139)$$

These results also apply for partial imaging ($C-D$ type) provided $\Delta\Psi_a$ is calculated for the pertinent imaging situation.

For $O-C$ imaging with the OHP approximated as a conducting equipotential surface, specific adsorption still involves transferring adions from the OHP to the IHP. In this case, however, it is almost always pertinent to take $q_1 = -q_2$, a grounded OHP situation. If we measure potential and Z from the OHP rather than from the ESP, as in the $C-D$ case, the actual situation is equivalent to that of $C-O$ imaging with $q = -q_1$ and a conducting ESP except that the roles of β and γ are reversed. Further, the potential is then zero at the OHP and thus $\psi_{12} = \psi(1) = \psi_a(1)$

for this situation. It then follows that

$$\Lambda = \psi_{12}/V_{20} = \psi_a(1)/\Gamma\psi_\infty \equiv \Psi_a(1) \quad (140)$$

In this equation V_{20} equals $-V_{02}$ except that the roles of γ and β must be interchanged. If, for convenience, we maintain our usual definitions of $\Gamma \equiv \gamma/\beta$, $B \equiv \beta/\gamma$, and $\lambda \equiv \Gamma/(1 + \Gamma)$, changing from $C-D$ to $D-C$ imaging as above causes ψ_∞ to change to $\Gamma\psi_\infty$. Since Z , however, is now measured from the OHP, it is logical to take $Z \equiv z/\gamma$; then $Z = 1$ still corresponds to the IHP. It will be clear that Eq. 140 applies for either $O-C$ or $D-C$ imaging if $\psi_a(1)$ is calculated for the imaging pertinent. Clearly, Λ values for $-1 \leq \omega \leq 1$ $D-C$ imaging lead directly to the normalized potential at the IHP. If they are given as a function of R_1 , then R_1 must be interpreted as r_1/γ in this case. The same values of $\Lambda(R_1)$ may be used to obtain $\Psi_a(1)$ directly in the $C-D$ case also provided that in this case R_1 is once again interpreted as r_1/β and $D-C$ imaging Γ values are transformed to numerically identical $C-D$ B values and *vice versa*.

The early work of Esin and Shikov (34), Ershler (32), and Grahame (52) already discussed, involves various approximations to $O-C$ or $C-O$ single imaging. Before discussing further work in this area, it will be valuable to summarize the modified cutoff model predictions for quantities such as Λ and Δ . For simplicity, take $q = -q_1$. Then for $C-O$ imaging we obtain

$$\begin{aligned} \Psi_a(1) &= \frac{1}{2}[\{(pR_1)^2 + 4\}^{1/2} - (pR_1)] \\ &\cong (pR_1)^{-1} - (pR_1)^{-3}, \quad (pR_1 \gg 2) \end{aligned} \quad (141)$$

in agreement with Eq. 120 if the $R_1 \equiv 2\gamma/r_1$ used there is replaced by $2\beta/r_1$ before comparison and the p here set equal to p_0 . Similarly,

$$\begin{aligned} \Psi_a(Z_0) &= \frac{1}{2}[\{(pR_1)^2 + (Z_0 + 1)^2\}^{1/2} - \{(pR_1)^2 + (Z_0 - 1)^2\}^{1/2}] \\ &\cong Z_0(pR_1)^{-1} - \frac{1}{2}(Z_0^3 + Z_0)(pR_1)^{-3}, \\ &\quad [(pR_1) \gg (Z_0 + 1)] \end{aligned} \quad (142)$$

Using these results and Eq. 138, we find for $pR_1 \gg (Z_0 + 1)$

$$\Lambda = -\Delta\Psi_a \cong \Gamma(pR_1)^{-1} - \frac{1}{2}(Z_0^3 + Z_0 - 2)(pR_1)^{-3} \quad (143)$$

for $q = -q_1$, and for $q = 0$

$$\begin{aligned} \Delta &\equiv \Delta_0 = B[1 + (1 + B)\Delta\Psi_a] \\ &\cong B - (1 + B)(pR_1)^{-1} \end{aligned} \quad (144)$$

We see from Eq. 144 that the limiting value of Δ_0 is not zero but B , also the limit for $C-O$ imaging when $R_1 \rightarrow 0$. If $R_1 \gg 7$, the appropriate value of p in these formulas is p_0 . Finally, we should point out that in view of Eq. 140, in the $O-C$ case Λ is given by just the $\Psi_a(1)$ of Eq. 141 provided R_1 in this equation is interpreted as r_1/γ .

In 1961, Mott and Watts-Tobin (94) carried out an approximate $C-O$ single image treatment in which the discrete adion images were completely smeared while the adion array itself was treated by the cutoff method with a hole of the usual Grahame radius, $r_0 = (\pi N)^{-1/2}$. Such a treatment retains very little of the original discreteness of the system. Further, it includes the image of an adion at point "d" but smears out this image over a circular region, making its potential contribution erroneously depend on N and r_1 . In calculating the energy equivalent to ψ_{12} with the self image energy included, Mott and Watts-Tobin should have properly considered the difference $[\phi_{iZ}(1) - \phi_{iZ}(Z_0)]$, which allows the image of an ion being adsorbed to move with the ion as it progresses from the OHP to the IHP. Instead, they considered only $\phi_{iZ}(1)$ and smeared its effect.

We have shown (6) that the Mott and Watts-Tobin model leads to the following expression for Λ when $q = -q_1$

$$\begin{aligned} \Lambda &= -\psi_{12}/\psi_\infty = -\Delta\Psi_a \\ &= \frac{1}{2}[\Gamma + (p_\infty R_1) - \{(p_\infty R_1)^2 + \Gamma^2\}^{1/2}] \end{aligned} \quad (145)$$

where we have replaced r_0/β by $p_\infty R_1$. In the limits $p_\infty R_1 \gg \Gamma$ and $p_\infty R_1 \ll \Gamma$, the above equation reduces to approximately

$$\Lambda \cong \frac{1}{2}[\Gamma - (\Gamma^2/2)(p_\infty R_1)^{-1}], \quad (p_\infty R_1 \gg \Gamma) \quad (146)$$

and

$$\Lambda \cong \frac{1}{2}[(p_\infty R_1) - (p_\infty R_1)^2(2\Gamma)^{-1}], \quad (p_\infty R_1 \ll \Gamma) \quad (147)$$

Mott and Watts-Tobin implicitly considered only the condition $p_\infty R_1 \gg \Gamma$ from the outset and obtained Eq. 146. Discreteness is so little evident that the corresponding ψ_{12} p.d. does not depend at all on β . The cutoff model for this case leads to Eq. 143 with $p = p_\infty$. In addition to the difference in the sign and magnitude of the coefficient of $(p_\infty R_1)^{-1}$, there is an additional term in Eq. 146 which does not disappear as $R_1 \rightarrow \infty$. This term arises from the overly approximate treatment of the self-image charge, not included in

the cutoff model but easily incorporated in it properly when desired. These results indicate that the Mott and Watts-Tobin result is less appropriate even than the earlier Esin-Shikov (34) expression. When $\Gamma \gg p_\infty R_1$, the image term becomes of negligible importance. In this case, in fact, the cutoff model leads to

$$\Lambda \cong \frac{1}{2}[(p_\infty R_1) - \{(Z_0^2 + 3)/4(Z_0^2 - 1)\}(p_\infty R_1)^2] \quad (148)$$

the same to first order as Eq. 147 and nearly the same to second order when $\Gamma = 1$.

Next, Levine et al. (75) used the Grahame cutoff model to examine an $O-C$ situation for which ϵ_0 (pertaining to a colloid plate region to the left of the ESP) was taken as 15, as was ϵ_1 . Further, ϵ_s was assumed infinite as well and the OHP taken as an equipotential surface. Since the average potential at the IHP will be $\Gamma\psi_\infty$ for $O-C$ imaging, again measuring Z and potential from the grounded OHP, we may write in the spirit of Levine's approach

$$\psi_a(1) = \Gamma\psi_\infty + \phi_1 = \Gamma\psi_\infty - \lambda\psi_\infty g \quad (149)$$

and

$$\Psi_a(1) \equiv \Lambda = 1 - \lambda Bg \quad (150)$$

where we have used Eq. 140. It follows that

$$g = (1 + \Gamma)[1 - \Psi_a(1)] \quad (151)$$

considerably different from the equation for g in the $C-C$ case. Had $C-O$ imaging been considered, Eq. 151 with $(1 + \Gamma)$ replaced by $(1 + B)$ would have obtained. Both Eqs. 150 and 151 apply for $-1 \leq \omega \leq 1$ as well as $\omega = 0$ provided $\Psi_a(1)$ is calculated for the pertinent ω value.

It is important to remember that in equations such as Eq. 151, which involves defined quantities taken from treatments by different authors, all constitutive parameters such as g and $\Psi_a(1)$ must refer to the same model. Thus, if in Eq. 151 $\Psi_a(1)$ is given by Eq. 141 with p equal to the Grahame p_∞ , then the corresponding g refers to the ordinary cutoff model. Note that since $\Psi_a(1) = 1$ and 0 when $R_1 \rightarrow 0$ and ∞ , respectively, g changes from zero to $(1 + \Gamma)$ over the full range of R_1 . Levine et al. (75) give a curve of g vs. $\tau \equiv p_\infty R_1/2$ from $\tau = 2$ to $\tau = 10$ for $\beta = \gamma$. By $\tau = 10$, g is nearly $(1 + \Gamma) = 2$.

In 1963, Bockris, Devanathan, and Müller (10) derived an isotherm (the BDM isotherm) intended to account for interactions between anions and the metallic electrode and those within the anion layer. Discussion of their result is of special interest because they found rather good agreement with experiment using this isotherm. In this $C-O$ treatment, Bockris et al. state that the work of transferring an ion from the OHP to the IHP was neglected. Instead, the potential at the OHP was neglected, in that the quantity $\psi(1)$ was used where the difference $\psi(1) - \psi(Z_0)$ should have been. Thus, their treatment essentially involves only the single imaging $\psi(1)$. Their expression corresponds to

$$\psi(1) = \frac{4\pi q\beta}{\epsilon} - \frac{Me_0\beta^2(\pi N)^{3/2}}{4\epsilon_c} [1 - \frac{3}{4}\beta^2\pi N] \quad (152)$$

where ϵ , ϵ_c , e_0 and M are undefined. Bockris et al. used the inconsistent relation $\pi N(\tau_1/2)^2 = 1$ in arriving at this result. This differs from the relation between these quantities for a hexagonal lattice by a ratio of about 0.68. Although these authors do not mention the adion array structure they consider, it will become evident later that their approach is only logically consistent with a fixed hexagonal array. The use of the above relation between N and τ_1 means that Eq. 152 is not fully related in a logical fashion to the model from which it was derived. Since Eq. 152 was apparently used in comparing theory and experiment, however, we shall compare it as is rather than derive the expression corresponding to the model begun with.

The matter of the meaning of undefined and unspecified parameters in reference 10 is somewhat clarified in later work by Wroblowa, Kovac, and Bockris (130). There, ϵ and ϵ_c are written as ϵ , the dielectric constant. Unfortunately, the region of applicability of ϵ and its value are not discussed; we shall take it as ϵ_1 , the effective dielectric parameter for the inner layer. Although e_0 is still undefined, we assume it to be the magnitude of the electron charge, e . Finally, M is defined as a two-dimensional analogue of the Madelung constant. It was taken as 11.4 on the authority of Langmuir (66). Langmuir considers a fixed hexagonal array of ideal dipoles and obtains 11.044 by a summation-integration method. The value 11.4 must, therefore, be a misprint, and we hazard a guess that in the comparisons with experiment

carried out by Bockris et al. the value 11.044 was used. It is now clear that Eq. 152 must involve a hexagonal lattice model and that M actually equals the Topping quantity we have denoted σ ($\cong 11.034$).

In the later paper, the term (πN) is written as $(\pi q_1 \mathbf{N}/\mathbf{F})$, where \mathbf{N} is Avogadro's number and \mathbf{F} must be the Faraday. Now q_1 is negative for adions, so \mathbf{F} must also be negative to avoid the appearance of imaginary numbers. Then $q_1 \mathbf{N}/\mathbf{F} = |q_1/e|$, equal to our N , the adion surface density, for $|z_v| = 1$.

There is one remaining difficulty before Eq. 152 may be compared with other approaches. The second term in Eq. 152 is negative there but positive in the later work (130). Equation 8 in the Wroblowa paper indicates, however, that the plus sign must be a misprint.

We shall compare the modified cutoff model prediction (with $p = p_0$) for $\psi(1)$ with Eq. 152. To maintain the same order of approximation, we employ the form of $\psi_a(1)$ valid when $p_0 R_1 \gg 2$. Note, however, that the unexpanded form of $\psi_a(1)$ with $p = p(\xi)$ would yield higher accuracy for smaller R_1 values. We obtain

$$\begin{aligned} \psi(1) &= \psi_a(1) + \psi_e(1) \\ &\cong [(p_0 R_1)^{-1} - (p_0 R_1)^{-3} - \{1 + (q/q_1)\}] \psi_\infty \quad (153) \end{aligned}$$

Let us now take $z_v = -1$ and express the above result in terms of N where appropriate. We obtain

$$\begin{aligned} \psi(1) &= -\frac{4\pi q\beta}{\epsilon_1} - \frac{4\pi q_1\beta}{\epsilon_1} \\ &\quad - \left(\frac{3^{3/4}\sigma}{\sqrt{2}}\right) \frac{e\beta^2 N^{3/2}}{\epsilon_1} \left[1 - \left(\frac{3^{3/2}\sigma^2}{2^5\pi^2}\right) \beta^2 N\right] \quad (154) \end{aligned}$$

which may now be directly compared with Eq. 152.

It is first evident (see also Eq. 136) that the constant field contribution ψ_e has been incorrectly taken into account in the BDM expression for $\psi(1)$. Since $q_1 < 0$ for the present case, it turns out, however, that $-(4\pi\beta/\epsilon_1)(q_1 + q)$ will generally remain positive and vary qualitatively with q roughly like the BDM term $(4\pi\beta/\epsilon)q$ for $q > 0$. Next, taking $M \equiv \sigma$, it is evident that we should compare $(\pi^{3/2}/4)$ and $(3^{3/4}/\sqrt{2})$. These numbers turn out to be about 1.39 and 1.61, respectively, adventitiously close to

one another. Similarly, for the $N^{5/2}$ term we should compare $(3\pi/4)$ and $(3^{3/2}\sigma^2/2^5\pi^2)$. Most surprisingly, these numbers are also accidentally close, about 2.36 and 2.02 respectively. Further, the term involving σ^2 involves p_0^{-2} , but p_0 is only strictly the right value for a hexagonal array (if it could exist) with $R_1 \rightarrow \infty$. For $R_1 \gg 2$ but finite, p is slightly less than p_0 , leading to a decrease in the difference between the last pair of numbers above.

We thus see that in spite of its theoretical inconsistencies and inadequacies, the BDM $\psi(1)$ turns out to be reasonably close to the $C-O$ hexagonal lattice $\psi(1)$. Nevertheless, the use of single imaging, of a hexagonal array (at the lower concentrations), the introduction of ϵ_1 , a $p_0 R_1 \gg 2$ expansion over the entire range of R_1 , and the neglect of the potential at the OHP are such inadmissible approximations that the usefulness found by Bockris and co-workers of the BDM $\psi(1)$ as the micropotential in an adsorption isotherm can only be considered fortuitous. No valid theoretical basis for the use of this $\psi(1)$ in an electrolyte adsorption isotherm should be asserted. While its empirical usefulness has been unquestioned, its considerable agreement with experiment nevertheless does not allow one to infer from it much of significance about the structure and behavior of the electrolyte inner layer.

Recently, the present authors (6) have presented a $C-O$ single-imaging treatment of the hexagonal lattice micropotential for comparison with $C-C$ results. Using an accurate summation method, many curves of Λ , Δ_0 , and Δ_0^0 were calculated and presented. It was found, for example, that Δ_0^0 varied from about 0.4 at $R_1 = 2$ to unity as $R_1 \rightarrow \infty$. As expected for single imaging, Λ departed considerably from its approximate value λ pertinent with $C-C$ imaging and appreciable R_1 . In fact, since $\Delta\Psi_a \rightarrow 0$ as $R_1 \rightarrow \infty$, Ψ_{12} becomes dominated by $[\psi_e(1) - \psi_e(Z_0)]/\psi_\infty$ in this limit, and Λ thus approaches unity when $q = 0$. Although the micropotential results of this paper (6) were calculated using a rather complicated formula, similar accurate results may now be obtained in a much simpler fashion using Eqs. 141 and 142 and the appropriate $p(\xi = R_1^{-1})$ and $p(\xi = Z_0/R_1)$ functions.

In Fig. 31 we have presented single-imaging Δ and Δ_0 curves calculated using Grahame's (51) 1.0N KI q, q_1 pairs. These curves should be compared with the corresponding $C-C$ curves of Fig. 29. As expected, both Δ and Δ_0 values are generally larger in the

single-imaging case. They are not as pertinent to the real situation, however, as are the $C-C$ ones since the actual inner-layer conditions must approximate $C-C$ imaging more closely than $C-O$. In fact, were single imaging appropriate in the electrolyte case, the large r_c pertinent in this situation would limit the maximum $|q_1|$ to a value considerably smaller than that derived from

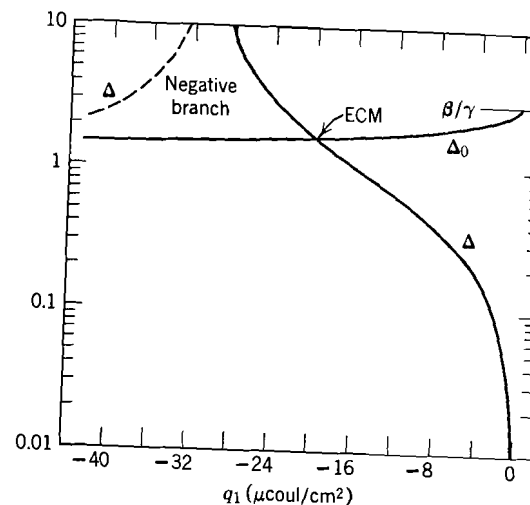


Fig. 31. Dependence of Δ_0 and Δ on q_1 for $C-O$ imaging with $\beta = 3 \text{ \AA}$, $\gamma = 1 \text{ \AA}$, and $Z_0 = \frac{4}{3}$ using Grahame's (51) 1N KI q and q_1 results (6).

experiment. The value $r_c = 14 \text{ \AA}$ discussed earlier corresponds to a maximum $|q_1|$ of only about $10 \text{ microcoul/cm}^2$.

Single imaging represents only one point on the continuum of $C-D$ imaging possibilities ranging from $-1 \leq \omega \leq 1$. Although it is the only imaging case of importance for adsorption from a gas phase, it is primarily of significance in the electrolyte case only for historical reasons and as a special limiting case for which the analysis becomes simpler. As we have seen earlier, however, although not of much physical significance for the electrolyte double layer, single imaging is of mathematical importance because results of $\omega = 0$ calculations can be combined to yield potentials and fields for any other pertinent ω values. Such a mode of calculation, using the ordinary or modified cutoff method

to calculate the input single-imaging potentials, represents probably the simplest method of calculating $\omega \neq 0$ results. Such partial imaging situations are considered in the next section.

D. Other Imaging Conditions. Some $D-C$ partial imaging results based on the ordinary cutoff model were given in the 1962 paper of Levine, Bell, and Calvert (75). The method of calculation was not described, but curves were given of g vs. τ for $\beta = \gamma$ and $\omega = 1, 0.9, 0.7, 0.5, 0,$ and -0.5 . This g is that of Eq. 151 of Section V-2-C.

Buff and Stillinger (17) then published a complicated statistical theory of the double layer with specific adsorption. This theory, applicable for $-1 \leq \omega \leq 1$ at the OHP, made use of the GFA Fourier-Bessel integral technique (17,77,115) to sum up the contribution to the potential from an infinite line of images. A doubly infinite sum of integrals had then to be carried out to account for every adion in the IHP. Buff and Stillinger bypassed this sum by means of a cluster theory approach which included only low-order interaction-induced correlations in adion position. They then considered only the thermally averaged, or expectation value, potential. Although this approach accounts properly for short-range forces, long-range forces are treated as a small perturbation, and all Mayer f -bonds are linearized in the long-range interaction. This treatment is valid, therefore, for a highly disordered situation, either the HTL or the LDL, but is inapplicable when an array with appreciable long-range order begins to form. Even in the applicable quasi-random situation, however, we believe that our modified cutoff methods are as valid as the above approach and are far easier to apply. It is perhaps significant that Buff and Stillinger present no numerical results at all and no assessment of the range of applicability of their analysis. Although the Buff-Stillinger approach might help one penetrate a short distance into the difficult transition region between quasi-random and regular array behavior, it cannot be expected to contribute much in its present form to bridging the gap. Were it generalized to include higher-order interactions, both analysis methods and computational techniques would be strained outside the realm of present practicality.

Next followed Krylov's (61) $\alpha_1(\omega = 1)$ and $\alpha_2(\omega = -1)$ hexagonal lattice and cutoff curves already presented in Fig. 30.

These results also pertain only for $\beta = \gamma$. The $\omega = 1$ $\alpha = \alpha_1$ curves have already been discussed. For $\omega = -1$, Krylov deals with a $D-C$ imaging situation and writes $\alpha = \alpha_2$ and

$$\psi_{12} = \alpha \Gamma \psi_{\infty} \quad (155)$$

Comparison with Eq. 140 of Section V-2-C shows us that $\alpha_2 \equiv \Psi_a(1)$ in this case. Comparison of Krylov's hexagonal lattice α_2 values with our corresponding $\Psi_a(1)$ values calculated entirely differently also yields good agreement. Note that as in the $C-C$ case, the $p = p_{\infty}$ cutoff α 's always exceed the hexagonal array ones.

Levine, Mingins, and Bell (77) next presented an extension of the earlier work of Levine, Bell, and Calvert (75). This new treatment is also based on the Grahame cutoff method, but the cutoff model hole size variable, $r_0 \equiv (\pi N)^{-1/2}$, is often replaced by r_{β} , a quantity which may vary with r_1 differently from r_0 . This replacement leads to what the authors term the revised cutoff model, equivalent in principle to our modified cutoff approach if their r_{β} is identified with our general cutoff model radius variable, r_b . Since no complete qualitative or quantitative relation between r_{β} and N or r_1 is presented, the authors frequently use r_0 in place of r_{β} and sometimes seem to confuse the two quantities. Although some curves and tables are given with r_{β} as the independent variable, the results cannot be related to the appropriate values of q_1 without a definite relation between r_{β} and N .

In the new work, Levine et al. included dielectric imaging at both the ESP and the OHP, took the ESP either conducting or insulating, and also investigated the effect of diffuse-layer screening as a function of the solute concentration and the potential drop across this layer, $V_{2\infty}$. Their treatment is thus both ambitious and comprehensive—and correspondingly complex and approximate. Although Levine and his co-workers have applied the cutoff model primarily in the regime where thermal motion is of some importance, the model can be extended outside this range, as we have shown in the prior discussion of cutoff approaches, by using r_{1m} for r_b in the HTL case, r_c for r_b in the LDL situation, and $p(\xi)r_1$ for r_b in the rigid hexagonal-array case.

Since the quantity r_{β} is of considerable importance to the Levine et al. approach, it warrants additional discussion. Using

a grand canonical ensemble, Levine and co-workers arrived at the (approximate) result

$$S^*(\rho) = q_1[\exp(-V(\rho)/kT) - 1] \quad (156)$$

where $S^*(\rho)$ is the fluctuation surface charge density, ρ the distance between two ions in the IHP, and $V(\rho)$ the potential of mean force between the two ions under the actual conditions applying in the inner region. They used this result to obtain

$$\begin{aligned} r_\beta^2 &= 2 \int_0^\infty \rho [1 - \exp(-V(\rho)/kT)] d\rho \\ &= r_{1m}^2 + 2 \int_{r_{1m}}^\infty \rho [1 - \exp(-V(\rho)/kT)] d\rho \end{aligned} \quad (157)$$

where the condition $V(\rho) = \infty$ for $\rho \leq r_{1m}$, consistent with r_{1m} (denoted a in the paper in question) being the minimum distance of approach in the plane because of hard-core steric effects, was used to arrive at the second form. It is clear that when $V(\rho) = 0$ for $\rho > r_{1m}$ as well, $r_\beta = r_{1m}$.

For sufficiently small $|q_1|$, the authors approximate $V(\rho)$, a function of q_1 and the imaging-shielding conditions as well as ρ by $V_0(\rho)$, the interaction energy of an isolated pair of adions separated by the distance ρ in the presence of the diffuse layer. The above equations are probably most appropriate in this limit. By means of an approximate treatment of the effect of the diffuse layer, they then calculate for various imaging conditions first $V_0(\rho)$ then $(r_\beta)_0$, which is the quantity corresponding to r_β when $V(\rho)$ is replaced by $V_0(\rho)$, itself independent of q_1 by definition. Asserting that $V(\rho)$ will decay more rapidly than $V_0(\rho)$, Levine and his associates interpret $(r_\beta)_0$ as the upper limit to the value of r_β . This limit must clearly be applicable only when $q_1 \rightarrow 0$ and $r_1 \rightarrow \infty$, the LDL regime. Thus, one concludes that r_β must vary from some minimum value to $(r_\beta)_0$ as $|q_1|$ decreases from its maximum possible value towards zero.

Since we may identify $R_\beta \equiv r_\beta/\beta$ with the R_b of Fig. 13, we may compare our conclusions concerning its variation with those of Levine and co-workers. The latter authors take $r_{1m} \leq r_\beta < r_0$, or $R_{1m} \leq R_\beta < R_0$. They seem to be primarily concerned with the quasi-random region and perhaps somewhat with the transition region, although they do not discuss the existence of the latter

region explicitly. Certainly, they do not intend their treatment to cover the regular-array region.

From their definitions, it is clear that our R_c and $(R_\beta)_0 \equiv (r_\beta)_0/\beta$ are identical in principle, even though the ways used to calculate them by ourselves and Levine et al. differ. For given imaging conditions, R_c is approximately the minimum distance of approach of two isolated ions. It is generally greater than r_{1m} because of the coulomb repulsion effective under the given conditions. In our calculations of an approximate R_c , diffuse-layer shielding has been ignored for C-O single imaging, while it has been included in our C-C imaging treatment and in the work of Levine and his associates.

Reference to Fig. 13 shows us that indeed $R_\beta < R_0$, as expected by Levine et al., in the quasi-random region where $R_\beta \equiv R_c$, a constant. We also see, however, that while R_c is the $q_1 \rightarrow 0$ limiting value of R_β , it is not necessarily the upper limit of R_β as stated by Levine et al. Depending upon the value of R_c and the widths of the hexagonal and transition regions, R_β may or may not reach a greater value than R_c . For the C-C imaging conditions of Fig. 13, it almost certainly exhibits a peak, as shown.

Using our modified cutoff approach, we are able to extend consideration of R_β into the regular-array region. In this region, we have seen that the cutoff equations can be made to represent a hexagonal-array model provided $r_0/\beta \equiv R_0$ is replaced by $p(\xi)R_1$. This quantity, R_b , is only equal to R_0 when $p(\xi) = p_\infty$, Grahame's value, which we find to be appropriate for the hexagonal array only for $\xi \gg 1$. Figure 13 was calculated for $Z = 1$; thus, $\xi (= R_1^{-1})$ ranges from 0.5 down towards zero. For this range, $p(\xi)$ varies only from about 0.62 to 0.657, nearly equal to p_0 . Therefore, in the available hexagonal-array region, from $R_1 = R_c$ to the transition region, $R_\beta = R_b$ is roughly $0.64R_1$, not equal to R_0 , which is given by $0.525R_1$. In this range we see that $R_\beta > R_0$, opposite to the Levine et al. conclusion. If the adions could actually be close packed in the plane, R_1 would equal R_{1m} , but the appropriate R_β which should be used in the cutoff model formulas would be $p(\xi_m)R_{1m}$, about equal to $0.62R_{1m} = 1.24$ for $R_{1m} = 2$.

Let us compare our and Levine's results for r_c for as analogous situations as possible. Initially, let us restrict attention to the

situation where the dielectric constant of the region to the left of the ESP is taken infinite. This appears to correspond in the Levine et al. treatment to taking the ESP electrically conducting. In this case, with $\beta = 3 \text{ \AA}$, $\epsilon_s = 80.1$, $\epsilon_1 = 10$, and $T = 20^\circ\text{C}$, Levine and his co-workers obtain $(r_\beta)_0 = 9.5 \text{ \AA}$ for $\gamma = 1 \text{ \AA}$, a solute concentration of 0.1 moles/liter, and the potential $V_{2\infty}$ taken zero. They further find $(r_\beta)_0 = 9.3$ and 11.0 \AA for $\gamma = 2 \text{ \AA}$ and concentrations of 0.1 and 0.01 moles/liter, respectively, again with $V_{2\infty} = 0$. The situation considered approximates that of C - D imaging with $\epsilon_s \sim \infty$ and hence perfect infinite imaging. In this case, concentration changes should be relatively unimportant, as indeed was found by Levine et al.

It is interesting to compare the above results with the values $r_c \cong 6.9 \text{ \AA}$ for $\beta = 3 \text{ \AA}$ and $\gamma = 1 \text{ \AA}$ and $r_c \cong 9.2 \text{ \AA}$ for $\beta = 3 \text{ \AA}$ and $\gamma = 2 \text{ \AA}$ obtained from the results of Appendix I in the simpler and more physically transparent manner discussed previously for the C - C case. These results are surprisingly close to those found by Levine and his associates, although the variation with γ is opposite. We believe that the degree of agreement is primarily an accident, however. Not only were our r_c 's and Levine's $(r_\beta)_0$'s calculated in quite different ways for slightly different situations, but our analysis used a shielding dielectric constant of unity, a value we believe to be close to that appropriate in the situation, while Levine used $\epsilon_1 = 10$.

Although no value of $(r_\beta)_0$ for O - C single imaging is given by Levine et al., they do present values for O - D imaging with $\epsilon_s = 80.1$ and some ionic diffuse-layer shielding. The combination of this high value of ϵ_s and some conductive shielding may again be taken to approximate conductive imaging quite closely. If we convert from O - C to C - O imaging ($\gamma \leftrightarrow \beta$), then the input values used by Levine and co-workers in this case correspond to $\beta = 1$ and 2 \AA , $T = 20^\circ\text{C}$, a solute concentration of 0.1 mole/liter and $\epsilon_2 = \epsilon_1 = 15$. The quantity $(r_\beta)_0$ was found to be 15.8 \AA for $\beta = 1 \text{ \AA}$ and 16.4 \AA for $\beta = 2 \text{ \AA}$. In contradistinction, our semiquantitative single-imaging result, appropriate for $\epsilon_1 = \epsilon_s = 1$, leads to $r_c \cong 9.5 \text{ \AA}$ for $\beta = 1 \text{ \AA}$ and $r_c \cong 15 \text{ \AA}$ for $\beta = 2 \text{ \AA}$. We note especially the considerably smaller value of r_c for $\beta = 1 \text{ \AA}$ and the lack, in the Levine results, of much dependence of $(r_\beta)_0$ on β . We believe this virtual independence to be

incorrect. Had we also used in our calculation a value of 15 for the dielectric constant effective in shielding the interaction, our values of r_c would have been reduced by a factor of more than 2.4, making the above disagreement even more pronounced.

Lack of space prohibits us from giving a detailed discussion of the lengthy and courageous work of Levine, Mingins, and Bell already discussed. We believe, however, that the following additional brief comments are worthwhile. Since a general form of $V(\rho)$ valid for all q_1 is not given, r_β cannot be calculated as a function of q_1 or r_1 . When $|q_1|$ is sufficiently large that $V_0(\rho)$ is no longer a good approximation, we believe that Eq. 157 is also no longer likely to be an adequate approximation even were the pair interaction potential $V(\rho)$ known exactly. Certainly this equation is inadequate when a regular array forms; we believe the combination of it and the cutoff model to be also inadequate over most of the transition region as well. Next, the treatment of diffuse-layer screening is based on the linearized Poisson-Boltzmann equation. The inadequacy of this equation for many pertinent electrolyte double-layer situations has already been discussed at length in an earlier section. It is easy to show that the linearization used by Levine et al. depends on the perturbation potential at the OHP being much less than $1.7(kT/e)$, about 42 mV at 20°C . No check of the validity of this stringent condition was presented; it is not likely to be satisfied, for example, when $|V_{2\infty}| = 97 \text{ mV}$, a value frequently used by these authors.

Finally, of less basic but of considerable practical importance is the lack in the Levine, Mingins, and Bell work of any experimental or theoretical correlation between q , q_1 , and q_2 . No values of q are given and potentials are calculated as functions of r_β or r_0 , hence presumably of N and q_1 . The potential $V_{2\infty}$, related to q_2 , is taken, however, as an independent parameter not directly associated, as it should be, with appropriate values of q and q_1 .

In Figs. 32 and 33 we reproduce results for ϕ_1^* and $\Delta\phi_1$ calculated by Levine et al. The fluctuation potential $\phi_1(0,0) \equiv \phi_1$ already discussed is written as $\phi_1^*(0,0) + \Delta\phi_1(0,0)$. The quantity ϕ_1^* is calculated for an infinite Debye length; then $\Delta\phi_1$ represents the correction arising from the ionic screening produced by mobile ions in the diffuse layer. The ordinate designations of both curves should be multiplied by $-e$, as should similar

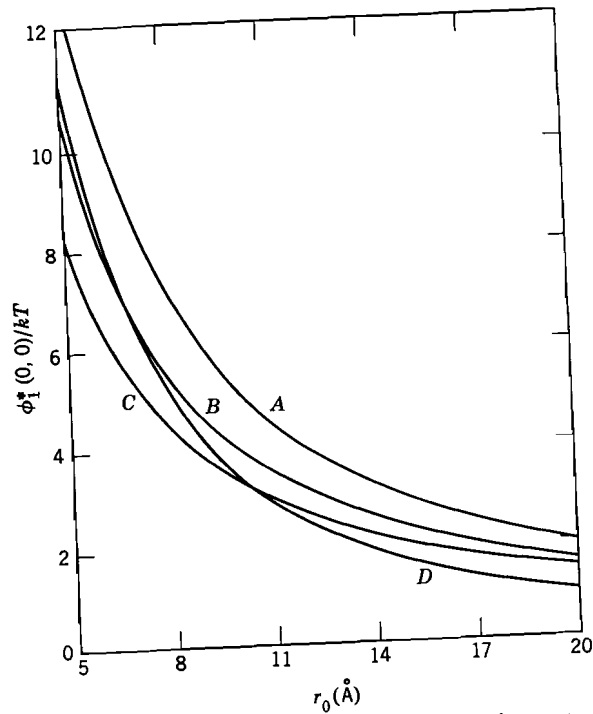


Fig. 32. The Levine et al. (77) unscreened discrete-ion potential ϕ_1^* versus r_0 (\AA). The ordinate designation should be $-e\phi_1^*/kT$. Here $\epsilon_s = 80.1$, $T = 20^\circ\text{C}$.

Curve	ϵ_0	ϵ_1	β (\AA)	γ (\AA)
A	15	10	3	2
B	15	10	3	1
C	15	15	—	1
D	∞	10	3	2

quantities presented in the tables included in the paper. In the text of the paper, the abscissa is referred to as r_β , not r_0 . Information received by private communication makes it clear that r_0 was actually meant here.

Note that had a more realistic value of $\epsilon_1 \approx 6$ been used in calculating the curves of these figures instead of the values of 10 and 15 actually used, the maximum values of ϕ_1 would have been about twice as many times (kT/e) as shown. The perturbation potential at the OHP would then be even less likely to satisfy the condition of being much smaller than $1.7(kT/e)$. Incidentally,

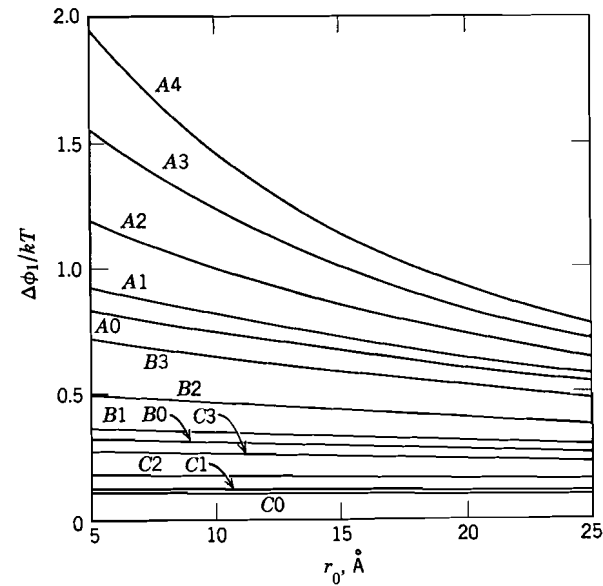


Fig. 33. The Levine et al. (77) diffuse-layer screening correction $\Delta\phi_1$ vs. r_0 (\AA). The ordinate designation should be $-e\Delta\phi_1/kT$. Here $\epsilon_s = 80.1$, $T = 20^\circ\text{C}$, $\epsilon_0 = 15$, $\epsilon_1 = 10$, $\beta = 3 \text{\AA}$, $\gamma = 1 \text{\AA}$. (A.) $M/10$; (B.) $M/100$; (C.) $M/1000$. The numbers 4, 3, 2, 1, and 0 refer to the value of $|\xi_d|$, equal to $|V_{2\infty}|/24.36$ when $V_{2\infty}$ is in mV.

Levine, Mingins, and Bell expect the results shown in these figures to be most reliable for the smallest r_β values. They seemingly set $r_\beta = r_0$ in some of their work and calculate q_1 from the Grahame cutoff relation $q_1 = z_v e / \pi r_0^2$. Their minimum value $r_0 = r_\beta = 5 \text{\AA}$ then corresponds to about $20 \mu\text{coul}/\text{cm}^2$, the $|q_1|$ region where they expect a hexagonal lattice to start to form. Since we believe their approach does not adequately span the transition region, we feel that their curves are most appropriate near the LDL region specified by $r_0 \equiv (r_\beta)_0$ where a smeared-charge model is most applicable.

There is a further interesting anomaly. It is clear from the form and derivation of Eq. 157 for r_β that Levine et al. expect r_{1m} to be the minimum value of r_β . But r_{1m} is the close-packed hexagonal array nearest distance of approach of ion centers, enforced by steric effects. On the other hand, r_β is a mathematical cutoff model

variable which specifies the radius of the circle of removed charge in this model. It is thus not limited in the same way that r_1 is, and instead of taking $r_{\beta \min} = r_{1m}$, Levine et al. should have used $r_{\beta \min} = p(\xi_m)r_{1m}$, a considerably smaller quantity. Since a close-packed array is not attained experimentally nor expected theoretically for either $C-C$ or $O-C$ imaging, this matter is not of great practical importance. It is confused, however, by Levine's choice of the minimum value of r_{β} (or r_0) as 5 \AA , a value he and his associates also use consistently as that of r_{1m} . If r_{1m} were equal to 5 \AA , the corresponding $|q_1|$ would have the far-too-large value of 74 \mu coul/cm^2 .

The most recent work on partial imaging is that of the present authors (91). The entire range of $-1 < \omega < 1$ was covered for both $C-D$ and $D-C$ imaging. Calculations for $\omega \neq 0$ were made by the method described earlier which sums individual single-image contributions. It thus involves only a single infinite series for $\omega \neq 0$ and converges rapidly for small ω . Convergence is slower the larger $\xi_0 \equiv Z_0/R_1$, and the closer $|\omega|$ to unity. It may be greatly speeded up, when needed, by application of the epsilon algorithm (83).

Figure 34 shows some Δ_0 results obtained for ordinary $C-D$ imaging, covering the range $0 \leq \omega < 1$ of interest in this case. The dashed and dotted lines of Fig. 34b were calculated using the ordinary cutoff model, not a hexagonal array (solid lines) for the fixed values $p = p_{\infty}$ (dotted) and $p = p_0$ (dashed). The differences between these curves and the corresponding hexagonal-array lines is not great out in the large R_1 region where they all run approximately parallel. The difference is large, however, for smaller R_1 values and becomes greater the smaller R_1 ($R_1 \geq 2$) and the closer ω to unity. Because p_0 and p_{∞} are the largest and smallest values, respectively, attained by the $p(\xi)$ of a fixed hexagonal array, it is not surprising that the limiting hexagonal lines lie between those for p_0 and p_{∞} . Since the region of maximum deviation between the cutoff model predictions and those of the hexagonal array is for small R_1 where the hexagonal array is likely to be the best approximation to the actual structure, the hexagonal array results are definitely preferable in this region.

Comparison in the case $\omega = 1$ is interesting. Let us temporarily denote the present $C-D$ Δ_0 for $\omega = 1$ as $\Delta_0^{(1)}$ and the $C-C$ imaging

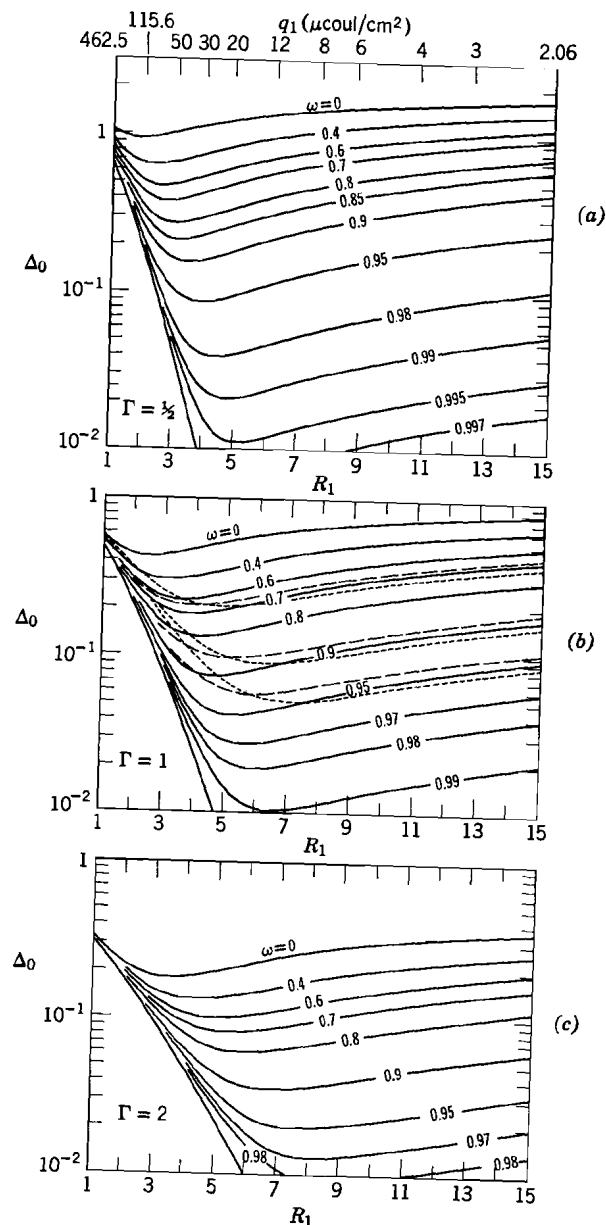


Fig. 34. The nonlinearity parameter for $q = 0$, Δ_0 , vs. $R_1 = r_1/\beta$ for a hexagonal array, three Γ values, and $\omega \geq 0$. Dotted lines were calculated from the cutoff model using the Grahame $p = p_{\infty}$ and dashed lines with $p = p_0$. The q_1 scale at the top of the figure is only appropriate for the choice $\beta = 2 \text{ \AA}$ (91).

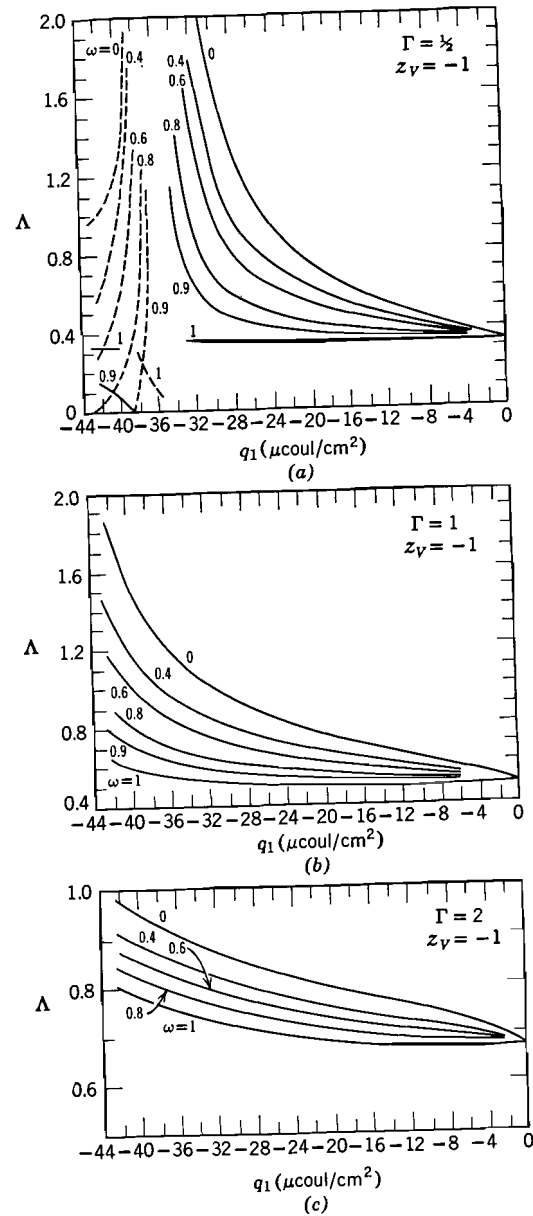


Fig. 35. The micropotential quantity $\Delta \equiv \psi_{12}/V_{02}$ vs. Grahame's (51) 1N KI derived $q_1(q)$ for $\beta = 2 \text{ \AA}$, three Γ 's and $\omega \geq 0$. Dashed lines here denote negative values (91).

Δ_0 of Section V-2-C as $\Delta_0^{(2)}$. Since $\Psi_a^{(1)}(Z_0) \equiv 1$, comparison of the relevant definitions shows that $\Delta_0^{(1)}$ and $\Delta_0^{(2)}$ are identical, as they should be. Comparison of numerical values of the two Δ_0 's calculated from $\psi_a^{(1)}$ and $\psi_a^{(2)}$ values obtained by tremendously different series, bears out this identity. To obtain the normalized potentials from Δ_0 values, we need only use either $\Psi_a^{(2)}(1) = \lambda\Gamma\Delta_0$ or $\Psi_a^{(1)}(1) = \lambda[\Gamma\Delta_0 + B]$. Finally, note that for any ω but unity the limiting value of Δ_0 is B as $R_1 \rightarrow \infty$ or 0. For $\omega = 1$, $\Delta_0 \rightarrow B$ only for $R_1 \rightarrow 0$.

Figure 35 shows C - D curves of the micro/macro potential ratio Δ calculated for several ω values using the paired values of q and q_1 which follow from Grahame's (51) 1N KI data. Here, Δ is presented both because it is more directly significant than Δ in the present case of many ω values and because it lends itself to the interesting comparison discussed below. The dashed lines in Fig. 35a denote negative parts of the curves and arise because the theoretical V_{02} passes through zero for $\Gamma = \frac{1}{2}$ within the q_1 range covered. Note that all curves go to the limiting value $\Delta = \lambda$ when $q_1 = 0$ and there is no adsorption. In the opposite limit of large $|q_1|$, $\Delta \rightarrow 1$, again when $q = 0$. The curves of Fig. 35 cover the full range of q_1 derived from the data.

In Fig. 36 we show the results of some calculations by Grahame and Parsons (53) using their KCl data and the above Grahame KI data. The quantity $\lambda \equiv \gamma/(\beta + \gamma)$ given as the ordinate designation in the figure was calculated in two different ways. The lack of agreement found bespeaks one or more inconsistencies in the model and equations used to obtain λ . The curves marked "equation 8" were calculated from experimentally derived values of q_1 , V_{02} , and $V_{2\infty}$ using a simple Boltzmann distribution adsorption isotherm. The quantity obtained, although termed $\gamma/(\beta + \gamma)$, is operationally equivalent to $\psi_{12}/V_{02} \equiv \Delta$ in some sense, however.

Let us write V_{02}^e for the experimentally derived V_{02} and V_{02}^t for the theoretical V_{02} which enters our Δ . Further, employ the same superscripts for ψ_{12} , Δ , and λ . Then the "λ" obtained with the aid of "equation 8" is actually

$$\begin{aligned} \Lambda^e &= (\psi_{12}^e/V_{02}^e) = (\psi_{12}^t/V_{02}^t)(\psi_{12}^e/\psi_{12}^t)(V_{02}^t/V_{02}^e) \\ &= \Lambda^t(\psi_{12}^e/\psi_{12}^t)(V_{02}^t/V_{02}^e) \end{aligned}$$

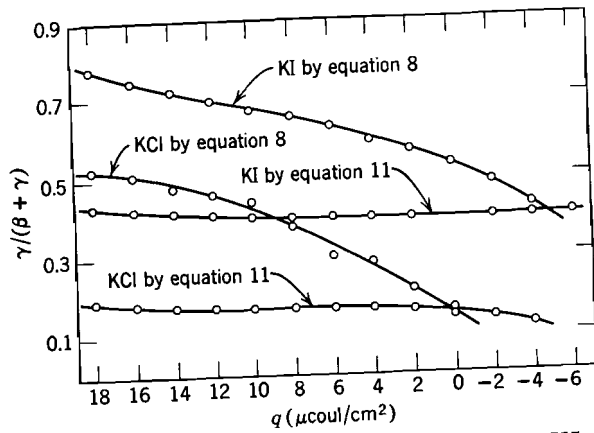


Fig. 36. The putative quantity $\lambda \equiv \gamma/(\beta + \gamma)$ vs. q for KI (51) and KCl (53), calculated from experimental results by two different methods (53).

If the last two ratios were each unity, Λ^e would equal the theoretically calculated Λ . There are a number of difficulties. First, even if the proper value of ω were known the resulting ψ_{12}^e would probably differ from ψ_{12}^e because of inadequate treatment of diffuse-layer screening and the use of the dielectric continuum assumption in the inner region. Second, (V_{02}^t/V_{02}^e) is not even unity, as we shall see later, when q and q_1 vary together. At present, we cannot even calculate the average quantity V_{02} sufficiently accurately to achieve agreement with V_{02}^e . Third, Λ^e is derived from an isotherm which is certainly incorrect for the higher $|q_1|$ values. Note that if the Ershler-Grahame linearity condition applied, as assumed by Grahame and Parsons, then $\Lambda = \lambda$ and "equation 8" would indeed give an estimate of λ^e , still not likely to equal λ^t . Finally, the determination of Λ^e requires its independence of q_1 when q is held fixed and q_1 varied by changing solute concentration. Although such independence was found, this restriction does not give us great confidence that the resulting Λ^e , which involves variable diffuse layer screening as pointed out by Payne (108) will be a good approximation to Λ^t calculated using experimental data taken at constant concentration and with q and q_1 varying together. Although the diffuse-layer shielding will also vary in this latter situation, it may be expected to vary differently from that involved in Λ^e . If

dielectric imaging is dominant ($\omega \approx 1$), however, such a difference in diffuse-layer shielding behavior will be unimportant. Finally, it should be mentioned that Parry and Parsons (101) have suggested an improved, but still nondiscrete, method of calculating ψ_{12} which seems to yield somewhat better agreement between the λ obtained from an adsorption isotherm and that obtained by the method of "equation 11" discussed below (101,107).

Although the "equation 8" Λ^e curves cannot be expected to agree closely with our theoretical Λ curves for the reasons already discussed it is still of interest to compare them. In making such a comparison, note that the Λ^t curves of Fig. 35 are plotted versus q_1 while the Λ^e 's of Fig. 36 use q as the abscissa. In the range $q > 0$, where most of the variation in the "equation 8" curves occurs, $-q_1$ and q are approximately proportional. Thus, the difference in scales is not of much importance here. Comparison shows that for KI reasonable values of Γ and ω , such as 1 and 0.9, respectively, can be selected that yield at least semiquantitative agreement between Λ^t and Λ^e . Nevertheless, too much should not be read into such agreement.

The curves marked "equation 11" were derived in a different way. It is found possible to derive the average quantities $\psi^v \equiv \Gamma\psi_\infty$ and $\psi^{02} \equiv (q/q_1)Z_0\psi_\infty$, which together make up our usual V_{02} , directly from manipulations of the experimental results. Then, if ψ^v and ψ^{02} are well approximated by the above equations, the ratio $(q/q_1)(\psi^v/\psi^{02})$ is $(\Gamma/Z_0) \equiv \lambda$. The result is thus really a measure of λ , not Λ as is the other approach. It is helpful that the λ obtained from "equation 11" is nearly independent of q , in keeping with one's expectations that γ and β should not vary very much with q and might tend to vary together if they did depend on q appreciably. Although the two sets of curves do not generally measure the same quantity, as we have seen, they should become identical at the right, where $q_1 \rightarrow 0$ and $\Lambda^t \rightarrow \lambda^t \equiv \gamma/(\beta + \gamma)$. Although such identity is by no means perfect, we note considerable tendency for the curves to come together on the right side of the figure. We shall further discuss these results in Section VI.

Finally, in Fig. 37 we present some curves of Λ ($\equiv \Lambda^t$) taken from our partial imaging work (91) calculated for the $D-C$ case.

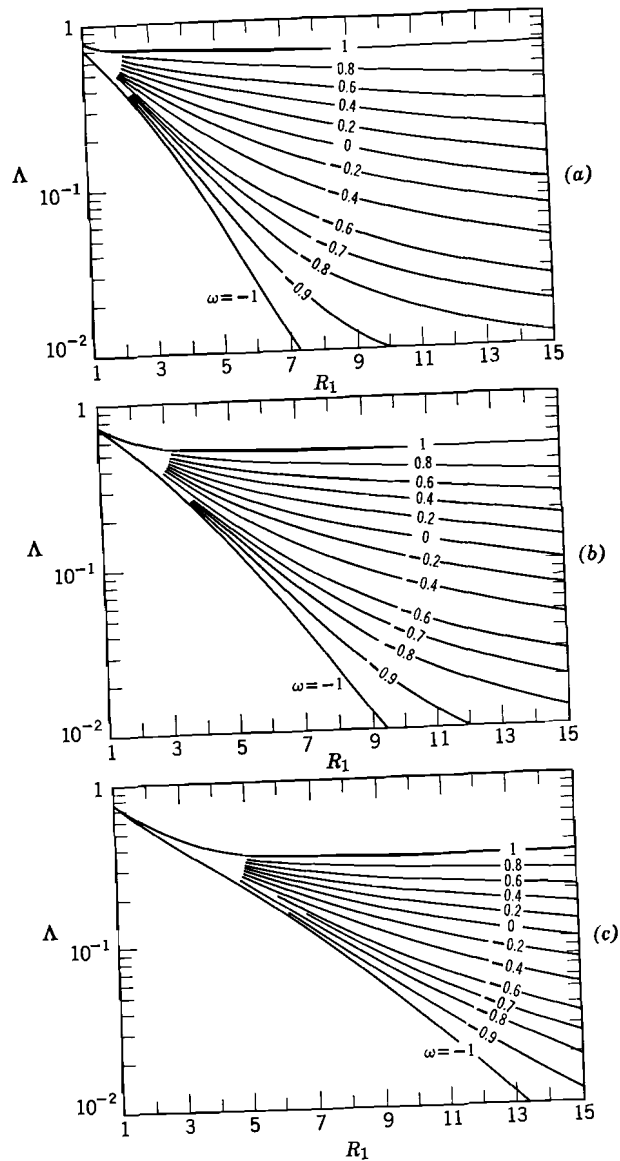


Fig. 37. The micropotential quantity Λ , here equal to $\Psi_a(1)$, vs. R_1 for a hexagonal array and a full range of ω values. For C - D imaging, $q = -q_1$ and $R_1 \equiv r_1/\beta$, while for D - C imaging $q_1 = -q_2$ and $R_1 \equiv r_1/\gamma$. C - D imaging: (a) $\Gamma = \frac{1}{2}$; (b) $\Gamma = 1$; (c) $\Gamma = 2$. D - C imaging: (a) $B = \frac{1}{2}$; (b) $B = 1$; (c) $B = 2$ (91).

In this situation, the OHP is taken conducting and a dielectric discontinuity (except at $\omega = 0$) occurs at the nonconducting ESP. As we have seen earlier, in this case $\Lambda \equiv \Psi_a(1)$. Thus, the curves shown give the normalized potential at the IHP directly for the case of overall neutrality, $q_1 = -q_2$. Note that for D - C imaging, the quantity R_1 is r_1/γ .

If, as before, we keep the same definitions of β and γ for both C - D and D - C imaging, such quantities as Γ and B also retain their usual definitions in passing between these cases, but their numerical values change. If fixed values of B and Γ are used first in a C - D calculation, then in a D - C one, the value of Γ appropriate in the first case becomes equal to the value of B in the second, and *vice versa*. The same curves may thus be used for either C - D or D - C situations with the proper changes of Γ , B , and R_1 . The pertinent values of these quantities for both cases are shown in the caption of Fig. 37. Note that in order to obtain the actual unnormalized potential $\psi_a(1)$ from the Λ values shown in the figure, one must multiply Λ by $\Gamma\psi_\infty \equiv 4\pi\gamma q_1/\epsilon_1$ in the D - C case and by $\psi_\infty \equiv 4\pi\beta q_1/\epsilon_1$ in the C - D situation. When $\omega = 1$, the final limiting value of $\Lambda [= \Psi_a^{(1)}(1)]$, is λ for D - C and $B\lambda$ for C - D imaging. The curves shown span the entire range of ω since the partition $-1 \leq \omega \leq 0$ is usually of most pertinence in the D - C case and its complement $0 < \omega \leq 1$ of corresponding interest for C - D imaging.

The results of Fig. 37 may be used to assess the magnitude of the fluctuation potential ϕ_1 used by Levine et al. (75,77). Normalizing as usual with $\Gamma\psi_\infty$ for D - C and ψ_∞ for C - D imaging, we may write

$$\Phi_1 = \Psi_a(1) - 1 \quad (158)$$

Note that when $\Psi_a(1) \approx 0$ the fluctuation potential ϕ_1 is nearly equal in magnitude to the average potential. This result is, of course, in agreement with $g \ll 1 + \Gamma$ (O - C imaging) or $(1 + B)$ (C - O imaging) in the same situation of negligible $\Psi_a(1)$.

In this part of the article, we have considered potentials and micropotentials over R_1 ranges which frequently cover the low R_1 excluded region, span the hexagonal-array region, and sometimes even reach through the transition region into the LDL regime. No real effort has been made by anyone thus far to try to bridge the transition region properly; currently the most

advanced approach, albeit still somewhat qualitative, is that contained in the present work, leading to Fig. 13 for $R_b(R_1)$.

Although a full and adequate account of discrete-element dielectric effects in the inner region may be long in coming, perhaps even longer than an accurate treatment of the transition region, we believe that something useful can be learned by considering how some of the curves of Fig. 37 would change if some account were taken of the transition and LDL regions. We can readily do this for the $\omega = 1$ ($\Gamma = 1$) and $\omega = 0$ cases using the $R_b(R_1)$ numbers discussed in Section IV and curve *b* of Fig. 13.

The peak of curve *b* of Fig. 13 occurs at $R_1 \approx 7.4$, where $R_b \approx 4.4$. This value of R_b leads, eventually, to $\Psi_a^{(1)}(1) \cong 0.5014$, very nearly the same as the corresponding $\omega = 1$ value shown in Fig. 37*b*. Similarly, the LDL value of R_b , 3.5, which is pertinent for $R_1 \geq 12.6$, leads to $\Psi_a^{(1)}(1) \cong 0.5052$, again very nearly equal to the $\omega = 1$ final limiting value $\lambda B = 0.5$ shown in Fig. 37*b*. Thus, in this case, the change in the $\omega = 1$ curve using R_b instead of $p(\xi)R_1$ is negligible.

Calculations are simpler in the $\omega = 0$ case. We estimate that the peak value of R_b is about 9.6 and occurs at $R_1 \approx 16$. As R_1 increases beyond this point, R_b will decrease towards its final limiting value of 7, appropriate for $R_1 \geq 32$. For the two values $R_b = 9.6$ and 7, we find $\Psi_a^0(1) \cong 0.10$ and 0.14, respectively. Thus, the normalized IHP potential will reach a shallow minimum of about 0.10 near $R_1 = 16$, then finally increase to 0.14 by $R_1 = 32$. For this case, only for $R_1 > 16$ will there be appreciable difference between the hexagonal array $\Psi_a^0(1)$ and the LDL $\Psi_a^0(1)$, providing our estimate for the value of R_1 at the crossover between the hexagonal-array and transition region, $R_1 \approx 15$, is reasonably close to the correct value. An interesting project for future work would be the calculation of curves like those of Fig. 37 covering the full range of ω , indicating excluded, hexagonal, transition, and LDL regions for each curve (the boundaries all change with change of ω), and using the most plausible interpolation values of $R_b(R_1)$ in the transition regions.

There has, thus far, been little experimental evidence directly bearing on the question of the importance and type of imaging at the OHP. Dutkiewicz and Parsons (31) have, however, carried out differential capacitance studies of the specific adsorption

behavior of the KI + KF system at constant overall ionic strength. In such a system, the Debye shielding length should remain constant with KI concentration change, as opposed to its variability in a simple KI system. Dutkiewicz and Parsons conclude that although such an experiment is unlikely to provide information about dielectric imaging, which is expected to remain relatively unchanged when the Debye length varies, it should allow some conclusions about the effect of diffuse-layer mobile-ion shielding with change in I^- adsorption.

In the mixed system, both types of imaging should be essentially independent of I^- adsorption, while for adsorption from a simple KI solute, conductive imaging at the OHP should change with KI concentration and Debye length. By comparing their results for the mixed system with Grahame's KI results (51), Dutkiewicz and Parsons in fact conclude that ionic imaging in the diffuse layer must be taken into account and is imperfect at least in solutions of lower ionic strength. If these conclusions are correct, we may further conclude that dielectric imaging is also imperfect and/or takes place on a plane further from the ESP than that associated with the conductive imaging effect of the diffuse-layer ions, since if it were perfect and took place at least as close to the ESP as the conductive imaging, changes in diffuse-layer imaging potentiality would have no effect on the overall (perfect) imaging present. In spite of these conclusions, we believe that the overall imaging at the OHP is likely to be much closer to perfect (or infinite) imaging, even at low ionic strengths, than to the single-imaging situation of no imaging at the OHP at all.

VI. Discussion of Results: Average Quantities

1. Permanent/Polarizable Dipoles

We have already discussed some of the difficulties which occur when two or more different discrete kinds of entities are present in the inner region. Here we shall briefly and approximately consider the dielectric effects of a single species, namely solvent molecules, and shall usually take these to be water, the species of greatest interest. The situation we therefore consider is appropriate in the absence of specific adsorption, thus probably in NaF over most of the q range.

Since a review of work on some of the dielectric properties of a monolayer of water molecules has already been given elsewhere (87) we shall here discuss the subject only briefly. Grahame (49) seems to have been one of the first to suggest that the high electric-field strength generally present in the inner layer produces some dielectric saturation and compression of the material therein. In spite of an implication to the contrary by Bockris, Devanathan, and Müller (10), one of present authors (80) was the first to treat the above qualitative suggestions of Grahame quantitatively and consider dielectric saturation in both the inner layer and the diffuse region. By including compression as well, good agreement with the results of differential capacitance measurements (50) on NaF was obtained for $q < 0$. From this work, it was found that the effect of dielectric saturation in the diffuse layer, but not the inner layer, was negligible.

This early work further introduced the value $\epsilon_\infty = 5$ for the completely saturated part of the dielectric constant. It was pointed out there (and also several times later independently by other authors) that ϵ_∞ should not equal n^2 , the square of the optical index of refraction, which only includes electron polarizability, and that it should include no permanent dipole orientation contribution. It should differ from n^2 because of inclusion of unsaturated librational and atomic polarization effects. The actual value of ϵ_∞ is of considerable importance in calculating inner-layer behavior and that of molecules immediately adjoining ions in solution. The value $\epsilon_\infty = 6$, which we introduced somewhat later on the basis of new experimental evidence (82,84) has been widely used thereafter. Now, however, recent evidence (18) seems to indicate that the high-frequency limiting value of ϵ for water at 20°C (appropriate at frequencies below those where the librational and atomic polarization effects begin to relax) is about 4.3–4.6. These measurements, which were carried out at wavelengths between 0.1 and 0.01 cm, yield values which, in at least an approximate sense, may be identified with the orientationally saturated value of ϵ , ϵ_∞ . We therefore currently incline to a value of ϵ_∞ for water at 20°C somewhere between 4.5 and 5.

The earlier paper (80) also introduced for the first time in this context the concept that a completely unsaturated monolayer of water dipoles should exhibit a dielectric constant, ϵ_0 , much below

that of bulk water. One reason suggested there for the low value of about 15 which was found necessary to achieve agreement with experiment near $q \approx 0$ was the absence of the usual bulk number of water molecules surrounding a given monolayer molecule. Considerably later, Watts-Tobin (128) [without reference in this connection to the earlier work of Macdonald (80)] and the authors (82,84) independently carried out at essentially the same time detailed treatments of the matter which largely explained the low effective value of ϵ_0 in terms of the different surroundings of the monolayer of water and the concomitant likelihood of low association between molecules.

Actually, Watts-Tobin's treatment involved a two-state treatment of the dielectric effects of a water molecule. It was assumed that the molecule would lie against the surface with either a lone-pair bond or a proton bond to a surface mercury atom. Later, Mott and Watts-Tobin (94) adopted the somewhat simpler picture of the full dipole moment of the water molecule lying perpendicular to the surface, either parallel or antiparallel to the normal field. A similar model was later used by Bockris, Devanathan, and Müller (10) and Bockris, Green, and Swinkels (11). In contradistinction, the earlier treatments of the authors (80,84) allowed all intermediate positions of the adsorbed water molecule and used either an empirical saturation law proposed by Grahame (47) and/or in the later work (84) a Langevin function or a more complicated function which took some account of imaging of the water dipoles in the mercury electrode. Although we now believe that the two opposite orientations of the water molecule at the surface are the most likely states, other less likely intermediate positions should not be entirely neglected. The actual differences in behavior of the different saturation functions may, however, be sufficiently small that distinction between them is unimportant at the present level of attainable experimental and theoretical accuracy.

One of the present authors (81) also suggested that there would be a "natural" field, \mathcal{E}_n , present at the surface of the electrode and directed perpendicular to it, even at the ECM, which would tend to orient dipoles along it. This effect was incorporated into the later treatment (84,87) and used, in part, to explain the appearance of a hump on the $q > 0$ side of the NaF differential

capacitance curves. Such an explanation required that the water molecules lie with their positive poles next to the electrode at the ECM. Frumkin et al. (42), however, suggest on the basis of other evidence that the orientation is with the oxygen (negative) pole toward the mercury at the ECM.

In our treatment of the differential capacitance in NaF (84), we suggested a number of causes for preferential alignment of an adsorbed molecule at the ECM (all of which were subsumed into the natural field or anisotropy energy). Among such causes may be mentioned nonspherical molecules, molecules having their effective dipole at a noncentral position, the influence of inhomogeneous polarization of the molecule, quadrupole and higher moments, electron overlap and bonding, and the nonplanarity of the metallic surface on an atomic scale. The appreciable electron wave-function overlap at the surface of a metal will tend to polarize adsorbed molecules with their negative poles inwards (84). There is another interesting effect which tends to produce the same response. A metal will tend to image negative charges better than positive ones because as a result of the Pauli exclusion principle, or statistical degeneracy of the conduction electrons, a depletion region can be formed near the surface of the metal with less expenditure of energy than can an accumulation region of electrons. Thus, a dipole directed outwards from the metal would be imaged at less expense than one directed toward it.

Bockris, Devanathan, and Müller (10, see also 11) have also suggested that the outward orientation is the more likely for adsorbed water dipoles because the oxygen atom is closer to the surface of the molecule, allowing that end of the dipole to be nearer the metal than would be possible for the positive pole in the opposite orientation. Further, measurements by Parsons and Zobel (106) also suggest that when the water molecules are most free to rotate, their natural orientation is with the oxygen toward the mercury. We now believe that the weight of the evidence and mechanisms discussed above are against the possible explanation of the hump we have given, and thus that the water dipole is more likely to lie with its negative pole toward the electrode at and near the ECM. Hills and Payne (56), on the basis of the results of differential capacitance measurements carried out under high

pressures, believe that the occupation of the surface by water molecules in a nonadsorbed electrolyte situation increases (at constant external pressure) with increasing positive polarization. This is one possible effect that we can't claim we suggested and/or treated first in earlier work, although our treatment of electrostatic compression in the inner layer considered a reduction in the thickness of the layer as the field there increased in magnitude. Finally, Frumkin et al. (44) ascribe the appreciable differences in the differential capacitance curves they obtain with liquid mercury and gallium electrodes in part to differences between the two metals in their orienting effects on water molecules at the ECM. Such differences would probably involve different natural fields.

The foregoing discussion indicates that even the "simple" case of a monolayer made up only of water molecules is still far from being understood in its entirety as far as its electrical properties are concerned. We shall conclude this section by giving a general expression (85,87,89,90) for the average p.d., V_{02} , across a layer of such discrete elements in the $C-O$ imaging regime, ignoring compression effects but including the polarizability of the elements, α , and their permanent dipoles, treated as ideal dipoles. We ignore the Onsager-type corrections here which should be included when permanent dipoles are involved.

In order to account for possible changes in the surface density of adsorbed molecules, take their number per unit area as N , assume a regular hexagonal array (exact on close packing when $N = N_s$), and write $r_1 = (\frac{4}{3})^{1/4} N^{-1/2}$, the nearest-neighbor distance. Note that in most of this article r_1 has measured the average or hexagonal nearest-neighbor distance between adions. Here, we have switched to molecules. Let $\Delta V \equiv -4\pi \mathcal{P}d$ be the difference in the potential at the electrode when the adsorbed layer is present and the potential in its absence. Here \mathcal{P} is the average volume polarization of the layer and d is its thickness. Then it is readily shown that $V_{02} = 4\pi qd + \Delta V$. Note that ΔV is the change in the average electron work function of the surface on establishment of the layer.

Although we shall not give the derivation of V_{02} in detail (85,89,90), it is worth pointing out that single imaging of the induced and permanent dipoles is taken into account accurately

and the treatment employs a self-consistent field. Work is in progress to extend this treatment to the infinite image regime. Let β be here the distance between the effective centers of the (ideal) dipoles (both induced and permanent) of the adsorbed molecules and the electrode imaging plane. Then again $R_1 \equiv r_1/\beta$, and we shall here take $R_{1m} = 2$ so that $\theta = 4/R_1^2$. We use the modified cutoff method to deal with the hexagonal array of image dipoles. The field inducing dipoles in adsorbed molecules is thus required a distance 2β in front of the image array, at the position of an adsorbed entity. Thus, $\xi \equiv z/r_1$ becomes $2\beta/r_1 = 2/R_1$, and for the choice $R_{1m} = 2$, $\theta = \xi^2$. Since our result involves $p(\xi)$ and $F(\xi)$, we shall express it entirely in ξ rather than in terms of N , θ , r_1 , or R_1 . Then

$$V_{02} = 4\pi qd - (2\pi/\sqrt{3})\xi^2\epsilon_1^{-1} \times [J\beta(4\pi q + \mathcal{E}_{n1}) + \beta^{-2}\langle\mu(\mathcal{E}_2)\rangle] \quad (159)$$

where

$$\epsilon_1 \equiv 1 + J \left[(\sigma/8)\xi^3 - \frac{1}{4} + \left(\frac{\pi}{2\sqrt{3}} \right) \frac{\{p(\xi)\}^2\{1 + F(\xi)\}}{[1 + \{\xi^{-1}p(\xi)\}^2]^{3/2}} \right] \quad (160)$$

The above equations contain a great deal of meat which we shall expose bit by bit. First, $J \equiv \alpha/\beta^3$ as ever. Since α for water seems (15) to be about 1.3 \AA^3 or more, $J \approx 0.53$. On the other hand, α for cesium atoms may be (7,96) as large as 55 or 60 \AA^3 and $\beta \approx 2.35 \text{ \AA}$. Using this value of β and $\alpha \approx 53 \text{ \AA}^3$, $J \approx 3.85$ and might (90) possibly exceed 4. The quantity ϵ_1 is here an effective dielectric constant arising entirely from the polarizability α . Note, however that this "dielectric constant" does not enter into the expression for V_{02} in the usual way; in general, it is not possible to meaningfully define a monolayer dielectric constant which does enter in the usual way. Taking $J = 0.53$, $\xi = 1$, and evaluating $p(\xi)$ and $F(\xi)$ for the ideal-dipole situation, one finds that the maximum likely value of ϵ_1 for water is about 1.7. The three terms within the square bracket in Eq. 160 arise, going from left to right, from the induced dipoles in the plane with a given dipole, the image of that dipole, and from all remaining induced dipole images.

The quantity \mathcal{E}_{n1} in Eq. 159 is the natural field effective in inducing polarization in adsorbed polarizable molecules when

$q = 0$. The field acting to orient permanent dipoles, \mathcal{E}_2 , is approximately $\mathcal{E}_{n2} + n^{-2}\mathcal{E}_{\text{eff}}$. Here \mathcal{E}_{n2} , not necessarily equal to \mathcal{E}_{n1} , is the natural field orienting permanent dipoles at $q = 0$ and n^2 is a shielding factor taken here to be the square of the optical index of refraction. Using the proper expression for \mathcal{E}_{eff} , we obtain

$$\mathcal{E}_2 = \mathcal{E}_{n2} + n^{-2}\epsilon_1^{-1}[4\pi q + \alpha^{-1}(1 - \epsilon_1)\{\alpha\mathcal{E}_{n1} + \langle\mu(\mathcal{E}_2)\rangle\}] \quad (161)$$

Since \mathcal{E}_2 occurs as the argument of $\langle\mu(\mathcal{E}_2)\rangle$, this equation must generally be solved for \mathcal{E}_2 by iteration when the form of $\langle\mu(\mathcal{E}_2)\rangle$, such as a two-state or Langevin function, is known. This process is of course unnecessary when the dipoles are completely pinned and $|\langle\mu(\mathcal{E}_2)\rangle| = \mu$, the full dipole moment. We still require \mathcal{E}_2 in this case, however, in order to see whether full pinning is likely.

Let us return now to the expression for V_{02} for water adsorbed on the electrode. Then $\xi \ll 1$, and we find (85) that the two main terms in the equation are opposite in sign and nearly equal in magnitude at the extremes of the q range. Thus, although ΔV may be quite large, several volts or more, V_{02} will be much smaller, as observed, throughout the full variation of q . We have found, in unpublished work, good but not excellent agreement between the predictions of Eq. 159 and experimental determination of $V_{02}(q)$ for NaF using both two-state and Langevin functions for $\langle\mu(\mathcal{E}_2)\rangle$. Slightly better agreement can be produced if compression effects are included. If any variation of θ (or ξ) with q were present and known, Eq. 159 could be used to account for this effect as well. Finally, it could be used, at least as a fair approximation, to account for the effects of displacement of solvent molecules on the electrode by adions during specific adsorption.

Although the permanent dipole moment of water of about 1.85×10^{-18} esu dominates its induced polarization, it is of interest to examine briefly the different situation of an inner layer composed of polarizable molecules or atoms with $\mu = 0$. The present description which ignores Onsager corrections is most appropriate for this case, as no such corrections are necessary for induced polarization. Such a system occurs, for example, when cesium or potassium atoms are adsorbed from a gas phase onto a conducting electrode such as tungsten. Equation 159

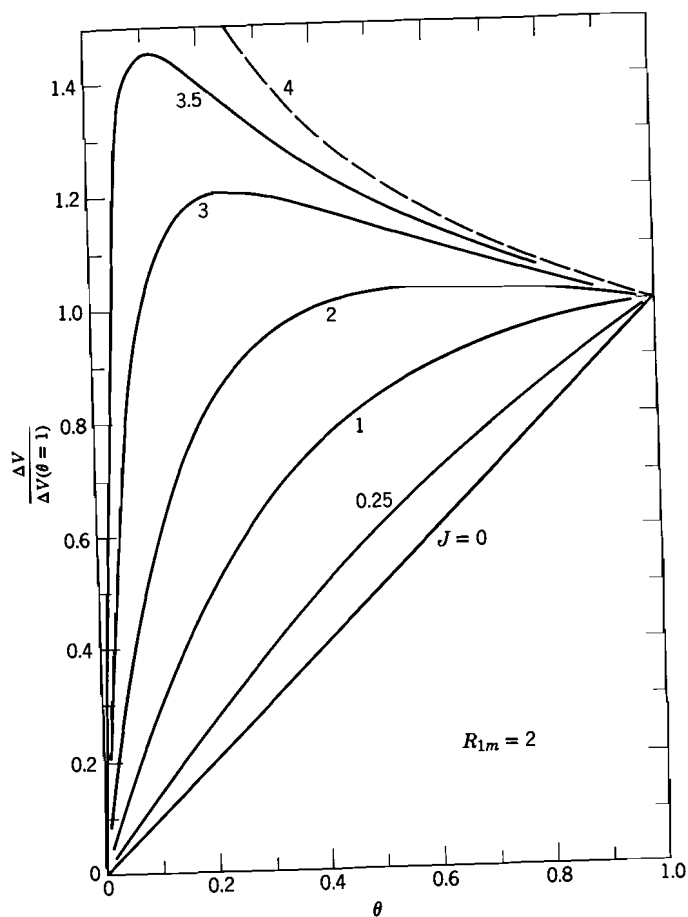


Fig. 38. The normalized $C-O$ imaging electron work function change, ΔV , vs. θ for a hexagonally arrayed adsorbed layer of polarizable molecules or atoms with $\mu = 0$. The parameter is $J = \alpha/\beta^3$ (90).

simplifies considerably in this situation, and we have presented in Fig. 38 some resulting curves of $\Delta V/\Delta V(\theta = 1)$ for several J values. Here $\Delta V/\Delta V(\theta = 1)$ becomes just $\theta\epsilon_1(\theta = 1)/\epsilon_1$, and the curves are appropriate for q zero or a constant. It is assumed that \mathcal{E}_{n1} is independent of θ . The curves for $J \geq 2$ show peaks, in agreement with experiment for such a material as cesium on tungsten. Note that the treatment breaks down (90) when $J \geq 4$.

2. Nonpolarizable Adions

In this section, we shall be less concerned with discreteness effects than with indicating some of the deficiencies of the simple space-averaged treatment of V_{02} which we have used throughout most of this work when adions are present in the inner region.

Consider nonpolarizable adions and smear the dielectric effects (moderated by appropriate imaging and screening) of the surrounding water molecules to yield the ϵ_β and ϵ_γ of Fig. 4. For greater generality, we shall not initially take $\epsilon_\beta = \epsilon_\gamma = \epsilon_1$. As usual, however, we assume that ϵ_β , ϵ_γ , γ and β are independent of q . Then, simple electrostatics yields

$$\begin{aligned} V_{02} &= (4\pi q_1 \gamma / \epsilon_\gamma) + 4\pi q \{ (\beta / \epsilon_\beta) + (\gamma / \epsilon_\gamma) \} \\ &\equiv 4\pi q_1 s [w + (1+w)(q/q_1)] \\ &\equiv 4\pi q_1 [t + (s+t)(q/q_1)] \end{aligned} \quad (162)$$

where we have set $s \equiv \beta/\epsilon_\beta$, $t \equiv \gamma/\epsilon_\gamma$, and $w \equiv (\gamma/\beta)(\epsilon_\beta/\epsilon_\gamma) = t/s = (\epsilon_\beta/\epsilon_\gamma)\Gamma$. Note that when $\epsilon_\beta = \epsilon_\gamma$, w becomes simply Γ .

We have used Grahame's (51) $1N$, $0.1N$, and $0.025N$ V_{02} , q , and q_1 results for KI to calculate values of s and t by a least-squares procedure. Some of the results obtained are presented in Table V. In this table, s and t are expressed in Angstroms. The

TABLE V
Parameters Obtained from Least-Square
Fitting of V_{02} Formula Using KI Data

	Normality		
	0.025	0.1	1
s	0.1805	0.2017	0.2459
t	0.1306	0.1389	0.1493
w	0.7234	0.6885	0.6071
λ_1	0.4197	0.4085	0.3777
σ	0.0135	0.0250	0.0586
s	0.21	0.21	0.21
t	0.1518	0.1418	0.1482
w	0.7229	0.6752	0.7055
λ_1	0.4196	0.4031	0.4137
σ	0.0239	0.0250	0.0746

quantity λ_1 is defined as $w/(1+w)$, equal to the ordinary λ when the assumption $\epsilon_\beta = \epsilon_\gamma$ is made. Finally, σ is the standard error obtained in the fitting. Its units are volts. It may involve contributions from both random and systematic experimental errors as well as systematic deviations arising from inadequacy of the model.

The first set of results in Table V was obtained with s and t both free to vary. In the second set, s was held fixed at 0.21 Å and the least-squares t obtained. Twelve data points were used for the 0.025*N* calculation, 14 for 0.1*N*, and 20 for 1*N*. In each case, they covered the q range where $|q_1|$ was sensibly greater than zero. Although the σ 's seem reasonably low, the degree of fit between theory and experiment was actually rather poor. For the top set of results shown in Table V, the greatest deviations between predicted and experimental values occurred roughly at the ends and middle of the q range and amounted to about 10% of V_{02} for all three concentrations shown.

We note from Table V that none of s , t , or w is very constant with concentration change. Further, when it is free, s varies even more strongly than t , a surprise since a possible change in the average imaging plane distance with concentration might have been expected to affect γ more than β . In fact, it seems reasonable to define the OHP operationally as being located at the average imaging-shielding plane. The results in the table show that provided ϵ_γ remains relatively constant, γ apparently increases with increasing concentration, contrary to the expected behavior.

Another anomaly appeared when we looked at the correlation factor, r_{st} , obtained between s and t . These quantities may very well be correlated, since if they do vary with q and q_1 , one would expect them to depend in much the same way on the same physical factors. We found that r_{st} was 0.7309, 0.5122, and 0.0553 for concentrations of 0.025*N*, 0.1*N*, and 1*N*, respectively. Guessing that the vast changes in r_{st} with concentration might depend in part on the different number of points and parts of the q range employed in the fitting for these three cases, we investigated the 1*N* situation in more detail. Table VI shows the results obtained with different selections of the data, all within the range where $|q_1| > 0$. We see that taking every other point makes relatively little difference in the results, but that restricting the fit to the

high end of the q range makes a great deal of difference. This same effect was doubtless operating to affect the results obtained in the variable concentration case of Table V.

Least-squares fitting has also been carried out for similar KCl data (53). In this case, s and t were roughly 0.3 and 0.1, respectively, but again they showed considerable variation with concentration and generally poor fits between theoretical and experimental values of V_{02} . The variation of r_{st} was again wild, changing from essentially zero at 2.449*N* to -0.53 at 0.02*N*.

TABLE VI
Parameters Obtained from V_{02} Fitting of 1*N* KI Data

No. of points	Data choice		Results			
	$q_{\text{initial}}/q_{\text{final}}$	q step, $\mu\text{coul}/\text{cm}^2$	s	t	σ	r_{st}
20	-20/18	2	0.2459	0.1493	0.0586	0.0553
10	-20/16	4	0.2529	0.1486	0.0603	-0.0428
12	-8/14	2	0.2023	0.1278	0.0196	0.5054
12	-4/16	2	0.1703	0.1203	0.0186	0.7716

We can conclude quite unambiguously that s and t should really depend on q and q_1 and that the equation for V_{02} used here, even with its unusual generality of taking $\epsilon_\beta \neq \epsilon_\gamma$, is quite inadequate for representing the data well. It is not even a good caricature of the system. Delahay and Susbielles (25) have also stated that an equation of the form of Eq. 162 is not justified for the cation specific adsorption situation they investigated.

In Section V-2-D, we discussed the method of obtaining λ , considered purely as the distance ratio $\gamma/(\beta + \gamma)$, by the average "capacity-ratio" method denoted there as "equation 11." To emphasize that the result is a distance ratio some authors (101,107) have written $(x_2 - x_1)/x_2$ in place of $\gamma/(\beta + \gamma)$. We prefer, however, to use β and γ as nothing but distances in all our work, so do not need to make this distinction.

If $\epsilon_\beta \neq \epsilon_\gamma$, the "equation 11" approach actually yields, to the degree that Eq. 162 is appropriate at all,

$$\lambda_1 \equiv w/(1+w) = \epsilon_\beta \gamma / [\epsilon_\gamma \beta + \epsilon_\beta \gamma] \quad (163)$$

rather than λ . The quantities ϵ_β and ϵ_γ might be expected to decrease, (probably somewhat differently) with increasing $|q_1|$ because of the displacement of neighboring water molecules which contribute their dielectric effects to produce ϵ_β and ϵ_γ . We must emphasize, however, that the model really seems too crude; an all-discrete treatment (without direct introduction of dielectric constants at all) of all entities present in the inner region is a greatly preferable approach. Although the actual procedure of the capacity-ratio method involves using the ratio of average quantities, such quantities can depend very appreciably on the presence of discrete particle interactions, and we have no real assurance that the λ or λ_1 which results from the procedure has much connection with a simple distance ratio.

One must also be particularly suspicious because the λ or λ_1 which results from the "equation 11" approach or the least-squares procedure (which yields nearly the same results) is considerably larger for KI than for KCl, yet the radii are about 2.05 and 1.64 Å, respectively (65). If γ were about 1.5 Å in both cases, λ for KI would be about 0.42, near the value obtained, but the KCl λ would be about 0.48, a change in the opposite direction from the value of 0.2 or less found for this system by the above approaches. Although one could think of many reasons to explain this result, we believe they should not be invoked unless a much more exact theory of V_{02} yields similar anomalies when compared with experiment.

As we have stated before in this article, an equation is still needed even for such a space-averaged quantity as V_{02} which adequately takes into account the contributions to the polarization arising from all discrete entities in the inner layer, moderated by imaging and shielding effects present at the boundaries. Although no such equation is currently available and obtaining it will be a most difficult task, it is clear that it will not subsume overall polarization effects entirely into either constant or variable dielectric constants. Further, until an average quantity such as V_{02} can be calculated accurately, it seems misguided for one to spend much more time refining a discreteness-of-charge model to calculate ψ_{12} or $\psi_{1\infty}$. We believe that the current uncertainty concerning both the proper form of $\psi_{1\infty}$ and the form of the adsorption isotherm for adion adsorption combine to make it

more important first to improve the theory of V_{02} (and so of the differential capacitance), and only when this is in a satisfactory state then to apply the models developed and insights gained to evolve a much improved theory of $\psi_{1\infty}$.

3. Polarizable Adions

In this section, we consider the situation of an adsorbed layer populated only by polarizable adions which only undergo C-O imaging (85,89). The results will apply therefore primarily to adsorption of ions from a gas phase, although they shed light on the behavior of an array of adions adsorbed from solution in situations which approximate C-O or O-C imaging when all effects of inner-region solute molecules are neglected. For example, the present results will be relevant in the O-C situation of high ionic concentration where the OHP can be well approximated as an equipotential and the (nonconducting) ESP dielectric constant approximately matches that of the inner region.

The expression for $\psi_\infty \equiv V_\infty$ we have used throughout this article applies, for $\epsilon_1 = 1$, when the polarization of adions (and all effects of solute molecules) is completely neglected. How much will the space-average quantity ψ_∞ change when α , here the ionic polarizability, is taken into account in a treatment which properly includes discreteness effects? This question will be answered in this section. The approach used is very much like that employed for polarizable molecules in Section VI-1; thus, we shall give the principal results and explain their genesis rather than setting out the entire somewhat complicated calculation in detail (89).

First, let us consider V_{02} for arbitrary q and q_1 . It is straightforward to show that in the present case

$$V_{02} = 4\pi\gamma(q + q_1) + 4\pi\beta q - 4\pi\mathcal{P}d \quad (164)$$

where \mathcal{P} is the average volume polarization of the layer. It is given by

$$\mathcal{P} = (\alpha N/d)[\mathcal{E}_{n1} + \mathcal{E}_a + 4\pi(q + q_1)] \quad (165)$$

In this equation, \mathcal{E}_a is a depolarizing field made up of five distinct contributions arising from: (a) the image charge of a given adion; (b) the image of the induced dipole of that adion; (c) the induced dipoles of the adions surrounding and in the plane with the given one; (d) the nonideal dipoles surrounding the given adion and

arising from the other adions and their $z_v e$ images, and; (e) the dipole images of the induced dipoles of all adions in the plane with the one considered.

The calculation of \mathcal{P} and V_{02} is carried out on the assumption that the induced dipoles are ideal and leads to

$$V_{02} = \psi_{\infty}^0 [\Gamma + Z_0(q/q_1) + g(R_1)] \quad (166)$$

where $\psi_{\infty}^0 \equiv 4\pi q_1 \beta$, the proper expression for ψ_{∞} when $\alpha = 0$ and there are no surrounding solute molecules. From now on, we shall use the symbol ψ_{∞} to denote the generalized quantity which applies when $\alpha \neq 0$. Further, let $\Psi_{\infty} \equiv \psi_{\infty}/\psi_{\infty}^0$. It turns out that

$$\Psi_{\infty} \equiv 1 - g(R_1) \quad (167)$$

and that when $q = -q_1$, $V_{02} \equiv -\psi_{\infty}$, consistent with our general definition for ψ_{∞} .

All that now remains is to give an expression for the complicated function $g(R_1)$. To do so we shall again use the modified cutoff method and assume a hexagonal array of adions. Here, we must distinguish between $p(\xi)$ for nonideal dipoles, which we denote $p_n(\xi)$ and that for ideal dipoles, $p_i(\xi)$. The arguments of these functions are somewhat different, so we shall write the entire result in terms of R_1 . We find

$$g(R_1) = (J/2\epsilon_1)[(8\pi/\sqrt{3})R_1^{-2}M_0 + \frac{1}{2} - S] \quad (168)$$

$$\text{where} \quad S \equiv 2(\beta/z_v e)(\beta \mathcal{E}_{n1}) \quad (169)$$

$$M_0 \equiv \frac{2 - [R_1 p_n(R_1^{-1})]^2 F_n(R_1^{-1})}{[\{R_1 p_n(R_1^{-1})\}^2 + 4]^{1/2}} - [R_1 p_n(R_1^{-1}) F_n(R_1^{-1})] \quad (170)$$

and

$$\epsilon_1 \equiv 1 + J \left[\sigma R_1^{-3} - \frac{1}{4} + \left(\frac{\pi}{2\sqrt{3}} \right) \frac{[p_i(2R_1^{-1})]^2 [1 + F_i(2R_1^{-1})]}{[1 + \{R_1 p_i(2R_1^{-1})/2\}^2]^{3/2}} \right] \quad (171)$$

Here, the expression for ϵ_1 turns out to be identical with that given in Eq. 160; it is merely written in terms of R_1 in Eq. 171. For many purposes, sufficient accuracy will be maintained if the small F_i and F_n terms are ignored and all p_i and p_n 's are replaced by $p_0 \equiv 4\pi/\sqrt{3}\sigma$ or even by 0.607. We have not given before the accurate expression for $g(R_1)$ above but have instead essentially made the above simplifications in our prior work (89).

When $R_1 \rightarrow \infty$, it is easy to show that $\epsilon_1 \rightarrow 1 - (J/4)$ and that $g(R_1) \rightarrow g(\infty) \equiv J(1 - 2S)/(4 - J)$. The quantity $J \equiv \alpha/\beta^3$ will never approach 4 for ions and will usually be of the order of unity or less. Further, $|S|$ will probably not exceed 0.25 for reasonable values of \mathcal{E}_{n1} , β , and $z_v = 1$. Thus, $g(\infty)$ is not likely to exceed 0.5. The quantity $g(R_1)$ may, however, approach and even exceed unity for small R_1 and $J \leq 2$. Thus, we see that under favorable conditions, the inclusion of adion polarizability may affect V_{02} quite appreciably.

In Fig. 39 we show how $\psi_{\infty}/(\psi_{\infty}^0 \text{ at } R_1 = 1) \equiv R_1^{-2}\Psi_{\infty}$, here termed Γ_1 , varies with R_1^{-2} . The ordinate is thus proportional to ψ_{∞} . The abscissa may be converted into a θ scale by multiplying by R_{1m}^2 . The solid curves were calculated with $S = 0$ from Eq. 167 with essentially the slight simplifications mentioned above (89). The dashed curves are very approximate, do not include all the proper contributions to \mathcal{E}_{n1} , and approximate nonideal dipoles by ideal dipoles. We see that even J values considerably less than unity can make ψ_{∞} considerably different from ψ_{∞}^0 (see the $J = 0$ curve). Note that to represent ψ_{∞} as ψ_{∞}^0/ϵ , where ϵ is even a "variable" dielectric constant, would be stretching the concept of a dielectric constant past bearing when ψ_{∞} changes sign and ψ_{∞}^0 doesn't.

If ΔV is the change in average electron work function on establishing the adion array, then for the $q = -q_1$ grounded electrode situation appropriate for adsorption from a gas phase, $\Delta V = -\psi_{\infty}$. Thus, Fig. 39 also shows how the work function change depends upon surface occupation. Note that we here define ΔV as the difference in the potential at the electrode (with reference to "infinity") with the adion array present and that with the array absent (a bare electrode).

In earlier work (89), the foregoing formula for ψ_{∞} was fitted to experimental data for the adsorption of cesium (as ions) on tungsten. A good fit to the data could be obtained for the range $5 < R_1 \leq \infty$ using reasonable values of the parameters. The tungsten temperature was sufficiently high that the appropriate single-imaging R_c , even including the effect of nonzero ionic polarizability, should be less than 4, however. Thus, the $R_1 \geq R_c$ restriction still allows R_1 values as small as the smallest values contained in the good fit range. Note that the room-temperature

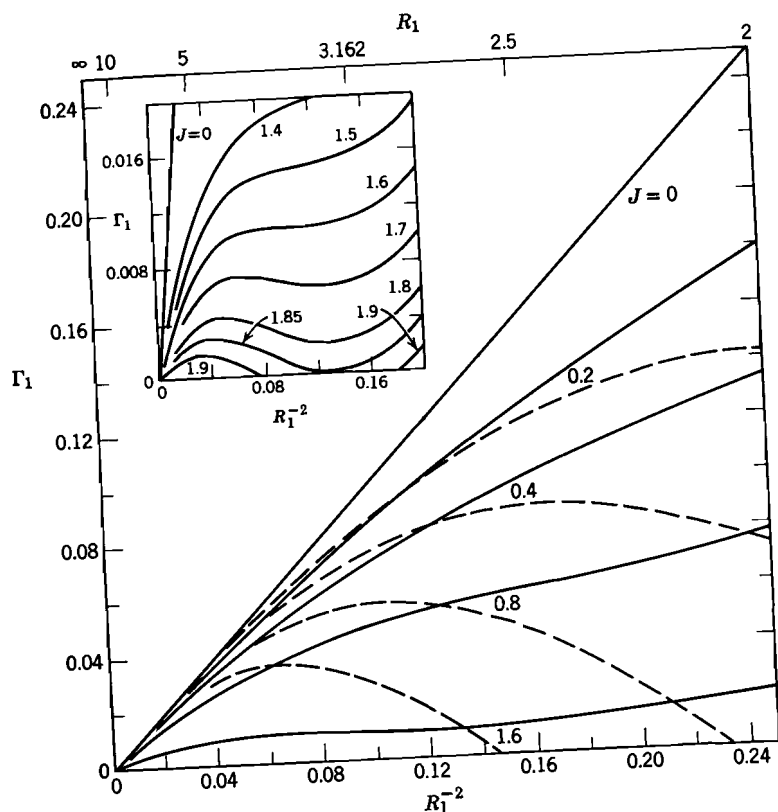


Fig. 39. The hexagonal array quantity $\Gamma_1 \equiv \psi_\infty / [\psi_\infty^0 \text{ at } R_1 = 1]$ vs. R_1^{-2} for $C-O$ imaging of a hexagonal array of polarizable ions ($|z_v| = 1$) adsorbed on a conducting electrode. The parameter is $J = \alpha/\beta^3$; note the R_1 scale at the top. The dashed lines were calculated using an overly approximate theory (89).

$R_c \approx 7$ value does limit the applicable parts of the curves of Fig. 39 to the extreme left region where $R_1^{-2} < 0.02$.

We now believe that the following situation is likely for gas phase adsorption, at least at room temperature. In the initial phases of adsorption when R_1 is large, we believe it will be energetically favorable for the discrete entities to be adsorbed as ions. When R_1 becomes smaller than about 15, the adion array should tend to become hexagonal and Eq. 167 should apply quite well. Finally, when the surface occupation is high enough

that R_1 approaches 7, we believe that either the entities will be adsorbed as atoms, or electrons will be shared with the electrode and $|z_v|$ will begin to decrease (decreasing R_c), or perhaps both processes will occur concomitantly. In any event, for $R_1 < R_c$ and approaching R_{1m} , we believe that most if not all of the discrete adsorbed entities can be considered to be atoms. Thus, in the range $R_{1m} \leq R_1 \leq R_c$, the polarizable atom or molecule results of Section VI-1 should apply.

Finally, it is of interest to give some results for J for ions of interest in electrolyte situations. We shall use some recently calculated (111) values of α and shall use the radii of the ions for β (65). The most likely choices of α and β then lead to $J \approx 0.15, 0.27, 0.38, 0.56, 0.67,$ and 0.73 for $\text{Na}^+, \text{K}^+, \text{Cs}^+, \text{F}^-, \text{Cl}^-$, and I^- , respectively. Particularly because of uncertainty in appropriate values of β (which enters as β^3) to use, these values must be considered very crude. The values used probably lead to the smallest likely values of J . Using more favorable but probably less likely values of α and β , we found elsewhere (89), for example, a J of about unity for Cs^+ .

VII. Discussion of Results: Local Potentials—Polarizable Adions

In this concluding section, we shall discuss briefly the potential variation through point 0 arising from an array of polarizable adions. The difficult case of partial or infinite imaging of a polarizable array has not yet been treated in detail; thus, again we consider only the $C-O$ imaging situation of a layer consisting only of polarizable adions. The potential with which we are concerned, $\psi(X, Y, Z) = \psi(0, 0, Z)$, is actually $\psi_a^0(Z)$ since we shall take $q = -q_1$ here and it is a single imaging situation; for simplicity, however, we shall omit both the superscript and subscript.

Again we shall use the modified cutoff approach and shall write the equation for $\Psi(Z) \equiv \psi(Z)/\psi_\infty$ on the basis of a regular hexagonal array of adions. Some consideration of the LDL situation will follow. The quantity $\Psi(Z)$ is made up of a part arising from the nonideal dipoles formed by the adions and their monopole images and another part stemming from the induced dipoles and their images. Let us again make use of the $p_n(\xi)$

and $p_i(\xi)$ functions and introduce the function

$$B_j^\pm(\xi) \equiv [\{R_1 p_j(\xi)\}^2 + (Z \pm 1)^2]^{1/2} \quad (172)$$

Then, it turns out (92) that $\Psi(Z)$ may be written

$$\begin{aligned} \Psi(Z) = & \frac{1}{2}[B_n^+(Z/R_1) - B_n^-(Z/R_1)] \\ & - g(R_1)\{(Z+1)[B_i^+\{(Z+1)/R_1\}]^{-1} \\ & + (Z-1)[B_i^-\{(Z-1)/R_1\}]^{-1}\}[1 - g(R_1)]^{-1} \end{aligned} \quad (173)$$

where some of the Z dependence is not shown explicitly since only the Z 's occurring in ξ appear in the arguments of the B functions. The function $g(R_1)$ appearing here is that of Eq. 168.

Figure 40 shows curves of $\Psi(Z)$ calculated from Eq. 173 with the relatively good approximation of setting $p_n(\xi) = p_i(\xi) = p_0$. Note that the abscissa scale is Z/R_1 and that we have taken $S \equiv 0$. The most interesting feature of these curves is that for $J \gtrsim 1$, $\Psi(Z)$ can exceed unity over part of the Z/R_1 range. The table in Fig. 40a shows $\Psi_\infty \equiv \psi_\infty/\psi_\infty^0$ for various situations, where again $\psi_\infty^0 \equiv 4\pi q_1\beta$. Since $\Psi_\infty \equiv 1 - g(R_1)$, the values listed may be used to illustrate how $g(R_1)$ varies as well.

The work on which the curves of Fig. 40 were based was carried out before we realized that R_c for single imaging is likely to be of the order of 7 for room temperature. The $R_1 = 5$ curves shown apply, therefore, only for temperatures sufficiently high that $R_c < 5$ and yet a hexagonal array is maintained and the HTL is not reached. The $R_1 = 2$ curves are really nonphysical. For $R_1 = R_c = R_{1m} = 2$, the HTL situation should apply, not the regular hexagonal array on which these curves were calculated. At room temperature, a regular hexagonal array with $R_1 \gtrsim 7$ would lead to curves which showed a peak only for appreciable J values, probably beyond the experimentally likely range. It should be further mentioned that even when Ψ_∞ exceeds unity, the quantity $\psi(Z)/\psi_\infty^0$ decreases for all Z as J increases.

Let us now define f as the ratio of the change of ionic work function to the change of electronic work function (92). Then one relatively crude definition of f , which we shall term f_1 , states that $f_1 \equiv 1 - [\psi_a(1)/\psi_\infty] = 1 - \Psi_a(1)$. Compare the Levine perturbation potential Φ_1 of Eq. 158, which is, of course, written for $\alpha = 0$. If we write f_1^0 for f_1 when $\alpha = 0$, then $\Phi_1 \equiv -f_1^0$. The quantity f_1 may be readily written from our foregoing equations and is,

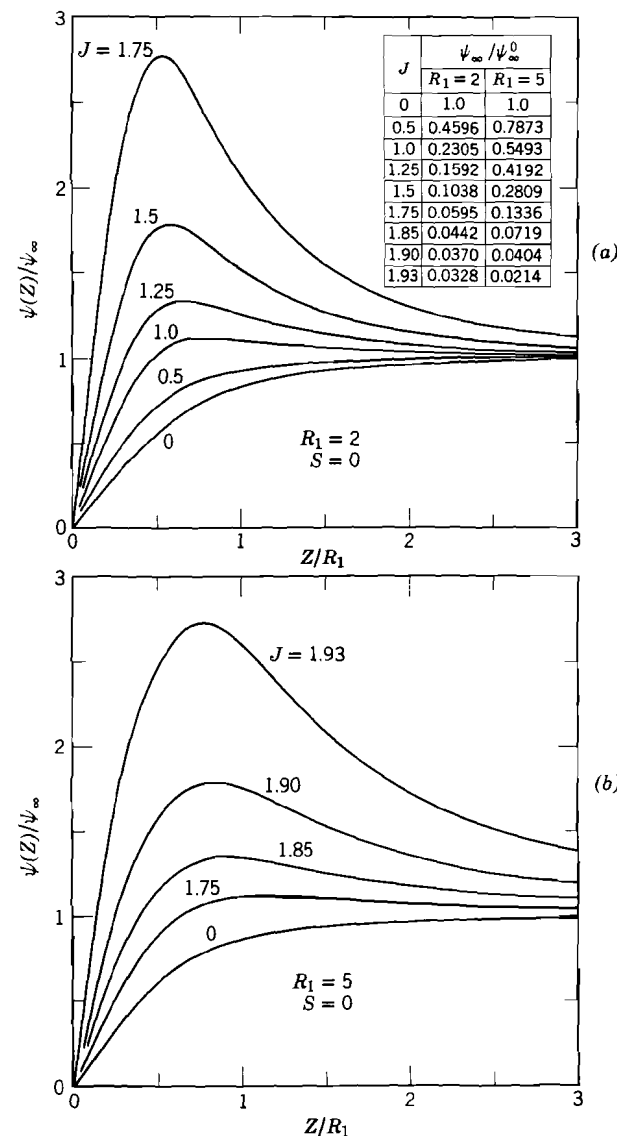


Fig. 40. The normalized local potential $\Psi(Z) \equiv \psi(Z)/\psi_\infty$, equal to $\psi_a(Z)/\psi_\infty$ here, for C-O imaging of a hexagonal array of polarizable adions ($|z_v| = 1$) vs. $\xi \equiv Z/R_1$ for two different R_1 values. The parameter is $J \equiv \alpha/\beta^3$ (92).

for a regular hexagonal array

$$f_1 \equiv \frac{f_1^0 - g(R_1)[1 - 0.5\{1 + [R_1 p_i(2/R_1)/2]^2\}^{-1/2}]}{1 - g(R_1)} \quad (174)$$

where

$$f_1^0 \equiv 1 + 0.5R_1 p_n(R_1^{-1}) - \{1 + [R_1 p_n(R_1^{-1})/2]^2\}^{1/2} \quad (175)$$

It turns out that a definition for f which takes nonzero polarizability into account more fully is $f_2 \equiv f_1 + T$, where

$$T \equiv (\sqrt{3}/64\pi)R_1^2[1 - g(R_1)]^{-1}[g(R_1) - g(\infty)] \quad (176)$$

None of the above f 's includes redistribution of the adion array upon removal of an adsorbed ion. As we have mentioned, redistribution effects should not be included in the micropotential used in an adsorption isotherm. On the other hand, redistribution exerts an effect on the energy necessary to remove to infinity an adion from a regular array provided the redistribution occurs in a sufficiently short time that the adion being removed is still within the influence of the surface array during the rearrangement. In such a case, redistribution makes it easier to remove the ion. Naturally, if the adion is removed from the neighborhood of the surface so rapidly that little or no redistribution has time to take place, redistribution effects are unimportant and $f = f_2$. Let us denote the f which includes redistribution as f_3 .

Figure 41 shows curves of f_2 and f_3 vs. θ for $R_{1m} = 4$ (probably appropriate for cesium on tungsten) and $S = 0$. Also shown as broken lines are two curves derived from cesium-tungsten experimental data (124). We see that the agreement between theory and experiment is not excellent. Although the adsorbent temperature was sufficiently high that $R_c \leq 4$ and thus there was no R_c restriction leading to $\theta < 1$, we believe, as mentioned in Section VI-3, that for some nonzero θ appreciably less than unity, z_v may begin to decrease and/or additional adsorption will occur as atoms, not ions. Since these possibilities were not incorporated in the calculation of the theoretical curves of Fig. 41, agreement with experiment beyond a maximum of $\theta \approx 0.6$ should not necessarily be expected. Further, the agreement should be poor also at very small θ 's because the curves were calculated for a fixed hexagonal array, not the transition region and LDL situation pertinent for θ less than 0.1 or 0.2.

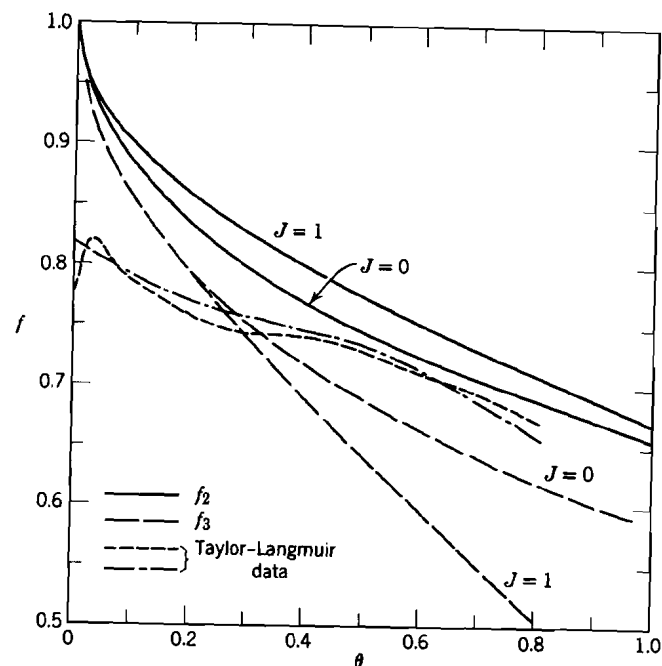


Fig. 41. Comparison of experimentally derived curves for cesium on tungsten with theoretical f results for $R_{1m} = 4$, $z_v = 1$, $S = 0$, and various J values (92).

Although we shall not illustrate how the curves would change in the transition region, we will point out how the theory may be modified to calculate such curves. The quantity $R_1 p_n(\xi)$ occurs in f_1^0 and $g(R_1)$ while $R_1 p_i(\xi)$ occurs in f_1 , f_2 , $g(R_1)$ and ϵ_1 . All that is necessary to effect the transformation is to replace all these $R_1 p$'s by R_b , a function of N (or R_1). The quantity σR_1^{-3} which appears in ϵ_1 merely needs to be written as $4\pi R_1^{-2}/\sqrt{3}p_0 R_1$, then replaced by $4\pi R_1^{-2}/\sqrt{3}R_b$.

We shall illustrate the result for f_2 in the LDL, where $R_b \equiv R_c$, first for the specific choice $R_c = 7$. One might think that in this limit only the $R_1 p_n$'s should be replaced since they only are associated with the monopoles and their images. The induced dipoles are a part of the adions, however, and are thus also restrained from approaching one another any closer than R_c . Thus, all $R_1 p_i$ terms should also be replaced by R_c .

In the LDL case, one first makes the $R_b = R_c$ replacements discussed above, then lets $R_1 \rightarrow \infty$ keeping R_c constant. One finds then that $\epsilon_1 \rightarrow 1 - (J/4)$ and $g(R_1) \rightarrow g(\infty)$. The quantity T does not go to zero, however, but to

$$J/\{4(4 - 2J)[1 + (R_c/2)^2]^{1/2}\}$$

For $J = 0.5$ and $R_c = 7$, $T \cong 0.011$, essentially negligible. For $R_c = 7$, we find $f_1^0 \cong 0.86$ and

$$f_1 \cong [0.86 - 0.863g(\infty)]/[1 - g(\infty)]$$

For this value of R_c , therefore, it turns out that $f_1 \cong f_1^0$ unless $g(\infty)$ is very near unity. Even for $g(\infty) = 0.5$, the largest likely value of this quantity, $f_1 \cong 0.857$. The largest likely value of f_2 is thus about 0.87. For the more reasonable choice of $R_c = 4$ in the present high-temperature situation, we find $f_1^0 \cong 0.764$, and on using $J = 0.5$, $f_1 \cong 0.761$, and $f_2 \cong 0.780$, in excellent agreement with one of the experimental curves at $\theta = 0$. Incidentally, on taking $\alpha = 0$, the appropriate expression for f_3^0 leads to about 0.825 for $R_c = 7$ and to 0.705 for $R_c = 4$. These results suggest that redistribution does not appreciably affect the f values determined from experiment in the present case.

Finally, it seems pertinent to discuss briefly the appropriateness of the classical image force law used throughout this article and in most treatments of ionic adsorption. We have taken the electrostatic potential at $z = \beta$ arising from the image, at $z = -\beta$, of a charge of effective valence z_v at $z = \beta$ to be $\phi_{i,z} = -z_v e/2\beta$. No contribution from the charge at $z = \beta$ appears in $\phi_{i,z}$. How applicable to the actual adion situation is this expression for $\phi_{i,z}$?

First, quantum-mechanical calculations (4,21,113) indicate that the classical image potential may be too large in magnitude by about 9% for β as small as 1 Å. Further, no deviations in emitted current from the Fowler-Nordheim theory of field emission, which is based on the classical image law, were observed experimentally by Barbour et al. (3, see also ref. 97) until the field magnitude exceeded about 5×10^7 V/cm. Even at 10^8 V/cm, the deviation was only 4 to 5%. Cutler and co-workers (20,21) have discussed a correction to the classical law which would lead to $\phi_{i,z} \cong (-z_v e/2\beta)(1 - \eta\beta^{-1})$. Values of the constant η used

ranged from about 0.07 to 0.09 Å. For $\beta = 2$ Å, the correction amounts therefore to about 4%.

Although a correction of the above form has been suggested as appropriate for ions by Andersen and Bockris (2), it is important to note that the correction and the above discussion all pertain only to electron imaging. There is perhaps some room for doubt concerning the applicability of electron-derived criteria for the usefulness of the classical image potential to cation adsorption situations. For $\beta \geq 2$ Å, we believe, however, that it is as appropriate to use the classical law as the corrected one for simple ions. Even were the corrected potential the more appropriate, the correction could be neglected compared with the greater uncertainties which abound in the inner layer.

There is, however, an ion correction to the classical image law which should be mentioned. An ion is not a bare charge and its charge will tend to be somewhat self shielded. Such a reduction in $\phi_{i,z}$ is likely to be very small for the usual ions of interest in electrolyte situations and can either be ignored to good approximation or incorporated, again to good approximation, by a small field-independent change in the ion-image distance. Finally, we have already mentioned the possibility of a difference in the imaging by a metal of positive and negative charges. This effect too may be small enough to neglect to good approximation, although the situation is not so clear for permanent dipoles inasmuch as any slight difference would exhibit itself as a contribution to the natural field \mathcal{E}_{n2} .

The treatments of discreteness effects discussed in this article have been meant to help expose and elucidate a number of gross features of the equilibrium double-layer system without incorporating all high-order effects which could be imagined. Although double-layer theory is still in an early stage of development, we hope this article will help advance the subject a step closer to maturity.

Appendix I

C-C Imaging for a Single Charge

We first consider the potential produced by a point charge at $x = y = 0$, $z = \beta$ between two perfect imaging planes each a distance β from the charge. This corresponds to the potential

produced by a charge on the IHP and its infinite regress of images in the $C-C$ imaging situation for $\beta = \gamma$. The first derivation here is extremely simple and relates back to some of the physical arguments in the main text, but unfortunately it is somewhat difficult to generalize; a less amusing but also more generally applicable method is considered afterward. Throughout this Appendix the dielectric constant ϵ_1 is taken as unity.

According to the method of images the potential at $r \equiv (x, y, z)$ is given by

$$\phi(\mathbf{r}) = z_0 e \sum_{n=-\infty}^{\infty} (-1)^n [\rho^2 + (z - \beta + 2n\beta)^2]^{-1/2}$$

where $\rho \equiv (x^2 + y^2)^{1/2}$. This expression for ϕ is not very useful as it stands, since the convergence rate is extremely slow. Therefore, we seek another expression for this potential. According to Laplace's equation

$$\frac{\partial^2 \phi}{\partial z^2} + \rho^{-1} \frac{\partial}{\partial \rho} \left(\rho \frac{\partial \phi}{\partial \rho} \right) = 0$$

everywhere in the domain $0 < z < 2\beta$ except at the site of the charge. Separating the variables and requiring that ϕ vanish at the two imaging planes $z = 0$ and $z = 2\beta$, one obtains

$$\phi(\mathbf{r}) = \sum_{n=1}^{\infty} A_n \frac{\sin(n\pi z/2\beta)}{\sin(n\pi/2)} K_0\left(\frac{n\pi\rho}{2\beta}\right)$$

where for convenience the unknown constants have been written $A_n \{\sin(n\pi/2)\}^{-1}$, the function K_0 is a modified Bessel function of the third kind, and the particular way we have written the unknown constants requires that the sum extend only over odd values of n as indicated by a prime on the summation. (Thus, that we are able to live with our "convenient" manner of writing is somewhat fortuitous.)

We now determine the values of A_n such that the potential properly behaves as $z_0 e [\rho^2 + (z - \beta)^2]^{-1/2}$ very close to the charge.* Taking $z = \beta$ we require

$$\sum_{n=1}^{\infty} A_n K_0\left(\frac{n\pi\rho}{2\beta}\right) \doteq z_0 e \rho^{-1}, \quad \text{as } \rho \rightarrow 0$$

* It turns out that it is easier to maintain rigor by requiring that the field behave as $z_0 e [\rho^2 + (z - \beta)^2]^{-1}$ close to the charge, but the results are the same in any case.

Now defining $\chi_n \equiv (2\beta)^{-1} n\pi\rho$, $\Delta\chi \equiv \beta^{-1} \pi\rho$ as the difference between successive values of χ_n in the sum, we find

$$\begin{aligned} \sum_{n=1}^{\infty} A_n K_0\left(\frac{n\pi\rho}{2\beta}\right) &= (\pi\rho)^{-1} \beta \sum_{n=1}^{\infty} A(\chi_n) K_0(\chi_n) \Delta\chi \\ &\doteq \beta (\pi\rho)^{-1} \int_0^{\infty} A(\chi) K_0(\chi) d\chi \end{aligned}$$

provided the function $A(\chi)$ is smoothly varying as $\rho \rightarrow 0$. We shall verify that this is indeed the case, for we shall obtain that $A(\chi) \equiv A$, a constant.

Write

$$\int_0^{\infty} A(\chi) K_0(\chi) d\chi = A \int_0^{\infty} K_0(\chi) d\chi = \frac{1}{2} \pi A$$

where we have employed the frequently useful relation,

$$\int_0^{\infty} K_0(\delta\chi) \cos(\theta\chi) d\chi = (\pi/2)(\theta^2 + \delta^2)^{-1/2}$$

which applies for real θ and δ provided $\delta > 0$. Thus our condition on the potential near the charge implies $\frac{1}{2} \rho^{-1} \beta A = \rho^{-1} z_0 e$; therefore, $A = 2z_0 e \beta^{-1}$, and

$$\phi(\mathbf{r}) = 2z_0 e \beta^{-1} \sum_{n=1}^{\infty} \frac{\sin(n\pi z/2\beta)}{\sin(n\pi/2)} K_0\left(\frac{n\pi\rho}{2\beta}\right)$$

The more mundane (and more rigorous) derivation of ϕ for the more general case, β and γ not necessarily equal, proceeds from the appropriate expression for potential obtained by the method of images

$$\begin{aligned} \phi(\mathbf{r}) &= z_0 e \sum_{n=-\infty}^{\infty} \{[\rho^2 + (z - \beta - 2nd)^2]^{-1/2} \\ &\quad - [\rho^2 + (z + \beta - 2nd)^2]^{-1/2}\} \end{aligned}$$

where $d \equiv \beta + \gamma$. We prefer to write this sum in the form

$$\phi(\mathbf{r}) = (2d)^{-1} z_0 e \sum_{n=-\infty}^{\infty} \{g^+(n | \mathbf{r}) - g^-(n | \mathbf{r})\}$$

with

$$g^{\pm}(n | \mathbf{r}) \equiv [(\rho/2d)^2 + \{n - (2d)^{-1}(z \mp \beta)\}^2]^{-1/2}$$

Next, we define the Fourier transforms $G^\pm(k | \mathbf{r})$

$$\begin{aligned} G^\pm(k | \mathbf{r}) &\equiv \int_{-\infty}^{\infty} d\xi \exp(2\pi i k \xi) g^\pm(\xi | \mathbf{r}) \\ &= 2 \exp\{i\pi(k/d)(z \mp \beta)\} K_0(\pi \rho |k|/d) \end{aligned}$$

Finally, we use the Poisson summation formula, relating the sum of the g -functions to the sum of the G -functions to obtain

$$\phi(\mathbf{r}) = (2d)^{-1} z_0 e \sum_{k=-\infty}^{\infty} \{G^+(k | \mathbf{r}) - G^-(k | \mathbf{r})\}$$

This is readily shown to give

$$\phi(\mathbf{r}) = 4 \frac{z_0 e}{\beta} (1 + \Gamma)^{-1} \sum_{n=1}^{\infty} \sin\left(\frac{\pi n}{1 + \Gamma}\right) \sin\left(\frac{\pi n Z}{1 + \Gamma}\right) K_0\left(\frac{\pi n P}{1 + \Gamma}\right)$$

where here $P \equiv \rho/\beta$.

When $\Gamma = 1$, all terms of even n vanish, and our earlier result is recovered. As a simple corollary to our general equation above, we find that the potential on the IHP ($Z = 1$) is given by

$$\phi(P, 1) = 4(z_0 e/\beta)(1 + \Gamma)^{-1} \sum_{n=1}^{\infty} \sin^2\left(\frac{\pi n}{1 + \Gamma}\right) K_0\left(\frac{\pi n P}{1 + \Gamma}\right)$$

We note that the potential on the IHP is invariant under the interchange of β with γ , as it must be for C - C imaging. All the foregoing series involving the modified Bessel functions converge quite rapidly, and usually the summations may be truncated after several terms with little loss of accuracy.

Appendix II

Distribution Function for Nearest Neighbors without Interaction

Define $P(r) dr$ as the probability of finding the nearest neighbor of a given particle somewhere in the annular ring of width dr and inner radius r about that particle. In order for such a situation to obtain, two conditions are necessary: (1) the nearest neighbor must not lie within the circle of radius r , and (2) the nearest neighbor must not lie outside the circle of radius $r + dr$. The probability that the first condition is satisfied is evidently given

by the expression

$$1 - \int_0^r P(\xi) d\xi$$

Given the first condition, the probability of realizing the second condition depends upon the correlation between particle positions; however, if it is assumed that no correlation exists, that is that the particles do not interact, then the probability of realizing the second condition is simply given by $2\pi Nr dr$, where $N \equiv$ mean surface density of particles. We obtain

$$P(r) dr = 2\pi Nr dr \left\{ 1 - \int_0^r P(\xi) d\xi \right\}$$

from whence

$$P(r) \equiv \frac{d}{dr} \left\{ \int_0^r P(\xi) d\xi \right\} = 2\pi Nr \left\{ 1 - \int_0^r P(\xi) d\xi \right\}$$

Solving the differential equation for

$$\int_0^r P(\xi) d\xi$$

produces

$$\int_0^r P(\xi) d\xi = 1 + A \exp(-\pi Nr^2)$$

where A is a constant yet to be determined. Differentiating, we find

$$P(r) = -2\pi NAr \exp(-\pi Nr^2)$$

and integrating again we may determine A from the normalization condition on $P(r)$. When such a normalization condition is imposed, we find* $A = -1$, and therefore

$$P(r) = 2\pi Nr \exp(-\pi Nr^2)$$

Now we use the distribution function just obtained for nearest-neighbor distances to find the expectation value of nearest-neighbor distance in the absence of interaction-induced correlations.

* Had there been a hard-core interaction excluding particles from the circle of radius r_{1m} , the lower limits of integration would have been r_{1m} , A would become $-\exp(-\pi Nr_{1m}^2)$, and $P(r)$ would be $2\pi Nr \exp\{-\pi N(r^2 - r_{1m}^2)\}$ for $r > r_{1m}$ and zero for $r < r_{1m}$.

Writing this expectation value as $\langle r_1 \rangle$, we find

$$\langle r_1 \rangle \equiv \int_0^\infty r P(r) dr = 2\pi N \int_0^\infty r^2 \exp(-\pi N r^2) dr$$

On transforming the variable to $\xi \equiv \pi N r^2$, we obtain

$$\langle r_1 \rangle = (\pi N)^{-1/2} \int_0^\infty \xi^{1/2} \exp(-\xi) d\xi = (\pi N)^{-1/2} \Gamma(\frac{3}{2})$$

Finally, noting that $\Gamma(\frac{3}{2}) \equiv \frac{1}{2}\sqrt{\pi}$, we may write

$$\langle r_1 \rangle = \frac{1}{2} N^{-1/2}$$

which is a very simple result.*

List of Symbols

Abbreviations

ASC	All system configurations
BDM	Bockris, Devanathan, and Müller
CHM	Cell and hexagonal lattice model: the approach of Bell, Mingins, and Levine
ECM	Electrocapillary maximum (potential)
ESP	Electrode surface plane
GEM	Generalized Ewald method
GFA	Green's function approach
HTL	High temperature limit
IHP	Inner Helmholtz plane
LDL	Low density limit
MHB	Mackenzie, van der Hoff, and Benson: a method for transforming lattice summations
OHP	Outer Helmholtz plane

* Again, were we to consider a hard-core interaction, the lower limits of integration would become finite and the final resulting expression for $\langle r_1 \rangle$ would become

$$\begin{aligned} \langle r_1 \rangle &= r_{1m} (\pi N r_{1m}^2)^{-1/2} \exp(\pi N r_{1m}^2) \Gamma(\frac{3}{2}, \pi N r_{1m}^2) \\ &= r_{1m} (\pi N r_{1m}^2)^{-1/2} \Psi(-\frac{1}{2}, -\frac{1}{2}; \pi N r_{1m}^2) \end{aligned}$$

where the first manner of writing involves the incomplete gamma function and the second, the confluent hypergeometric function. The function $\chi^{-1/2} \times \Psi(-\frac{1}{2}, -\frac{1}{2}, \chi)$ diverges as $\sqrt{\pi/4\chi}$ for small values of the argument; for large values its asymptotic behavior is as $1 + (2\chi)^{-1} + O(\chi^{-2})$, while for $\chi = 1, 2,$ and 3 its values are approximately 1.36, 1.21, and 1.14, respectively.

PZC	Point of zero charge: according to theory, equivalent to ECM
TSE	Thermal stability according to an Einstein approximation: the method of Macdonald and Barlow
C-O, C-C, etc	Such abbreviations refer to the imaging conditions applying in the double layer; the first letter pertains to the ESP, the second to the OHP. The letter <i>O</i> designates that the plane in question does not image; the letter <i>C</i> designates ideal conductive imaging, and <i>D</i> , dielectric imaging.

Standard Mathematical Functions

erf (<i>x</i>)	Error function $\equiv 2\pi^{-1/2} \int_0^x \exp(-t^2) dt$
erfc (<i>x</i>)	$1 - \text{erf}(x)$
$J_n(x)$	Bessel function of the first kind
$K_n(x)$	Modified Bessel function of the third kind (Macdonald's function)
$\Gamma(x)$	Gamma function $\equiv \int_0^\infty t^{x-1} \exp(-t) dt$
$\Gamma(x, y)$	Incomplete gamma function $\equiv \int_y^\infty t^{x-1} \exp(-t) dt$
$\gamma(n, x)$	$\Gamma(n) - \Gamma(n, x)$
$\psi(a, b; x)$	Confluent hypergeometric function

Main Symbols

c_0	Ionic concentration in the bulk solution
d	$\beta + \gamma \equiv$ compact layer thickness
\mathcal{D}	Electric displacement
e	Protonic charge
\mathcal{E}, \mathcal{E}	Generic symbols for local electric field; when the symbol is not boldface, it generally refers to the component normal to the ESP.
$\mathcal{E}_{\text{ext}}, \mathcal{E}_{\text{ext}}$	External field
$\mathcal{E}_{\text{eff}}, \mathcal{E}_{\text{eff}}$	Field effective in polarizing elements
$\mathcal{E}_r, \mathcal{E}_r, \mathcal{E}_d$	Depolarization field arising from dipoles
$\mathcal{E}_{\parallel}, \mathcal{E}_{\perp}$	Field components parallel to and normal to the ESP, respectively
E_∞	$-\psi_\infty/\beta$, a normalizing quantity having dimensions of electric field
f, f_1, f_2, f_3	The penetration parameter, the subscripts referring to specific situations
F	$\equiv -d \ln p(\xi)/d \ln \xi$
g	A discreteness parameter used by Levine et al. to characterize the perturbation potential

$g(R_1)$	A function involved in the effect of nonzero ionic polarizability upon ψ_∞
$G(\Gamma)$	A function characterizing the effect of Γ upon critical fluctuation lengths
$\mathbb{G}(\mathbf{r}, \mathbf{r}'_{mn})$	Green's function at \mathbf{r} for charge placed at \mathbf{r}'_{mn}
h	Height of a basic array triangle $\equiv (3)^{1/2}r_1/2$
J	A parameter measuring the increase in effective polarizability as a result of imaging $\equiv \alpha/\beta^3$
\mathbf{k}, k	Generic symbols for wave-vector, wave-number
k	Boltzmann's constant
l	Characteristic distance in the compact layer; also normalized distance from symmetry line $\equiv \rho/h$
l_{\max}	Maximum normalized motion allowable along given line
L, L_1, L_2	r.m.s. normalized (with h) fluctuation distance: the subscripts refer to one and two dimensional motion, respectively; the symbols L_1 and L_2 also refer to a normalized variable in the IHP applying to Figs. 21 and 22.
N	Particle surface density
N_v	Particle volume density
N_0	Total particle number
N_s	Maximum possible particle surface density for a monolayer
$p \equiv p(\xi), p_0, p_\infty$	Ratio of cutoff-model radius, r_b , to r_1 for hexagonal array; the subscripts 0 and ∞ refer to the values pertaining when $\xi \rightarrow 0$ and $\xi \rightarrow \infty$ respectively. In particular, $p_0 \cong 0.65752$, $p_\infty \cong 0.52504$. Sometimes, the subscripts i and n are used with $p(\xi)$, e.g., $p_i(\xi)$, to indicate ideal and nonideal dipole situations.
\hat{p}	A probability ratio defined by Bell and co-workers = (probability of occupying outer half of proximity cell)/(probability of occupying inner half).
P, \mathbf{P}	Dipole moment of an element; a subscript refers to which element is involved.
\mathcal{P}, \mathcal{P}	Polarization \equiv volume density of dipole moment.
q	Charge density on ESP
q_1	Charge density on IHP
q_2	Charge density on OHP
$\mathbf{r}, \mathbf{r}', \mathbf{r}_i$	Variouly used as an unnormalized position variable
r_1	Nearest-neighbor distance
$\langle r_1 \rangle$	Mean nearest-neighbor distance
$\mathbf{r}_1, \mathbf{r}_2, \mathbf{r}_3, \dots, \mathbf{r}_N$	Positions of particles in statistical assemblage
r_0	Grahame cutoff radius: $\pi N r_0^2 \equiv 1$
r_b	Generalized cutoff radius
r_c	Coulombic hard-core diameter
r_M	Quantity analogous to l_{\max} used in CHM and there set equal to r_0

r_{1m}	Minimum possible value allowed for r_1 ; usually the hard-core diameter
R	Normalized r ($\equiv r/\beta$)
R_1	Normalized value of r_1 ; generally $R_1 \equiv r_1/\beta$. However, when no hexagonal array is presumed, $R_1 \equiv (r_0/\beta_\infty)\beta$ in the cutoff model. For $D-C$ imaging, $R_1 \equiv r_1/\gamma$. When γ is the separation between discrete layers of charge, we have also used $R_1 = 2r_1/\gamma$.
R_0	$\equiv r_0/\beta$
R_b	$\equiv r_b/\beta$
R_c	Normalized r_c ($\equiv r_c/\beta$)
R_{1m}	Normalized r_{1m} ($\equiv r_{1m}/\beta$)
\mathbf{R}_k	Vector position of \mathbf{k} 'th lattice point
S	Structure factor relating \mathcal{E}_r to \mathcal{P} . Also the quantity $2(\beta/z_0 e)(\beta \mathcal{E}_{n1})$.
T	Absolute temperature
U	Generically employed to designate interaction energy: a superscript zero refers to single image conditions; a superscript two refers to $C-C$ conditions; the subscript "pair" designates that a single pair is being considered; U_{ij} is the interaction energy between the i 'th and j 'th particles; U_{total} is the total interaction energy; U_T is also used for total energy; U_{int} is sometimes used to mean interaction energy, and sometimes, internal energy.
V	Generically employed for average potentials and potential differences. A single subscript determines the plane where the average is taken: (0, 1, 2, " ∞ ") refers respectively to the ESP, the IHP, the OHP, and " ∞ " (see discussion concerning " ∞ " in the text). A double subscript denotes a potential difference; for example $V_{02} \equiv V_0 - V_2$, etc.
V_0	This is also used to designate the average p.d. across charge layers. In terms of the definitions above, V_0 is analogous to V_{02} .
x	Component of \mathbf{r} parallel to IHP
X	Normalized x : $\equiv x/\beta$
y	Component of \mathbf{r} parallel to IHP
Y	Normalized y : $\equiv y/\beta$
z	Variouly used, but most often the distance from the ESP
z_0	Effective adion valence
Z	Normalized value of z : $\equiv z/\beta$
Z_0	Value of Z at OHP $\equiv 1 + \Gamma \equiv d/\beta$
\mathcal{Z}	Partition function
$\alpha, \alpha_0, \alpha_{ }$	Polarizability of an element; low field limit $\equiv \mu^2/3kT$ for permanent dipoles; "parallel component" of polarizability giving dipole-moment component parallel to IHP

$\alpha, \alpha_1, \alpha_2$	Potential parameter used by Krylov and Levich. The subscripts 1 and 2 refer to $\omega = +1$ and $\omega = -1$, respectively.
β	Distance from ESP to IHP
B	$\beta/\gamma \equiv$ the ratio of two dimensions
γ	Distance from IHP to OHP
Γ	The ratio γ/β
$\delta\psi, \delta\rho_{\pm}$	Small perturbation in the potential and positive and negative diffuse-layer ion number densities, respectively
Δ	A parameter measuring the nonlinearity of the potential in the compact layer. A subscript 0 refers to the situation $q = 0$; a superscript 0, to the condition $\beta = \gamma$.
$\Delta\Psi_a$	The difference between the $Z = 1$ normalized potential at point a' and point 0: $\Delta\Psi_a \equiv \Psi_a(a') - \Psi_a(0)$
ϵ	Generic symbol for dielectric constant. Subscripts β and γ refer to the values pertinent for the regions $0 < Z < 1$ and $1 < Z < Z_0$, respectively. ϵ_s pertains to the region to the right of the OHP ($Z > Z_0$). ϵ_0 pertains to the region to the left of the ESP ($Z < 0$). ϵ_1 is the value pertinent to the compact layer when ϵ_β and ϵ_γ are considered identical. The quantity ϵ_2 is either ϵ_0 or ϵ_s depending on which plane is considered to be a dielectric imaging plane. ϵ_{eff} is a quantity involved in the C-O imaging calculation of \mathcal{E}_{eff} .
η	A dielectric imaging parameter: $\eta\epsilon_1/\epsilon_2 \equiv 1 - \omega$
θ	Fractional surface coverage $\equiv N/N_s$
λ	The ratio $\gamma/(\beta + \gamma) \equiv \Gamma(1 + \Gamma)^{-1} \equiv \Gamma Z_0^{-1}$
λ_D	The Debye shielding length $\equiv (kT\epsilon_s/4\pi c_0 e^2)^{1/2}$
$\lambda_D(\mathbf{r})$	A local Debye-length for a uni-univalent electrolyte: $\lambda_D(\mathbf{r}) \equiv (kT\epsilon_s/4\pi e^2)^{1/2} \{\rho_+(\mathbf{r}) + \rho_-(\mathbf{r})\}^{-1/2}$
λ'	The coefficient in the parabolic approximation to the potential on a line of n -fold symmetry
λ_k	Reciprocal lattice vectors
Λ	A potential ratio playing a central role in the theory of the double layer: $\Lambda \equiv \psi_{12}/V_{02}$
$\mu, \langle \mu \rangle$	Magnitude of the permanent dipole moment and thermal average value of its z -component, respectively
ξ	The dimensionless ratio z/r_1
ξ_m	The ratio $z/r_{1,m}$
ξ_c	The ratio z/r_c
ρ	Used both as a radial coordinate and as a charge density
$\langle \rho^2 \rangle$	Mean square unnormalized fluctuation distance
$\hat{\rho}$	Radial distance from line of symmetry
ρ_{mn}	Radial distance from (m,n) lattice point: $\rho_{mn} \equiv \{(x - x'_{mn})^2 + (y - y'_{mn})^2\}^{1/2}$
ρ_0	Equivalent to c_0

ρ_{\pm}	Positive and negative ion number densities
ρ_{\pm}^0	Positive and negative ion number densities pertaining when $\psi = \psi^0$ (before a perturbation is applied)
P	Normalized radial coordinate $\equiv \rho/\beta$
σ	Topping's parameter $\cong 11.034$
τ	A parameter used by Levine et al.: $\tau \equiv p_{\infty} R_1/2$
ϕ	A generic symbol for potential when it is desired to avoid identification with one of the more specific ψ potentials
ϕ_0	An artificial potential used to calculate interaction energy of a pair in the presence of polarization
ϕ_{iz}	Potential arising from the image of a charge at $(0,0,z)$
$\phi_{\beta}, \phi_1, \phi_1(0,0)$	These symbols are various representations of the self-atmosphere perturbation potential of Levine et al. ϕ_1 is generally used in the present article.
ψ	A generic symbol for local potential and for p.d. There are many variations on this symbol, and not all will be listed here. The basic rules for interpretation are as follows: (1) a capital ψ designates that the unnormalized potential has been normalized by ψ_{∞} ; (2) a superscript zero usually refers to C-O imaging (except when the quantity ψ_{∞}^0 is the value of ψ_{∞} for $\alpha = 0$); (3) a superscript (1) refers to the C-D limit $\omega \rightarrow 1$; (4) a superscript (2) refers to the C-C imaging situation; (5) a subscript a designates a lattice with a single vacancy; (6) single subscripts $(0,1,2,\infty)$ designate respectively the ESP, IHP, OHP, and " ∞ ," as for the case of the V 's; (7) doubly subscripted symbols containing two numbers out of the set $(0,1,2,\infty)$ refer to the appropriate potential difference along a line through point 0, analogous to the usage in the case of the V 's. Thus, $\psi_{12} \equiv \psi_1 - \psi_2 \equiv \psi(1) - \psi(Z_0)$. In addition to these general rules, we have the following specific definitions.
Ψ	Normalized potential $\equiv \psi(z)/\psi_{\infty}$; infrequently denoted by ψ^N
Ψ_{∞}	$\equiv \psi_{\infty}/\psi_{\infty}^0$
ψ_e	The uniform field part of the total potential ψ
ψ_{a1Z_0}	$\psi_a(1) - \psi_a(Z_0)$
ψ_{aic}	Potential arising from a complete array, i.e., one without a vacancy
ψ_i	Potential which includes the contribution ϕ_{iz} from the image of a charge at $(0,0,z)$
ψ_i	Ideal dipole potential
ψ_n	Nonideal dipole potential
ψ_c	Krylov's constant field potential
ψ_0, ψ_p	Potentials calculated by Esin and Shikov at points 0 and p of Fig. 26a

ψ_{0p}	$\psi_0 - \psi_p$
ψ_∞	Potential at "infinity"; also denoted by V_∞
ψ_∞^0	ψ_∞ when $\alpha = 0$ ($\equiv 4\pi z_0 e \beta N$)
ω	Dielectric imaging parameter $\equiv (\epsilon_2 - \epsilon_1)/(\epsilon_2 + \epsilon_1)$; sometimes used as a circular frequency.

References*

1. S. Adler, *Physica*, **27**, 1193 (1961).
2. T. N. Andersen and J. O'M. Bockris, *Electrochim. Acta*, **9**, 347 (1964).
3. J. B. Barbour, W. W. Dolan, J. K. Trolan, E. E. Martin, and W. P. Dyke, *Phys. Rev.*, **92**, 45 (1953).
4. J. Bardeen, *Phys. Rev.*, **49**, 653 (1936).
5. C. A. Barlow, Jr. and J. R. Macdonald, *J. Chem. Phys.*, **40**, 1535 (1964). In Eq. 23 of this paper, the term in square brackets should be in the denominator, not the numerator, of the equation. The term $\mathbf{h} - \mathbf{h}$ which appears twice on p. 1543 should be $\mathbf{h} - \mathbf{h}_\lambda$.
6. C. A. Barlow, Jr. and J. R. Macdonald, *J. Chem. Phys.*, **43**, 2575 (1965). On p. 2578 of this paper, \mathcal{E} in the Glossary should be \mathcal{E}_a ; reference 8 on p. 2579 should read 199-247; on p. 2590 Mignolet²⁸ should be Mignolet¹⁴.
7. B. Bederson and E. J. Robinson, in *Molecular Beams, Advances in Chemical Physics*, Vol. 10, J. Ross, Ed., Interscience, New York, 1966.
8. G. M. Bell, J. Mingins, and S. Levine, *Trans. Faraday Soc.*, **62**, 949 (1966).
9. J. O'M. Bockris and D. A. J. Swinkels, *J. Electrochem. Soc.*, **111**, 736 (1964).
10. J. O'M. Bockris, M. A. V. Devanathan, and K. Müller, *Proc. Roy. Soc. (London)*, **A274**, 55 (1963); this paper in identical form, also appears in *Proc. Australian Conf. Electrochem.*, 1st, J. A. Friend and F. Gutmann, Eds., Pergamon, Oxford, 1965, p. 832.
11. J. O'M. Bockris, M. Green, and D. A. J. Swinkels, *J. Electrochem. Soc.*, **111**, 743 (1964).
12. J. O'M. Bockris, K. Müller, H. Wroblowa, and Z. Kovac, *J. Electroanal. Chem.*, **10**, 416 (1965).
13. G. H. Bolt, *J. Colloid Sci.*, **10**, 206 (1955).
14. M. Born and K. Huang, *Dynamical Theory of Crystal Lattices*, Oxford University Press, Oxford, 1956.
15. C. J. F. Böttcher, *Theory of Electric Polarization*, Elsevier, Amsterdam, 1952.
16. D. L. Bowers and E. E. Salpeter, *Phys. Rev.*, **119**, 1180 (1960).
17. F. P. Buff and F. H. Stillinger, Jr., *J. Chem. Phys.*, **39**, 1911 (1963).
18. J. E. Chamberlain, G. W. Chantry, H. A. Gebbie, N. W. B. Stone, T. B. Taylor, and G. Wyllie, *Nature*, **210**, 790 (1966).
19. B. E. Conway, *Theory and Principles of Electrode Processes*, Ronald Press, New York, 1965.
20. P. H. Cutler and J. C. Davis, *Surface Sci.*, **1**, 194 (1964).
21. P. H. Cutler and J. J. Gibbons, *Phys. Rev.*, **111**, 394 (1958).
22. B. B. Damaskin, "Differential Capacity and Structure of the Electrical Double Layer at the Mercury/Electrolyte Interface," *Russ. Chem. Rev.*, **30**, 220-242 [78-90] (1961). An excellent review, more comprehensive and critical than most.
23. P. Debye and E. Hückel, *Physik. Z.*, **24**, 185, 305 (1923).
24. P. Delahay, *Double Layer and Electrode Kinetics*, Interscience, New York, 1965. The most complete discussion of work on the double layer yet to appear. Includes some discussion of discreteness calculations.
25. P. Delahay and G. G. Susbielles, *J. Phys. Chem.*, **70**, 647 (1966).
26. P. Delahay, R. de Levie, and A.-M. Giuliani, *Electrochim. Acta*, **11**, 1141 (1966).
27. M. A. V. Devanathan and S. G. Canagaratna, *Electrochim. Acta*, **8**, 77 (1963).
28. M. A. V. Devanathan and B. V. K. S. R. A. Tilak, "The Structure of the Electrical Double Layer at the Metal-Solution Interface," *Chem. Rev.*, **65**, 635-684 (1965). Contains much discussion of a variety of experimental results and a great many references. Noncomprehensive; insufficiently critical of overly simplified earlier work by Devanathan and others.
29. O. F. Devereux and P. L. de Bruyn, *Interaction of Plane-Parallel Double Layers*, M.I.T. Press, Cambridge, Massachusetts, 1963. Earlier references to the subject may be found in this work.
30. O. F. Devereux and P. L. de Bruyn, *J. Colloid Sci.*, **19**, 302 (1964).
31. E. Dutkiewicz and R. Parsons, *J. Electroanal. Chem.*, **11**, 100 (1966).
32. B. V. Ershler, *Zh. Fiz. Khim.*, **20**, 679 (1946). English translation available.
33. O. A. Esin and B. F. Markov, *Zh. Fiz. Khim.*, **13**, 318 (1939).
34. O. A. Esin and V. M. Shikov, *Zh. Fiz. Khim.*, **17**, 236 (1943). English translation available.
35. P. P. Ewald, *Ann. Physik*, **54**, 519, 557 (1917); **64**, 253 (1921).
36. N. F. Fletcher, *Phil. Mag.*, **8**, 1425 (1963).
37. H. S. Frank and P. T. Thompson, *J. Chem. Phys.*, **31**, 1086 (1959).
38. A. N. Frumkin, *Phys. Z. Sowjetunion*, **4**, 239 (1933). (In German.)
39. A. N. Frumkin, "The Double Layer in Electrochemistry," *Usp. Khim.*, **4**, 987-1008 (1935).
40. A. N. Frumkin, "The Double Layer in Electrochemistry," *J. Electrochem. Soc.*, **107**, 461-472 (1960). A useful review primarily experimentally oriented; brief mention of discreteness effects.
41. A. N. Frumkin and B. B. Damaskin, "Adsorption of Organic Compounds at Electrodes," in *Modern Aspects of Electrochemistry*, Vol. III, J. O'M. Bockris and B. E. Conway, Eds., Butterworths, Washington, 1964, pp. 149-223.
42. A. N. Frumkin, Z. A. Iofa, and M. A. Gerovich, *Zh. Fiz. Khim.*, **30**, 1455 (1956).

* Where English translations have been found of Russian papers, we have inserted the initial English page number in square brackets following the initial Russian page number, e.g., Ref. 43.

43. A. N. Frumkin, R. V. Ivanova, and B. B. Damaskin, *Dokl. Akad. Nauk SSSR*, **157**, 1202 [822] (1964).
44. A. N. Frumkin, N. Polianovskaya, N. Grigoryev, and I. Bagotskaya, *Electrochim. Acta*, **10**, 793 (1965).
45. R. Gomer, *J. Chem. Phys.*, **21**, 1869 (1953).
46. D. C. Grahame, "The Electrical Double Layer and the Theory of Electrocapillarity," *Chem. Rev.*, **41**, 441-501 (1947). An excellent review; still an important part of the literature. No discussion of discreteness effects except that associated specifically with ion size.
47. D. C. Grahame, *J. Chem. Phys.*, **18**, 903 (1950).
48. D. C. Grahame, "Progress and Problems in the Study of the Electrical Double Layer," *Record Chem. Progr.*, **11**, 93 (1950).
49. D. C. Grahame, *Comite Intern. Thermodyn. Cinet. Electrochim., Compt. Rend. Réunion 3e*, Berne, 1951. References to earlier pertinent papers are given in this one.
50. D. C. Grahame, *J. Am. Chem. Soc.*, **76**, 4821 (1954).
51. D. C. Grahame, *J. Am. Chem. Soc.*, **80**, 4201 (1958).
52. D. C. Grahame, *Z. Elektrochem.*, **62**, 264 (1958).
53. D. C. Grahame and R. Parsons, *J. Am. Chem. Soc.*, **83**, 1291 (1961).
54. W. J. C. Grant, *Bell System Tech. J.*, **44**, 427, 2433 (1965).
55. E. A. Guggenheim, *Discussions Faraday Soc.*, **24**, 53 (1957).
56. G. J. Hills and R. Payne, *Trans. Faraday Soc.*, **61**, 326 (1965).
57. C. A. Hurst and E. St. A. Jordine, *J. Chem. Phys.*, **41**, 2735 (1964).
58. H. D. Hurwitz, "Theoretical Considerations of the Double Layer," in *Electrosorption*, E. Gileadi, Ed., Plenum, to be published. Primarily concerned with approximate statistical treatments of the double layer. Some discussion of discreteness, especially statistical treatments thereof.
59. E. St. A. Jordine, G. B. Bodman, and A. H. Gold, *Soil. Sci.*, **94**, 371 (1962).
60. V. S. Krylov, *Dokl. Akad. Nauk SSSR*, **144**, 155 [356] (1962).
61. V. S. Krylov, *Electrochim. Acta*, **9**, 1247 (1964). On p. 1248, the expression $x \geq \beta$ should read $x \geq \gamma$. On p. 1249, $e^2 z_1^2 2D_3 kT$ should read $e^2 z_1^2 / 2D_3 kT$. The concentrations in Fig. 1 should read 0.5M and 0.6M. On p. 1252, the expression $x = -\sigma/4$ should be replaced by $x = -\delta/4$. The relation $\theta = 0.9\xi^2$ on p. 1254 should be replaced by $\theta = \xi^2$. The term $\partial\psi_0/\partial \ln a_{\pm}$ on p. 1257 should have a minus sign preceding it.
62. V. S. Krylov and V. G. Levich, *Zh. Fiz. Khim.*, **37**, 106 [50] (1963).
63. V. S. Krylov and V. G. Levich, *Zh. Fiz. Khim.*, **37**, 2273 [1224] (1963).
64. V. S. Krylov and V. G. Levich, *Dokl. Akad. Nauk SSSR*, **159**, 409 [1037] (1964).
65. M. F. C. Ladd and W. H. Lee, in *Progr. Solid State Chem.*, **II**, H. Reiss, Ed., Pergamon, 1965.
66. I. Langmuir, *J. Am. Chem. Soc.*, **54**, 2798 (1932).
67. V. G. Levich and V. A. Kir'yanov, *Dokl. Akad. Nauk SSSR*, **131**, 1134 [349] (1960).
68. V. G. Levich and V. S. Krylov, *Dokl. Akad. Nauk SSSR*, **141**, 1403 [969] (1961).

69. V. G. Levich and V. S. Krylov, *Dokl. Akad. Nauk SSSR*, **142**, 123 [18] (1962). In the English translation, the second $\omega \rightarrow 1$ on p. 20 should read $\omega \rightarrow -1$.
70. V. G. Levich, V. A. Kir'yanov, and V. Yu. Filinovsky, Symposium in Commemoration of David C. Grahame, 138th Meeting of the American Chemical Society, New York, N.Y., September 14, 1960. Abstracts of papers, p. 14-I. The title and author which appear in these abstracts do not agree with those appearing on the actual paper finally submitted and presented.
71. V. G. Levich, V. A. Kir'yanov, and V. S. Krylov, *Dokl. Akad. Nauk SSSR*, **135**, 1425 [1193] (1960). The material to the right of $D/D_0\kappa$ in Eq. 11 should be eliminated. In Eq. 14, a_{\pm}^2 should be changed to a_{\pm} .
72. S. Levine and G. M. Bell, *Can. J. Chem.*, **38**, 1346 (1960). These authors state (after Eq. 6.1) that the ϵ_1 appearing there in what is essentially V_{02} should be a differential rather than integral dielectric constant. Insofar as an ϵ_1 in such a formula is a useful construct at all, we believe the above point of view to be incorrect.
73. S. Levine and G. M. Bell, *J. Colloid Sci.*, **17**, 838 (1962).
74. S. Levine and G. M. Bell, *J. Phys. Chem.*, **67**, 1408 (1963).
75. S. Levine, G. M. Bell, and D. Calvert, *Can. J. Chem.*, **40**, 518 (1962). Some errors in this paper are listed in the present reference 87.
76. S. Levine, J. Mingins, and G. M. Bell, *Intern. Congr. Surface Activity, IV* Brussels, September, 1964.
77. S. Levine, J. Mingins, and G. M. Bell, *Can. J. Chem.*, **43**, 2834 (1965). In this paper e_0 and e both denote the magnitude of the electron charge. The expression $\beta = 3$ in Table II should be $\beta = 3 \text{ \AA}$. The symbol $\phi_1(x, \rho)$ in Eq. 4.5 should be replaced by $\phi_1(0, 0)$. In Appendixes B and C, the symbols F and F_1 are apparently taken to mean the same thing. In Eq. C.22, $\phi_1(x)$ should be replaced by $\phi_1(\gamma)$.
78. A. L. Loeb, *J. Colloid Sci.*, **6**, 75 (1951).
79. J. Lyklema, "The Measurement and Interpretation of Electric Potentials from a Physico-Chemical Point of View," *Med. Electron. Biol. Eng.*, **2**, 265-280 (1964). Primarily deals with potentials but includes non-comprehensive discussion of the double layer. No discussion of discreteness effects.
80. J. R. Macdonald, *J. Chem. Phys.*, **22**, 1857 (1954).
81. J. R. Macdonald, *J. Chem. Phys.*, **25**, 364 (1956).
82. J. R. Macdonald, Symposium in Commemoration of David C. Grahame, 138th Meeting of the American Chemical Society, New York, September 14, 1960. Abstracts of papers, p. 14-I.
83. J. R. Macdonald, *J. Appl. Phys.*, **35**, 3034 (1964).
84. J. R. Macdonald and C. A. Barlow, Jr., *J. Chem. Phys.*, **36**, 3062 (1962). Some corrections to this paper appear in its reference in the present reference 87.
85. J. R. Macdonald and C. A. Barlow, Jr., *J. Chem. Phys.*, **39**, 412 (1963); **40**, 237 (1964). An important correction to a part of this work is discussed

- in the present reference 89. The quantity $-4\pi Ld$ in line 12 of the second column of p. 419 should be $-4\pi Pd$.
86. J. R. Macdonald and C. A. Barlow, Jr., *J. Phys. Chem.*, **68**, 2737 (1964).
 87. J. R. Macdonald and C. A. Barlow, Jr., "Equilibrium Double-Layer Theory," in *Proc. Australian Conf. Electrochem.* 1st, J. A. Friend and F. Gutmann, Eds., Pergamon, Oxford, 1965, pp. 199-247. Comprehensive discussion of various theories developed to explain equilibrium behavior of double layers. Includes some discussion of discreteness work, tables comparing notations of various authors, and values suggested for double layer parameters. More critical than most other reviews; lists errors and misprints in much earlier work.
 88. J. R. Macdonald and C. A. Barlow, Jr., *Can. J. Chem.*, **43**, 2985 (1965). In the caption of Fig. 1, the expression $\sqrt{3}/2$ should be $2/\sqrt{3}$, and in the caption of Fig. 2, $\frac{3}{4}$ should be $\frac{4}{3}$.
 89. J. R. Macdonald and C. A. Barlow, Jr., *J. Chem. Phys.*, **44**, 202 (1966). The misplaced "2" at the right side of Eq. 13 should be a superscript.
 90. J. R. Macdonald and C. A. Barlow, Jr., *Surf. Sci.*, **4**, 381 (1966).
 91. J. R. Macdonald and C. A. Barlow, Jr., Symposium on Electrode Reactions, Electrochemistry Society Meeting, Cleveland, Ohio, May, 1966. *J. Electrochem. Soc.*, **113**, 978 (1966).
 92. J. R. Macdonald and C. A. Barlow, Jr., *J. Appl. Phys.*, **37**, 3471 (1966).
 93. J. K. Mackenzie, Thesis, University of Bristol, Bristol, 1950.
 94. N. F. Mott and R. J. Watts-Tobin, *Electrochim. Acta*, **4**, 79 (1961). Some errors in this paper are listed in the present reference 87.
 95. N. F. Mott, R. Parsons, and R. J. Watts-Tobin, *Phil. Mag.*, **7**, 483 (1962).
 96. K. Murakawa and M. Yamamoto, *J. Phys. Soc. Japan*, **21**, 821 (1966).
 97. D. Nagy and P. H. Cutler, *Phys. Letters*, **10**, 263 (1964).
 98. L. Nemeč, K. Holub, and J. Koryta, "The Electrical Double Layer," *Chem. Listy*, **59**, 476-519 (1965). (In Czech.) Appears to be a thorough review; contains discussion of several discreteness calculations.
 99. B. R. A. Nijboer and F. W. de Wette, *Physica*, **23**, 309 (1957).
 100. J. Th. G., Overbeek, "Electrochemistry of the Double Layer," in *Colloid Sci.*, Vol. I, H. R. Kruyt, Ed., Elsevier, Amsterdam, 1952, pp. 115-193. A thorough review of theoretical and experimental aspects of the double layer. No mention of discreteness.
 101. J. M. Parry and R. Parsons, *Trans. Faraday Soc.*, **59**, 241 (1963).
 102. R. Parsons, "Equilibrium Properties of Electrified Interphases," in *Modern Aspects of Electrochemistry*, Vol. I, J. O'M. Bockris, Ed., Butterworths, London, 1954, pp. 103-179. A comprehensive review containing much still pertinent basic material, including some discussion of early discreteness calculations.
 103. R. Parsons, *Proc. Intern. Congr. Surface Activity*, 2nd, Butterworths, London, **3**, 38 (1957).
 104. R. Parsons, "The Structure of the Electrical Double Layer and its Influence on the Rates of Electrode Reactions," in *Advances in Electrochemistry and Electrochemical Engineering*, Vol. I, P. Delahay, Ed., Interscience, New York, 1961, pp. 1-64. An excellent, authoritative review. Emphasizes broadness of coverage over depth but does include some discussion of early discreteness calculations.
 105. R. Parsons, "The Electrode Double Layer and Electrode Reactions," *Chem. Soc. (London) Ann. Rept.*, **61**, 80-98 (1964). A valuable review covering publications in the period since 1958. Includes some discussion of discreteness work.
 106. R. Parsons and F. G. R. Zobel, *J. Electroanal. Chem.*, **9**, 333 (1965).
 107. R. Payne, *J. Chem. Phys.*, **42**, 3371 (1965).
 108. R. Payne, Discussion following paper No. 148, Symposium on Electron Reactions, Electrochemistry Society Meeting, Cleveland, Ohio, May, 1966. *J. Electrochem. Soc.*, **113**, 990 (1966).
 109. R. E. Peierls, *Quantum Theory of Solids*, Oxford Univ. Press, Oxford, 1964.
 110. D. Pines, *Elementary Excitations in Solids*, Benjamin, New York, 1963.
 111. J. Pirenne and E. Kartheusen, *Physica*, **30**, 2005 (1964).
 112. C. D. Russell, *J. Electroanal. Chem.*, **6**, 486 (1963).
 113. R. G. Sachs and D. L. Dexter, *J. Appl. Phys.*, **21**, 1304 (1950).
 114. É. S. Sevast'yanov and D. I. Leikis, *Elektrokhim.*, **1**, 239 [203] (1965).
 115. W. R. Smythe, *Static and Dynamic Electricity*, McGraw-Hill, New York, 1950, p. 182.
 116. M. J. Sparnaay, *Rec. Trav. Chim.*, **77**, 872 (1958).
 117. M. J. Sparnaay, "Electrical Double Layers," *Vortr. Originalfassung Intern. Kongr. Grenzflächenaktive Stoffe*, 3, Cologne, 1960, **2**, 232-253 (Pub. 1961). (In German.) Contains useful general material, some discussion of discreteness, and material related to semiconductor surfaces.
 118. O. Stern, *Z. Elektrochem.*, **30**, 508 (1924).
 119. D. Stigter, *J. Phys. Chem.*, **68**, 3603 (1964).
 120. F. H. Stillinger, Jr., *J. Chem. Phys.*, **35**, 1584 (1961).
 121. F. H. Stillinger, Jr. and F. P. Buff, *J. Chem. Phys.*, **37**, 1 (1962).
 122. F. H. Stillinger, Jr. and J. G. Kirkwood, *J. Chem. Phys.*, **33**, 1282 (1960).
 123. L. W. Swanson and R. Gomer, *J. Chem. Phys.*, **39**, 2813 (1963).
 124. J. B. Taylor and I. Langmuir, *Phys. Rev.*, **44**, 423 (1933).
 125. J. Topping, *Proc. Roy. Soc. (London)*, **A114**, 67 (1927).
 126. M. P. Tosi, *Solid State Physics*, **16**, 1 (1964).
 127. B. M. E. van der Hoff and G. C. Benson, *Can. J. Phys.*, **31**, 1087 (1953). References to articles where the summation-integration method is applied for solids are given in this paper.
 128. R. J. Watts-Tobin, *Phil. Mag.*, **6**, 133 (1961).
 129. W. E. Williams, *Proc. Phys. Soc.*, **A66**, 372 (1953).
 130. H. Wroblowa, Z. Kovac, and J. O'M. Bockris, *Trans. Faraday Soc.*, **61**, 1523 (1965).
 131. Yu. I. Yalamov, *Zh. Fiz. Khim.*, **37**, 1393 [744], 1429 [768] (1963).
 132. J. M. Ziman, *Electrons and Phonons*, Oxford Univ. Press, London, 1960.

Manuscript received by Publisher September 29, 1966.